

Criteria of Wave Breaking Onset and its Variability in Irregular Wave Trains

Von der Fakultät für Bauingenieurwesen und Geodäsie
der
Gottfried Wilhelm Leibniz Universität Hannover

zur Erlangung des Grades
Doktorin der Ingenieurwissenschaften
Dr.-Ing.

genehmigte Dissertation

von

Dipl.-Ing. Mayumi Louise Wilms
geboren am 21.09.1982
in Wuppertal

Hannover, 2018

Referent: Prof. Dr.-Ing. habil. Torsten Schlurmann
Korreferent: Prof. Dr.-Ing. Bettar Ould el Moctar
Tag der Promotion: 02.06.2017

Danksagung

Die vorliegende Arbeit entstand während meiner Zeit als wissenschaftliche Mitarbeiterin am Ludwig-Franzius-Institut für Wasserbau, Ästuar- und Küsteningenieurwesen der Leibniz Universität Hannover. Die grundlegende Idee zur Untersuchung der Wahrscheinlichkeit des Wellenbrechens im Übergangsbereich entstand dabei im Rahmen des Forschungsvorhabens “Probabilistische Sicherheitsbewertung von Offshore-Windenergieanlagen (PSB)”, gefördert vom Niedersächsischen Ministerium für Wissenschaft und Kultur. Mein besonderer Dank gilt Herrn Prof. Dr.-Ing. habil. T. Schlurmann, für die Begleitung und Förderung, für das mir entgegengebrachte Vertrauen sowie den überlassenen Freiraum zur inhaltlichen Ausgestaltung meiner Arbeit. Die fachlichen Diskussionen, Ideen und Vorschläge waren stets eine Bereicherung. Weiterer Dank gilt Herrn Prof. Dr.-Ing. B. O. el Moctar für die Anfertigung des Zweitgutachtens und seine Verbesserungsvorschläge für die schriftliche Ausfertigung. Auch den weiteren Mitgliedern der Prüfungskommission, Herrn Prof. Dr.-Ing. K.-H. Rosenwinkel mit Übernahme des Prüfungsvorsitzes, sowie Herrn Prof. Dr.-Ing. S. Köster möchte ich für ihren Einsatz und ihre Zeit danken. Mein großer Dank gilt Herrn Dr. Sriram Venkatachalam für die Bereitstellung seines numerischen Modells des Wellenkanals, ohne dessen Nutzung diese Arbeit nicht möglich gewesen wäre. Bei meinen Kolleginnen, Kollegen und Freunden am Ludwig-Franzius-Institut, die mich über die Jahre begleitet haben, bedanke ich mich herzlich für die stete Unterstützung, Zusammenarbeit und gute Arbeitsatmosphäre. Ein besonderer Dank gilt hierbei den Kollegen O. Lojek, Dr.-Ing. N. B. Kerpen, M. Welzel und G. David, welche alle zum Gelingen der hydronumerischen Simulationen im Rahmen meiner Arbeit beigetragen haben. Außerdem bedanke ich mich bei Prof. Dr.-Ing. A. Hildebrandt und Dr.-Ing. K.-F. Daemrich für ihre stete Motivation und Bereitschaft zu fachlichen Diskussionen. Weiterhin danke ich den Mitarbeitern aus Technik und Verwaltung sowie allen studentischen Mitarbeitern für ihre Unterstützung im Rahmen der Projekte und Modellversuche. Mein größter Dank gilt abschließend meiner gesamten Familie und meinen Freunden. Meinen Eltern danke ich für ihre Unterstützung und ihren Zuspruch während meines Studiums und meiner Zeit als wissenschaftliche Mitarbeiterin. Meinem Verlobten Dr.-Ing. J. Brökelmann danke ich vom ganzen Herzen für seine Liebe und Unterstützung, die er mir in der gesamten Zeit der Bearbeitung und darüber hinaus hat zuteil werden lassen.

Hannover, Juni 2017

Mayumi Wilms

Abstract

Wave breaking is a random process that causes extreme hydrodynamic loads on offshore structures which lead to structural degradation and destruction. The majority of studies in literature analysed single wave breaking events in (quasi-)monochromatic wave trains and focused on energy dissipation and slamming forces on structures. Due to the random nature of wave breaking, its parameters vary widely and cannot be predicted with an exact value at a future instant of time, but instead must be described with probabilistic statements and statistical averages. This thesis analyses the variability of wave breaking onset, in order to gain deeper knowledge of the frequency and likelihood of occurrence of wave breaking, providing many applications to a more economic design and safety of offshore structures. Breaking onset is defined as an instantaneous state of wave dynamics where a wave has not started to break but cannot return to a stable state either. Present investigations focus on the evolution of wave trains towards and at breaking onset to describe the stochastic process of breaking onset, to find precursors and indicators of breaking onset, and to determine the optimal sample size of test runs to get a reliable result of the parameters of breaking onset. By this means, insights on the variability of breaking onset and its distribution function are achieved, which have not been available beforehand. In this context, investigations on breaking onset in irregular wave trains (JONSWAP sea spectrum) in intermediate water depth are carried out using laboratory and hydronumerical model tests. The physical model tests are carried out in the wave flume of the Ludwig-Franzius-Institute in a length scale of 1:40. In parallel, hydronumerical model tests using a numerical wave flume developed by Sriram (2008) and Sriram et al. (2006; 2007; 2010), based on the fully non-linear potential flow theory (semi-arbitrary Lagrangian-Eulerian Finite Element Method (SALE-FEM, structured version)), are conducted in the same length scale to complement the laboratory investigations and to increase the possible test run length and number. As design database the wave measurements of research platform FINO1 in the North Sea for the time period 2004–2011 are used and JONSWAP spectra are selected in such a way that daily and storm events are covered. By means of the random phase angle distribution, every considered spectrum is transformed multiple times to artificial, but physically-sound time series of water surface elevations. The cause-effect relationship between input wave train and breaking onset is investigated with a dimensional analysis (BUCKINGHAM π theorem) and an analysis of the uni- and bivariate (copula) distribution functions. The optimal sample size of test runs is derived by means of a convergence analysis. Indicators of breaking onset are detected by analysing the surface elevation (over time and over flume length) and applying the

threshold method which assumes that breaking onset happens when a parameter exceeds a certain threshold value. A novel detection indicator based on the HILBERT transform is introduced. Precursors of breaking onset are presented with MARKOV chains of the geometrical and instantaneous parameters, which describe the conditions that had to be met stochastically for wave instability to occur.

Keywords

wave breaking, breaking onset, variability, detection, prediction, distribution function, intermediate water, SALE-FEM, physical modeling, numerical modeling, numerical wave flume.

Kurzfassung

Wellenbrechen an Offshore-Bauwerken verursacht extreme hydrodynamische Lasten, die zur strukturellen Degradation und ggf. Zerstörung führen können. Der Großteil der bisherigen Studien untersuchte einzelne Wellenbrechenereignisse in monochromatischen bzw. quasi-monochromatischen Wellenzügen und konzentrierte sich dabei auf die Energiedissipation oder Druckschläge auf die Struktur. Da Wellenbrechen ein Zufallsprozess ist, variieren seine Parameter stark und können nicht mit einem exakten Wert zu einem bestimmten Zeitpunkt vorhergesagt werden, sondern müssen mit probabilistischen Aussagen und statistischen Mittelwerten beschrieben werden. Diese Arbeit untersucht die Variabilität des Wellenbrechenanfangs, um neue Erkenntnisse über die Häufigkeit und die Wahrscheinlichkeit des Auftretens von Wellenbrechen zu gewinnen, und somit eine wirtschaftlichere und sichere Konstruktion von Offshore-Bauwerken zu ermöglichen. Der Wellenbrechenanfang beschreibt den instantanen Zustand der Wellendynamik, bei dem die Welle noch nicht begonnen hat zu brechen, aber auch nicht in einen stabilen Zustand zurückkehren kann. Diese Arbeit konzentriert sich auf die Untersuchung der Entwicklung der Wellenzüge vor Wellenbrechenanfang und der Ganglinien am Ort des Wellenbrechenanfangs, um den stochastischen Prozess des Wellenbrechenanfangs zu beschreiben, Indikatoren des Wellenbrechens zu finden, und die optimale Stichprobengröße der Testläufe zu bestimmen, um ein zuverlässiges Ergebnis der Parameter des Wellenbrechenanfangs zu erhalten. Somit werden Erkenntnisse über die Variabilität des Wellenbrechenanfangs und dessen Verteilungsfunktion gewonnen, die bisher nicht verfügbar waren. Im Rahmen der Arbeit wird das Wellenbrechen in irregulären Wellenzügen (JONSWAP Seegangsspektren) im Übergangsbereich mit Hilfe von physikalischen und hydronumerischen Modellversuchen untersucht. Die physikalischen Modellversuche werden im Wellenkanal des Ludwig-Franzius-Instituts in einem Längenmaßstab von 1:40 durchgeführt. Parallel dazu werden hydronumerische Modellversuche im von Sriram (2008) und Sriram et al. (2006; 2007; 2010) entwickelten numerischen Wellenkanal im gleichen Längenmaßstab durchgeführt, um die Laboruntersuchungen zu ergänzen und die mögliche Testlaufänge und Testanzahl signifikant zu erhöhen. Der numerische Wellenkanal basiert auf der Theorie der vollständig nichtlinearen Potentialströmung (semi-arbiträre Lagrange-Euler Finite Elemente Methode (SALE-FEM, strukturierte Version)). Als Datengrundlage werden die Seegangsmessungen der Forschungsplattform FINO1 in der Nordsee für den Zeitraum 2004–2011 verwendet. Die JONSWAP Seegangsspektren werden so gewählt, dass Tages- und Sturmereignisse abgedeckt werden. Durch die zufällige Phasenwinkelverteilung wird jedes betrachtete Spektrum mehrfach in künstliche, aber physikalisch mögliche Zeitreihen

von Wasserspiegelauslenkungen transformiert. Der Einfluss des Eingangswellenzuges auf den Wellenbrechenanfang wird zum einen mit der Dimensionsanalyse (BUCKINGHAM π Theorem) und zum anderen mit der Untersuchung der uni- und bivariaten (copula) Verteilungsfunktionen bestimmt. Die optimale Stichprobengröße der Testläufe wird mittels einer Konvergenzanalyse hergeleitet. Indikatoren des Wellenbrechenanfangs werden durch Analyse der Wasserspiegelauslenkung (über Zeit und über Ort) ermittelt und die Grenzwert-Methode wird angewendet, bei der angenommen wird, dass Wellenbrechen stattfindet, wenn ein Parameter einen bestimmten Grenzwert überschreitet. Es wird ein neuartiger Indikator zur Detektion von Wellenbrechen in Zeitreihen eingeführt, der auf der HILBERT Transformation basiert. Mit Hilfe von MARKOW-Ketten wird das Verhalten der geometrischen und instantanen Parameter der Wellenzüge vor Wellenbrechenanfang dargestellt und die Bedingungen beschrieben, die stochastisch erfüllt werden müssen, damit Wellenbrechen auftritt.

Schlüsselwörter

Wellenbrechen, Wellenbrechenanfang, Variabilität, Detektion, Vorhersage, Verteilungsfunktion, Übergangsbereich, SALE-FEM, physikalische Modellierung, numerische Modellierung, numerischer Wellenkanal.

Contents

List of Figures	xiii
List of Tables	xxi
List of Symbols	xxv
1. Introduction	1
1.1. Motivation	1
1.2. Objective	2
1.3. Outline	4
2. Background and Recent Work	7
2.1. Wave Breaking in Intermediate and Deep Water	7
2.1.1. Breaking Criteria and Thresholds	7
2.1.2. Breaking Mechanism and Types	12
2.1.3. Breaking Phases	15
2.1.4. Breaking Detection Method	16
2.1.5. Breaking Probability	19
2.2. Wave Breaking Onset	21
2.2.1. Definition of Wave Breaking Onset	21
2.2.2. Studies on Wave Breaking Onset	21
2.3. Statistical Variability of Wave Breaking	26
3. Hydronumerical Model Tests	29
3.1. Test Setup	30
3.2. Test Program and Procedure	31
3.2.1. Generation of the Input Spectrum and Wave Train	34
3.2.2. Post-Processing of NWF Output Data	38
3.3. Validation, Limitations and Uncertainties	40
3.3.1. Validation	40
3.3.2. Limitations and Uncertainties	42

4. Influencing Factors on Breaking Onset	47
4.1. Development of Time of Breaking Onset	47
4.2. Dimensional Analysis	54
4.3. Comparison with Physical Model Tests	60
4.4. Likelihood of Breaking Onset	61
5. Variability of Breaking Onset	65
5.1. Univariate Distribution Function	65
5.2. Bivariate Distribution Function	74
5.2.1. Copula Approach	77
5.2.2. Uncertainty assessment	89
5.3. Optimal Sample Size	89
5.3.1. Optimal Sample Size Based on NWF Data	89
5.3.2. Optimal Sample Size Based on Copula Generated Data	92
6. Detection and Prediction of Breaking Onset in Wave Trains	99
6.1. Detection of Breaking Onset in Wave Trains	99
6.1.1. Test Setup	100
6.1.2. Test Program and Procedure	100
6.1.3. Results and Extended Detection Method	102
6.1.3.1. Extended Detection Method	107
6.1.3.2. Conditions of the Breaking Detection Method	112
6.2. Deformation of Wave Crests before Breaking Onset	115
6.2.1. Deformation of Wave Crests before Breaking Onset	116
6.2.2. Comparison of Breaking and Non-Breaking Wave Crests	124
6.2.3. Comparison with Physical Model Tests	128
6.3. Prediction of Breaking Onset	129
6.3.1. MARKOV Chain	135
7. Summary & Outlook	147
7.1. Summary	147
7.2. Outlook	153
Bibliography	155
A. Test Program of Hydronumerical Model Tests	165
B. Additional Figures (copula)	169

C. Additional Figures (deformation of wave crest)	179
D. Curriculum Vitae	183

List of Figures

2.1. Definition of wave parameters based on the recommendations of IAHR (1989).	8
2.2. Wave breaker types. (Source: Kraaiennest (2015))	14
2.3. Measurement methods for wave breaking detection.	16
3.1. Work flow of data generation and data analysis. The resulting geometrical and instantaneous parameters of the single waves are listed in Tab. 3.4.	33
3.2. Flowchart of the test procedure of the hydronumerical model tests.	35
3.3. Comparison of wave gauge WG1 ($x_{WG1} = 14.9$ m) for numerical (NWF) and physical model test (WKS). Initial wave steepness $s_{Z,i} = 0.044$	42
3.4. Comparison of wave gauge WG1 and WG3 for numerical (NWF) and physical model test (WKS). Wave steepness is $s_Z = 0.043$	43
3.5. Difference of water surface elevation for wave flume length $L_{flume} = 50$ m and $L_{flume} = 100$ m for wave gauge WG1 (left, $x_{WG1} = 0.0$ m) and WG6 (right, $x_{WG6} = 49.9$ m) for three regular wave trains with different wave steepnesses s_Z	44
3.6. Development of normalised time of breaking onset t_{br}/T_P against initial spectral steepness $s_{Z,i} = H_S/L_P$ for each wave flume length L_{flume} (top) and their median values (below).	45
4.1. Development of normalised time of breaking onset t_{br}/T_P against initial spectral steepness $s_{Z,i} = H_S/L_P$ for each number of waves in initial wave train N_W . Median values (black markers) and fitting line (black dashed line). Minimal duration of simulation (grey dashed line).	49
4.2. Development of normalised time of breaking onset t_{br}/T_P against number of waves in initial wave train N_W for each initial spectral steepness $s_{Z,i} = H_S/L_P$. Median values (black markers) and fitting line (black dashed line).	49

LIST OF FIGURES

4.3. Development of normalised time of breaking onset t_{br}/T_P against the normalised water depth H_S/h (top) and the water depth h (bottom) for each initial spectral steepness $s_{Z,i} = H_S/L_P$. Median values (black markers) and fitting line (black dashed line). 51

4.4. Development of normalised time of breaking onset t_{br}/T_P against the normalised water depth H/h for each water depth h . H is the wave height of the breaking wave. 53

4.5. Development of normalised time of breaking onset t_{br}/T_P against the enhancement factor γ of the JONSWAP spectrum for each initial spectral steepness $s_{Z,i} = H_S/L_P$. Median values (black markers) and fitting line (black dashed line). 53

4.6. Dimensional analysis of normalised time of breaking onset t_{br}/T_P (plotted against predicted results). Total number of data points $n_{max} = 291$. Normal (top) and logarithmic (bottom) presentation. 56

4.7. Dimensional analysis of normalised location of breaking onset x_{br}/L_P (plotted against predicted results). Total number of data points $n_{max} = 291$. Normal (top) and logarithmic (bottom) presentation. 57

4.8. Development of normalised time of breaking onset t_{br}/T_P against initial spectral steepness $s_{Z,i} = H_S/L_P$ for each number of waves in initial wave train N_W . Median values for the total data points (black markers). . . . 59

4.9. Development of normalised time of breaking onset t_{br}/T_P against number of waves in initial wave train N_W for each initial spectral steepness $s_{Z,i} = H_S/L_P$. Median values for the total data points (black markers). 59

4.10. Development of normalised location of breaking onset x_{br}/L_P against initial spectral steepness $s_{Z,i} = H_S/L_P$ in comparison with results from WKS model tests, NWF simulations, dimensional analysis, and Babanin et al. (2007). 61

4.11. Histograms of normalised time of breaking onset t_{br}/T_P for the data sample with all test runs (non-breaking and breaking wave trains) and with only breaking wave trains. Number of bins was 10. Initial spectral steepness $s_{Z,i} = 0.01$ (top) and $s_{Z,i} = 0.02$ (bottom). 63

5.1. Histograms of normalised time of breaking onset t_{br}/T_P with different PDFs for different initial spectral steepnesses $s_{Z,i}$ 69

LIST OF FIGURES

5.2.	Empirical cumulative distribution function of normalised time of breaking onset t_{br}/T_P with different CDFs for the test runs with initial spectral steepness $s_{Z,i} = 0.033, 0.044, 0.055, 0.067$	70
5.3.	Histograms of normalised location of breaking onset x_{br}/L_P with different PDFs for different initial spectral steepnesses $s_{Z,i}$	71
5.4.	Empirical cumulative distribution function of normalised location of breaking onset x_{br}/L_P with different CDFs for the test runs with initial spectral steepness $s_{Z,i} = 0.033, 0.044, 0.055, 0.067$	72
5.5.	qq-plots of output parameter time of breaking onset t_{br}/T_P against theoretical distributions for the test runs with initial spectral steepness $s_{Z,i} = 0.033$	75
5.6.	qq-plots of output parameter location of breaking onset x_{br}/L_P against theoretical distributions for the test runs with initial spectral steepness $s_{Z,i} = 0.033$	76
5.7.	qq-plot of output parameter location of breaking onset x_{br} against time of breaking onset t_{br} for the test runs with initial spectral steepness $s_{Z,i} = 0.033$	77
5.8.	Value pairs $(t_{br}/T_P, x_{br}/L_P)$ and their respective histograms for the test runs with initial spectral steepness $s_{Z,i} = 0.033$	78
5.9.	Ranked values (R, S) and their respective histograms for the test runs with initial spectral steepness $s_{Z,i} = 0.033$	79
5.10.	Normalised ranked values (U, V) and their respective histograms for the test runs with initial spectral steepness $s_{Z,i} = 0.033$	80
5.11.	The influence of the parameter Θ on the form of the copula shown exemplarily for the GUMBEL copula.	81
5.12.	Contour plots of the empirical copula $C_n(u, v)$ and the three ARCHIMEDEAN copulas for the test runs with initial spectral steepness $s_{Z,i} = 0.033$	83
5.13.	Comparison of original NWF simulated data (red cross markers) and copula generated data (black round markers) for the test runs with initial spectral steepness $s_{Z,i} = 0.033$	83
5.14.	Development of normalised time of breaking onset t_{br}/T_P against initial spectral steepness $s_{Z,i} = H_S/L_P$ for original NWF simulated data (red cross markers) and copula generated data (black round markers) for FRANK, GUMBEL and CLAYTON copula.	85
5.15.	qq-plots with original NWF simulated data and copula generated data of t_{br}/T_P and x_{br}/L_P	86

LIST OF FIGURES

5.16. Cumulative distribution function $H(x, y)$ calculated with the GUMBEL copula for the test runs with spectral steepness $s_{Z,i} = 0.033$, with original NWF simulated data (red cross markers) and copula generated data (black round markers). 88

5.17. Exceedance probability P_E calculated with the GUMBEL copula for the test runs with spectral steepness $s_{Z,i} = 0.033$, with original NWF simulated data (red cross markers) and copula generated data (black round markers). 88

5.18. Convergence analysis for the normalised time of breaking onset t_{br}/T_P against the number of considered test runs with mean value of all convergence curves (red). Repeats: 3,000. 91

5.19. Optimal sample size N_{opt} for the median value of the normalised time of breaking onset t_{br}/T_P with a permissible deviation of 1%, 2%, 5% and 10% based on the NWF data for all $s_{Z,i}$. Repeats: 10,000. 93

5.20. Optimal sample size N_{opt} for the median value of the normalised time of breaking onset t_{br}/T_P with a permissible deviation of 1%, 2%, 5% and 10% based on the NWF data for different repetitions of the convergence analysis. 94

5.21. Optimal sample size N_{opt} for the median value of the normalised time of breaking onset t_{br}/T_P with a permissible deviation of 1%, 2%, 5% and 10% based on the NWF data and copula generated data with the same initial sample size per spectral steepness. Repeats: 3,000. 95

5.22. Optimal sample size N_{opt} for the median value of the normalised time of breaking onset t_{br}/T_P with a permissible deviation of 1%, 2%, 5% and 10% based on copula generated data with different initial sample sizes n_{max} . Repeats: 3,000. 96

6.1. Test setup in the wave flume. Top: side view of setup. Bottom: top view of setup. wg: wave gauge. 101

6.2. Reproducibility of test run with $H_S = 0.2$ m and phase angle distribution "a". 104

6.3. Wave breaking probability P_{br} for the test runs with $h = 0.7$ m. 106

6.4. Time series of test run 1 for wave gauge WG2 with $H_S = 0.2$ m and phase angle distribution "a" with the geometrical parameters wave steepness s_Z , frequency f , skewness $S_K = \frac{a_c}{a_T} - 1$ and asymmetry $A_S = \frac{L''}{L'} - 1$. Position of wave breaking is marked with dashed lines. 108

LIST OF FIGURES

6.5. Geometrical parameters for test run 1 for wave gauge WG2 with $H_S = 0.2$ m and phase angle distribution “a”. Position of wave breaking is marked with dashed lines. 110

6.6. Time series of test run 1 for wave gauge WG2 with $H_S = 0.2$ m and phase angle distribution “a” with the instantaneous parameters $a(t)$ (instantaneous amplitude), $f(t)$ (instantaneous frequency) and $s_Z(t)$ (instantaneous steepness). The two spilling breakers occur at approximately 33 s and 61 s. The suggested thresholds are marked with dashed lines. 113

6.7. Computed wave crest evolution (chronological) until breaking onset with time step $\Delta t = 0.04$ s. 116

6.8. Development of the median of the geometrical parameters against the time step ($\Delta t = 0.04$ s) until breaking onset with the simulated NWF data for the test runs with different spectral steepnesses $s_{Z,i}$ (part 1, amplitudes and frequencies). 117

6.9. Development of the median of the geometrical parameters against the time step ($\Delta t = 0.04$ s) until breaking onset with the simulated NWF data for the test runs with different spectral steepnesses $s_{Z,i}$ (part 2, steepnesses and asymmetries). 118

6.10. Development of the median of the geometrical parameters against the time step ($\Delta t = 0.04$ s) until breaking onset with the simulated NWF data for the test runs with different spectral steepnesses $s_{Z,i}$ (part 3, steepnesses). 119

6.11. Normalised instantaneous amplitude of the breaking and non-breaking wave crest for the test runs with initial spectral steepness $s_{Z,i} = 0.01$ and $s_{Z,i} = 0.02$. In case of the breaking wave crest, the parameter is a median of all test runs. 125

6.12. Normalised instantaneous frequency of the breaking and non-breaking wave crest for the test runs with initial spectral steepness $s_{Z,i} = 0.01$ and $s_{Z,i} = 0.02$. In case of the breaking wave crest, the parameter is a median of all test runs. 125

6.13. Instantaneous steepness of the breaking and non-breaking wave crest for the test runs with initial spectral steepness $s_{Z,i} = 0.01$ and $s_{Z,i} = 0.02$. In case of the breaking wave crest, the parameter is a median of all test runs. 126

LIST OF FIGURES

6.14. Development of geometrical parameters against time steps ($\Delta t = 0.04$ s) with the simulated NWF data (black circle markers) for the test with $s_{Z,i} = 0.071$ and the measured data (filled red circle markers) by Bonmarin and Ramamonjariisoa (1985). The breaking onset is marked by a dashed line. 130

6.15. Development of geometrical and instantaneous parameters (part 1, amplitudes and frequencies) of the wave train at location of breaking onset for the test runs with initial spectral steepness $s_{Z,i} = 0.027, 0.044, 0.067$ over the last ten waves before the breaking wave. 132

6.16. Development of geometrical and instantaneous parameters (part 2, steepnesses and asymmetries) of the wave train at location of breaking onset for the test runs with initial spectral steepness $s_{Z,i} = 0.027, 0.044, 0.067$ over the last ten waves before the breaking wave. 133

6.17. Development of geometrical and instantaneous parameters (part 3, steepnesses) of the wave train at location of breaking onset for the test runs with initial spectral steepness $s_{Z,i} = 0.027, 0.044, 0.067$ over the last ten waves before the breaking wave. 134

6.18. Boxplots of geometrical and instantaneous parameters (part 1, amplitudes and frequencies) of the wave train at location of breaking onset for $s_{Z,i} = 0.044$ over the last ten waves before the breaking wave. 138

6.19. Boxplots of geometrical and instantaneous parameters (part 2, steepnesses and asymmetries) of the wave train at location of breaking onset for $s_{Z,i} = 0.044$ over the last ten waves before the breaking wave. 139

6.20. Boxplots of geometrical and instantaneous parameters (part 3, steepnesses) of the wave train at location of breaking onset for $s_{Z,i} = 0.044$ over the last ten waves before the breaking wave. 140

B.1. Cumulative distribution function $H(x, y)$ with the Gumbel copula for the test runs with spectral steepness $s_{Z,i} = 0.01$, with original NWF simulated data (red cross markers) and copula generated data (black round markers). 170

B.2. Exceedance probability P_E for the test runs with spectral steepness $s_{Z,i} = 0.01$, with original NWF simulated data (red cross markers) and copula generated data (black round markers). 170

B.3. Cumulative distribution function $H(x, y)$ with the Gumbel copula for the test runs with spectral steepness $s_{Z,i} = 0.02$, with original NWF simulated data (red cross markers) and copula generated data (black round markers). 171

LIST OF FIGURES

B.4. Exceedance probability P_E for the test runs with spectral steepness $s_{Z,i} = 0.02$, with original NWF simulated data (red cross markers) and copula generated data (black round markers). 171

B.5. Cumulative distribution function $H(x, y)$ with the Gumbel copula for the test runs with spectral steepness $s_{Z,i} = 0.027$, with original NWF simulated data (red cross markers) and copula generated data (black round markers). 172

B.6. Exceedance probability P_E for the test runs with spectral steepness $s_{Z,i} = 0.027$, with original NWF simulated data (red cross markers) and copula generated data (black round markers). 172

B.7. Cumulative distribution function $H(x, y)$ with the Gumbel copula for the test runs with spectral steepness $s_{Z,i} = 0.035$, with original NWF simulated data (red cross markers) and copula generated data (black round markers). 173

B.8. Exceedance probability P_E for the test runs with spectral steepness $s_{Z,i} = 0.035$, with original NWF simulated data (red cross markers) and copula generated data (black round markers). 173

B.9. Cumulative distribution function $H(x, y)$ with the Gumbel copula for the test runs with spectral steepness $s_{Z,i} = 0.044$, with original NWF simulated data (red cross markers) and copula generated data (black round markers). 174

B.10. Exceedance probability P_E for the test runs with spectral steepness $s_{Z,i} = 0.044$, with original NWF simulated data (red cross markers) and copula generated data (black round markers). 174

B.11. Cumulative distribution function $H(x, y)$ with the Gumbel copula for the test runs with spectral steepness $s_{Z,i} = 0.05$, with original NWF simulated data (red cross markers) and copula generated data (black round markers). 175

B.12. Exceedance probability P_E for the test runs with spectral steepness $s_{Z,i} = 0.05$, with original NWF simulated data (red cross markers) and copula generated data (black round markers). 175

B.13. Cumulative distribution function $H(x, y)$ with the Gumbel copula for the test runs with spectral steepness $s_{Z,i} = 0.055$, with original NWF simulated data (red cross markers) and copula generated data (black round markers). 176

LIST OF FIGURES

B.14. Exceedance probability P_E for the test runs with spectral steepness $s_{Z,i} = 0.055$, with original NWF simulated data (red cross markers) and copula generated data (black round markers). 176

B.15. Cumulative distribution function $H(x, y)$ with the Gumbel copula for the test runs with spectral steepness $s_{Z,i} = 0.067$, with original NWF simulated data (red cross markers) and copula generated data (black round markers). 177

B.16. Exceedance probability P_E for the test runs with spectral steepness $s_{Z,i} = 0.067$, with original NWF simulated data (red cross markers) and copula generated data (black round markers). 177

B.17. Cumulative distribution function $H(x, y)$ with the Gumbel copula for the test runs with spectral steepness $s_{Z,i} = 0.071$, with original NWF simulated data (red cross markers) and copula generated data (black round markers). 178

B.18. Exceedance probability P_E for the test runs with spectral steepness $s_{Z,i} = 0.071$, with original NWF simulated data (red cross markers) and copula generated data (black round markers). 178

C.1. Development of the median of the geometrical parameters against time steps ($\Delta t = 0.04$ s) until breaking onset with the simulated NWF data for different spectral steepnesses $s_{Z,i}$ (part 1, amplitudes and frequencies). . . 180

C.2. Development of the median of the geometrical parameters against time steps ($\Delta t = 0.04$ s) until breaking onset with the simulated NWF data for different spectral steepnesses $s_{Z,i}$ (part 2, steepnesses and asymmetries). . 181

C.3. Development of the median of the geometrical parameters against time steps ($\Delta t = 0.04$ s) until breaking onset with the simulated NWF data for different spectral steepnesses $s_{Z,i}$ (part 3, steepnesses). 182

List of Tables

1.1. Overview of objectives of the thesis.	3
2.1. Wave parameters and ratio values for steepness and asymmetry based on the recommendations of IAHR (1989).	9
2.2. Compilation of wave steepness thresholds from literature.	10
2.3. Compilation of steepness and asymmetry thresholds from literature.	11
2.4. Compilation of threshold parameter α for the dynamic breaking criterion from literature.	13
3.1. Parameters for the setting of the numerical wave flume.	31
3.2. Limit values for geometrical parameters in post-processing of NWF output data.	34
3.3. Combinations of enhancement width σ_L and σ_H used in the hydronumerical simulations.	36
3.4. Compilation of dimensionless geometrical and instantaneous parameters as used in the analysis.	40
3.5. Overview of the thesis' chapters of results and the covered output data.	41
4.1. Overview of number of test runs for data sets with different initial spectral steepnesses and the frequency of breaking.	62
5.1. Statistics of normalised time of breaking onset t_{br}/T_P for dataset with all test runs (breaking wave trains).	66
5.2. Statistics of normalised time of breaking onset t_{br}/T_P for dataset with all test runs (breaking wave trains) and $h = 0.7$ m, $N_W = 192$ and $\gamma = 3.3$	66
5.3. Statistics of normalised location of breaking onset x_{br}/L_P for dataset with all test runs (breaking wave trains).	67
5.4. Statistics of normalised location of breaking onset x_{br}/L_P for dataset with all test runs (breaking wave trains) and $h = 0.7$ m, $N_W = 192$ and $\gamma = 3.3$	67
5.5. Probability density functions.	68

LIST OF TABLES

5.6.	Cumulative distribution functions, $\gamma(k, ax)$ is the lower incomplete Gamma function.	73
5.7.	KS-statistics of two-sample KOLMOGOROV-SMIRNOV tests for the normalised time of breaking onset t_{br}/T_P	73
5.8.	KS-statistics of two-sample KOLMOGOROV-SMIRNOV tests for the normalised location of breaking onset x_{br}/L_P	74
5.9.	Summary of the three one-parameter (Θ) ARCHIMEDEAN copulas. $t = u$ or $t = v$. $s = \varphi(u) + \varphi(v)$	81
5.10.	Compilation of the results of the parameter Θ for the copula families FRANK, GUMBEL, and CLAYTON for each spectral steepness $s_{Z,i}$	82
5.11.	RMSEs and values for the KS-statistic from comparing theoretical and empirical copula functions for the parameters t_{br}/T_p and x_{br}/L_P , and for the test runs with initial spectral steepness $s_{Z,i} = 0.033$	84
5.12.	Geometrical parameters for the breaking wave crest for the exemplary value pairs in Fig. 5.17.	87
5.13.	Optimal sample size N_{opt} for the median value of the normalised time of breaking onset t_{br}/T_P with a permissible deviation of 1%, 2%, 5% and 10% based on the NWF data. Repeats: 10,000.	92
5.14.	Optimal sample size N_{opt} for the median value of the normalised time of breaking onset t_{br}/T_P with a permissible deviation of 1%, 2%, 5% and 10% based on the NWF simulated data and copula generated data (in italic) for the test runs with initial spectral steepness $s_{Z,i} = 0.033, 0.044, 0.055, 0.071$. Repeats: 10,000 (NWF) and 3,000 (GUMBEL copula).	97
6.1.	Compilation of conducted model test runs in the WKS wave flume with random wave trains.	103
6.2.	Compilation of conducted model test runs in the WKS wave flume with regular wave trains.	104
6.3.	Compilation of results of number of breaking waves with their respective time stamp relative to the start of the wave maker.	105
6.4.	Median values for every geometrical and instantaneous parameter for every 5th time step (every 0.2s) until time of breaking onset (tbo) for the test runs with initial spectral steepness $s_{Z,i} = 0.044$	121

6.5. Absolute value of the gradient of the median values for every geometrical and instantaneous parameter for every 5th time step (every 0.2 s) until time of breaking onset (tbo) for the test runs with initial spectral steepness $s_{Z,i} = 0.044$ 122

6.6. Minimum and maximum values of the geometrical and instantaneous parameters at breaking onset for initial spectral steepness $s_{Z,i} = 0.01 - 0.035$ 123

6.7. Minimum and maximum values of the geometrical and instantaneous parameters at breaking onset for initial spectral steepness $s_{Z,i} = 0.044 - 0.071$ 123

6.8. Geometrical and instantaneous parameters for the highest (and steepest) wave crest at the time of simulation end for non-breaking test runs, and minimum and maximum values for the breaking test runs. 128

6.9. Minimum and maximum values of geometrical and instantaneous parameters for the 10th wave (last wave before the breaking wave) for the test runs with initial spectral steepness $s_{Z,i} = 0.01 - 0.035$ 136

6.10. Minimum and maximum values of geometrical and instantaneous parameters for the 10th wave (last wave before the breaking wave) for the test runs with initial spectral steepness $s_{Z,i} = 0.044 - 0.071$ 136

6.11. Median values for every geometrical and instantaneous parameter for the last six waves before the breaking wave for the test runs with initial spectral steepness $s_{Z,i} = 0.044$ 137

6.12. Absolute value of the gradient of the median values for every geometrical and instantaneous parameter for the last six waves before the breaking wave for the test runs with initial spectral steepness $s_{Z,i} = 0.044$ 141

6.13. Relative frequency of the median values for every geometrical and instantaneous parameter for the last six waves before the breaking wave for the test runs with initial spectral steepness $s_{Z,i} = 0.044$ 142

6.14. Maximum relative frequency for every geometrical and instantaneous parameter for the last six waves before the breaking wave for the test runs with initial spectral steepness $s_{Z,i} = 0.044$ 143

6.15. Minimum and maximum values of the geometrical and instantaneous parameters for their respective maximum relative frequencies (see Tab. 6.14) for the last six waves before the breaking wave for the test runs with initial spectral steepness $s_{Z,i} = 0.044$ 144

LIST OF TABLES

A.1. Test program of the hydronumerical model tests.	165
A.1. Test program of the hydronumerical model tests.	166
A.1. Test program of the hydronumerical model tests.	167

List of Symbols

Roman Symbols

$(ak)_0$	initial steepness of regular waves by Banner et al. (2000)	[-]
Δf	spectral bandwidth	[Hz]
Δt	time step	[s]
Δt_{NWF}	time step of simulation	[s]
\dot{u}	downward surface acceleration	[m/s ²]
a	wave amplitude	[m]
$a(t)$	instantaneous amplitude	[m]
A_S	asymmetry by Babanin et al. (2007), $L''/L' - 1$	[-]
a_C	zero-crossing wave crest height	[m]
a_T	zero-crossing wave trough excursion (positive)	[m]
b_T	wave breaking probability by Babanin et al. (2011)	[-]
C	copula function	[-]
c	wave velocity	[m/s]
C_n	empirical copula function	[-]
c_r	velocity scale	[-]
cv	coefficient of variation	[-]
DWT	duration of wave train, time length of input signal	[s]
dx	distance between nodes in x-axis direction	[m]

List of Symbols

f	wave frequency	[Hz]
$f(t)$	instantaneous frequency	[Hz]
$F(x), G(y)$	marginal distributions	[-]
f_P	peak wave frequency	[Hz]
F_r	Froude number	[-]
f_{br}	breaking frequency, ratio of breaking test runs to total number of test runs	[-]
f_{max}	upper integration limit for spectrum	[Hz]
f_{min}	lower integration limit for spectrum	[Hz]
g	acceleration of gravity	[m/s ²]
H	wave height	[m]
h	water depth	[m]
$H(x, y)$	joint cumulative distribution function	[-]
H_P	peak wave height by Banner et al. (2000)	[m]
H_S	significant wave height	[m]
k	wave number, $2\pi/L$	[1/m]
k_P	peak wave number, $2\pi/L_P$	[1/m]
L	wave length measured in the direction of wave propagation	[m]
$L(t)$	instantaneous wave length	[m]
L''	crest rear wave length	[m]
L'	crest front wave length	[m]
L_0	wave length in deep water	[m]
L_P	peak wave length	[m]
L_{flume}	wave flume length	[m]
m_0	0th moment of spectral energy density $S(f)$	[m ²]

List of Symbols

m_4	4th moment of spectral energy density $S(f)$	[m ² s ⁻⁴]
N_W	number of waves in wave train	[-]
n_{br}	number of breaking wave crests	[-]
n_{freq}	number of frequency components	[-]
n_{max}	total number of test runs	[-]
N_{opt}	optimal sample size	[-]
$n_{tot,c}$	actual counted number of wave crests	[-]
n_{tot}	number of total wave crests in a wave train	[-]
n_x	number of nodes in x-axis direction	[-]
n_z	number of nodes in z-axis direction	[-]
P_E	exceedance probability	[-]
P_{br}	breaking probability	[-]
R, S	ranked values	[-]
R^2	coefficient of determination	[-]
R_p	characteristic measure of the wave steepness by Dawson et al. (1991)	[-]
$S(f)$	spectral energy density	[m ² s]
S_K	skewness by Babanin et al. (2007), $a_C/a_T - 1$	[-]
$s_Z(t)$	instantaneous steepness, $2a(t)/L(t)$	[-]
s''_C	crest rear steepness, a_C/L''	[-]
s'_C	crest front steepness, a_C/L'	[-]
$s_{Z,i}$	initial spectral steepness, H_S/L_P	[-]
s_{ZC}	crest steepness, a_C/L	[-]
s_{ZT}	trough steepness, a_T/L	[-]
s_Z	wave steepness by zero-crossing analysis, H/L	[-]

List of Symbols

T	wave period	[s]
$T(t)$	instantaneous period	[s]
T_b	time to breaking onset by Banner et al. (2000)	[s]
T_D	main temporal scale of the wave field	[s]
T_R	duration of the wave record	[s]
t_{br}	time of breaking onset, temporal distance from simulation start to end	[s]
T_P	peak wave period	[s]
t_{Rampe}	time span to start the input signal for the wave maker with zero displacement	[s]
t_{simul}	maximal duration of simulation	[s]
u	horizontal surface wave orbital velocity	[m/s]
U, V	normalised ranked values	[-]
$X(t)$	analytical signal	[-]
$X_i(t)$	Hilbert transform	[-]
$X_r(t)$	real function, original signal	[-]
x_{br}	location of breaking onset, spatial distance from inlet to breaking wave crest	[m]
x_{WG1}	distance of wave gauge WG1 from wave maker	[m]

Abbreviations

CDF	cumulative distribution function
FFT	fast Fourier transform
FZK	Forschungszentrum Küste
GoF	goodness of fit
KS	Kolmogorov-Smirnov
MI	modulational instability
NWF	numerical wave flume

PDF	probability density function
qq-plots	quantile-quantile plots
RMSE	root-mean-square error
SALE-FEM	semi-arbitrary Lagrangian-Eulerian Finite Element Method
tbo	time of breaking onset
WG	wave gauge
WKS	wave flume Schneiderberg of the Ludwig-Franzius-Institute
wmt	wave maker theory

Greek Symbols

α	Phillip's constant of JONSWAP spectrum	[-]
$\delta(t)$	local energy growth rate by Song et al. (2002)	[-]
ϵ	significant spectral peak steepness by Banner et al. (2000)	[-]
η	water surface elevation	[m]
γ	enhancement factor of JONSWAP spectrum	[-]
λ	length scale	[-]
μ	location parameter	[-]
μ_H	horizontal asymmetry factor, a_C/H	[-]
μ_V	vertical asymmetry factor, L''/L'	[-]
$\omega(t)$	instantaneous angular frequency	[rad/s]
ω_P	peak angular frequency	[rad/s]
ρ	Spearman's ρ	[-]
σ	standard deviation	[-]
σ_H	enhancement width of JONSWAP spectrum	[-]
σ_L	enhancement width of JONSWAP spectrum	[-]

List of Symbols

τ	time scale	[-]
τ_n	Kendall's τ_n	[-]
Θ	copula parameter	[-]
$\Theta(t)$	instantaneous phase	[-]
φ	phase angle distribution	[-]

Subscripts

$()_0$	deep water
$()_C$	crest
$()_H$	higher
$()_i$	initial
$()_L$	lower
$()_m$	model dimension
$()_n$	nature dimension
$()_P$	peak
$()_r$	ratio
$()_S$	significant
$()_T$	trough
$()_Z$	steepness
$()_{br}$	breaking
$()_{freq}$	frequency
$()_{max}$	maximum
$()_{min}$	minimum
$()_{opt}$	optimal
$()_{tot}$	total

Mathematical Symbols

- $\bar{()}$ mean value
- $\dot{()}$ time derivative
- $\tilde{()}$ median value

1. Introduction

1.1. Motivation

For about 50 years the phenomenon of wave breaking has been closely studied with the aim of the analytical description of the underlying processes and its prediction. Several authors (e.g. Ochi (2005); Babanin (2011); Barthélémy et al. (2011); Zakharov and Shamin (2012)) have investigated the statistical properties of wave breaking by different measurement methods in the field, in controlled laboratory environments or by means of hydronumerical models. Most of the laboratory experiments were performed with monochromatic waves, few in random seas and only a marginal part is conducted in three-dimensional seas. However, there is not yet a complete, i.e. universal analytical description of wave breaking, as the process is highly non-linear, irregular and intermittent. Despite the random and intermittent nature of wave breaking, it is a significant phenomenon in the sea state environment as it plays an important role in the ocean-atmosphere interaction and represents the key role in wave energy dissipation. Furthermore, breaking waves may cause extreme hydrodynamic loads on offshore structures or vessels, which induce significant singular stresses and thereby lead to degradation or destruction of the structure. An estimation of the frequency or likelihood of occurrence and type of breaking waves in a given sea state are valuable information for the design engineer in order to enable economical and safe constructions.

It is important to keep in mind that the wave breaking process, as the sea state process in general, is a random process, and thus, there is no way to predict an exact value at a future instant of time. The data must be described in terms of probability statements and statistical averages. Waves do not break at a single well defined value of wave steepness, but instead, break over a wide value range (Kjeldsen and Myrhaug, 1979b; Bonmarin et al., 1989; Kriebel, 2000; Toffoli et al., 2010).

So far the majority of studies focused on the analysis of a single breaking wave to describe the underlying processes, estimate the energy dissipation, or study the slamming forces on structures. There are no studies which take into account or analyse the variability of parameters of the breaking wave. Although previous investigations contributed to

1. Introduction

the fundamental understanding of wave breaking, there is little consensus on the influencing factors that control breaking onset or breaking probability (Nath and Ramsey, 1976; Melville, 1996; Babanin et al., 2001; Banner et al., 2000). Breaking onset is defined as an instantaneous state of wave dynamics where a wave has not started to break but cannot return to a stable state either. Furthermore, there is an absence of established breaking criteria, and therefore a lack of progress in the development of an efficient method to detect wave breaking in time series of water surface elevations (Sharkov, 2007; Toffoli et al., 2010; Babanin et al., 2011b; Perlin et al., 2013). Concerning the question how large a sample size has to be to have a reliable result of the likelihood of wave breaking and of the geometry of a breaking wave at breaking onset, previous studies recommends solely that the sample size has to be large enough without specifying the size (Banner et al. (2000, p. 3156), Goda (2010), Babanin et al. (2011b, p. 176)).

1.2. Objective

Breaking waves are highly non-linear and the result of a certain propagation of multiple waves. Therefore, it is obvious that the time history of a wave train is essential to describe such phenomenons like breaking waves. One objective of this thesis was to investigate the evolution of a wave train (two-dimensional) right before and at breaking onset by means of laboratory and hydronumerical experiments to describe the stochastic process of breaking onset. The cause-effect relationship between the input wave train and breaking onset was investigated in two ways: 1) a dimensional analysis (BUCKINGHAM π theorem) and 2) an analysis of the uni- and bivariate (copula) distribution functions.

Another objective of this thesis was to investigate the water surface elevation at breaking onset (as a function of the flume length) to determine the critical geometrical and instantaneous parameters to detect breaking onset (threshold method). Moreover, the progress of the geometrical and instantaneous properties of single waves in the wave train (as a function of time) towards breaking onset was investigated in order to determine precursors of wave breaking and as such progress indicators of probability of breaking. This information was used to describe which conditions have to be met stochastically for wave instability to occur (MARKOV chain) and, thus, enables to find robust indicators, i.e. precursor of wave breaking onset from times series history.

Because the wave breaking process is highly irregular, the geometrical and instantaneous parameters of breaking onset spread. The distributions of those describing parameters are presented, and their variability and sensitivity are described. Thus, the required measurement duration and area to determine the properties of breaking onset was de-

Table 1.1.: Overview of objectives of the thesis.

Objective	Methodology	Results	Chapter
Investigate the evolution of wave trains towards and at breaking onset to describe the stochastic process of breaking onset.	Dimensional analysis (BUCKINGHAM π theorem)	Influencing factors on breaking onset	4.1 and 4.2
	Uni- and bivariate distribution functions		5.1 and 5.2
Investigate the optimal sample size to get a reliable result of breaking onset.	Convergence analysis	Optimal sample size of test runs	5.3
Investigate the evolution of wave trains towards and at breaking onset to find precursors and indicators of breaking onset.	Threshold method	Detection of breaking onset	6.1 and 6.2
	MARKOV chain	Prediction and likelihood of breaking onset	6.3

terminated. The main reason for the variability of breaking onset is the wave sequence in a wave train (phase angle distribution). Another objective of this thesis was to investigate the optimal sample size of test runs (convergence analysis), so that the output parameters (time and location of breaking onset) were independent of the wave sequence and phase angle distribution respectively, in other words uninfluenced by the initial input signal.

An overview of all objectives of this thesis is given in Tab. 1.1. The more detailed flowcharts of the work flow of the data collection, post-processing, and data analysis are given in chapter 3, see especially Figs. 3.1 and 3.2 and Tabs. 3.4 and 3.5.

The physical model tests were carried out in the wave flume ‘‘Schneiderberg’’ of the Ludwig-Franzius-Institute for Hydraulic, Estuarine and Coastal Engineering (WKS, 100 m x 2.2 m x 2.0 m) in a length scale of 1:40. The record length was limited to max. 100 waves to avoid wave reflections in the testing area. In parallel, hydronumerical model tests using a numerical wave flume (NWF) developed by Sriram (2008) and Sriram et al. (2006; 2007; 2010), based on the fully non-linear potential flow theory (semi-arbitrary Lagrangian-Eulerian Finite Element Method (SALE-FEM, structured version)), were conducted to complement the laboratory investigations and to increase the possible test run length and number. Although the hydronumerical model tests took a certain computing time, their use had the important advantage that test run length and test number

1. Introduction

could be increased significantly, which would not have been possible with the physical model tests in the same time. The hydronumerical model tests were also conducted in a length scale of 1:40. Due to potential flow theory the NWF calculations are terminated when the water surface becomes discontinuous. However, this limitation is not detrimental because the focus is set on the wave train evolution until breaking onset. The discontinuity in the NWF may be of numerical or physical nature. To sort out the test runs with numerical discontinuities, solely the test runs were considered here which contain wave trains where the maximum wave crest and the maximum wave steepness were less than one single waves apart. Wave trains were divided into single waves by the zero-downcrossing method. The point of termination of simulation was characterized by the two parameters: time to breaking onset t_{br} (time span from simulation start to end) and location of breaking onset x_{br} (spatial distance from inlet to breaking wave crest).

As design database the wave measurements of research platform FINO1 in the North Sea was used (Neumann et al., 2003), and a scatter diagram for the time period 2004 - 2011 was derived. The significant wave height H_S and wave peak period T_P for the JONSWAP spectra was selected in such a way that daily and storm events were considered, and the initial spectral steepness $s_{z,i} = H_S/L_P$ with $L_P = g/(2\pi)T_P^2$ varied between $0.01 \leq s_{z,i} \leq 0.071$. Further input parameters were the enhancement factor γ ($2 \leq \gamma \leq 7$), water depth h ($0.5 \text{ m} \leq h \leq 0.9 \text{ m}$), phase angle distribution φ , and the number of waves in a wave train N_W ($192 \leq N_W \leq 3072$). By means of the random phase angle distribution, every considered spectrum was transformed multiple times (up to 500 times) to artificial, but physically-sound time series of water surface elevations.

1.3. Outline

In chapter 2 a summary of the background and recent work about wave breaking, with focus on wave breaking onset in intermediate and deep water, is given.

In chapter 3 the validation, test setup, program and procedure of the hydronumerical model tests are explained. Especially Figs. 3.1 and 3.2 and Tabs. 3.4 and 3.5 explain the work flow of data collection, post-processing, and data analysis.

In chapter 4 the results of the investigation of the cause-effect relationship between input factors and time and location of breaking onset with the dimensional analysis (BUCKINGHAM π theorem) are given. The analysis was based on the results of the hydronumerical model tests.

In chapter 5 the results of the investigation of the variability of breaking onset with the uni- and bivariate (copula) distribution functions are given. Furthermore, the con-

vergence analysis to determine the optimal sample size of test runs is presented. The analysis was based on the results of the hydronumerical model tests.

In chapter 6 a detection method based on the physical and numerical model tests is developed with the threshold method; the test setup, program and procedure of the laboratory model tests are explained in section 6.1. The prediction of breaking onset in a time series was investigated with the MARKOV chain.

In chapter 7 the thesis is summarised and an outlook is given.

2. Background and Recent Work

In this chapter, a synopsis of wave breaking in intermediate and deep water with focus on breaking onset is given. After a short summary of breaking criteria and mechanisms, the focus is on the recent work on detection and prediction of wave breaking onset and its variability and probability.

2.1. Wave Breaking in Intermediate and Deep Water

Wave breaking is the process of the deformation and destabilization of wave crests, followed by water-air mixture and wave energy dissipation. The physics that lead to wave breaking are elusive, but previous studies suggested various criteria which supposedly indicate a breaking onset and therefore may help to detect it. It is an assumption that a wave crest has to exceed a critical threshold before the wave can break; this is called the threshold method. According to Babanin et al. (2007) “a criteria of breaking may be indicative of a wave approaching an instable state, but is not a reason or a cause for the breaking”. However, to investigate the wave breaking phenomenon, a criterion to define the breaking onset of a wave crest has to be chosen. Previous studies show that there is no universal value, but a value range in which the wave breaking parameters lie. In the following, the different approaches to define a criterion are summarised. Please note, that the focus of this thesis is on dominant wave breakers, and not on small breaking waves; the selection of the measurement and detection method depends on this.

2.1.1. Breaking Criteria and Thresholds

The three main criteria to define the conditions of wave breaking are:

1. geometrical criterion: the wave steepness ($s_z = H/L$) exceeds a threshold parameter.
2. Kinematic criterion: the surface wave orbital velocity u exceeds a threshold parameter. At breaking onset, the streamlines of fluid particles stagnate relative to the wave form.

2. Background and Recent Work

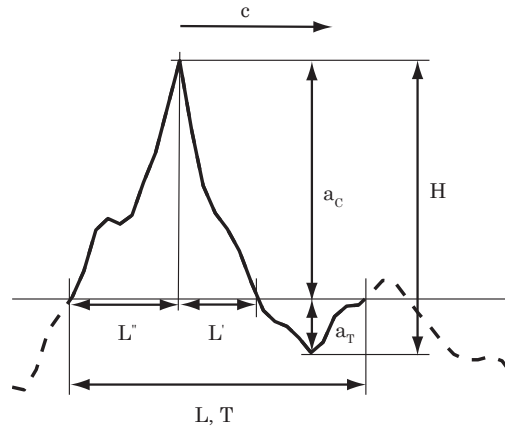


Figure 2.1.: Definition of wave parameters based on the recommendations of IAHR (1989).

3. Dynamic criteria: the downward surface acceleration \dot{u} exceed a threshold parameter.

Geometrical Breaking Criteria

The geometry of a single wave in a time series is described with the following wave parameters, see Fig. 2.1. Based on those wave parameters, various ratio values are derived, which describe steepness and asymmetry of the single wave, see Tab. 2.1.

The most widely known wave steepness threshold is the limiting steepness for a STOKES wave, analytically derived by Michell (1893), for which a wave crest breaks when the wave height exceeds $s_Z = 1/7$ of the STOKES limiting wavelength. The wave steepness threshold for breaking onset has been examined extensively in laboratory and hydronumerical experiments. In Tab. 2.2, an overview of the critical wave steepness thresholds determined by different authors is given. The threshold spreads because of different methods of wave breaking generation and the ambiguity in definition of breaking onset. The wave steepness s_Z may be enough to describe a sinusoidal wave, but not a steep asymmetric wave, because asymmetric waves can exist with the same wave steepness s_Z . Therefore, Kjeldsen and Myrhaug (1979b, 1981) introduced the crest-front and -rear steepness (s'_C and s''_C), and the vertical and horizontal asymmetry parameters (μ_V and μ_H), see Tab. 2.1. These parameters describe the geometry of a breaking gravity wave crest, i.e. the sharpened crest, flattened trough and the very steep crest-front face. For a second-order STOKES wave in deep water, these parameters are $s'_C = s''_C = 0.40$, $\mu_V = 1$

2.1. Wave Breaking in Intermediate and Deep Water

Table 2.1.: Wave parameters and ratio values for steepness and asymmetry based on the recommendations of IAHR (1989).

Symbol	Description	Unit
H	Wave height	m
T	Wave period	s
L	Wavelength measured in the direction of wave propagation	m
c	Wave velocity	m/s
a_C	Zero-crossing wave crest height	m
a_T	Zero-crossing wave trough excursion (positive)	m
L'	Crest front wavelength	m
L''	Crest rear wavelength	m
s_Z	Wave steepness by zero-crossing analysis, H/L	
s_{ZC}	Crest steepness, a_C/L , based on Bonmarin and Ramamonjiarisoa (1985)	
s_{ZT}	Trough steepness, a_T/L , based on Bonmarin and Ramamonjiarisoa (1985)	
s'_C	Crest front steepness, a_C/L'	
s''_C	Crest rear steepness, a_C/L''	
μ_V	Vertical asymmetry factor, L''/L'	
μ_H	Horizontal asymmetry factor, a_C/H	

2. Background and Recent Work

Table 2.2.: Compilation of wave steepness thresholds from literature.

Author	$s_Z = \frac{H}{L}$	Note
Michell (1893)	0.143	regular STOKES wave
Duncan (1981)	0.200	breaking produced by towed hydrofoil
Ochi and Tsai (1983)	0.126	irregular wave
Xu et al. (1986)	0.119	irregular wave
Ramberg and Griffin (1987)	0.132	irregular wave
Rapp and Melville (1990, fig. 21)	0.048 - 0.070	dispersive focusing
Wu (2004)	0.048 - 0.121	dispersive focusing
Tian et al. (2008)	0.089 - 0.137	dispersive focusing
Tian et al. (2012)	0.064 - 0.153	dispersive focusing and modulational instability
Bonmarin and Ramamonjjarisoa (1985, fig. 9)	0.120	modulational instability
Tulin and Waseda (1999, fig. 15)	0.070 - 0.131	modulational instability
Babanin et al. (2010)	0.127	modulational instability
Babanin et al. (2010)	0.140	modulational instability (while breaking)
Babanin (2011, p. 152)	0.146 - 0.153	short-crested directional waves
Babanin (2011, p. 152)	0.175	short-crested directional waves (while breaking)

and $\mu_H = 0.61$. The corresponding thresholds determined by different authors are given in Tab. 2.3.

The determination of the geometrical parameters in laboratory experiments is non-trivial, because the wave profile is highly irregular and unsteady and the profile deforms rapidly. There are difficulties of spatial surface profile measurement. There are no straightforward transformation between measurements in the temporal domain and those in the spatial domain available. Temporal measurements may not fully represent the spatial characteristics. Yao and Wu (2005) showed that the wave steepness ak , with a as amplitude and k as wave number $k = 2\pi/L$ and the crest's geometrical parameters of the same incipient breaking wave may vary up to 50% dependent on the measurement

Table 2.3.: Compilation of steepness and asymmetry thresholds from literature.

Author	$s'_C = \frac{aC}{L'}^2$	$s''_C = \frac{aC}{L''}$	$\mu_V = \frac{L''}{L'}$	$\mu_H = \frac{aC}{H}$	Note
Kjeldsen and Myrhaug (1979b), Kjeldsen and Myrhaug (1981)	0.32 - 0.78	0.26 - 0.39	2.0	0.84 - 0.95	different kinds of breaking
Bonmarin and Ramamonjarisoa (1985)	0.25 to 0.55	0.25 to 0.28		0.50 to 0.85	from 2 <i>T</i> before breaking to breaking onset
Bonmarin and Ramamonjarisoa (1985, fig. 10)	0.20	0.26			after breaking
Bonmarin et al. (1989)			1.20 - 2.14	0.69 - 0.77	
Bonmarin et al. (1989)	0.38				for spillers
Bonmarin et al. (1989)	0.61				for plungers
She et al. (1994)	0.51 to 1.02			0.65 to 0.67	3D breaking, directional focusing, increasing angle
Nepf et al. (1998)	0.32 to 0.52				directional spreading, side to centre
Nepf et al. (1998)	0.56				2D breaking
Nepf et al. (1998)	0.30 to 1.02				from directional spreading to directional focusing
Wu and Nepf (2002)	0.39				for onset of 3D spilling, dir. spreading
Wu and Nepf (2002)	0.41				for onset of 3D spilling, dir. focusing
Wu and Nepf (2002)	0.38				onset of 2D spillers

2. Background and Recent Work

(temporal or spatial).

Kinematic Breaking Criteria

The kinematic criterion postulates that before the inception of breaking the horizontal fluid velocity at the surface of the wave crest u exceeds the phase speed of the wave c .

$$\frac{u}{c} \geq 1 \quad (2.1)$$

The difficulties with this breaker criterion are, on the one hand, the calculation of the phase velocity and, on the other hand, the measurement of the particle velocity in the laboratory. Linear theory overestimates the magnitude of the phase speed (Skjelbreia et al., 1991; Gudmestad, 1993), but even local phase speed definitions do not satisfy the kinematic breaking criterion, see Stansell and MacFarlane (2002). The investigation by Stansell and MacFarlane (2002) showed that the ratio of particle to phase velocity was between $0.68 \leq u/c \leq 0.95$. Experimental studies performed by Melville and Rapp (1988), Kjeldsen (1989), Perlin et al. (1996), Chang and Liu (1998) and Stansell and MacFarlane (2002) did not verify the kinematic criterion. Therefore, the condition described in Eq. (2.1) may be sufficient condition for breaking but it is not a necessary condition, and thus, the kinematic criterion is not an universal predictor of wave breaking.

Dynamic Breaking Criteria

The classic dynamic criterion describes the vertical component of surface acceleration exceeding a certain threshold, see Eq. (2.2).

$$a_{downward} \geq \alpha g \quad (2.2)$$

with α as an unknown constant and g as acceleration of gravity. The corresponding thresholds determined by different authors are given in Tab. 2.4.

2.1.2. Breaking Mechanism and Types

When discussing the physical mechanisms behind the wave breaking phenomenon, a distinction is made between whether the wave breaking is depth induced or wave induced (induced by wave-wave interaction). Depth induced wave breaking occurs when the ratio of wave height to water depth H/h comes into a critical range. This happens, for example, when waves enter from deep into shallow water; the wave height increases (shoaling), the wave becomes unstable and breaks. The breaking criterion for extreme shallow water

2.1. Wave Breaking in Intermediate and Deep Water

Table 2.4.: Compilation of threshold parameter α for the dynamic breaking criterion from literature.

Author	α	Note
Stokes (1847)	0.5	monochromatic STOKES wave
Longuet-Higgins and Fox (1977)	0.388	numerical calculations
Snyder et al. (1983)	0.5	dominant waves in the field
Longuet-Higgins (1985)	1.0	natural wave field
Ochi and Tsai (1983)	0.4	natural wave field
Liu and Babanin (2004)	0.3	natural wave field

is $H/h = 0.89$ according to Miche (1944), and $H/h = 0.78$, respectively, based on the theory of solitary waves according to McCowan (1891).

Wave-wave induced wave breaking occurs when the wave steepness exceeds a critical threshold, see section 2.1.1. In intermediate and deep water, on the one hand, superposition mechanisms such as wave-wave interaction (frequency, amplitude or directional focusing), or on the other hand instability mechanisms such as modulational instability (MI), can lead to wave breaking. The modulational instability, or BENJAMIN-FEIR instability, is an instability that only occurs to weakly non-linear wave groups in deep water, and describes amplitude modulation due to sideband instabilities. Dependent on the initial wave steepness, a wave train with active modulational instability may develop to a breaking wave or to a very large and steep, but non-breaking wave. Modulational instability do not always lead to wave breaking (Chalikov, 2007). Wave groups, and thus the temporal sequence of waves and their superposition, play an immense role in the breaking of waves in intermediate and deep water, see Banner et al. (2000, p. 3148) and Babanin et al. (2011b, p. 146). To identify if non-linear wave groups are present in a wave record, the kurtosis k can be determined. The kurtosis is the fourth-order moment of the probability density function of the surface elevation. If $k > 3$, then non-linear wave groups are present. Once the modulational instability happens, the breaking probability only depends on steepness regardless of the directional spreading (Babanin et al., 2011b, p. 154). The steepness defines whether and what kind of instability develops (Babanin et al., 2011b, p. 147).

In general, a distinction is made between five different types of wave breakers (Babanin, 2011, p. 40):

1. Spilling breaker: the wave crest destabilises and collapses, spilling the water over

2. Background and Recent Work

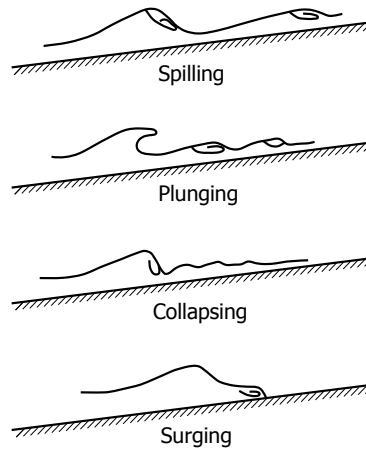


Figure 2.2.: Wave breaker types. (Source: Kraaiennest (2015))

the front slope of the wave. Small wave steepness. More frequent than plunging breakers (Babanin, 2011, p. 40).

2. Plunging breaker: the wave crest curves forward and forms a plunging jet that impacts the water surface in front of the wave and entrains air and turbulence under the surface. This leads to gas exchange across the interface, loss of energy/momentum, and produces acoustic noise, which can be used as a detection method, see section 2.1.4. Large wave steepness.
3. Collapsing breaker: a cross between plunging and surging, in which the crest never fully breaks, yet the bottom face of the wave gets steeper and collapses, resulting in foam.
4. Surging breaker: a wave with a low steepness runs up the steep beach profile, its base swash up the slope, and the wave crest disappears. There is either no breaking at all or relatively smooth with little foam or bubbles.
5. Micro-breaker: short gravity waves whose breaking intensity is too weak to warrant air entrainment visible as whitecapping. Their wavelength is less than 0.25 m and their wave frequency is greater than 2.5 Hz.

The first four types of breakers are illustrated in Fig. 2.2.

2.1.3. **Breaking Phases**

It is important to define breaking phases to avoid uncertainties and ambiguities in measurement of breaking events and rates. The breaking phases are distinguished from both the external appearance of breaking and the underlying physics involved. According to Sharkov (2007) wave breaking is noticeably shorter than the wave period T of the carrier wave. The detection method depends on the scope of a study and what kind of wave breaking is investigated. Of course, influencing factors are whether the investigation takes place in the laboratory, numerically or in the field, and which means are available. Since the functioning of the detection methods, as described in subsection 2.1.4, are based on certain definitions of wave breaking, the detection method must be adapted to the desired examination scope. The four breaking phases defined by Babanin (2011) are:

1. Incipient phase (least investigated): the incipient breaker is defined as a wave which has already reached its limiting stability, but has not yet started the irreversible breaking progress. Lasts according to Sharkov (2007) tenth of seconds and thus is difficult to measure.
2. Developing phase: breaking in progress, very rapidly, high loss of energy/wave height, highly non-linear, different mechanism than those which lead to breaking, driven by gravity and inertia of moving water mass, “but the pre- and post-breaking physics are not entirely disconnected”, see Babanin (2011, p. 15). Developing breaker exhibits an increase in wave front steepness before it subsides.
3. Subsiding / relaxing phase (least investigated): breaking in progress.
4. Residual phase: a follow-up dynamic impact of the breaking event, introduced by Rapp and Melville (1990), whitecap is already left behind, but the underwater turbulent front is still moving downstream, not detectable by wavelet or similar analytical methods based on interpretation of surface elevation, or whitecapping-oriented measurement. Rapp and Melville (1990) generated the breaking waves by superposition of linear waves. The outcome of these breakers can be different to those resulting, for example, of non-linear modulation or superposition of non-linear waves. It is not clear if residual stage is a general feature of wave breaking. Diorio et al. (2009), who has generated wave breaking with dispersive focusing, modulational instability and wind forcing, says that independent of the generation, the bulge and the capillary waves were self-similar on the crest-front face of the spillers (at breaking onset). The geometrical similarity is limited to the crest-front

2. Background and Recent Work

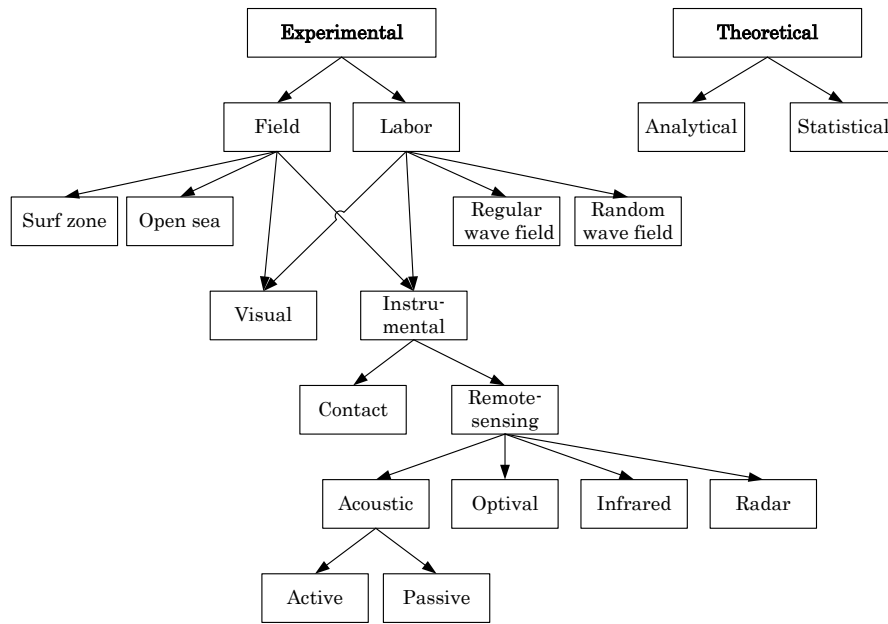


Figure 2.3.: Measurement methods for wave breaking detection.

profiles of the spillers. Thus, Diorio et al. do not disagree with Rapp and Melville (1990).

2.1.4. Breaking Detection Method

When investigating wave breaking, the main question is usually the frequency of occurrence (probability) of wave breaking and magnitude of the energy dissipation. The choice of the measuring method depends on where and what is to be measured. In Fig. 2.3, an overview of the common measurement methods concerning wave breaking is presented. All methods, apart from the statistical method, aim to measure individual events of wave breaking. The statistical method, however, combines the statistical properties of wave fields (for example, joint probability distributions of wave height and period) with breaking criteria in order to be able to make statistical statements about the probability of wave breaking. This is discussed in section 2.1.5.

The oldest method is the visual observation of a wave field and the manual counting of wave breaking events; usually the dominant breakers are counted, which break with whitecapping. Thus the phase "breaking in progress" is observed. The first major study using this method is from Holthuijsen and Herbers (1986). Holthuijsen and Her-

2.1. Wave Breaking in Intermediate and Deep Water

bers (1986) observed the wave breaking at/under a buoy in their field measurement and marked the time of the wave breaking with the aid of a trigger signal. Thus, in post-processing, the corresponding individual wave could be linked to the wave breaker event. Holthuijsen and Herbers (1986) showed that the wave steepness is not a good parameter to distinguish breaking and non-breaking waves, and therefore is not a reliable breaking criterion. Banner et al. (2000) agreed that wave steepness is not a well-founded breaking criterion because it shows a range of values at the onset of breaking. However, Banner et al. (2000) said that the front rear steepness is a functional criterion. In contrast to that, Babanin et al. (2007) stated that wave steepness seemed to be the single robust criteria for breaking.

An extension of the visual observation method is the use of high-resolution video recordings and corresponding image recognition software. Although the visual method is basically reliable and non-invasive, the disadvantages are that it is very time-consuming in post-processing and is subject to human errors. In addition, it can only be measured whether or not a wave breaks; further information such as the geometry of the breaking wave is missing (except there was a buoy or wave gauge at the location of breaking). The use of video recording and image recognition software is very complex and has not yet been developed far enough to be a robust, universally applicable measuring method. Besides, the video evaluations are very sensitive to the local conditions such as light and the permeability of the water.

In addition to visual observation, there are other remote-sensing methods, such as radar or infrared measurements of the water surface, where the wave breaking is associated with a discontinuity or a particular phenomenon in the measured time series and is thus detected. For example, sea spikes are measured in the backscatter signal of radar measurements when wave breaking (whitecapping) occurs. Investigations using this method have been described, for example, by Kwok and Lake (1984).

Another remote-sensing method is the acoustic method, which is either passive (hydrophone) or active (sonar). In the active acoustic method, for example, acoustic Doppler velocimeters (ADV) or acoustic Doppler current profilers (ADCP) are used to measure the velocity field under a wave field; in combination with the kinematic breaking criterion and an empirical threshold wave breaking can be detected. The acoustic method can, however, also be used to measure the sound of the wave breaking or the air bubbles in the water; in combination with a critical threshold, the frequency of occurrence of wave breaking can be measured, see, for example, Ding and Farmer (1994) and Manasseh et al. (2006). The advantage of this method is that the measuring instruments such as hydrophones are relatively cheap, robust and easy to maintain. The disadvantage, however,

2. Background and Recent Work

is that wave breaking in the field occurs multiscale and the differentiation between the different noises is difficult. Investigations using a combination of the acoustic and radar backscatter method have been described, for example, by Melville et al. (1992).

In addition to the remote-sensing methods, there are the contact measurement methods, in which either physical (geometry, kinematics, dynamics) or rarer chemical properties of the wave field are directly measured. It is searched either for discontinuities or for physical limits in the measured time series to detect wave breaking. The best known measuring instruments are buoys in the field, wave gauges in the laboratory, and velocimeters or acceleration sensors. The advantages of this method are that the use of the measuring instruments is tested and the characteristics of the wave are directly measured. The disadvantages of the method are that it is invasive, pointwise and it requires a breaker criterion with a corresponding critical threshold. In this thesis the contact measurement method with wave gauges was used and is described in section 6.1 in more detail.

In addition to the experimental methods described so far, there are also the analytical methods, which, like the statistical methods, fall under the theoretical methods. They are, strictly speaking, not pure theoretical methods, since the analytical methods depend on empirical criteria and are thus semi-empirical. Since a wave breaking event is non-linear, highly non-stationary and sporadic, the analytic methods aim to find such discontinuities or their derivatives in time series. Such a time series can consist of water surface, speed, acceleration or underwater acoustics measurements. An overview of non-stationary analytical methods is provided by Huang et al. (1998). Often used are the wavelet method (in combination with the dynamic breaking criterion), see Liu and Babanin (2004), and the HILBERT transformation or the phase-time method, respectively, see Zimmermann and Seymour (2002). The HILBERT transformation is a method that can analyse mathematical functions when they are single-valued, see Huang et al. (1999). In the breaking onset, however, the water surface can become vertical and thus no longer single-valued. At the same time, a wave gauge measures only single-valued functions, and air gaps can lead to measurement errors. Thus, the combination of wave gauge measurement and HILBERT transformation contains error sources, which must be taken into account when interpreting the results. Nonetheless, the HILBERT transformation and the phase-time method are valuable instruments for the detection of wave breaking in time series, and a sensible combination of critical parameters enables a robust detection method. See chapter 2.2 for more information.

When investigating wave breaking or wave breaking onset, the desired objective must be clear to choose a suitable measuring and detection method. A detection method

will not be universally applicable in all cases, especially in a natural wave field that is multiscale. A clear target definition, for example, dominant wave breaking in irregular waves, is necessary.

2.1.5. Breaking Probability

There are two general concepts to approach wave breaking probability:

- the breaking probability P_{br} is determined for a fixed point, and is the percentage of breaking crests n_{br} within a sequence of n_{tot} wave crests according to Babanin (2011)
- the breaking probability P_{br} is the fraction of the area of the sea surface over which wave breaking occur for a fixed point in time according to Snyder and Kennedy (1983)

In the first approach, the breaking probability P_{br} is:

$$P_{br} = \frac{n_{br}}{n_{tot}} = \frac{n_{br}T_D}{T_R} \quad (2.3)$$

where $T_R = n_{tot}T_D$ is the duration of the wave record and T_D is the main temporal scale of the wave field. However, because wind-generated waves have a continuous spectrum, the methods to determine T_D and n_{tot} have to be stated very clearly. To define T_D , a spectral bandwidth $f \pm \Delta f$ has to be specified. In Banner et al. (2000) and Babanin et al. (2001) the spectral bandwidth was $\Delta f = \pm 0.30f_p$, which was later reassigned as $\Delta f = \pm 0.35f_p$ by Manasseh et al. (2006). The physical meaning for the spectral band in the breaking probability definition of dominant waves is, that the width of the spectral peak defines the characteristics of the groups of dominant waves, and the wave breaking probability depends on these wave groups. Next to T_D , the total number of wave crests in a sequence n_{tot} has to be defined clearly as well. For each determined breaker the frequency f (period T) of the wave is extracted, for example, by zero-crossing analysis. Thus, the total number of breaking waves $n_{br}(f)$ is found for each frequency. The total number of expected waves at a frequency is according to Babanin et al. (2011a):

$$n_{tot}(f) = T_R/T = T_R f \quad (2.4)$$

$n_{tot}(f)$ is a nominal reference count, and there will be no match between $n_{tot}(f)$ and the actual counted number of wave crests in each frequency bin $n_{tot,c}(f)$. The resulting

2. Background and Recent Work

count $n_{tot,c}(f)$ would be less than the nominal reference count $n_{tot}(f)$, because in real seas waves of periods other than $1/f$ will occupy some part of the duration T_R .

For the second approach, Snyder and Kennedy (1983) measured a certain area of the sea surface by camera and wave array measurements. They introduced a breaking variable which is set equal to 1 inside a whitecap and 0 outside. Their breaking probability is the percentage of sea surface covered by breaking waves (whitecaps).

In general, the different statistical approaches to the evaluation of breaking probability, theoretical as well as experimental studies, can be organized into four models. All of these model combine a property of the wave field with a breaking criterion (limiting steepness, orbital velocity or downward acceleration, or their derivatives).

Model 1 Gaussian Distribution and STOKES' Limit

The Gaussian/normal distribution of surface elevation is used to predict the appearance of wave heights exceeding the limiting steepness of the STOKES wave, or its limiting orbital velocity, or its limiting acceleration at the crest. It is an analytical model proposed by Longuet-Higgins (1969) and further developed by Yuan et al. (1986), Hua and Yuan (1992) and Yuan et al. (2008, 2009).

Model 2 Probability Function and Empirical (Local) Breaking Criterion

The probability density function of some property of the wave system is combined with an empirical, rather than theoretical, breaking criterion. Since wave measurements are most often time series of surface elevations, mostly the joint probability distribution of wave height H and wave period T is used. As an empirical breaking criterion, e.g. the local wave steepness or the local downward wave crest acceleration is used. Studies that used this model are e.g. Nath and Ramsey (1976), Longuet-Higgins (1983), Ochi and Tsai (1983), Huang et al. (1984), Hwang et al. (1989), Dawson et al. (1993), Song et al. (1997) and Zheng and Xu (2004).

Model 3 Spectral Density and Global Breaking Criterion

The spectral density of the sea state is connected with a global breaking criterion, e.g. the global wave steepness or the global downward wave crest acceleration. The most important study in this model class are the field measurements and analytical considerations conducted by Snyder and Kennedy (1983), Kennedy and Snyder (1983), and Snyder et al. (1983).

Model 4 Wave Groups

Wave groups and wave breaking are linked together, and the breaking probability is concluded from the wave group statistics / occurrence. The most important studies in this model class are by Donelan et al. (1972), Holthuijsen and Herbers (1986), Babanin and Polnikov (1995), Babanin et al. (2007), and Tian et al. (2010).

2.2. Wave Breaking Onset

This section summarises the most important studies on breaking onset, in which analytical methods were applied.

2.2.1. Definition of Wave Breaking Onset

Breaking onset is defined as an instantaneous state of wave dynamics where a wave has already reached its limiting stability state, but has not yet started the irreversible breaking process. That is, breaking onset is the ultimate point where the wave has not started to break but cannot return to a stable state either. Breaking onset is the first phase, thus the incipient phase, of the breaking process, see 2.1.3. The location of the wave breaking onset is the peak of the wave crest.

2.2.2. Studies on Wave Breaking Onset

State-of-the-art is that the initial wave steepness (for monochromatic or quasi-monochromatic wave trains), see Babanin et al. (2010), or the spectral peak steepness (for natural wave fields), see Banner et al. (2000), or the dimensionless growth rate parameter (rate of change of local wave steepness), see Song and Banner (2002), controls the breaking onset (and thus indirectly the probability of wave breaking). The use of the kinematic and dynamic criterion do not come into effect; presumably the accurate determination of the velocity field or acceleration field is too complicated. Babanin et al. (2007) stated that the wave steepness seemed to be the single robust criteria for breaking; they then further explained that “a criteria of breaking may be indicative of a wave approaching an instable state, but is not a reason or a cause for the breaking”. In contrast, Phillips (1985) and Bonmarin and Ramamonjiarisoa (1985), among others, stated that a single local wave parameter was not a robust indicator for breaking onset, but instead the time history of the water surface elevation had to be analysed. However, the vast majority of previous studies (regarding breaking onset) is based on the investigation of quasi-monochromatic wave groups, not on irregular wave trains (sea spectra).

2. Background and Recent Work

Rapp and Melville (1990) investigated deep water wave breaking generated by dispersive focusing and introduced the non-dimensional wave amplitude ak_c with $a = a_n N$ as the amplitudes of each wave, N as the number of components of the wave packet and k_c as the central wave number, which were calculated with the central frequency $f_c = 0.5(f_N + f_1)$ and the dispersion relation for intermediate water depths. For wave groups with constant steepness the global wave steepness is $S = \sum k_n a_n$, see Drazen et al. (2008). Tian et al. (2010) introduced the spectrally weighted wave number k_s , which is calculated with the spectrally weighted wave frequency f_s , see Eq. (2.5), and defined the global wave steepness as $S = k_s \sum a_n$. They also introduced the local wave steepness S_b , prior to wave breaking, with $S_b = k_b \sum a_n$.

$$f_s = \frac{\sum (f_n a_n^2) (\Delta f)_n}{\sum (a_n^2) (\Delta f)_n} \quad (2.5)$$

A more sophisticated parameter, proposed by Banner and Tian (1998) and further developed by Song and Banner (2002), is the dimensionless growth rate

$$\delta(t) = \frac{1}{\omega_c} \frac{D\langle\mu(t)\rangle}{Dt}$$

with ω_c as the centre angular wave frequency, $\langle\mu(t)\rangle$ as the mean of the upper and lower envelopes of $\mu(t) = [E_{max}/\rho g] k^2$, and E_{max} as the local wave energy density at the maximum surface displacement

$$E(x, t) = \int_{-h}^{\eta} \frac{1}{2} \rho_w (u^2 + v^2) dy + \frac{1}{2} \rho_w g \eta^2$$

Song and Banner (2002) calculated the local wave number k from the x derivative of the unfolded phase function computed from the HILBERT transform of the water surface elevation. They applied a low-pass filter to smoothen the development of the local wave number. With a threshold value of $\delta(t) = (1.4 \pm 0.1) * 10^{-3}$, the criterion was shown to successfully differentiate wave groups that would eventually break from those that would not, see Tian et al. (2008). Tian et al. (2010) used the characteristic wave frequency ($\omega_s = 2\pi f_s$) instead of ω_c to reduce data scatter and calculate the growth rate at breaking onset δ_{br} . The correlation between the local wave steepness S_b , prior to wave breaking, and the growth rate at breaking onset δ_{br} based on $\mu(t) = S_b^2$ was approximated by

$$\delta_{br} = 8.77 * 10^{-3} S_b^2 \frac{\omega_b}{\omega_s}$$

with $\omega_b = 2\pi f_b$. Furthermore, Tian et al. (2010) found out that the global wave steepness threshold S_0 , which indicated incipient wave breaking, varied between $S_0 = 0.31 - 0.35$. When considering the case that no wave breaking occurred, S_0 was approximately 0.339. Based on the correlation $S_b = 1.237S$, the maximum local wave steepness for incipient wave breaking was roughly $(S_b)_0 = 0.419$, which is $s_Z = H/L = 0.13$ and thus smaller than the maximum steepness of a deep water STOKES' waves with $s_Z = 0.14$, compare also Tab. 2.2. However, the application of the dimensionless growth rate $\delta(t)$ in phase-resolving, deterministic prediction of the evolution of non-linear wave fields may be limited, as the calculation of the diagnostic parameter is non-trivial and it is not possible to determine this parameter from routinely available wave data (Banner et al., 2000, p. 3152).

The author's own approach to link the envelope of the water surface elevation and the wavelength is explained and discussed in subsection 6.1.3.1.

Banner et al. (2000) investigated the breaking probability of dominant waves in the field (Lake Washington, Black Sea, Southern Ocean). They introduced the significant wave steepness with $H_S k_P / 2$. Because of the shorter and higher frequency components in $H_S = 4\sqrt{m_0}$, they also introduced the significant spectral peak steepness ϵ , see Eq. (2.6).

$$\epsilon = \frac{H_P k_P}{2} \tag{2.6}$$

where

$$H_P = 4 \left\{ \int_{0.7f_P}^{1.3f_P} S(f) df \right\}^{1/2}$$

In this thesis, the initial wave steepness $s_{Z,i} = H_S / L_P$ is introduced with $L_P = g / (2\pi) T_P^2$, and the relation to Banner et al.'s significant wave steepness is $H_S k_P / 2 = s_{Z,i} * \pi$. Banner et al. observed that the spectral peak steepness needs to be $\epsilon \gtrsim 0.05 - 0.06$ ($s_{Z,i} \gtrsim 0.016 - 0.019$) for dominant wave breaking to exist.

Babanin et al. (2007, 2010) carried out a pilot study in which they investigated the properties of breaking waves and the processes responsible for breaking onset in two-

2. Background and Recent Work

dimensional initially monochromatic waves. Focus was on the processes leading to breaking, and not on the process of wave collapse itself. They conducted numerical simulations with the fully non-linear CHALIKOV-SHEININ model, see Chalikov (2005), and carried out physical experiments to validate the numerical simulations. The wave trains broke due to modulational instability. Their main finding was, see Babanin (2011): “The nearly-breaking wave is the highest and most skewed, but is almost symmetric. The two waves immediately preceding and following the breaker are asymmetric: the preceding wave is tilted backward (positive asymmetry) and the following wave is tilted forward (negative asymmetry). The preceding wave is smaller than the following wave, and, at least in these observations, the preceding trough is shallower. This may be a key feature to distinguish the linear-focusing breaking onset from the modulational-instability breaking, as the former is not expected to exhibit uneven front and rear troughs.”

Furthermore, Babanin et al. (2007) observed that for their numerical model tests the wave trains broke within one wavelength and with an initial wave steepness of $(ak)_0 \geq 0.3$; no breaking occurred for the wave trains with $(ak)_0 < 0.1$. For their physical model tests the wave trains always broke with an initial wave steepness of $(ak)_0 \geq 0.44$ and no breaking occurred for wave trains with $(ak)_0 < 0.08$. Dold and Peregrine (1986) observed in their numerical model tests with monochromatic wave trains similar threshold values ($(ak)_0 \geq 0.1$, $H/L \geq 0.03$) for which wave trains developed to breaking. Babanin et al. further deduced an relationship between the dimensionless distance to breaking x_{br}/L and the initial wave steepness $(ak)_0$, see Eq. (2.7)¹.

$$\frac{x_{br}}{L} = -11 \operatorname{atanh} [5.5 ((ak)_0 - 0.26)] + 23 \text{ for } 0.08 \leq (ak)_0 \leq 0.44 \quad (2.7)$$

Babanin et al. (2007) stated that the dimensionless distance to breaking x_{br}/L was related to the probability of wave breaking b_T with $x_{br}/L = 1/b_T$. They concluded based on the Black Sea data set of Babanin et al. (2001) the following relationship between the initial spectral steepness ϵ and the probability of breaking, see Eq. (2.8). Their values for x_{br}/L ranged from $17 \leq x_{br}/L \leq 21$.

$$\frac{1}{b_T} = -10 \operatorname{atanh} [13.3 (\epsilon - 0.13) + 17] \text{ for } 0.055 \leq \epsilon \leq 0.205 \quad (2.8)$$

Babanin (2011) and Babanin et al. (2011b) were concerned with the breaking of waves

¹The original equation as found in the publication had the term “+23” inside of the brackets, which is false, else the equation does not produce the graph described in the quoted publication.

in three-dimensional wave fields. Their laboratory model tests showed that modulational instability is still active in three-dimensional wave fields and is the most likely cause for wave breaking in the oceanic wave fields.

The part of the research, which is concerned with wave trains (or fields) based on sea spectra, i.e. irregular waves, consists of the studies of Dawson et al. (1991), Kriebel and Dawson (1991), Dawson et al. (1993) and Kriebel (2000) who studied the two-dimensional BRETSCHNEIDER and JONSWAP wave trains with breaking waves in the laboratory and compared the results with a self-developed theoretical approach to estimate the breaking probability. The theoretical approach was based on the RAYLEIGH distribution and the distribution function of non-linear amplitudes (modulated STOKES wave). In their work, Dawson et al. did not investigate the evolution of the descriptive wave parameters towards breaking onset, but quantified the wave breaking probability. They introduced the characteristic measure of the wave steepness R_p , see Eq. (2.9).

$$R_p = \frac{\omega_P^2 H_S}{g} \quad (2.9)$$

with the peak angular frequency ω_P . The relation to the initial wave steepness introduced in this thesis here is $s_{Z,i} = R_p/(2\pi)$. The special feature of their work was that they studied the wave breaking probability for both a fixed point and a region, and also measured and analytically predicted the time between two breaking events. Due to the simplifications in its theoretical approach, the study showed weaknesses, e.g. the wave breaking probability was only so well predicted, because the approach overestimated and underestimated wave breaking. Nonetheless, the study by Dawson et al. is a good basis for the author's own work here.

Similar to Dawson et al., Song et al. (1997) also developed a theoretical approach for the wave breaking probability in JONSWAP sea states, based on the wave breaking criterion of Ochi and Tsai (1983) and the two-dimensional probability distribution of Fu (1987).

Nath and Ramsey (1976) developed a theoretical approach to the probability of wave breaking based on the geometrical wave breaking criterion (wave steepness), the assumption that the wave height and wave period are independent of each other, and field data. The assumption that the wave height and the wave period are independent of one another is, of course, a highly simplified assumption.

Zimmermann and Seymour (2002), beside Dawson et al. (1993), were the only ones who generated two-dimensional JONSWAP wave trains in the laboratory and focused on the detection of wave breaking. With the help of the phase-time method, Zimmer-

2. Background and Recent Work

mann and Seymour worked out two parameters with critical thresholds which determined wave breaking in a time series, namely the water surface elevation ($\eta(t) \geq 0.38H_S$) and the instantaneous frequency ($f(t) \geq 0.8f_p$). Their results are opposed to the results of Griffin et al. (1996), but Griffin et al. (1996) investigated wave breaking due to dispersive focusing. This observation indicates that the breaking criteria depends on the physical mechanism which leads to breaking, see Chalikov and Babanin (2012). Babanin et al. (2007) says, however, that “if a critical wave steepness is reached, the wave will break, independent of the physical reason for the critical wave steepness.” Moreover, Zimmermann and Seymour applied these thresholds to field measurements, but had no visual confirmation as to whether there were breaking waves in the measured time series, so only a subjective assessment of the authors was possible, whether the results are realistic or not. Another finding regarding the use of wave buoys in the field was that buoys following the waves avoid the steepest wave. Thus, the possibility of detecting wave breaks in time series from field measurements is restricted.

The thresholds by Zimmermann and Seymour (2002) and Babanin et al. (2007, 2010) to detect wave breaking in a time series of water surface elevation is compared with the results of the thesis in subsection 6.1.3.1.

2.3. Statistical Variability of Wave Breaking

To the author’s knowledge, there are no studies in literature solely about the variability of wave breaking parameters, breaking onset, or breaking probability. Studies about the deformation of the wave train before breaking onset often only present one exemplary wave train. However, Kjeldsen and Myrhaug (1979a) stated that the crest front steepness $\epsilon = s'_C = a_C/L'$ varied between $s'_C = 0.32 - 0.78$ and the crest rear steepness $\delta = s''_C = a_C/L''$ varied between $s''_C = 0.26 - 0.39$ in their experiments. Furthermore, Babanin et al. (2007) stated that the wave steepness $Hk/2 = s_Z\pi$ varied between $Hk/2 = 0.37 - 0.44$ ($s_Z = 0.12 - 0.14$), the skewness $S_K = a_C/a_T - 1$ varied between $S_K = 0 - 1$, and the asymmetry $A_S = L''/L' - 1$ varied between $A_S = -0.4 - 0.8$ in their experiments. A more detailed analysis, e.g. about the distribution of those parameters or the time and location of breaking onset were not given.

There are only very few qualitative mentions about the required record length to determine the wave breaking probability in a robust manner, for example by Babanin et al. (2011a), who wrote: “Measurements of b_T [wave breaking probability] require averaging over a large number of wave groups since the breaking process is characterised by long-period intermittences [...]” Exact numbers or at least estimations are not available.

2.3. Statistical Variability of Wave Breaking

The only source which was a little bit more in-depth was Banner et al. (2000, p. 3156), who gave a short note about the observed long-term variability of wave breaking probability: “An interesting result on the sensitivity of the correlation to the averaging time was found during our analysis of the Black Sea data. While 20-min records are usually regarded as sufficient for determining wave spectra, the number of wave groups required to provide stable breaking probabilities is found to be longer. The result of splitting several of the 40-min records into two 20-min records produced significantly more scatter in the dependence of b_T on ϵ [significant spectral peak steepness $\epsilon = Hpk_P/2$, see Eq. (2.6)]. [...] Our limited duration data records and the relatively infrequent onset of dominant wave breaking did not allow us to further identify the source of this variability and future studies involving longer data records are clearly needed.” The presumption of the author of this thesis is that wave breaking does not occur evenly in a wave train, therefore wave breaking probability varies for different study areas and investigation periods.

3. Hydronumerical Model Tests

The hydronumerical experiments were carried out with the numerical wave flume (NWF) developed and verified by Sriram (2008) and Sriram et al. (2006; 2007; 2010). The NWF is based on the fully non-linear potential flow theory (semi-arbitrary Lagrangian-Eulerian Finite Element Method (SALE-FEM, structured version)) and has been applied to study, for instance:

- numerical and physical speed of non-linear waves
- rogue/freak waves
- sloshing

Due to potential flow theory the NWF simulations are terminated when the water surface becomes discontinuous. However, this limitation is not detrimental because focus was set on the wave train evolution until breaking onset. The discontinuity in the NWF may be of numerical or physical nature. A form of numerical instability happens, when waves get steeper, node crossing will take place, leading to negative elements in the free surface, as the free surface nodes are moved in Lagrangian fashion. To sort out the test runs with numerical discontinuities, solely the test runs were considered here which contained wave trains where the waves with the maximum wave crest and the maximum wave steepness were less than two single waves apart. Wave trains were divided into single waves by the zero-downcrossing method. The point of termination of simulation was characterized by the two parameters: time to breaking onset t_{br} (temporal distance from simulation start to end) and location of breaking onset x_{br} (spatial distance from inlet to breaking wave crest).

The main advantages of the application of hydronumerical simulations with a numerical wave flume were the speed of carrying out the simulations and the spatial measurement of the entire water surface elevation per time step. However, it has to be considered that the measurement was only quasi-spatial, since the wave flume was spanned by means of nodes. Thus, a hydronumerical simulation with the numerical wave flume was a quasi-pointwise measurement. The number of nodes and the spatial distance between the nodes

3. Hydronumerical Model Tests

had an influence on the result. The instability of the water surface could only occur there and thus could only be measured where a node existed. If the spatial distance between the nodes was changed with the input signal remaining constant, the time and location of instability varied.

In the following chapter the test setup, program and procedure of the hydronumerical simulations are presented. Then, the post-processing of the output data is described. Finally, the validation, limitations, and uncertainties of the hydronumerical model are investigated.

3.1. Test Setup

Tab. 3.1 summarises the relevant parameters describing the NWF settings. As described in Sriram (2008, p. 70ff), the number of nodes in horizontal direction must be at least 30 nodes per wavelength for simulation of medium steep waves ($s_Z \geq 0.03$) and at least 60 nodes per wavelength for steep waves ($s_Z \geq 0.05$). These minimum requirements were taken into account in this thesis, and nx varied between $51 < nx < 68$ per wavelength depending on the wave period, whereby the distance between nodes was constantly $dx = L_{flume}/nx = 0.0833$ m. As mentioned above, the result may vary if the spatial distance between the nodes is changed with the input signal remaining constant, for more details see subsection 3.3.2. According to Sriram (2008, p. 70ff), the recommended number of nodes in vertical direction is $nz = 13$, independent of water depth. For the thesis, a constant value of $nz = 28$ was chosen (recommended by Prof. A. Hildebrandt in personal communication). With a high number of nodes per wavelength, collisions of nodes may occur and therefore the mesh must be regridded after a certain number of time steps; the recommended step size is 40 s, see Sriram (2008, p. 70ff).

Based on the smallest selected wave period of $T_P = 1.42$ s the time step of simulation was chosen $\Delta t_{NWT} = 0.02$ s for all test runs. The maximum duration of simulation t_{simul} corresponds to the time length of the input wave train, $t_{simul} = DWT = N_W * T_P$; the test runs with small initial spectral steepness $s_{Z,i}$ showed that this maximum duration of simulation was sufficient and the simulations aborted before due to discontinuities. It is shown later that only a very small fraction of simulations passed through t_{simul} . The flume length was $L_{flume} = 50$ m by default, as the physical tests showed that the wave trains break beforehand; however, selected experiments were also repeated with $L_{flume} = 100$ m. For more details about the influence of the flume length on the result see subsection 3.3.2.

Table 3.1.: Parameters for the setting of the numerical wave flume.

Symbol	Description	Unit
L_{flume}	Flume lengths	m
nx	Number of nodes in x-axis direction (along L_{flume})	
nz	Number of nodes in z-axis direction (along flume height)	
dx	Distance between nodes in x-axis direction	m
Δt_{NWF}	Time step of simulation, $\Delta t_{NWF} \leq \frac{T}{60}$	s
t_{simul}	Maximum duration of simulation	s

3.2. Test Program and Procedure

In hydraulic model investigations free-surface flows, which in principle also involve the wave motion, are modelled according to the prevailing gravitational and inertial forces according to FROUDE's law of similarity. This law requires equal FROUDE numbers for flow processes in the model (index m) and in nature (index n):

$$F_r = \frac{c}{\sqrt{gL}}$$

with wave velocity c , wavelength L and acceleration of gravity g . The length scale λ is:

$$\lambda = \frac{l_n}{l_m}$$

The time scale τ is:

$$\tau = \frac{t_n}{t_m} = \sqrt{\lambda}$$

The velocity scale c_r is:

$$c_r = \frac{c_n}{c_m} = \sqrt{\lambda}$$

Both the numerical and physical model tests, see section 6.1, were carried out in the length scale $\lambda = 40$. The length scale was obtained from the research platform FINO1 in the North Sea with a water depth of approximately 30 m (in the model 0.75 m) and the boundary conditions of the WKS wave flume with maximum possible water depth

3. Hydronumerical Model Tests

1.20 m and a maximum wave height of 0.40 m. The length scale was selected as small as possible to be as close to nature as possible, but as large as necessary so that water depth and wave height could be generated in the wave flume. The dimensions given in this thesis are to be interpreted as model values, if not specifically pointed out otherwise.

Fig. 3.1 shows the basic work flow of the data generation. Since the measurements of the research platform FINO1 in the North Sea were used as a design basis, the JONSWAP spectrum was the chosen input sea spectrum. The input JONSWAP spectrum was transformed from its frequency domain to time domain, resulting into the input wave signal $\eta_r(t)$ for the numerical wave flume. Each input spectrum $S(f)$ was transformed r -times to time domain to vary the phase angle distribution φ_r and thereby investigate the influence of the wave sequence in the wave train on breaking onset. In case the simulation terminated due to a instability, the output data were on the one hand the location and time of breaking onset (x_{br}, t_{br}) , and on the other hand the wave trains $\eta(x, t)$ over the whole flume for each time step $\Delta t=0.02$ s. The time of breaking onset t_{br} was the time span from simulation start to the last simulated time step t_{end} , and the location of breaking onset x_{br} was the spatial distance from inlet to the peak of the breaking wave crest. Special focus was given to the breaking wave and its deformation within the last 2 s before breaking onset, resulting into the waves $\eta_1(x, t_{br}), \dots, \eta_{50}(x, t_{br} - 2 \text{ s})$ with a time step of $\Delta t=0.04$ s. Further on, special focus was given to the wave train at the location of breaking onset over time $\eta(x_{br}, t)$ to analyse what happened at the location of breaking onset within the last ten waves before breaking onset. To describe and analyse the output, the geometrical and instantaneous parameters were determined for the breaking wave $\eta_1(x, t_{br}), \dots, \eta_{50}(x, t_{br} - 2 \text{ s})$ and the last ten waves of the wave train at breaking onset $\eta(x_{br}, t)$. The parameters are explained in more detail in subsection 3.2.2.

In Fig. 3.2 the main steps of the test procedure are shown, divided into "Data Generation", "Simulation" and "Post-Processing". The steps are explained in more detail below. As mentioned in the figure, the test runs were sorted out by introducing a permissible threshold, which was based on the physically possible maximum values of the geometrical parameters, as measured so far in laboratory tests from other authors, see Tab.3.2. This step was necessary to filter "spurious" waves which came about because the single waves in the wave trains were determined by the zero-downcrossing method. The zero-crossings were recognized as such when the minimum excursion of the surface elevation at at-rest water level was greater than $0.001 * a_{C,max}$. It happened, however, that even small oscillations around the rest water level were recognized as single waves. These "single waves" led to outliers for the geometrical parameters of the wave crest at

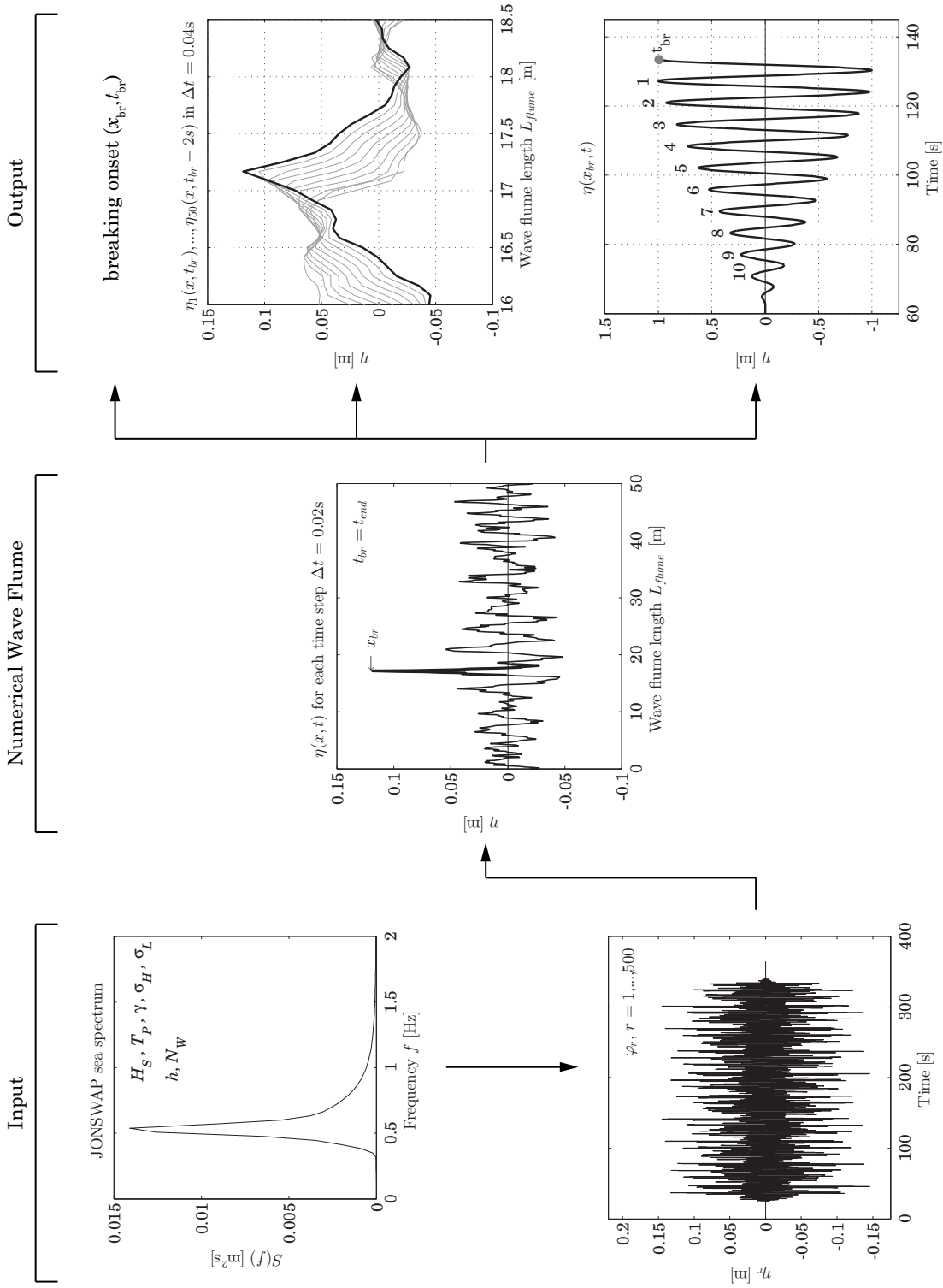


Figure 3.1.: Work flow of data generation and data analysis. The resulting geometrical and instantaneous parameters of the single waves are listed in Tab. 3.4.

3. Hydronumerical Model Tests

Table 3.2.: Limit values for geometrical parameters in post-processing of NWF output data.

Symbol	Limit value	Based on
$s_Z = H/L$	$s_{Z,lim} = 10 * 0.18$	Toffoli et al. (2010)
$s_{ZC} = a_C/L$	$s_{ZC,lim} = 10 * 0.10$	Bonmarin and Ramamonjariosa (1985)
$s_{ZT} = a_T/L$	$s_{ZT,lim} = 10 * 0.018$	Bonmarin and Ramamonjariosa (1985)
$s'_C = a_C/L'$	$s'_{C,lim} = 10 * 0.78$	Kjeldsen and Myrhaug (1979b)
$s''_C = a_C/L''$	$s''_{C,lim} = 10 * 0.39$	Kjeldsen and Myrhaug (1979b)
$\mu_H = a_C/H$	$\mu_H = 10 * 0.95$	Kjeldsen and Myrhaug (1979b)

breaking onset, and they needed to be filtered out.

The generation of the input spectrum and input wave signal is explained in more detail in subsection 3.2.1. The post-processing and data analysis is explained in more detail in subsection 3.2.2. An overview where which output parameter is analysed in this thesis is given in Tab. 3.5, see subsection 3.2.2.

3.2.1. Generation of the Input Spectrum and Wave Train

As design database the wave measurements of research platform FINO1 in the North Sea were used (Neumann et al., 2003), and a scatter diagram for the time period 2004 - 2011 was derived. The significant wave height H_S and wave peak period T_P for the JONSWAP spectra were selected in such a way that daily and storm events were considered, and the initial spectral steepness $s_{Z,i} = H_S/L_P$ with $L_P = g/(2\pi)T_P^2$ varied between $0.01 \leq s_{Z,i} \leq 0.071$. In total, 49 different sea spectra were chosen and, by means of the random phase angle distribution, were transformed multiple times (up to 500 times) to artificial, but physically-sound time series of water surface elevations. The whole test program with all 49 JONSWAP sea spectra is given in Tab. A.1 in the annex.

The significant wave height varied between $0.038 \text{ m} \leq H_S \leq 0.30 \text{ m}$ and $0.043 \text{ m} \leq H_S \leq 0.30 \text{ m}$ ($H_S = 0.043 \text{ m}, 0.083 \text{ m}, 0.15 \text{ m}, 0.2 \text{ m}, 0.225 \text{ m}, 0.25 \text{ m}, 0.30 \text{ m}$), respectively, after test runs with outliers were sorted out. The wave period varied between $1.42 \text{ s} \leq T_P \leq 1.90 \text{ s}$ and $1.65 \text{ s} \leq T_P \leq 1.9 \text{ s}$ ($T_P = 1.65 \text{ s}, 1.7 \text{ s}, 1.9 \text{ s}$), respectively, after test runs with outliers were sorted out. Further input parameters were the enhancement factor γ ($\gamma = 2, 3.3, 5, 7$), water depth h ($h = 0.5 \text{ m}, 0.6 \text{ m}, 0.7 \text{ m}, 0.8 \text{ m}, 0.9 \text{ m}$), phase angle distribution φ , and the number of waves in a wave train N_W ($N_W = 192, 768, 1536, 3072$). The enhancement width σ_L and σ_H modulate the width of the spectrum and

3.2. Test Program and Procedure

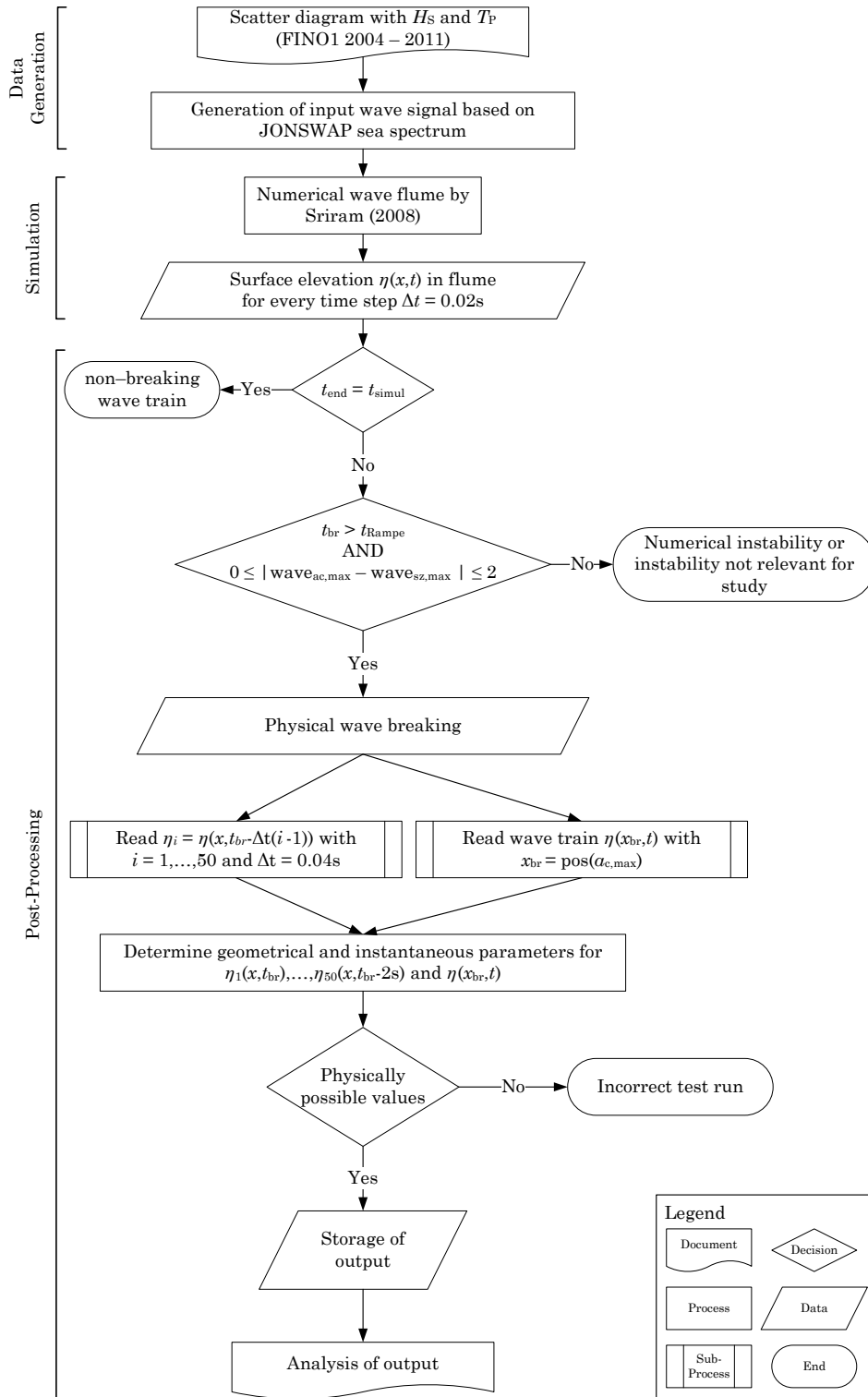


Figure 3.2.: Flowchart of the test procedure of the hydronumerical model tests.

3. Hydronumerical Model Tests

Table 3.3.: Combinations of enhancement width σ_L and σ_H used in the hydronumerical simulations.

σ_L	σ_H
0.070	0.090
0.065	0.095
0.060	0.100
0.055	0.105

were varied in such a way that the spectrum varied from narrow to wider, see Tab. 3.3. The purpose of this variation was to investigate the influence of the spectral form on the output, since Ochi and Tsai (1983) found that the shape of the spectrum (fourth moment m_4), has a large influence on the probability of wave breaking. However, the chosen variation of the parameters σ_L and σ_H were too small to detect an effect on the breaking onset.

The JONSWAP spectrum is described in Eq. (3.1).

$$S(f) = \frac{\alpha g^2 f^{-5}}{8 \arctan(1)^4} \exp \left[-\frac{5}{4} \left(\frac{f}{f_P} \right)^{-4} \right] \gamma^B \quad (3.1)$$

with

$$B = \exp \left[\frac{-(f - f_P)^2}{2\sigma^2 f_P^2} \right]$$

$$\sigma = \begin{cases} \sigma_L & \text{for } f \leq f_P \\ \sigma_H & \text{for } f > f_P \end{cases}$$

$$f_P = \frac{1}{T_P}$$

$$\alpha = 0.0081$$

When generating a spectrum, there has to be a minimal and maximal frequency con-

3.2. Test Program and Procedure

sidered; in this thesis they were $f_{min} = f_P/4$ and $f_{max} = 4 * f_P$, and Δf was a constant range dependent on the number of frequency components. The number of frequency components n_{freq} between f_{min} and f_{max} depended on the wanted N_W with $n_{freq} \leq N_W/3$. This relation was determined by realizing wave trains with different ratios of n_{freq} and N_W , and then comparing the distributions of the resulting wave heights in the wave train with the expected RAYLEIGH distribution. At the same time, care was taken to ensure that the length of the wave train on a natural scale lasted at least 30 min, which corresponds to the recommended duration for short-term statistics of sea state data. The time length of the input signal or the duration of the wave train $DWT = T_P * N_W$ was determined over the peak period and the desired number of waves in the wave train. As described in Eq. (3.1), the spectrum depends on the wave period T_P and enhancement factor γ . The code for the generation of the wave trains took the significant wave height H_S into account by a correction term, with which the once generated spectrum was multiplied, see Eq. (3.2).

$$S_{corrected}(f) = S(f) \left(\frac{H_S}{H_{m0}} \right)^2 \quad (3.2)$$

H_S is the chosen input parameter and H_{m0} is calculated with the 0th moment m_0 (area under the spectrum), see Eqs. (3.3) and (3.4).

$$H_{m0} = 4\sqrt{m_0} \quad (3.3)$$

$$m_0 = \int_{f_{min}}^{f_{max}} S(f) f^0 df \quad (3.4)$$

In the generation of the wave trains, both 1st and 2nd order of wave generation theory were considered. The code for generating the input signal converted the desired wave train into a paddle motion for the wave maker. Both signals, generated wave train and converted paddle motion, included a “fade in” and “fade out” time span to ensure that the paddle motion for the wave maker started and ended with zero displacement. The duration of the “fade in” and “fade out” time span is called t_{Ramp} and depends on the duration of the wave train with $t_{Ramp} = DWT/30$.

The paddle motion was passed along with the internal NWF settings, as described in section 3.1, to the code of the NWF. The NWF calculated the surface elevation over the entire flume for each time step until either a discontinuity occurred and the simulation

3. Hydronumerical Model Tests

was aborted or the end of the simulation duration was reached. When all test runs for an input spectrum had been performed, the output data were sorted in post-processing and processed for subsequent analysis, as described in chapter 4 to 6 in more detail.

3.2.2. Post-Processing of NWF Output Data

In the first step of post-processing, a check was carried out to determine whether the last simulated time step of the test run corresponded to the duration of the simulation or not. If so, that meant that the simulation was fully carried out and no discontinuity had occurred. In this thesis, this case was treated as a "non-breaking case"; there was no instability in the chosen duration of the simulation. It was, however, not known whether the wave train would have been unstable if the duration of the simulation had been chosen to be longer. The study showed that, even at low initial spectral steepness $s_{Z,i}$, the majority of the test runs broke before the simulation duration, and thus the simulation duration was selected to be sufficiently large. If the last simulated time step was less than the simulation duration, a discontinuity occurred during the simulation, and it had to be checked whether it was a numeric or physical instability.

For physical instability, the following conditions had to be met: a) The time of breaking onset t_{br} had to happen later than the duration of the "fade in" time span t_{Ramp} , and b) The wave with the maximum wave crest and the wave with the maximum wave steepness were at most one single wave away from each other. That condition was based on the findings from literature, e.g. Bonmarin and Ramamonjiarisoa (1985) and Babanin et al. (2007), which contributed to the detection of wave breaking in time series. 81% of the breaking test runs fulfilled the condition that the largest wave was also the steepest wave; 13% of the test runs fulfilled the condition that the largest wave was next to the steepest wave; 6% of the test runs fulfilled the condition that the largest and steepest waves were one single wave apart.

In the dimensional analysis, see section 4.2, another condition was added, namely $a_C/H_S \geq 0.9$, so as to reduce the data sample to the interesting cases of wave breaking, namely large, steepness-induced wave breaking.

After the test runs with numerical instabilities were sorted out, the time series was read out at the location of wave breaking $\eta(x_{br}, t)$; the location of wave breaking x_{br} was the spatial distance from the inlet to the maximum wave crest $a_{C,max}$. Because of the regridding of the mesh, the value for x_{br} varied slightly ($\mathcal{O}(10^{-3} - 10^{-4})$), therefore when reading out the displacement $\eta(x_{br}, t)$ for time steps smaller than t_{br} , the location closest to x_{br} was chosen. Later in chapter 6, these time series are used to develop a detection and prediction method for breaking onset.

3.2. Test Program and Procedure

Furthermore, the water surface elevation of the entire wave flume $\eta_1(x, t_{br})$ to $\eta_{50}(x, t_{br} - 2\text{s})$ were read out at a time interval of $\Delta t = 0.04\text{s}$ for the last 2.0 s before termination of the simulation, where η_1 was the water surface elevation at the last simulated time step t_{br} . The choice of $\Delta t = 0.04\text{s}$ was based on Bonmarin and Ramamonjiarisoa (1985), who chose the same time step for their experiments. The total investigation time of 2.0 s was based on the findings from literature, which states that the process of wave breaking takes a fraction of the wave period, see Sharkov (2007) and subsection 2.1.3. With a maximum peak period of $T_P = 1.9\text{s}$ the selected 2.0 s were sufficient. Later on in chapter 6.2, these results are taken to describe the deformation of the wave just before breaking onset.

In the next step, the geometrical and instantaneous parameters of the individual waves were calculated from the wave train $\eta(x, t_{br})$ and wave train $\eta(x_{br}, t)$. As summarised in Tab.3.2, the experimental maximum values for some parameters were known from literature. These were introduced as limit values and test runs with parameters that exceeded a multiple of those limit values were sorted out. Finally, the remaining test runs were saved and were ready for the subsequent analysis. In total, 15,500 simulations had been carried out. From those 15,500 simulations, 4,412 test runs did not terminate due to numerical instability, and from those again 4,329 test runs were within the limit values.

The output data considered in the analysis are

- the location and time of breaking onset (x_{br}, t_{br}) or rather their dimensionless quantities $(x_{br}/L_p, t_{br}/T_P)$
- the breaking wave and its deformation within the last 2 s before breaking onset, resulting into the waves $\eta_1(x, t_{br}), \dots, \eta_{50}(x, t_{br} - 2\text{s})$ with a time step of $\Delta t = 0.04\text{s}$
- the wave train at the location of breaking onset over time $\eta(x_{br}, t)$ and its last ten waves before breaking onset

The breaking wave and the single waves in the wave train at the location of breaking onset are described with the geometrical parameters, based on the recommended wave parameters by IAHR (1989) and Bonmarin and Ramamonjiarisoa (1985), and the instantaneous parameters computed with the HILBERT transform, see Tab.3.4. For more details on the HILBERT parameters see subsection 6.1.3.1. An overview where those output parameters were analysed in this thesis is given in Tab.3.5.

3. Hydronumerical Model Tests

Table 3.4.: Compilation of dimensionless geometrical and instantaneous parameters as used in the analysis.

Symbol	Description
a_C/H_S	dimensionless wave crest amplitude
f_0/f_P	dimensionless wave frequency
$s_Z = H/L$	wave steepness
$s_{ZC} = a_C/L$	crest steepness
$s_{ZT} = a_T/L$	trough steepness
$s'_C = a_C/L'$	crest front steepness
$s''_C = a_C/L''$	crest rear steepness
$\mu_V = L''/L'$	vertical asymmetry
$\mu_H = a_C/H$	horizontal asymmetry
$a(t)/H_S$	dimensionless instantaneous amplitude
$f(t)/f_P$	dimensionless instantaneous frequency
$s_Z(t) = 2a(t)/L(t)$	instantaneous steepness

3.3. Validation, Limitations and Uncertainties

3.3.1. Validation

The NWF code was extensively validated in Sriram (2008). Nonetheless, in this thesis, the quality of the NWF was also tested by means of physical model tests with regular and irregular wave trains. The physical model tests with irregular waves, described in detail in chapter 6, which were used for the development of the detection method, were only of limited use for the validation, since the first breaking waves occurred in the first few wavelength because the initial steepness was so high ($s_{Z,i} = 0.044$), but the first wave gauge was only located at 14.9 m in the wave flume. The wave breaking dissipated wave energy and modulated the wave train and, thus, limited a direct comparison of the hydronumerical and laboratory measurements. The physical model tests were nevertheless repeated with the NWF. In Fig. 3.3, three such tests (with different phase angle distributions) are compared with each other. Despite the modulation of the wave train by the wave breaking in the physical model tests, the correlation was sufficient.

In Fig. 3.4 the comparison for the regular wave trains ($H = 0.15$ m, $T = 1.5$ s, $s_Z = 0.043$) are shown. There was no wave breaking in the physical model tests, so the

3.3. Validation, Limitations and Uncertainties

Table 3.5.: Overview of the thesis' chapters of results and the covered output data.

Chapter	Content	Analysed output data
4.1	Development of time of breaking onset	t_{br}/T_P
4.2	Dimensional analysis	$t_{br}/T_P, x_{br}/L_p$
4.3	Likelihood of breaking onset	t_{br}
5.1	Univariate analysis	$t_{br}/T_P, x_{br}/L_p$
5.2	Bivariate analysis (copula approach)	$(t_{br}/T_P, x_{br}/L_p)$
5.3	Optimal sample size (convergence analysis)	t_{br}/T_P
6.1	Detection of breaking onset in wave trains (laboratory model tests)	Geometrical and instantaneous parameters of $\eta(x_{br}, t)$
6.2	Deformation of wave crests before breaking onset	Geometrical and instantaneous parameters of $\eta_1(x, t_{br}), \dots, \eta_{50}(x, t_{br} - 2s)$
6.3	Prediction of breaking onset (hydronumerical model tests)	Geometrical and instantaneous parameters of $\eta(x_{br}, t)$

3. Hydronumerical Model Tests

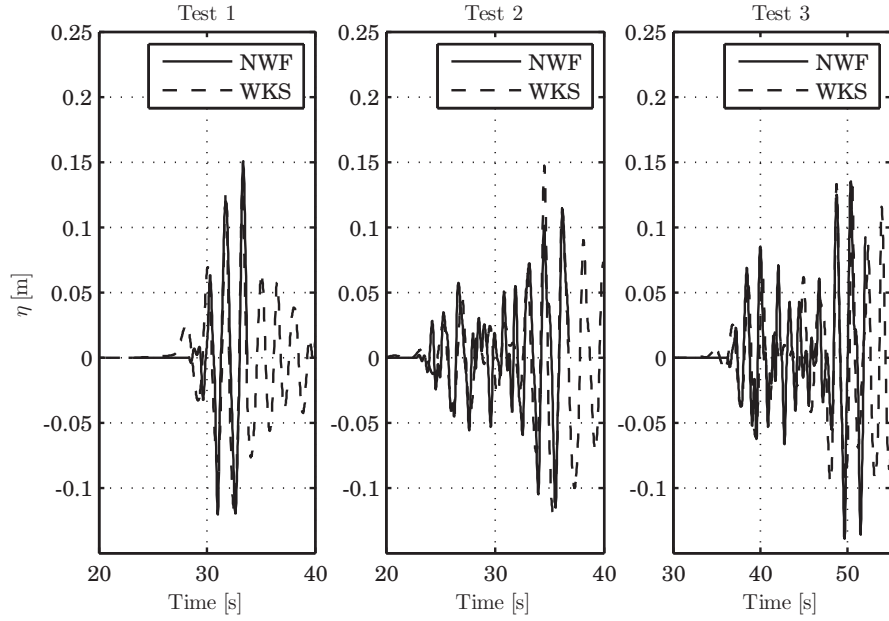


Figure 3.3.: Comparison of wave gauge WG1 ($x_{WG1} = 14.9$ m) for numerical (NWF) and physical model test (WKS). Initial wave steepness $s_{Z,i} = 0.044$.

wave train was not modulated. The correlation for WG1 was $R^2 = 0.98$ and for WG3 $R^2 = 0.99$. The correlation between experimental measurement and numerical simulation was good.

3.3.2. Limitations and Uncertainties

The model uncertainty was that due to potential flow theory simulations with the numerical wave flume were terminated when the water surface became discontinuous. Again, this limitation was not detrimental because the focus of this thesis was set on the wave train evolution until breaking onset. There were two parameter uncertainties that were investigated in more detail: the influence of the distance of nodes dx and the influence of the wave flume length L_{flume} on the results.

The analysis showed that the choice of dx had an impact on the output results. This was understandable, if one imagines that the equations were solved at the nodes; if there was no node at the location of a possible instability, it could not be found. In the thesis, care was taken to ensure that the experiments were carried out with a constant distance dx in order to ensure the comparability of the results.

The second parameter uncertainty was the influence of the wave flume length L_{flume}

3.3. Validation, Limitations and Uncertainties

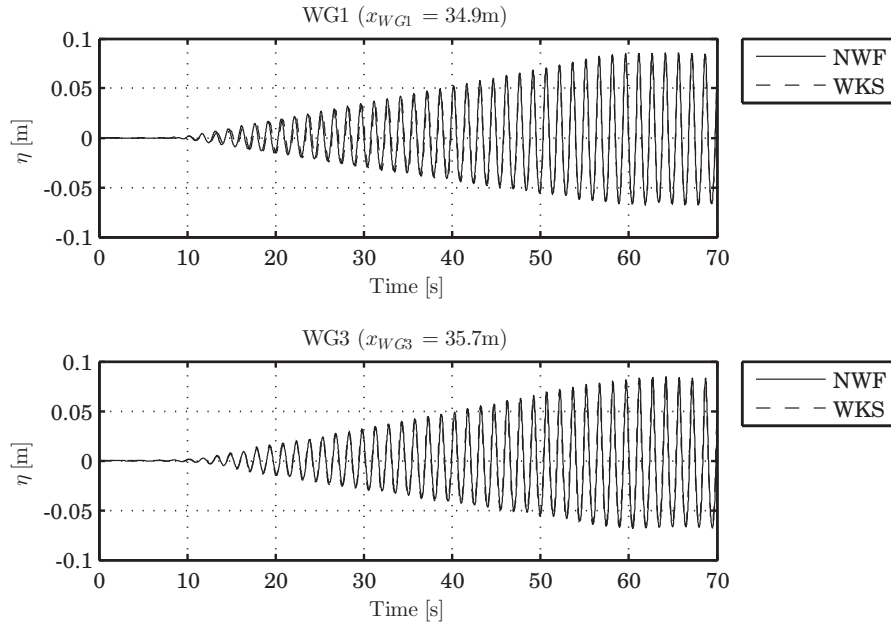


Figure 3.4.: Comparison of wave gauge WG1 and WG3 for numerical (NWF) and physical model test (WKS). Wave steepness is $s_Z = 0.043$.

on the water surface elevation. The question was when and how reflections of the wave flume end (outlet) occurred, despite the wave damping of the numerical code at the outlet. Three different regular wave trains with 150 waves ($N_W = 150$) in the wave train and increasing wave steepness $s_Z = 0.009, 0.029, 0.042$ were carried out in the numerical wave flume with the flume length $L_{flume} = 50$ m and $L_{flume} = 100$ m. The water surface elevation were “measured” (read out) at six positions $x = 0.0$ m, 10.0 m, 20.0 m, 30.0 m, 40.0 m, 49.9 m in the wave flume. The results for wave gauges WG1 and WG6 are shown in Fig. 3.5. The comparison showed that differences ($\Delta \geq 0.001$ m) in the water surface elevation occurred after approximately 50 s; the steeper the wave train the larger the differences were. Obviously, the differences were larger for WG6, which was just 0.1 m away from the outlet.

The influence of the flume length on the water surface elevation did not affect the overall result of the breaking onset as seen in Fig. 3.6. The figure shows the development of normalised time of breaking onset t_{br}/T_P against initial spectral steepness $s_{Z,i} = H_S/L_P$. For small $s_{Z,i} = 0.01$ and $s_{Z,i} = 0.02$ only test runs with $L_{flume} = 100$ m existed, except one test run with $s_{Z,i} = 0.02$, which lie in the same order of magnitude as the test runs with $L_{flume} = 100$ m. As can be seen, the median values for spectrum steepnesses

3. Hydronumerical Model Tests

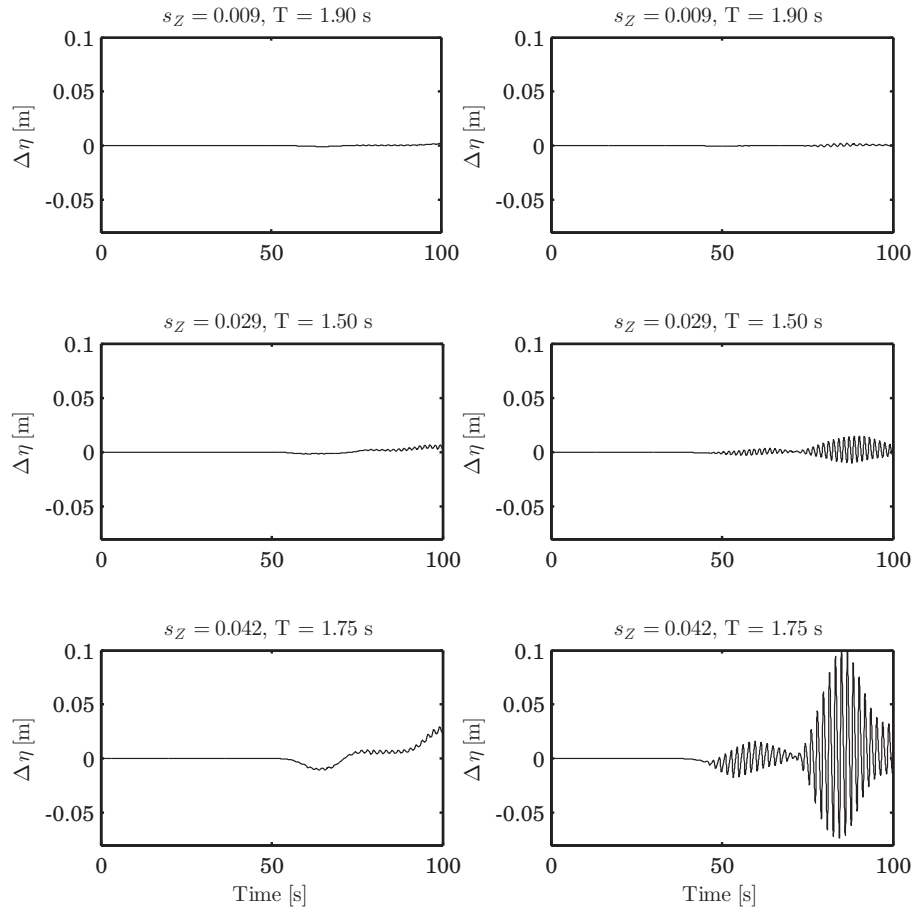


Figure 3.5.: Difference of water surface elevation for wave flume length $L_{flume} = 50$ m and $L_{flume} = 100$ m for wave gauge WG1 (left, $x_{WG1} = 0.0$ m) and WG6 (right, $x_{WG6} = 49.9$ m) for three regular wave trains with different wave steepnesses s_Z .

3.3. Validation, Limitations and Uncertainties

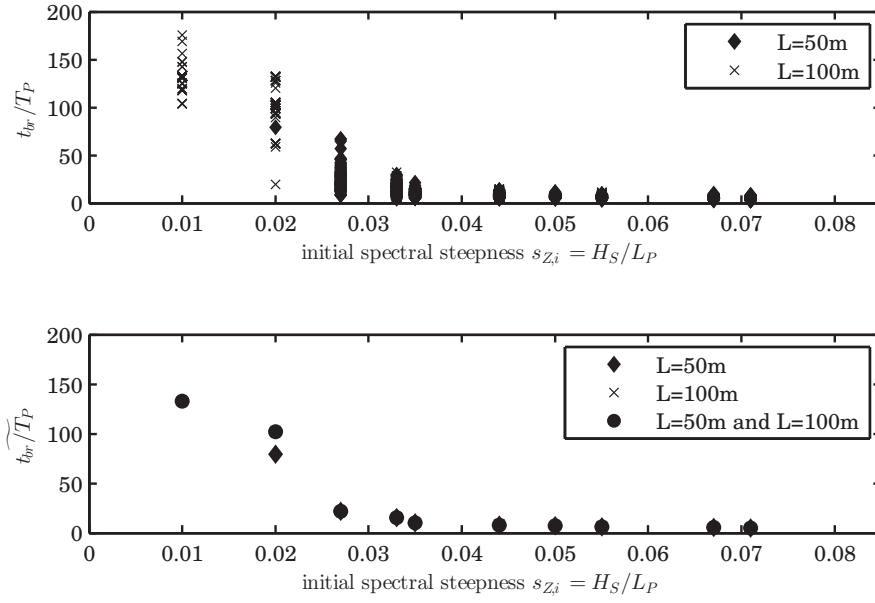


Figure 3.6.: Development of normalised time of breaking onset t_{br}/T_P against initial spectral steepness $s_{Z,i} = H_S/L_P$ for each wave flume length L_{flume} (top) and their median values (below).

$s_{Z,i} \geq 0.027$ for the data sets with only $L_{flume} = 50\text{ m}$, only $L_{flume} = 100\text{ m}$, or both data sets together resulted in the same values.

4. Influencing Factors on Breaking Onset

In the following chapter, the sensitivity, i.e. the cause-effect relationship between the input and output variables of breaking onset is investigated. Input variables were the characteristic parameters of the sea spectrum and wave train, respectively, $(H_S, T_P, \gamma, N_W, h)$ and their dimensionless characteristic values. Output variables were the time and location of breaking onset t_{br} and x_{br} . The influence of the input variables was firstly examined individually and secondly in a dimensional analysis. The test program for the hydronumerical model tests was based on the results of the physical model tests, which served as a first sensitivity analysis. Particular attention was paid to the parameters, which proved to be especially influential, namely the initial spectral steepness $s_{Z,i}$ and the phase angle distribution φ (wave sequence in the wave train). The randomness of the phase angle distribution, and thereby the randomness of the wave sequence in the time series, had a significant influence on the number of breaking waves; different realizations of the same energy density spectra in time domain did not produce same numbers of breaking waves. Therefore, each spectrum was repeated with a large sample number (up to 500 times). In the first step the relation between time of breaking onset t_{br} and the input variables H_S, T_P, γ, N_W, h was examined. The dimension analysis follows in section 4.2 and the investigation of the likelihood of breaking onset follows in section 4.4, where the frequency of non-breaking cases is investigated.

4.1. Development of Time of Breaking Onset

In this section the relation between time of breaking onset t_{br} , or rather the normalised time of breaking onset t_{br}/T_P , and the input variables H_S, T_P, γ, N_W, h is examined to determine the input variable with the greatest influence. All breaking test runs were considered here. For the analysis, the dimension-dependent input variables were sensibly standardized and yield the following dimensionless input variables:

- $s_{Z,i} = H_S/L_P$ with $L_P = \frac{g}{2\pi}T_P^2$
- $DWT/T_P = N_W * T_P/T_P = N_W$ ¹

¹The time length of the input signal or the duration of the wave train DWT is determined in the

4. Influencing Factors on Breaking Onset

- H_S/h
- γ

In Fig. 4.1 the development of normalised time of breaking onset t_{br}/T_P against initial spectral steepness $s_{Z,i} = H_S/L_P$ for each number of waves in initial wave train N_W is plotted. For each initial spectral steepness $s_{Z,i}$, multiple test runs (realizations of the wave spectrum) were performed which differed in their phase angle distribution. It can be observed that the median and the scattering of t_{br}/T_P decreased with increasing initial spectral steepness $s_{Z,i}$ (per N_W). In general, the greater the spectral steepness, the earlier the wave train broke. A scattering of the results (per $s_{Z,i}$ and N_W) showed the significance of the phase angle distribution, i.e. the significance of the wave sequence in the time series, to the time of breaking onset. For small spectrum steepnesses $s_{Z,i} \leq 0.044$, the dispersion of the output was relatively high; thus the wave sequence in the time series has a significant influence on the time of breaking onset. This observation was confirmed by the physical model tests, see section 6.1. In the case of large spectrum steepnesses $s_{Z,i} \geq 0.044$, the influence of the spectral steepness, in particular of the significant wave height H_S , and thus of the energy in the wave spectrum, predominated. The spread of the output parameters is investigated in more detail in section 5.1.

Banner et al. (2000) observed that the spectral peak steepness needed to be $\epsilon = H_P k_P / 2 \gtrsim 0.05 - 0.06$, see Eq. (2.6), for dominant wave breaking in natural wave fields to exist. This threshold value transferred to the initial spectral steepness leads to $s_{Z,i} \approx \epsilon / \pi \approx 0.016 - 0.019$, which goes along with the author's results. Babanin et al. (2007) and Dold and Peregrine (1986) observed in their numerical studies with monochromatic wave trains that wave trains needed an initial wave steepness of $(ak)_0 \geq 0.1$ ($H/L \geq 0.03$) to develop into a breaking wave train. In this thesis' numerical model tests non-breaking wave trains occurred for test runs with $s_{Z,i} = 0.01$ and $s_{Z,i} = 0.02$, but every test run with $s_{Z,i} \geq 0.027$ ($(ak)_0 \gtrsim 0.08$) broke, which also goes along with the results from literature. Babanin et al. (2007) found lower thresholds values in their physical model tests where monochromatic wave trains needed an initial wave steepness of $(ak)_0 \geq 0.08$ to break.

For the variation of the spectral steepness, primarily the significant wave height H_S ($0.043 \text{ m} \leq H_S \leq 0.30 \text{ m}$) was changed. The peak period T_P was only minimally changed ($1.65 \text{ s} \leq T_P \leq 1.90 \text{ s}$) because on the one hand it had to remain within the range of the possible values from the scatter diagram, and on the other hand it influenced the number of nodes of the mesh and thus the simulation duration. For the numerical simulation to

numerical code over the peak period and the desired number of waves in the wave train.

4.1. Development of Time of Breaking Onset

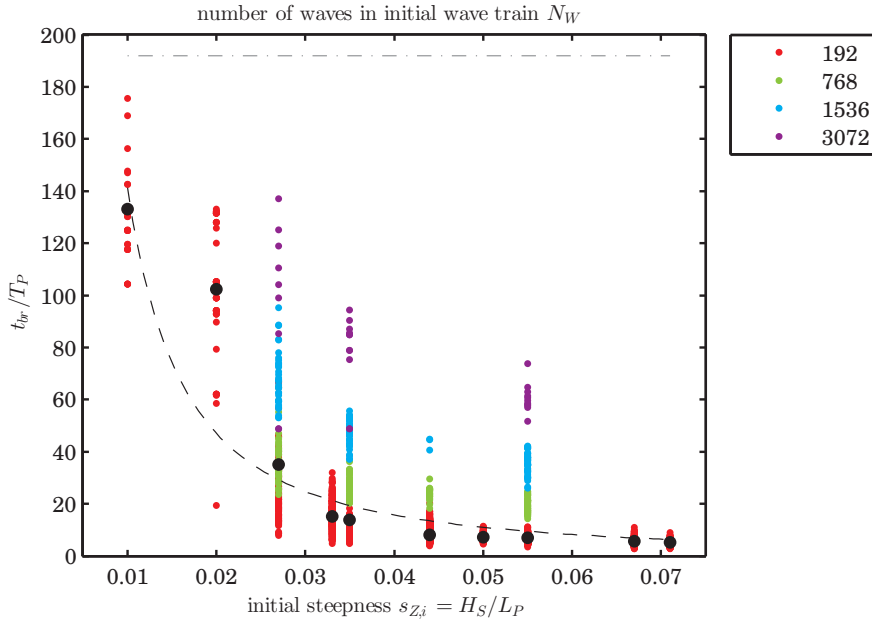


Figure 4.1.: Development of normalised time of breaking onset t_{br}/T_P against initial spectral steepness $s_{Z,i} = H_S/L_P$ for each number of waves in initial wave train N_W . Median values (black markers) and fitting line (black dashed line). Minimal duration of simulation (grey dashed line).

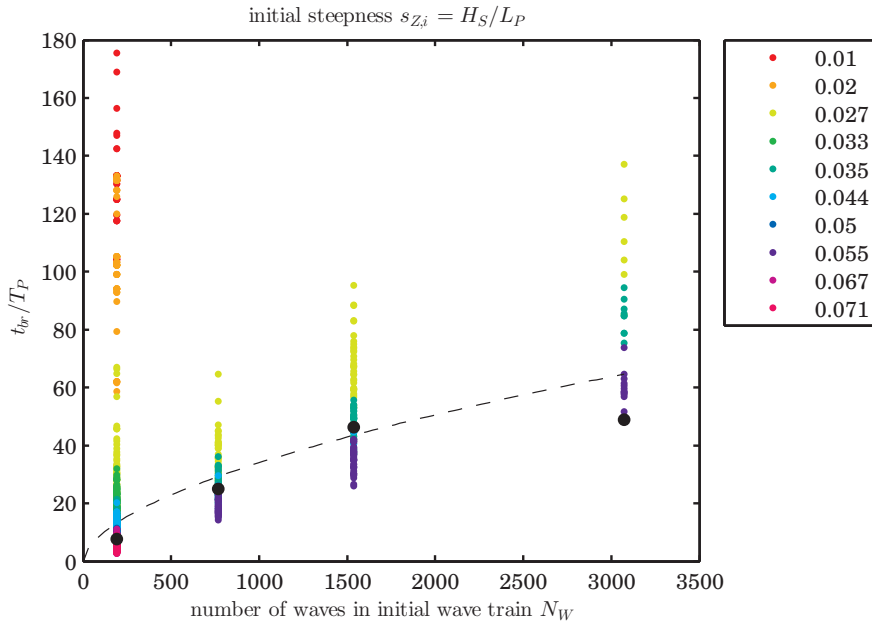


Figure 4.2.: Development of normalised time of breaking onset t_{br}/T_P against number of waves in initial wave train N_W for each initial spectral steepness $s_{Z,i} = H_S/L_P$. Median values (black markers) and fitting line (black dashed line).

4. Influencing Factors on Breaking Onset

continue to be efficient, the peak period was not further increased. Although the peak period has a quadratic influence on the spectral steepness, the significant wave height H_S and thus the energy content of the spectrum was the driving force that caused the wave breaking. The fitted curve has the Eq. (4.1) and the coefficient of determination $R^2 = 0.72$.

$$\frac{t_{br}}{T_P} = 0.095s_{Z,i}^{-1.59} \approx 0.1s_{Z,i}^{-\pi/2} \quad (4.1)$$

Banner et al. (2000) investigated breaking onset in an initial nearly uniform wave group configuration and concluded that the initial steepness $(ak)_0$ has the strongest influence on the time to breaking onset T_b , with the inverse time to breaking almost quadratically dependent on $(ak)_0$. This is similar with the author's result of the relation of the initial spectral steepness $s_{Z,i}$ and the time of breaking onset t_{br} in this investigations with irregular wave trains.

In Fig. 4.2 the development of normalised time of breaking onset t_{br}/T_P against number of waves in initial wave train N_W for each initial spectral steepness $s_{Z,i} = H_S/L_P$ is shown. It can be observed that the time of breaking onset increased as the number of waves in the wave train increased. In general, the longer the initial wave train, the later the wave train broke. When the course of the normalised time of breaking onset t_{br}/T_P was considered for each initial spectral steepness $s_{Z,i}$, the number of waves in the wave train N_W showed a linear influence. The fitted curve has the Eq. (4.2) and the coefficient of determination $R^2 = 0.14$.

$$\frac{t_{br}}{T_P} = 0.66N_W^{0.57} \quad (4.2)$$

In Fig. 4.3 the development of normalised time of breaking onset t_{br}/T_P against the normalised water depth H_S/h (top) and the water depth h (bottom) for each initial spectral steepness $s_{Z,i} = H_S/L_P$ is plotted. It can be observed that the time of breaking onset decreased with increasing ratio H_S/h , but the cause was the significant wave height H_S as Fig. 4.3 (bottom) shows. A change in water depth h did not significantly influence the time of breaking onset and no pattern in their behaviour were seen. The fitted curves have the Eqs. (4.3) and (4.4) and the coefficients of determination $R^2 = 0.85$ and $R^2 = 1.14 * 10^{-4}$, respectively.

$$t_{br}/T_P = 2 \left(\frac{H_S}{h} \right)^{-1.52} \approx 2 \left(\frac{H_S}{h} \right)^{-\pi/2} \quad (4.3)$$

4.1. Development of Time of Breaking Onset

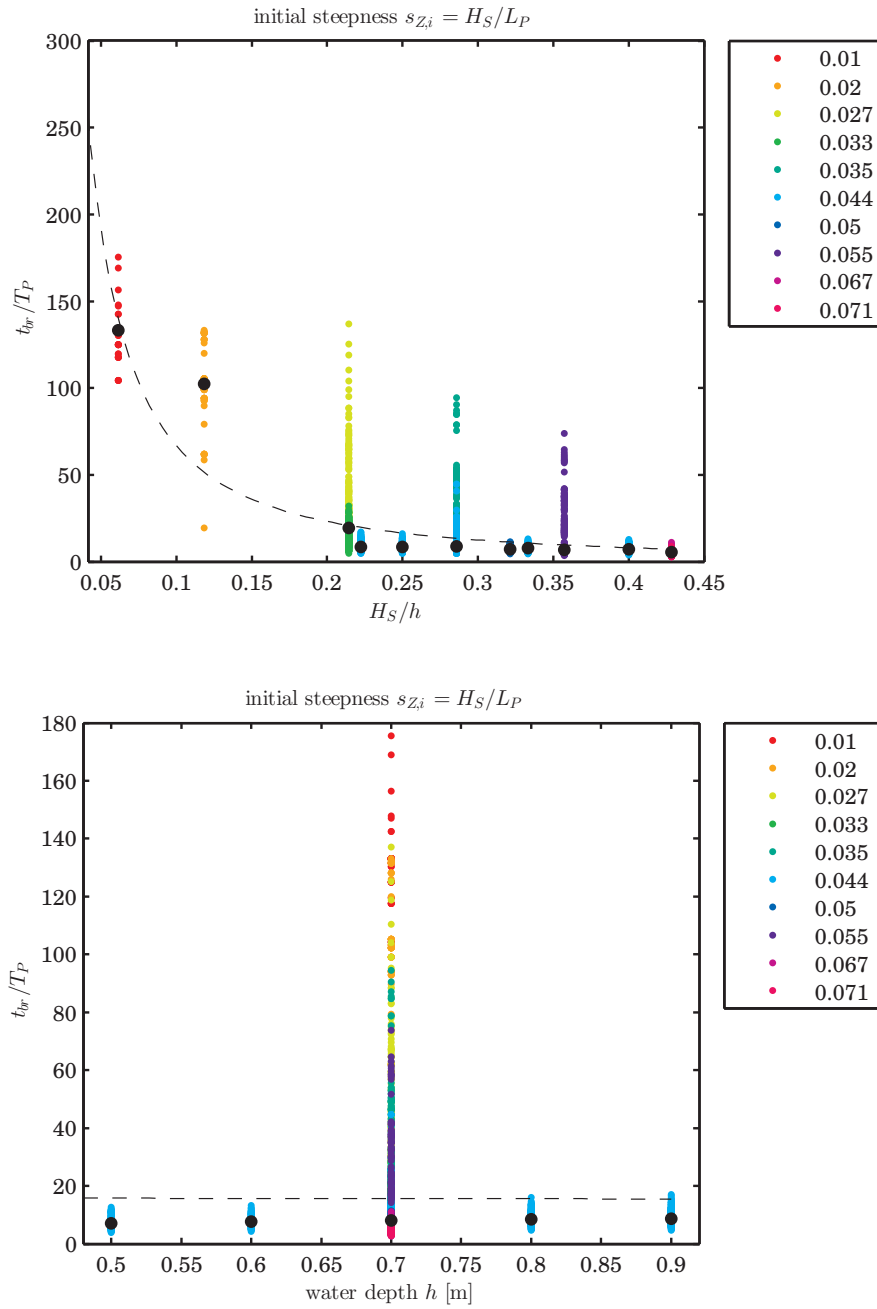


Figure 4.3.: Development of normalised time of breaking onset t_{br}/T_P against the normalised water depth H_S/h (top) and the water depth h (bottom) for each initial spectral steepness $s_{Z,i} = H_S/L_P$. Median values (black markers) and fitting line (black dashed line).

4. Influencing Factors on Breaking Onset

$$t_{br}/T_P = 15.46h^{-0.023} \quad (4.4)$$

Thus the occurring wave breaking was not depth-induced. To support that statement, the time of breaking onset is plotted over the normalised water depth H/h , with H as the wave height of the breaking wave, see Fig. 4.4. The breaking waves had a relative water depth of $0.027 \leq H/h \leq 0.64$, and were thus below the breaking criterion of $H/h = 0.78$, this criterion being based on the theory of solitary waves according to McCowan (1891). For irregular wave trains, the breaking criterion $H/h = 0.78$ and the assumption $H_{max}/H_S = 1.86$ leads to a critical threshold of $H_S/h = 0.42$. This theoretical value was just barely reached from the measurement results of $(H_S/h)_{max} = 0.429$, see Fig. 4.3.

In Fig. 4.5 the development of normalised time of breaking onset t_{br}/T_P against the enhancement factor γ of the JONSWAP spectrum for each initial spectral steepness $s_{Z,i} = H_S/L_P$ is plotted. The enhancement factor γ describes the peakedness of the JONSWAP sea spectrum (in relation to the PIERSON-MOSKOWITZ spectrum). A change in the enhancement factor γ did not significantly influence the time of breaking onset and no pattern were seen. The fitted curve has the Eq. (4.5) and the coefficient of determination $R^2 = 8.67 * 10^{-4}$.

$$\frac{t_{br}}{T_P} = 17.2\gamma^{-0.08} \quad (4.5)$$

Conclusions

- Breaking onset is highly sensitive to the initial spectral steepness $s_{Z,i}$, to the sequence of waves in the input wave train (phase angle distribution), and to the number of waves in the input wave train N_W .
- For small spectral steepnesses $s_{Z,i} \leq 0.044$, the sequence of waves in the input wave train is the main influence on breaking onset.
- For larger spectral steepnesses, the initial spectral steepness $s_{Z,i}$, especially H_S and, thus, the spectral energy, is the main influence on breaking onset.
- The inverse time of breaking onset $1/t_{br}$ is almost quadratically dependent on $s_{Z,i}$.

4.1. Development of Time of Breaking Onset

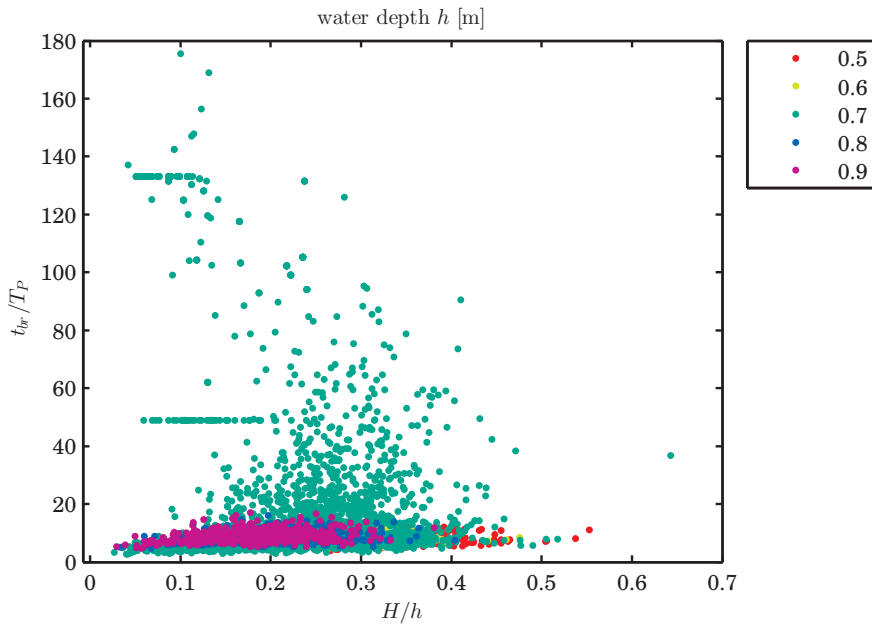


Figure 4.4.: Development of normalised time of breaking onset t_{br}/T_P against the normalised water depth H/h for each water depth h . H is the wave height of the breaking wave.

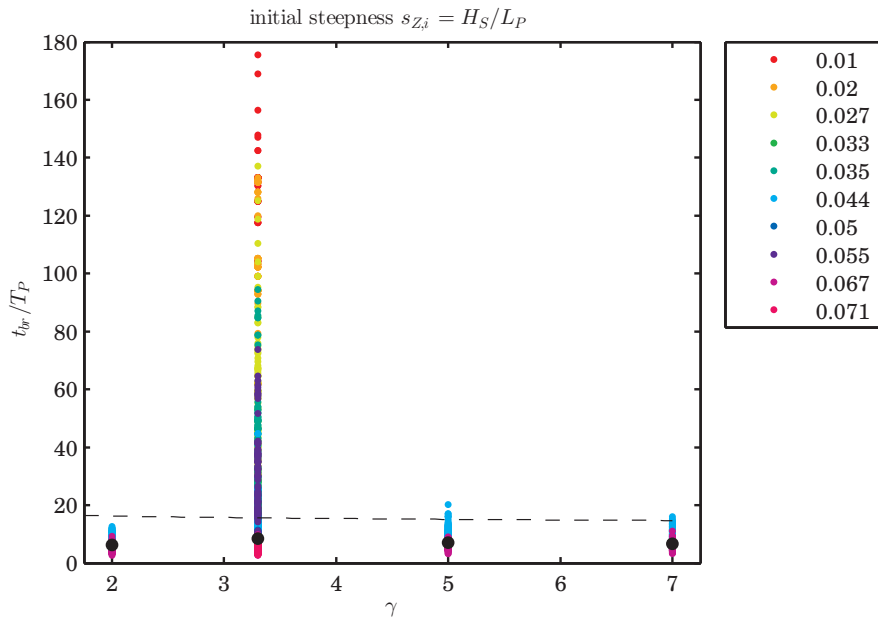


Figure 4.5.: Development of normalised time of breaking onset t_{br}/T_P against the enhancement factor γ of the JONSWAP spectrum for each initial spectral steepness $s_{Z,i} = H_S/L_P$. Median values (black markers) and fitting line (black dashed line).

4.2. Dimensional Analysis

The aim of the dimensional analysis according to Buckingham (1914) is to mathematically describe the influence of the input variables and predict the output value based on the results of the measurements. The output values to be determined were the time and the location of breaking onset t_{br} and x_{br} , or their dimensionless variants t_{br}/T_P and x_{br}/L_P . In addition to the input values H_S , T_P , N_W , h and γ , introduced in section 4.1, the following input variables were introduced for the dimension analysis to describe the phase angle distribution and the width of the sea spectrum:

- the spectral width $\nu_W = \sqrt{\frac{m_0 m_2}{m_1^2} - 1}$
- time of the first wave group in initial wave train $WaGo_{Time}$
- number of waves in first wave group in initial wave train $WaGo_{Num}$

The spectral width ν_W was introduced because the width of the peak of a narrow-banded spectrum is related to modulational properties in the train of dominant waves. m_i is the spectral moment of order i , see Eq. (4.6).

$$m_i = \int_{f_{min}}^{f_{max}} S(f) f^i df \quad (4.6)$$

The spectrum was determined from the input signal of the wave train and the the bandwidth was $f_{min} = 0.25 * f_P$ and $f_{max} = 4 * f_P$; those cut-off frequencies were also chosen to generate the wave train in the numerical code.

As described by Donelan et al. (1972) and Holthuijsen and Herbers (1986) for the first time, wave groups and wave breaking are connected to one another. Therefore the parameters $WaGo_{Time}$ and $WaGo_{Num}$ were also taken into account in the following dimension analysis. For the analysis, the input variables were normalised and yield the following dimensionless input variables:

- $s_{Z,i} = H_S/L_P$
- $DWT/T_P = N_W T_P/T_P = N_W$
- H_S/h
- γ
- ν_W

- $WaGo_{Num}/N_W$
- $WaGo_{Time}/T_P$

with the time length of the input signal DWT . The power function $y = ax^b$ was defined as the basic mathematical relation. The considered sample consisted of all test runs that broke and had the ratio $a_C/H_S \geq 0.9$. The restriction to consider only breaking waves with a minimum height was introduced to increase the quality of the dimensional analysis and to focus on the interesting data ranges. To investigate which input variables were relevant for dimensional analysis, three groups of input variables were used and the results were compared with one another.

In Group 1 all of the above listed input variables were considered. In Group 2 the four main input variables $s_{Z,i}$, N_W , H_S/h and γ were considered. As shown in the previous section 4.1, the initial spectral steepness $s_{Z,i}$ and the number of waves in the initial wave train N_W had the biggest influence on the time of breaking onset t_{br} . The normalised water depth H_S/h and the enhancement factor of the sea spectrum γ were considered because the water depth generally have an influence on wave breaking and γ is an indicator of the energy content and peakedness of the sea spectrum. Whether the two last-mentioned input variables were really relevant for dimensional analysis is to be shown here.

Furthermore, in Group 3 only $s_{Z,i}$ and H_S/h were considered; N_W and γ were left out since the number of waves (or the time length of the signal) and the enhancement factor are not standard information which is measured. In contrast, the variables H_S , T_P and h are default measured values, e.g. from the research platform FINO1.

In Fig. 4.6 the dimensional analysis of normalised time of breaking onset t_{br}/T_P is plotted against its predicted results. The coefficient of determination was $R^2 = 0.958$ for Group 1 and Group 2, and $R^2 = 0.885$ for Group 3. Whether the spectral width ν_W or the wave group parameters $WaGo_{Num}/N_W$ and $WaGo_{Time}/T_P$ were considered or not had no influence on the coefficient of determination. The exclusion of the number of waves N_W and the enhancement factor γ on the other hand decreased the coefficient of determination, consequently, N_W and γ were important input variables for the time of breaking onset.

In Fig. 4.7 the dimensional analysis of the normalised location of breaking onset x_{br}/L_P is plotted against its predicted results. The coefficient of determination was $R^2 = 0.901$ for Group 1 and $R^2 = 0.906$ for Group 2 and Group 3. Again the spectral width and the wave group parameters had no influence on the output. The spectral steepness $s_{Z,i}$ and the relative water depth H_S/h had the biggest influence on the location of breaking onset

4. Influencing Factors on Breaking Onset

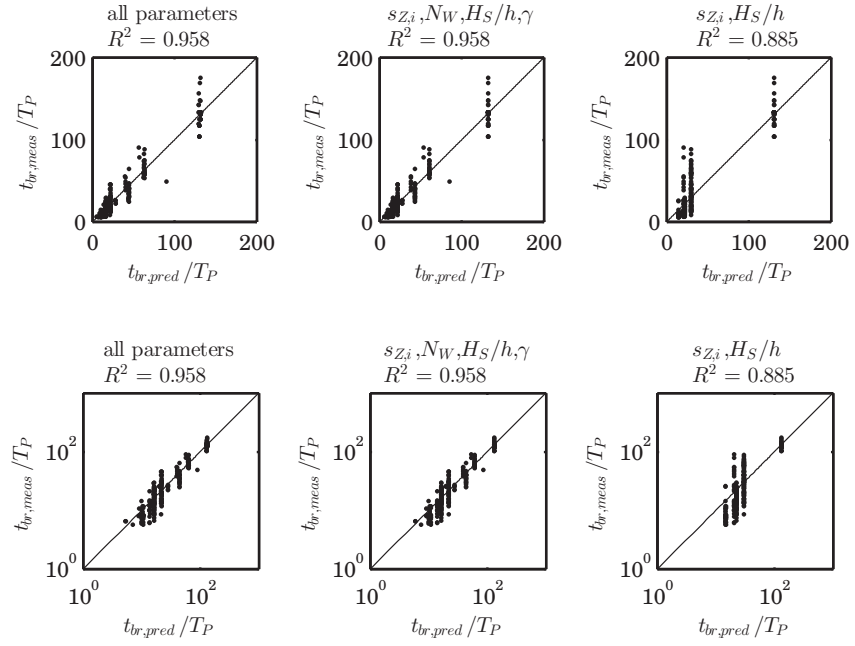


Figure 4.6.: Dimensional analysis of normalised time of breaking onset t_{br}/T_P (plotted against predicted results). Total number of data points $n_{max} = 291$. Normal (top) and logarithmic (bottom) presentation.

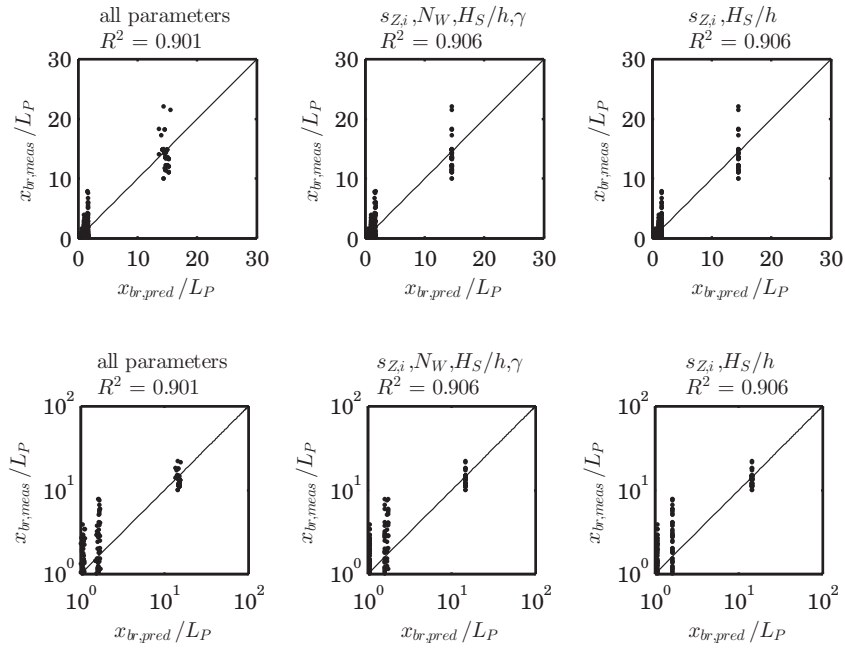


Figure 4.7.: Dimensional analysis of normalised location of breaking onset x_{br}/L_P (plotted against predicted results). Total number of data points $n_{max} = 291$. Normal (top) and logarithmic (bottom) presentation.

4. Influencing Factors on Breaking Onset

x_{br} .

The resulting equation for the time of breaking onset $t_{br,pred}$ is Eq. (4.7), the equation for the location of breaking onset $x_{br,pred}$ is Eq. (4.8).

$$\frac{t_{br,pred}}{T_P} = 0.0294 s_{Z,i}^{-1.43} N_W^{0.49} \left(\frac{H_S}{h} \right)^{-0.3} \gamma^{-0.71} \left(\frac{WaGoNum}{N_W} \right)^{-0.02} \left(\frac{WaGoTime}{T_P} \right)^{0.002} \nu_W^{0.76} \quad (4.7)$$

$$\frac{x_{br,pred}}{L_P} = 0.0053 s_{Z,i}^{-2.09} N_W^{0.05} \left(\frac{H_S}{h} \right)^{-0.11} \gamma^{-1.36} \left(\frac{WaGoNum}{N_W} \right)^{-0.01} \left(\frac{WaGoTime}{T_P} \right)^{-0.05} \nu_W^{0.44} \quad (4.8)$$

When only the initial spectral steepness $s_{Z,i}$ and the relative water depth H_S/h were taken into account, then the equation for $t_{br,pred}$ and $x_{br,pred}$ were as follows, see Eqs. (4.9) and (4.10).

$$\frac{t_{br,pred}}{T_P} = 0.158 s_{Z,i}^{-1.43} \left(\frac{H_S}{h} \right)^{-0.04} \quad (4.9)$$

$$\frac{x_{br,pred}}{L_P} = 0.0008 s_{Z,i}^{-2.09} \left(\frac{H_S}{h} \right)^{-0.09} \quad (4.10)$$

In Fig. 4.8 and 4.9, the resulting curves according to Eq. (4.7) are presented together with the measured data. The curves were calculated with the fixed parameters $\gamma = 3.3$ and $H_S/h = 0.061$ and then for variable numbers of waves in the initial wave train N_W and variable initial spectral steepnesses $s_{Z,i}$, respectively. The resulting curves fit the data good.

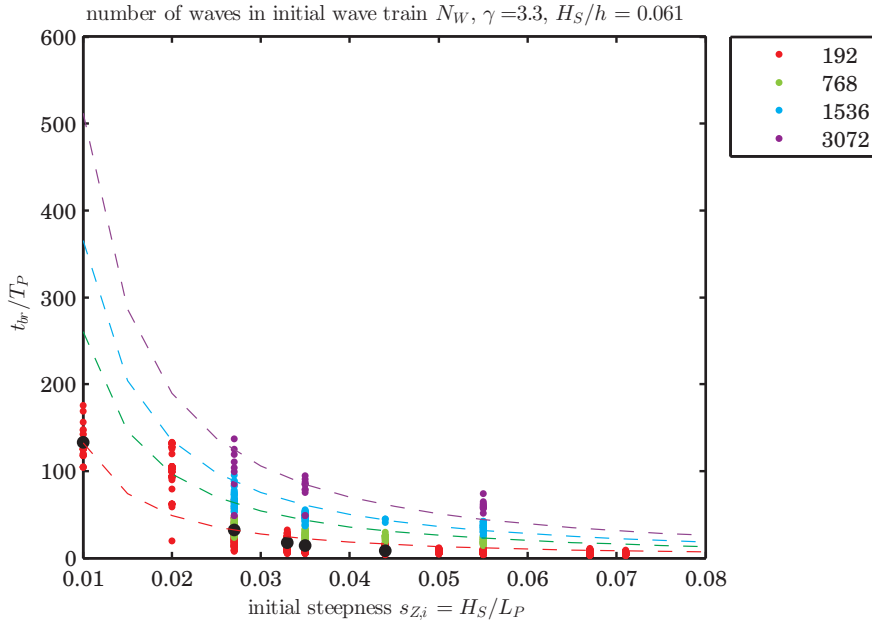


Figure 4.8.: Development of normalised time of breaking onset t_{br}/T_P against initial spectral steepness $s_{z,i} = H_S/L_P$ for each number of waves in initial wave train N_W . Median values for the total data points (black markers).

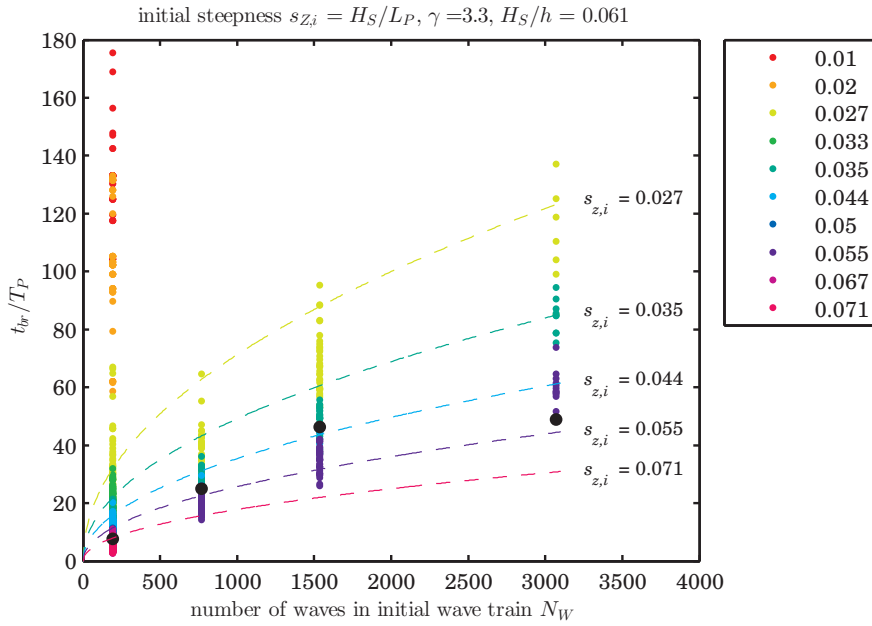


Figure 4.9.: Development of normalised time of breaking onset t_{br}/T_P against number of waves in initial wave train N_W for each initial spectral steepness $s_{z,i} = H_S/L_P$. Median values for the total data points (black markers).

Conclusions

- The dimensional analyse shows that the initial spectral steepness $s_{Z,i}$, the number of waves in the input wave train N_W , and the enhancement factor γ are influential variables for the time of breaking onset t_{br} .
- For the location of breaking onset x_{br} , only the initial spectral steepness $s_{Z,i}$ is a influential variable.
- The spectral width ν_W and the wave group parameters $WaGo_{Time}$ and $WaGo_{Num}$ show no influence on the coefficient of determination.

4.3. Comparison with Physical Model Tests

In this section, the results of the dimensional analysis, which was based on the data of the NWF simulations, are compared to the results of the physical model tests of this thesis, see section 6.1, and the results of the physical model tests by Babanin et al. (2007). Babanin et al. conducted model tests with two-dimensional initially monochromatic waves, which broke due to modulational instability. They deduced an relationship between the dimensionless distance to breaking x_{br}/L and the initial wave steepness $(ak)_0$, see Eq. (2.7).

Fig. 4.10 shows the normalised location of breaking onset x_{br}/L_P against initial spectral steepness $s_{Z,i} = H_S/L_P$. The results of the physical model tests in the WKS wave flume are shown as a grey area, and not as exact values, because it was not possible to measure the breaking onset of the first breaking wave in the laboratory. In the model tests, JONSWAP spectra with initial spectral steepnesses between $0.026 \leq s_{Z,i} \leq 0.082$ were carried out, and the video recordings showed, that the first wave breaking usually happened in the first $\sim 10\text{m}^2$ after the wave paddle, but the first wave gauge was installed in 14.9m distance. Nevertheless, the results of the WKS model tests and the NWF simulations are in good agreement, and the equations from the dimensional analysis follow the pattern of x_{br}/L_P well.

Please note, to present Babanin et al.'s resulting equation Eq. (2.7) in Fig. 4.10 the following assumption was made: $(ak)_0 \approx \pi * s_{Z,i}$. The resulting curve shows the same trend as Eq. (4.8) and (4.10), but with a higher offset. The comparison shows that monochromatic (regular) waves break spatially later than irregular waves with similar

² $x_{br}/L_P \approx 10\text{m}/3.1\text{m} \approx 3.2$ with 3.1m as the shortest wavelength in the model tests

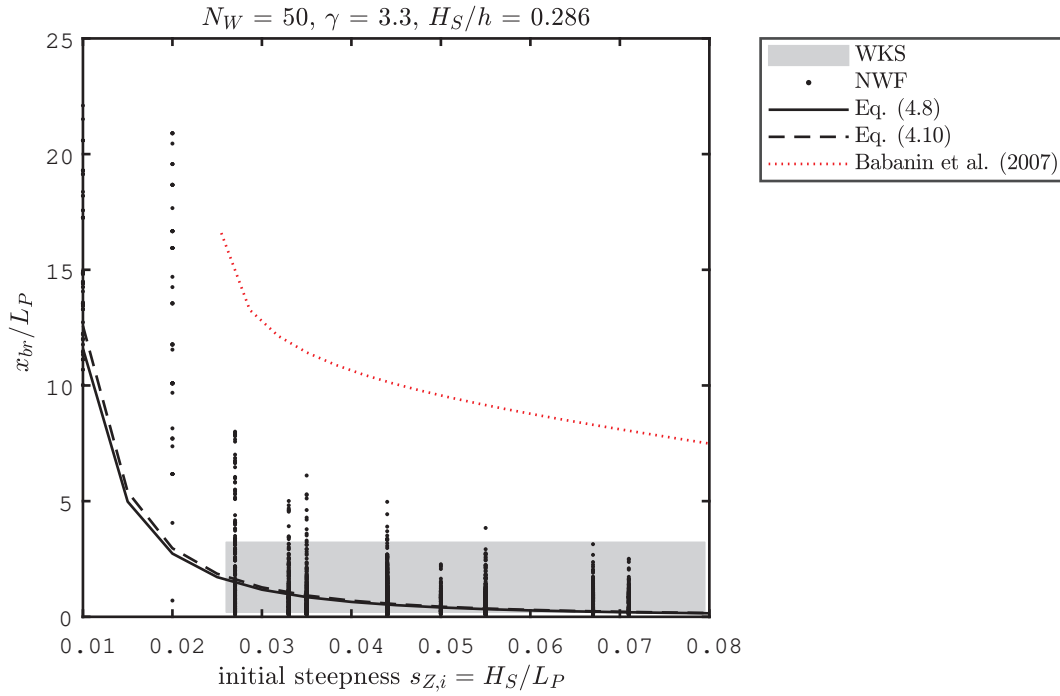


Figure 4.10.: Development of normalised location of breaking onset x_{br}/L_P against initial spectral steepness $s_{Z,i} = H_S/L_P$ in comparison with results from WKS model tests, NWF simulations, dimensional analysis, and Babanin et al. (2007).

initial wave steepnesses. Furthermore, the comparison shows the significant influences of the type of wave train and the type of wave breaking generation on the breaking process and its onset.

4.4. Likelihood of Breaking Onset

In addition to section 4.1, the frequency of occurrence of the breaking wave trains is investigated in this section. In Tab. 4.1, the number of test runs for the dataset with non-breaking and breaking wave trains n_{max} and the dataset with only breaking wave trains $n_{breaking}$ is presented for each initial spectral steepness. The frequency of breaking is:

$$f_{br} = \frac{n_{breaking}}{n_{max}} \quad (4.11)$$

4. Influencing Factors on Breaking Onset

Table 4.1.: Overview of number of test runs for data sets with different initial spectral steepnesses and the frequency of breaking.

$s_{Z,i}$	All wave trains	Breaking wave trains	Non-breaking wave trains	Breaking Frequency f_{br}
0.010	88	85	3	0.97
0.020	70	69	1	0.99
0.027	208	208	0	1
0.033	288	288	0	1
0.035	281	281	0	1
0.044	1918	1918	0	1
0.050	142	142	0	1
0.055	473	473	0	1
0.067	676	676	0	1
0.071	185	185	0	1
Sum	4412	4329	4325	

The difference to Eq. (2.3), $P_{br} = n_{br}/n_{tot}$, is that Eq. (2.3) considers one wave train in which n_{br} wave crests break, but Eq. (4.11) considers n_{max} wave trains of which $n_{breaking}$ wave trains break.

As can be seen in Tab. 4.1, only for the low initial spectral steepnesses $s_{Z,i} = 0.01$ and $s_{Z,i} = 0.02$ there were four non-breaking wave trains that propagated without any discontinuity in the NWF; the breaking frequency was $f_{br} = 0.97$ for $s_{Z,i} = 0.01$ and $f_{br} = 0.99$ for $s_{Z,i} = 0.02$. For all higher spectral steepnesses, the breaking frequency was $f_{br} = 1$, that is, each wave train broke in the course of the simulation. The result shows that a wave train also breaks with a low spectral slope, if it has enough running length. From a spectral steepness of $s_{Z,i} \geq 0.027$ all test runs broke; the low scattering of the results of t_{br}/T_P for high spectral steepnesses suggests that even with an increase in the number of test runs carried out, no wave train would had passed without instability. In Fig. 4.11, the corresponding histograms for the datasets with and without non-breaking wave trains are shown for $s_{Z,i} = 0.01$ and $s_{Z,i} = 0.02$. Since, as a whole, only four wave trains passed through without instability, the difference between the histograms was only minimal.

4.4. Likelihood of Breaking Onset

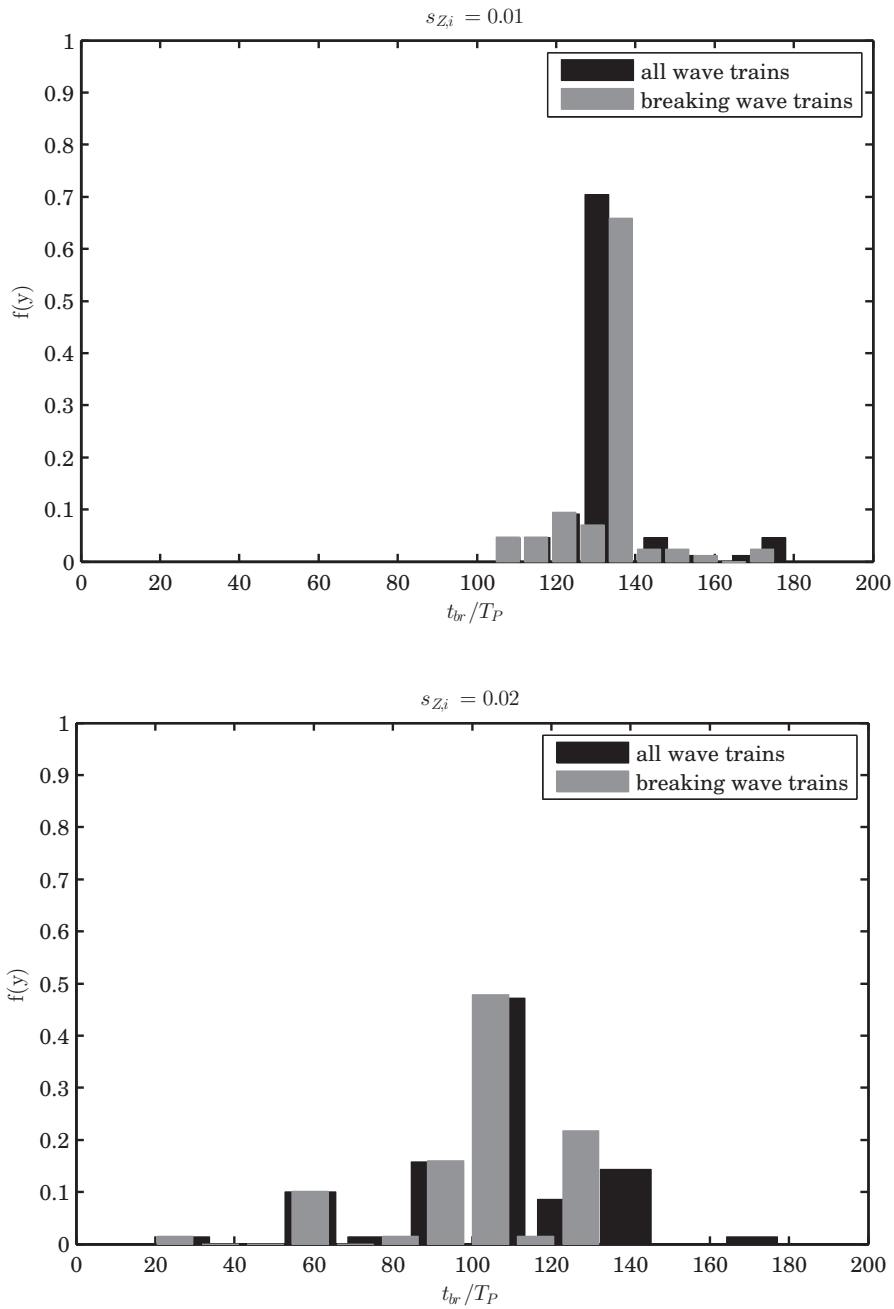


Figure 4.11.: Histograms of normalised time of breaking onset t_{br}/T_P for the data sample with all test runs (non-breaking and breaking wave trains) and with only breaking wave trains. Number of bins was 10. Initial spectral steepness $s_{Z,i} = 0.01$ (top) and $s_{Z,i} = 0.02$ (bottom).

5. Variability of Breaking Onset

In this chapter the scattering of the normalised time and location of breaking onset t_{br}/T_P and x_{br}/L_P , respectively, are investigated as a function of the spectral steepness $s_{Z,i}$, both with univariate and bivariate (copula) distribution functions. Thereby, the influence of the phase angle distribution, and thus of the wave sequence in the wave train, on the output parameters is analysed.

Furthermore, a convergence analysis for the normalised time of breaking onset t_{br}/T_P is carried out, and the optimum sample size N_{Opt} , that is, the necessary test number to calculate t_{br}/T_P with a permissible deviation is determined.

5.1. Univariate Distribution Function

In the following, the scattering of the normalised time and location of breaking onset t_{br}/T_P and x_{br}/L_P , respectively, for every initial spectral steepness $s_{Z,i}$ is analysed. An overview of the statistical values such as minimum value, maximum value, median value, standard deviation and total number of test runs for t_{br}/T_P for each $s_{Z,i}$ is given in Tabs. 5.1 and 5.2. In Tab. 5.1, all test runs that broke are taken into account. In Tab. 5.2, however, the data set is taken into account with all test runs that broke, but with fixed boundary conditions for the water depth, number of waves in the initial wave train and enhancement factor so that only the spectral steepness $s_{Z,i}$ varied. The boundary conditions were $h = 0.7\text{m}$, $N_W = 192$, and $\gamma = 3.3$.

The standard deviations varied between $\sigma \approx 1$ to $\sigma \approx 23$, where the scatter was particularly large for small spectral steepnesses $s_{Z,i} \leq 0.027$, and then decreased rapidly. As expected, both data sets differ only for the spectral steepnesses $s_{Z,i}$, which have varying water depths h , numbers of waves in the initial wave train N_W , or enhancement factors γ , see Fig. 4.1.

In Tabs. 5.3 and 5.4 the corresponding results for the location of breaking onset x_{br}/L_P are given. Again, the scatter was the largest for small steepnesses, but the standard deviation only varied between $\sigma \approx 0.5$ and $\sigma \approx 5$. The location and time of breaking onset did not need necessarily to correlate, since the breaking wave crest did not necessarily

5. Variability of Breaking Onset

Table 5.1.: Statistics of normalised time of breaking onset t_{br}/T_P for dataset with all test runs (breaking wave trains).

sZ_i	x_{min}	x_{max}	\tilde{x}	σ	n_{max}
0.010	104.21	175.54	133.10	10.44	85
0.020	19.30	133.10	102.27	21.82	69
0.027	7.91	137.01	35.09	23.20	208
0.033	4.75	31.99	15.24	5.58	288
0.035	4.85	94.43	13.66	19.17	281
0.044	3.93	44.75	8.11	3.11	1870
0.050	4.62	11.49	7.13	1.42	142
0.055	3.47	73.87	6.94	12.27	448
0.067	2.75	10.95	5.59	1.17	589
0.071	2.82	8.93	5.07	1.06	185

Table 5.2.: Statistics of normalised time of breaking onset t_{br}/T_P for dataset with all test runs (breaking wave trains) and $h = 0.7$ m, $N_W = 192$ and $\gamma = 3.3$.

sZ_i	x_{min}	x_{max}	\tilde{x}	σ	n_{max}
0.010	104.21	175.54	133.10	10.44	85
0.020	19.30	133.10	102.27	21.82	69
0.027	7.91	66.94	21.88	12.30	99
0.033	4.75	31.99	15.24	5.58	288
0.035	4.85	21.39	10.07	2.90	171
0.044	4.67	14.53	8.12	2.02	396
0.050	4.62	11.49	7.13	1.42	142
0.055	3.47	11.12	6.19	1.39	347
0.067	2.77	9.95	5.39	1.18	146
0.071	2.82	8.93	5.07	1.06	185

Table 5.3.: Statistics of normalised location of breaking onset x_{br}/L_P for dataset with all test runs (breaking wave trains).

sZ_i	x_{min}	x_{max}	\tilde{x}	σ	n_{max}
0.010	10.02	22.10	14.47	3.12	85
0.020	0.70	20.90	13.55	4.87	69
0.027	0.09	8.00	1.44	2.04	208
0.033	0.07	5.01	0.81	0.93	288
0.035	0.09	6.11	0.59	0.97	281
0.044	0.07	4.97	0.52	0.57	1870
0.050	0.13	2.27	0.55	0.45	142
0.055	0.09	3.84	0.65	0.54	448
0.067	0.07	3.14	0.68	0.45	589
0.071	0.08	2.51	0.67	0.47	185

Table 5.4.: Statistics of normalised location of breaking onset x_{br}/L_P for dataset with all test runs (breaking wave trains) and $h = 0.7$ m, $N_W = 192$ and $\gamma = 3.3$.

sZ_i	x_{min}	x_{max}	\tilde{x}	σ	n_{max}
0.010	10.02	22.10	14.47	3.12	85
0.020	0.70	20.90	13.55	4.87	69
0.027	0.09	7.91	1.40	1.89	99
0.033	0.07	5.01	0.81	0.93	288
0.035	0.09	3.23	0.47	0.57	171
0.044	0.07	3.36	0.55	0.57	396
0.050	0.13	2.27	0.55	0.45	142
0.055	0.09	2.75	0.64	0.47	347
0.067	0.07	3.14	0.67	0.47	146
0.071	0.08	2.51	0.67	0.47	185

5. Variability of Breaking Onset

Table 5.5.: Probability density functions.

PDF	
GUMBEL	$f(x) = a * \exp(-a(x - \mu)) * \exp(-\exp(-a(x - \mu)))$
Gamma	$f(x) = \frac{1}{b^a \Gamma(a)} x^{a-1} \exp(-\frac{x}{b})$
WEIBULL	$f(x) = \frac{b}{a} (\frac{x}{a})^{b-1} \exp(-(\frac{x}{a})^b)$
GAUSSIAN Normal	$f(x) = \frac{1}{\sigma\sqrt{2\pi}} \exp(-\frac{1}{2}(\frac{x-\mu}{\sigma})^2)$
RAYLEIGH	$f(x) = \frac{x}{b^2} \exp(-\frac{x^2}{2b^2})$

had to belong to the first wave, and thus the location and time were not connected to the running speed of the wave; due to wave-wave interaction, the location of the breaking could also be in the centre of the wave train, rather than at the beginning.

In the following, the histograms, empirical probability density functions (PDFs) and empirical cumulative distribution functions (CDFs) are shown; then they are compared with the theoretical GUMBEL, Gamma, WEIBULL, GAUSSIAN, and RAYLEIGH distribution functions. For the histograms, the class number m was determined according to Eq.(5.1), where N is the number of characteristic values (Papula, 2002, p. 475).

$$m = 5 \log_{10}(N) \quad (5.1)$$

The empirical density function was calculated with the matlab function *ksdensity*, which represents an estimate of the density function based on a normal kernel function (Bowman and Azzalini, 2004). The formulas for the probability density functions and distribution functions for GUMBEL, Gamma, WEIBULL, GAUSSIAN, and RAYLEIGH are summarised in Tabs.5.5 and 5.6. a is the shape parameter, σ and b are the scale parameters, and μ is the location parameter.

In Figs. 5.1 to 5.4, the PDFs and CDFs for the normalised time and location of breaking onset are shown exemplarily for $s_{Z,i} = 0.033, 0.044, 0.055, 0.067$. It can be seen that the larger $s_{Z,i}$ the smaller the scatter of t_{br}/T_P and x_{br}/L_P , and the smaller the mean value of t_{br}/T_P , that is, the sooner the train broke. Furthermore, it can be observed that the larger $s_{Z,i}$ the better all theoretical distribution functions followed the empirical distribution functions of t_{br}/T_P (except RAYLEIGH) and x_{br}/L_P . The GUMBEL and Gamma distributions best described the scattering of t_{br}/T_P , and the WEIBULL and Gamma distributions best described the scattering of x_{br}/L_P .

5.1. Univariate Distribution Function

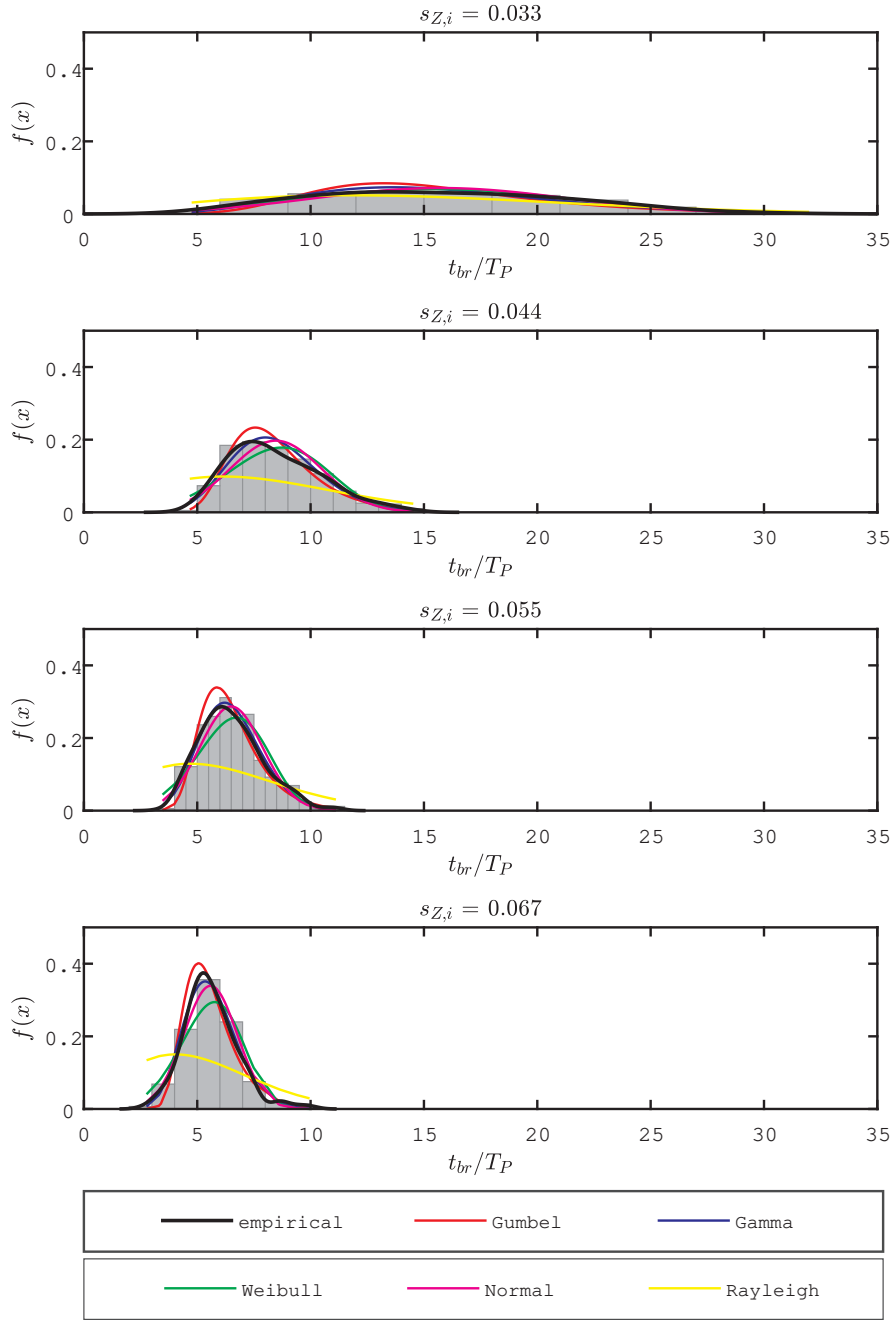


Figure 5.1.: Histograms of normalised time of breaking onset t_{br}/T_P with different PDFs for the test runs with initial spectral steepness $s_{Z,i} = 0.033, 0.044, 0.055, 0.067$.

5. Variability of Breaking Onset

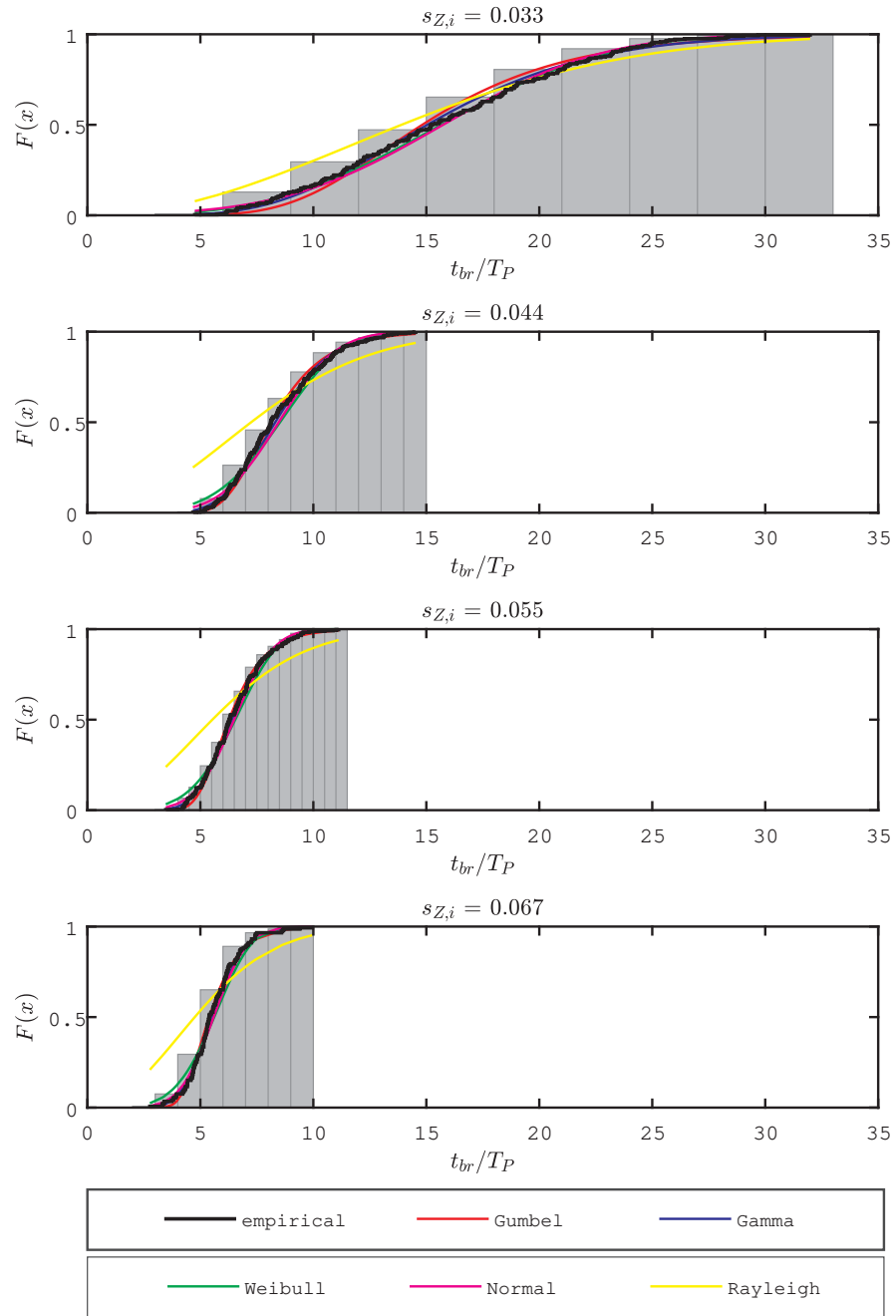


Figure 5.2.: Empirical cumulative distribution function of normalised time of breaking onset t_{br}/T_P with different CDFs for the test runs with initial spectral steepness $s_{Z,i} = 0.033, 0.044, 0.055, 0.067$.

5.1. Univariate Distribution Function

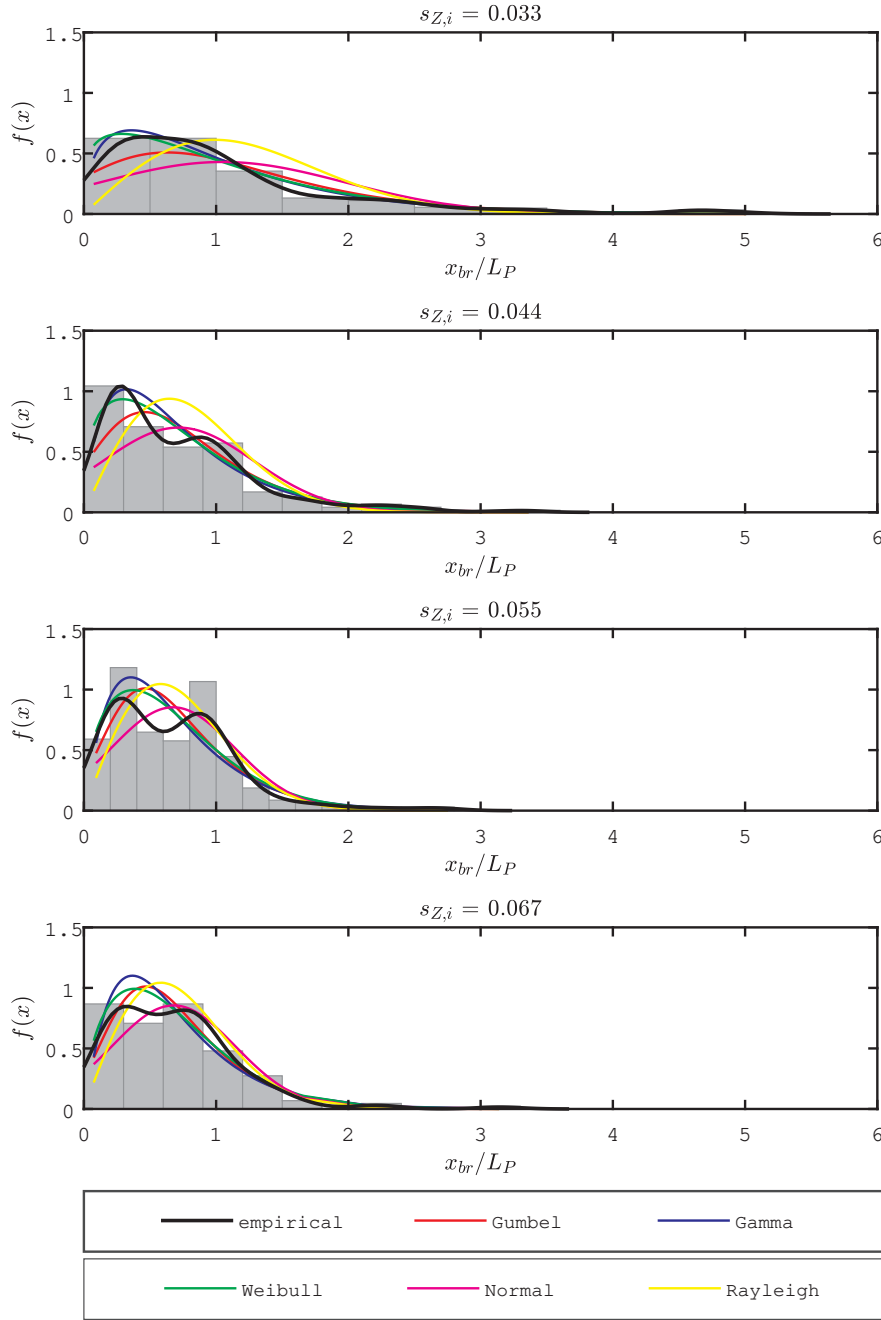


Figure 5.3.: Histograms of normalised location of breaking onset x_{br}/L_P with different PDFs for the test runs with initial spectral steepness $s_{Z,i} = 0.033, 0.044, 0.055, 0.067$.

5. Variability of Breaking Onset

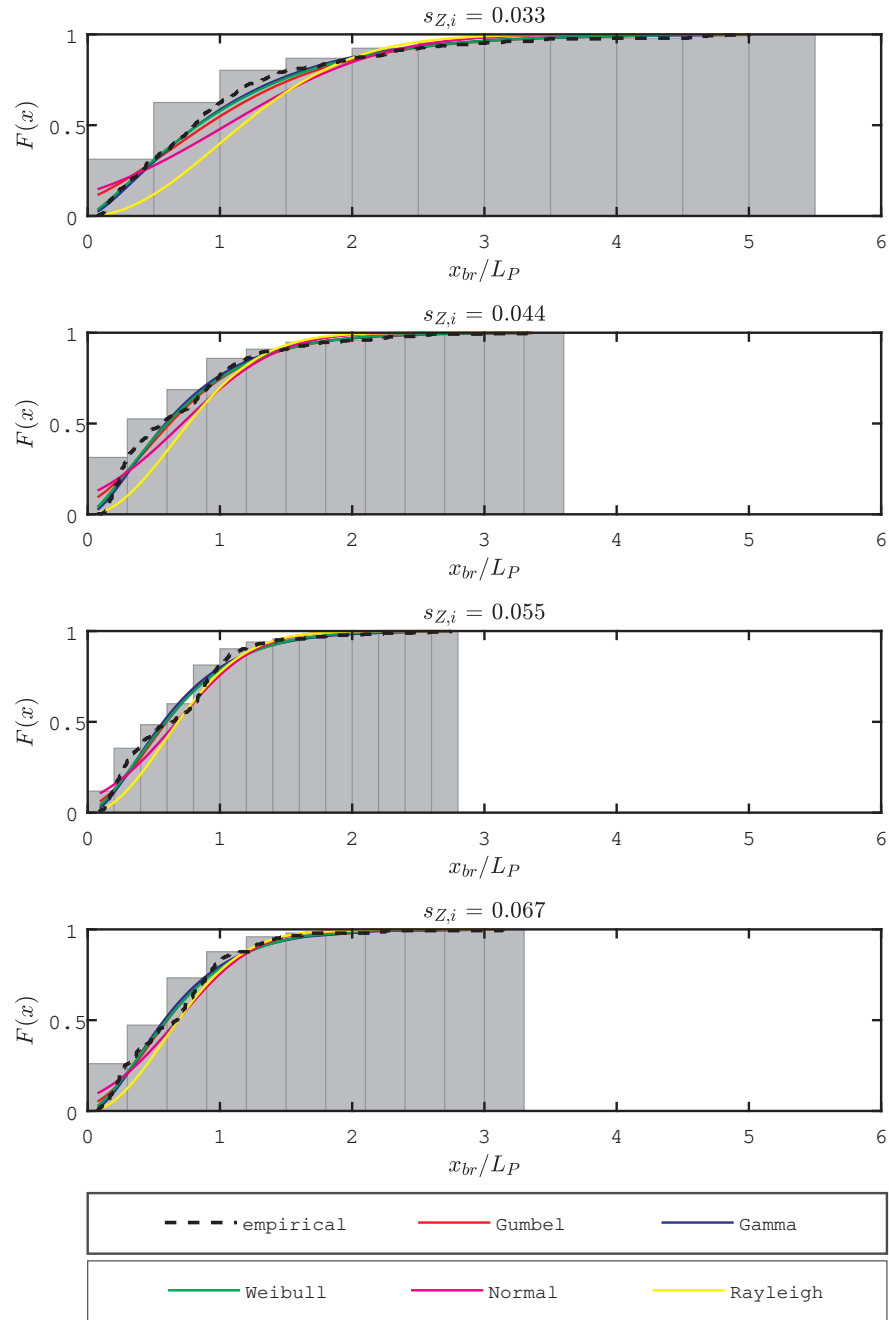


Figure 5.4.: Empirical cumulative distribution function of normalised location of breaking onset x_{br}/L_P with different CDFs for the test runs with initial spectral steepness $s_{Z,i} = 0.033, 0.044, 0.055, 0.067$.

Table 5.6.: Cumulative distribution functions, $\gamma(k, ax)$ is the lower incomplete Gamma function.

CDF	
GUMBEL	$F(x) = \exp(-\exp(-a * (x - \mu)))$
Gamma	$F(x) = \frac{\gamma(a, \frac{x}{b})}{\Gamma(a)}$
WEIBULL	$F(x) = 1 - \exp\left[-\left(\frac{x}{a}\right)^b\right]$
GAUSSIAN Normal	$F(x) = \frac{1}{\sigma\sqrt{2\pi}} \int_{-\infty}^x \exp\left(-\frac{1}{2}\left(\frac{t-\mu}{\sigma}\right)^2\right) dt$
RAYLEIGH	$F(x) = 1 - \exp\left(-\frac{x^2}{2b^2}\right)$

Table 5.7.: KS-statistics of two-sample KOLMOGOROV-SMIRNOV tests for the normalised time of breaking onset t_{br}/T_P .

$s_{Z,i}$	GUMBEL	Gamma	WEIBULL	Normal	RAYLEIGH
0.033	0.0632	0.0388	0.043	0.0517	0.1489
0.044	0.0516	0.0789	0.1156	0.1058	0.2942
0.055	0.0636	0.0937	0.1282	0.1192	0.3055
0.067	0.0679	0.0878	0.1405	0.1092	0.3457

In order to perform the goodness of fit (GoF) test not only qualitatively, the KS-statistics were determined using the two-sample KOLMOGOROV-SMIRNOV test, which are the maximum distance between the empirical and theoretical distribution function. The results of the KS-statistics of the two-sample KOLMOGOROV-SMIRNOV test are given in Tab. 5.7 for the time of breaking onset t_{br}/T_P and in Tab. 5.8 for the location of breaking onset x_{br}/L_P . The course of the time of breaking onset t_{br}/T_P was represented well by the GUMBEL and Gamma distribution. The course of the location of breaking onset x_{br}/L_P was represented well by the WEIBULL and Gamma distribution.

To complete the GoF test, the output parameters t_{br}/T_P and x_{br}/L_P , respectively, were visually compared with each other in quantile-quantile-plots (qq-plots) with different distribution functions, see Figs. 5.5 and 5.6. The comparison showed that the output parameters followed well the Generalized Extreme Value (GUMBEL's Type I), WEIBULL, and Gamma distribution. Generally, the time of breaking onset t_{br} was better represented by theoretical distribution functions than the location of breaking onset x_{br} . Since

5. Variability of Breaking Onset

Table 5.8.: KS-statistics of two-sample KOLMOGOROV-SMIRNOV tests for the normalised location of breaking onset x_{br}/L_P .

$s_{Z,i}$	GUMBEL	Gamma	WEIBULL	Normal	RAYLEIGH
0.033	0.1211	0.0544	0.0613	0.1582	0.2373
0.044	0.1158	0.0966	0.0840	0.1461	0.2302
0.055	0.0875	0.1019	0.0846	0.1063	0.1705
0.067	0.0714	0.0918	0.0714	0.1020	0.1451

GUMBEL, Gamma and WEIBULL are often used in the extreme value statistics, it is understandable that they represent the extreme values t_{br} and x_{br} very well.

Conclusions

- The GUMBEL and Gamma distribution functions are well suited to represent the distribution of the time of breaking onset t_{br}/T_P .
- The WEIBULL and Gamma distribution functions are well suited to represent the distribution of the location of breaking onset x_{br}/L_P .

5.2. Bivariate Distribution Function

Since the output parameters time and location of breaking onset t_{br} and x_{br} , respectively, depend on one another and did not follow the same marginal distribution, see Fig 5.7 and section 5.1, the classical multivariate approach, in which the marginal distribution functions are multiplied, could not be used to determine the bivariate distribution function. Instead, the copula functions were used which can represent dependent parameters with mixed marginal distributions.

Copula models are a relative new method (last ~ 15 years) in the field of hydraulics, coastal research and engineering. The advantages of the ARCHIMEDEAN copulas are that they are flexible and easy to construct. GUMBEL, CLAYTON and FRANK were chosen here because they are applicable for multivariate frequency analyses, that is, the analysis of the frequency of occurrence of values of a phenomenon less than a reference value, and they cover the full range of tail behaviour. The CLAYTON copula has lower tail dependence, while the FRANK copula has no tail dependence and the GUMBEL copula has only upper tail dependence. A brief summary of the theory of copulas is given below

5.2. Bivariate Distribution Function

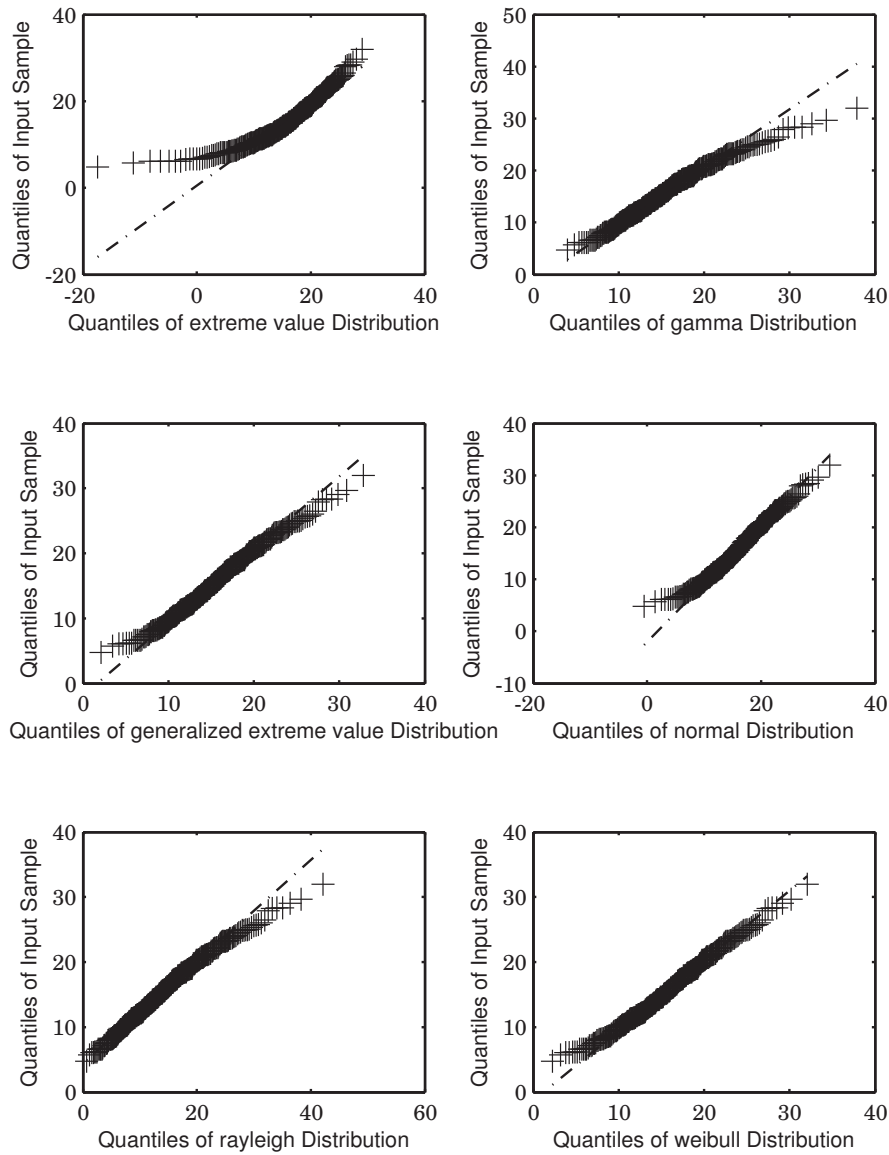


Figure 5.5.: qq-plots of output parameter time of breaking onset t_{br}/T_P against theoretical distributions for the test runs with initial spectral steepness $s_{Z,i} = 0.033$.

5. Variability of Breaking Onset

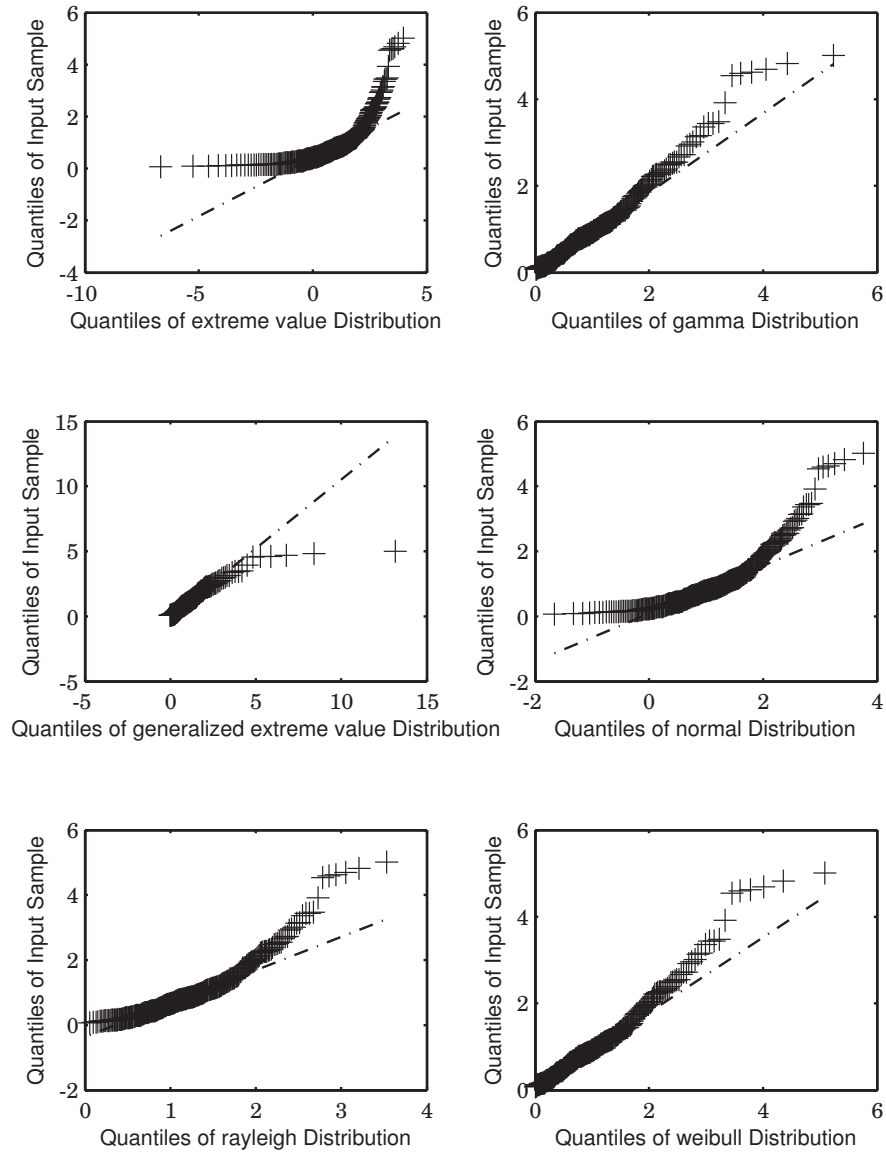


Figure 5.6.: qq-plots of output parameter location of breaking onset x_{br}/L_P against theoretical distributions for the test runs with initial spectral steepness $s_{Z,i} = 0.033$.

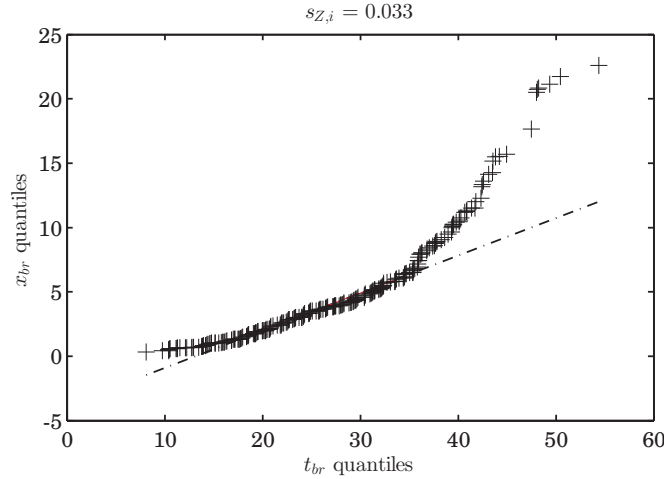


Figure 5.7.: qq-plot of output parameter location of breaking onset x_{br} against time of breaking onset t_{br} for the test runs with initial spectral steepness $s_{Z,i} = 0.033$.

and then demonstrated exemplarily with the value pair (X, Y) with $X = t_{br}/T_P$ and $Y = x_{br}/L_P$ for the test runs with a spectral steepness of $s_{Z,i} = 0.033$. The final results of the cumulative distribution functions $H(x, y)$ and the exceedance probabilities P_E for the other initial spectral steepnesses $s_{Z,i}$ are given in the annex.

5.2.1. Copula Approach

Copulas are multivariate distribution functions whose one-dimensional margins are uniform on the interval $(0, 1)$ (Nelsen, 2006). The copula approach to dependence modelling is rooted in a representation theorem due to Sklar (1959). It states that the joint cumulative distribution function $H(x, y)$ of any pair¹ (X, Y) of continuous random variables may be written in the form

$$H(x, y) = C\{F(x), G(y)\}, \quad x, y \in \mathbb{R} \quad (5.2)$$

where $F(x)$ and $G(y)$ marginal distributions; and $C : [0, 1]^2 \rightarrow [0, 1]$ = copula.

$$C(u) = H(F^{-1}(x), G^{-1}(y)) \quad (5.3)$$

with pseudo-inverse F^{-1} and G^{-1} (Genest and Favre, 2007).

The name ‘‘copula’’ was chosen to emphasize the manner in which a copula ‘‘couples’’

¹Restricting attention to the bivariate case for the sake of simplicity.

5. Variability of Breaking Onset

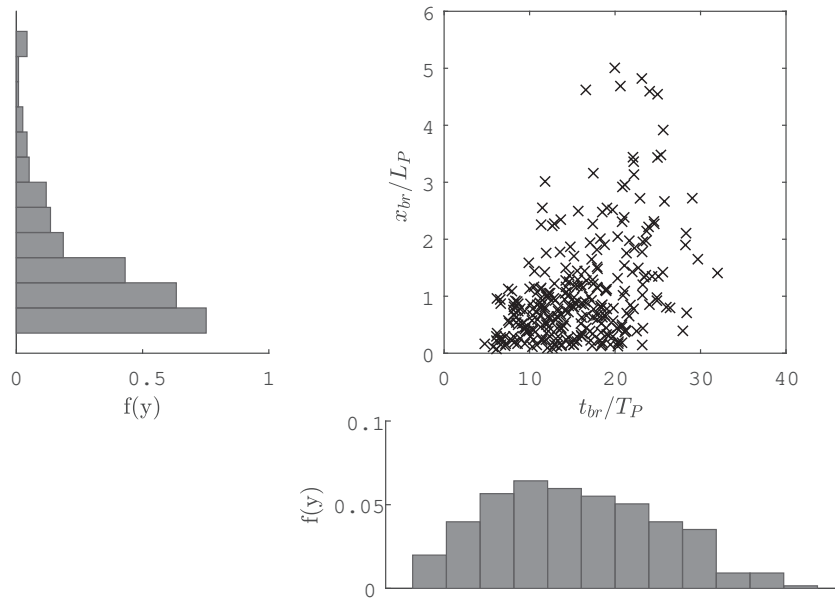


Figure 5.8.: Value pairs $(t_{br}/T_P, x_{br}/L_P)$ and their respective histograms for the test runs with initial spectral steepness $s_{Z,i} = 0.033$.

a joint distribution function to its univariate margins (Nelsen, 2006, p. 18/28). An unique copula associated with a random pair (X, Y) is invariant by monotone increasing transformations of the marginals (Genest and Favre, 2007). In order to determine the underlying dependency between two parameters (X, Y) using a copula function, all ties (duplicate values) of the pair must be removed in the first step since the parameters must be continuous.

The steps to determine an appropriate copula function were illustrated here exemplarily using the value pair (X, Y) with $X = t_{br}/T_P$ and $Y = x_{br}/L_P$ for the test runs with a spectral steepness of $s_{Z,i} = 0.033$. The total test number was $n_{max} = 288$, so there were 288 value pairs. In Fig. 5.8 the original pairs of values (X, Y) including their respective relative frequency as histograms are shown.

Then the value pairs (X, Y) were sorted according to the parameter $X = t_{br}/T_P$ so that the parameter increased in magnitude and $X = X_1, \dots, X_n$ with $X_1 < X_n$; thus, the value pairs were sorted according to their rank. The resulting ranked values (R, S) are shown in Fig. 5.9 including their respective histograms. The marginal distributions of R and S are uniform.

To test the dependence of the two parameters on each other, KENDALL's τ_n and SPEAR-

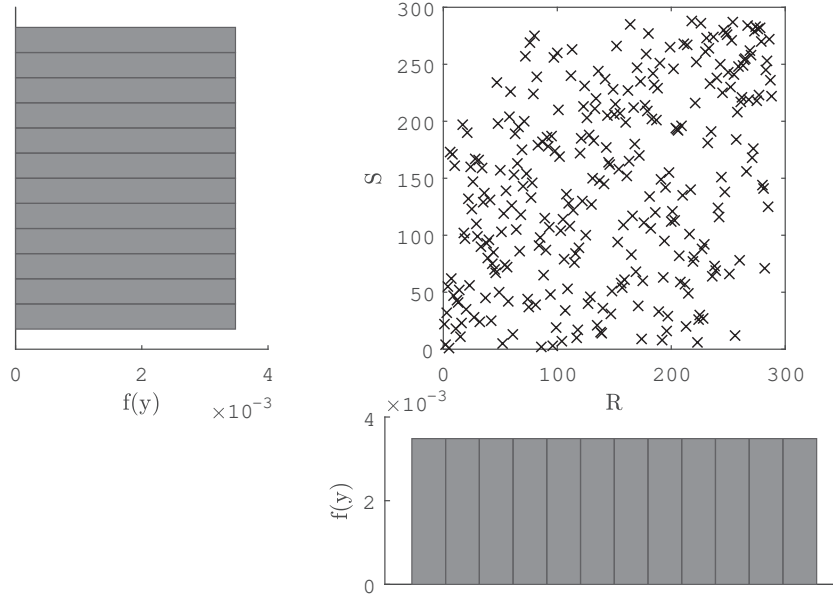


Figure 5.9.: Ranked values (R, S) and their respective histograms for the test runs with initial spectral steepness $s_{Z,i} = 0.033$.

MAN's ρ were used, see Eqs. (5.4) and (5.5). If τ_n and ρ are close to zero, the parameters are independent; if they are close to 1, the parameters are dependent.

$$\rho = \frac{\sum_{i=1}^n (R_i - \bar{R}) (S_i - \bar{S})}{\sqrt{\sum_{i=1}^n (R_i - \bar{R})^2 \sum_{i=1}^n (S_i - \bar{S})^2}} \in [-1, 1] \quad (5.4)$$

where

$$\bar{R} = \frac{1}{n} \sum_{i=1}^n R_i = \frac{n+1}{2} = \frac{1}{n} \sum_{i=1}^n S_i = \bar{S}$$

$$\tau_n = \frac{P_n - Q_n}{\binom{n}{2}} = \frac{4}{n(n-1)/2} P_n - 1 \quad (5.5)$$

For the data sample here KENDALL's τ was $\tau = -0.97$ and SPEARMAN's ρ was $\rho = 0.4$. Thus the value pair $(t_{br}/T_P, x_{br}/L_P)$ was dependent on each other.

5. Variability of Breaking Onset

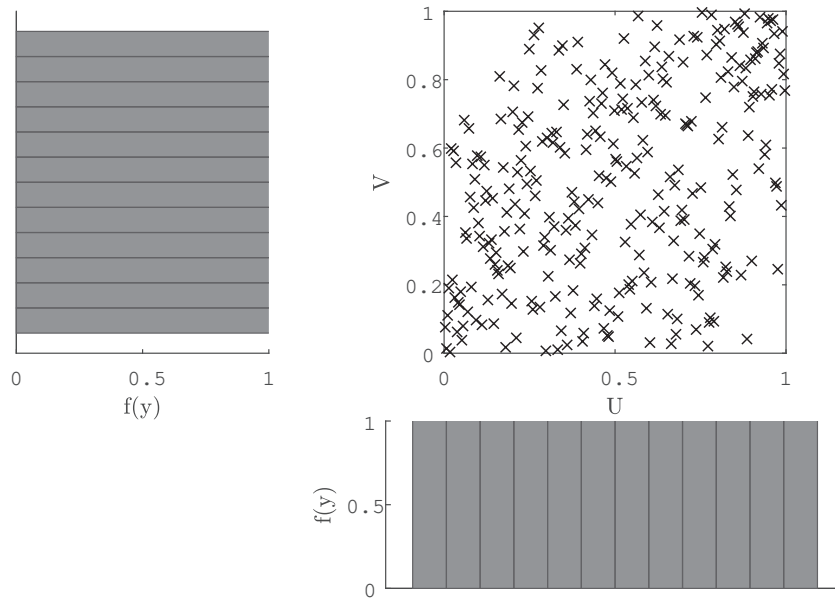


Figure 5.10.: Normalised ranked values (U, V) and their respective histograms for the test runs with initial spectral steepness $s_{Z,i} = 0.033$.

In the next step, the axes were re-scaled by normalising the ranked values with $1/(n+1)$, so that the marginal distributions of R and S were uniform in the range $[0, 1]$. The result of the normalised ranked values (U, V) is shown in Fig. 5.10. Normalising the ranked values forms the domain of the so-called empirical copula, see Deheuvels (1979), formally defined by

$$C_n(u, v) = \frac{1}{n} \sum_{i=1}^n \mathbf{1} \left(\frac{R_i}{n+1} \leq u, \frac{S_i}{n+1} \leq v \right)$$

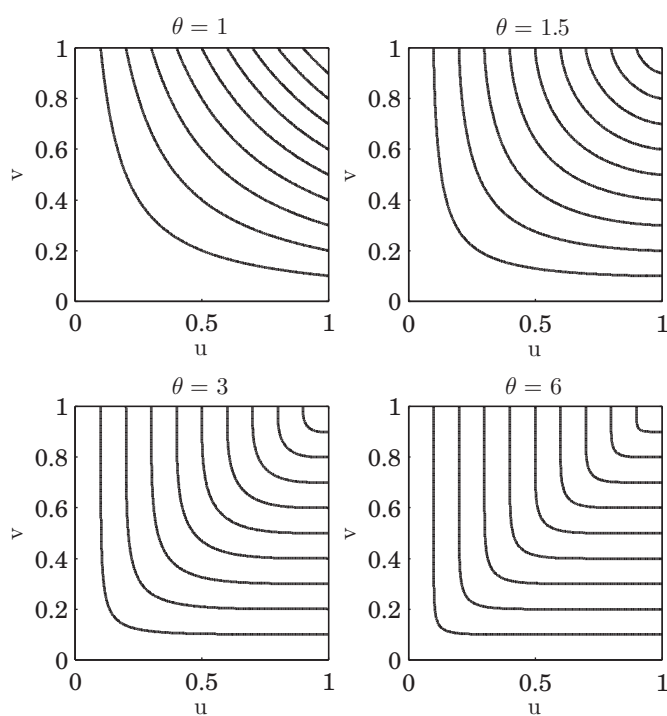
with $\mathbf{1}(A)$ denoting the indicator function of set A . The empirical copula can be seen as the empirical distribution of the rank transformed data.

In the next step, the empirical copula C_n was compared with the theoretical copula families FRANK, GUMBEL, and CLAYTON, and the parameter Θ was estimated. In Tab. 5.9 the three ARCHIMEDEAN copulas are summarised, which were used in the evaluation. The influence of the parameter Θ on the form of the copula is shown exemplarily for the GUMBEL copula in Fig. 5.11.

The results of the parameter Θ of the three copula families FRANK, GUMBEL, and CLAYTON are summarised for each spectral steepness $s_{Z,i}$ in Tab. 5.10. In the estimation

Table 5.9.: Summary of the three one-parameter (Θ) ARCHIMEDEAN copulas. $t = u$ or $t = v$. $s = \varphi(u) + \varphi(v)$.

Family	Generator $\varphi(t)$	Generator inverse or copula function $\varphi^{-1}(s) = C_{\Theta}(s)$	Parameter space
Frank (1979)	$-\ln \frac{e^{-\Theta t} - 1}{e^{-\Theta} - 1}$	$-\Theta^{-1} \ln(1 + e^{-s}(e^{-\Theta} - 1))$	$\Theta \geq 0$
Gumbel (1960)	$(-\ln t)^{\Theta}$	$\exp(-s^{1/\Theta})$	$\Theta \geq 1$
Clayton (1978)	$t^{-\Theta} - 1$	$(1 + s)^{-1/\Theta}$	$\Theta \geq 0$

Figure 5.11.: The influence of the parameter Θ on the form of the copula shown exemplarily for the GUMBEL copula.

5. Variability of Breaking Onset

Table 5.10.: Compilation of the results of the parameter Θ for the copula families FRANK, GUMBEL, and CLAYTON for each spectral steepness $s_{Z,i}$.

$s_{Z,i}$	FRANK	GUMBEL	CLAYTON
0.010	10.23	2.76	1.79
0.020	7.34	2.10	1.89
0.027	4.78	1.77	0.82
0.033	2.60	1.36	0.49
0.035	2.45	1.30	0.50
0.044	1.76	1.22	0.38
0.050	1.11	1.15	0.23
0.055	0.82	1.09	0.27
0.067	0.39	1.14	0.05
0.071	0.19	1.03	0.06

of Θ , the significance level for confidence intervals was $\alpha = 0.05$ and the fitting method was the maximum likelihood method.

The larger the initial spectral steepness $s_{Z,i}$ the smaller the optimal parameter Θ , that is, that for larger spectral steepnesses the theoretical copula did not need to be adjusted to the empirical copula as much as for smaller spectral steepnesses.

In order to get a first impression which copula family was best suited to represent the relation between t_{br}/T_P and x_{br}/L_P , the empirical copula $C_n(u, v)$ was compared with the three theoretical copula families, and their contour plots are shown in Fig. 5.12. It seems that the empirical copula $C_n(u, v)$ follow the GUMBEL copula best.

Another approach to get an impression which copula family was best suited to represent the relation between t_{br}/T_P and x_{br}/L_P , generic random samples from the copula families were generated in the copula space, and then transformed into the original scale of the parameters. The results for the test runs with a spectral steepness of $s_{Z,i} = 0.033$ is shown in Fig. 5.13. 500 value pairs were randomly generated based on the copula families. It seems that the value pairs $(t_{br}/T_P, x_{br}/L_P)$, follow the GUMBEL copula best.

For the other initial spectral steepnesses, in addition to $s_{Z,i} = 0.033$, generic random samples from the copula families were also generated and the normalised time of breaking onset t_{br}/T_P is plotted against the initial spectral steepness $s_{Z,i}$, see Fig. 5.14. The random samples generated from the copula families confirmed the observations that 1) wave trains break earlier with increasing spectral steepness and 2) the scatter of the

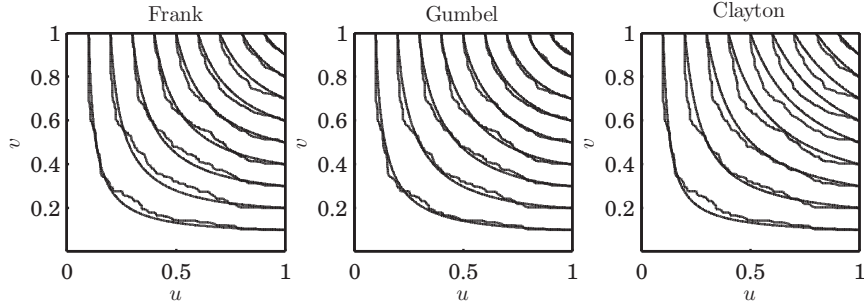


Figure 5.12.: Contour plots of the empirical copula $C_n(u, v)$ and the three ARCHIMEDEAN copulas for the test runs with initial spectral steepness $s_{Z,i} = 0.033$.

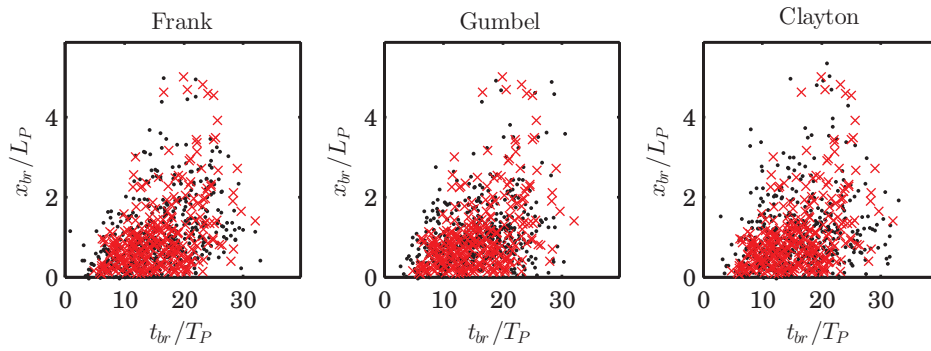


Figure 5.13.: Comparison of original NWF simulated data (red cross markers) and copula generated data (black round markers) for the test runs with initial spectral steepness $s_{Z,i} = 0.033$.

5. Variability of Breaking Onset

Table 5.11.: RMSEs and values for the KS-statistic from comparing theoretical and empirical copula functions for the parameters t_{br}/T_p and x_{br}/L_P , and for the test runs with initial spectral steepness $s_{Z,i} = 0.033$.

Function	RMSE	KS-statistic
FRANK copula	0.0129	0.0483
GUMBEL copula	0.0094	0.0306
CLAYTON copula	0.0198	0.0373

results decreases with increasing spectral steepness.

In order to determine the goodness of fit more precisely, qq-plots, root-mean-square-error-values (RMSE), and two-sample Kolmogorov-Smirnov tests (KS-statistics) were performed. The execution of several GoF tests intended to minimize the uncertainty of selecting a copula family. Particular attention was paid to which copula family suits the tail dependency best in the upper right corner, as this is important for probabilities of exceedance. In Fig. 5.15 the qq-plots for the original NWF simulated data and copula generated data for t_{br}/T_P and x_{br}/L_P are shown. The qq-plots for t_{br}/T_P were very similar to each other, with the GUMBEL und CLAYTON copula seeming to be the best fit. For the output parameter x_{br}/L_P , the differences between the copula families were clearer, but also here the GUMBEL and CLAYTON copula fit best.

In Tab. 5.11, the RMSE values and the values for the KS-statistic are shown. RMSE values described the deviations between the empirical copula C_n and the theoretical copula functions. The KS-statistic, on the other hand, described the maximum distance between two probability distributions, which in turn were based on the NWF simulated and on the randomly generated data from the copulas; therefore the values of the KS-statistic varied slightly according to the randomly generated data sample. The observed trend, however, remained the same: the GUMBEL copula showed the lowest RMSEs and values of the KS-statistic. The differences among the copula families, however, were small.

A convergence analysis regarding the parameter Θ showed that the analysis for the GUMBEL copula was the fastest convergence, that is, less data was needed for the GUMBEL copula to obtain the optimal parameter Θ . This result supported the choice for the GUMBEL copula.

The resulting cumulative distribution function $H(x, y)$ calculated with the GUMBEL copula, see Eq. (5.2), is represented in Fig. 5.16 for a spectral steepness $s_{Z,i} = 0.033$. The results for the other spectral steepnesses are given in the annex, see Figs. B.1 to B.17.

5.2. Bivariate Distribution Function

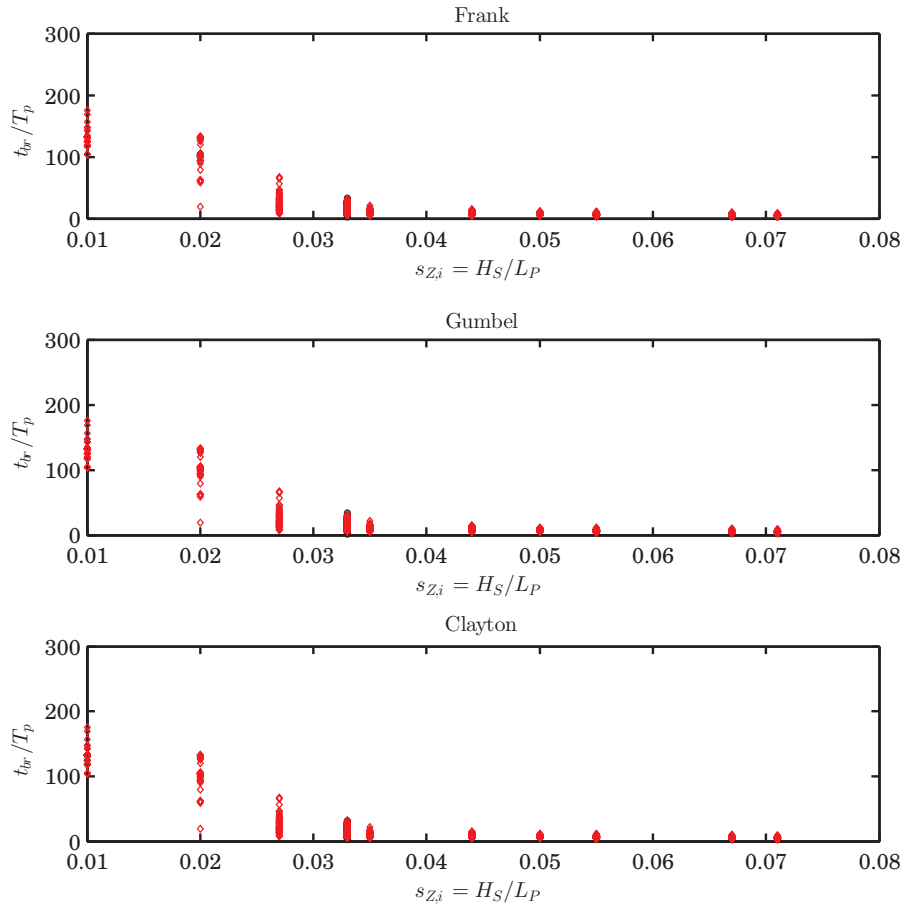


Figure 5.14.: Development of normalised time of breaking onset t_{br}/T_P against initial spectral steepness $s_{Z,i} = H_S/L_P$ for original NWF simulated data (red cross markers) and copula generated data (black round markers) for FRANK, GUMBEL and CLAYTON copula.

5. Variability of Breaking Onset

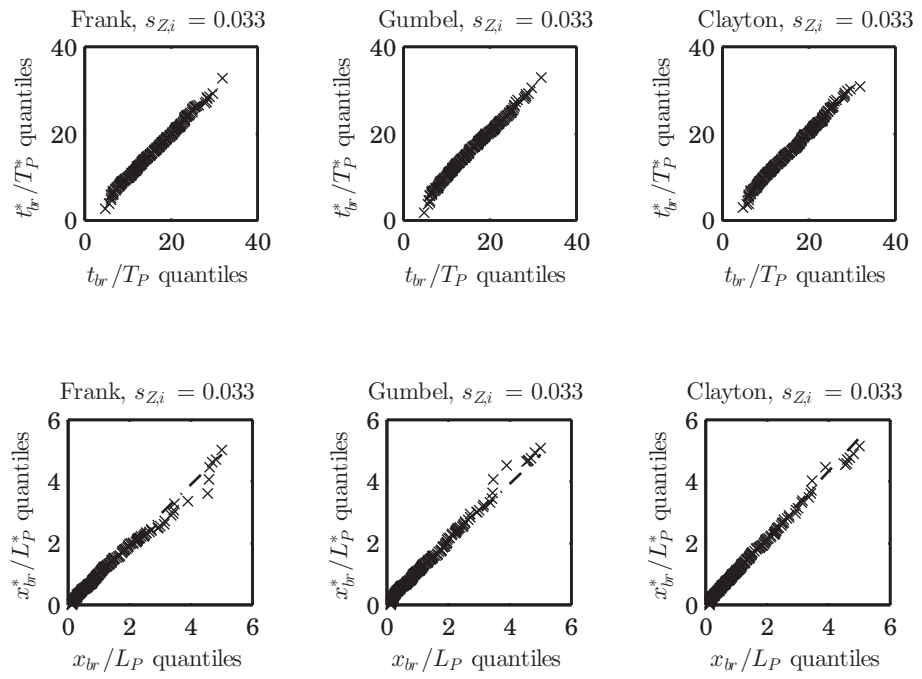


Figure 5.15.: qq-plots with original NWF simulated data and copula generated data of t_{br}/T_P and x_{br}/L_P .

Table 5.12.: Geometrical parameters for the breaking wave crest for the exemplary value pairs in Fig. 5.17.

t_{br}/T_P	x_{br}/L_P	s_Z	s'_C	μ_H
13.65	2.34	0.061	0.112	0.63
17.89	1.52	0.059	0.180	0.79
19.81	0.79	0.062	0.105	0.58

The resulting bivariate joint exceedance probability P_E is (Wahl et al., 2012, p. 101):

$$\begin{aligned} P_E &= P(X > x \wedge Y > y) = 1 - F(x) - G(y) + H(x, y) \\ &= 1 - F(x) - G(y) + C[F(x), G(y)] \end{aligned} \quad (5.6)$$

The contours of some joint exceedance probabilities calculated with the GUMBEL copula are shown in Fig. 5.17 for the test runs with spectral steepness $s_{Z,i} = 0.033$. The results for the other spectral steepnesses are given in the annex, see Figs. B.2 to B.18. The computation of the cumulative distribution function $H(x, y)$ and the bivariate joint exceedance probability P_E was based on 500 randomly generated value pairs whose distribution follows the GUMBEL copula. In Fig. 5.17 three exemplary value pairs from the numerical simulations, which have an exceedance probability of $P_E = 0.4$, are marked blue. Although they share the same exceedance probability, the shapes of the underlying wave are different. The steepness of the breaking wave crest $s_Z = H/L$, the crest front steepness $s'_C = a_C/L'$ and the horizontal asymmetry $\mu_H = a_C/H$ of the three exemplary value pairs from the numerical simulations are summarised in Tab. 5.12. The definition of the wave parameters can be found in Fig. 2.1.

Conclusions

- The GUMBEL copula is well suited to represent the relation between time and location of breaking onset $(t_{br}/T_P, x_{br}/L_P)$. However, the differences of the GoF tests among the three analysed copula families are small.
- By means of the computed cumulative distribution functions and joint exceedance probabilities for every spectral steepness $s_{Z,i}$, which were considered in this thesis, one can determine the probability with which a certain combination of time and location of breaking onset $(t_{br}/T_P, x_{br}/L_P)$ is undercut or exceeded.

5. Variability of Breaking Onset

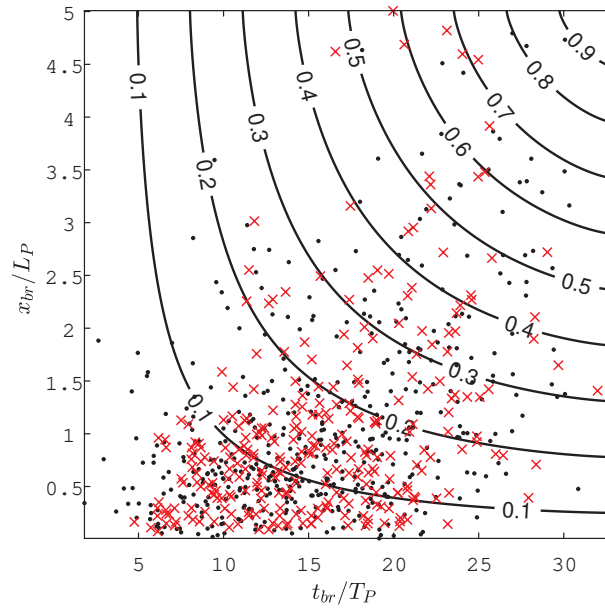


Figure 5.16.: Cumulative distribution function $H(x, y)$ calculated with the GUMBEL copula for the test runs with spectral steepness $s_{Z,i} = 0.033$, with original NWF simulated data (red cross markers) and copula generated data (black round markers).

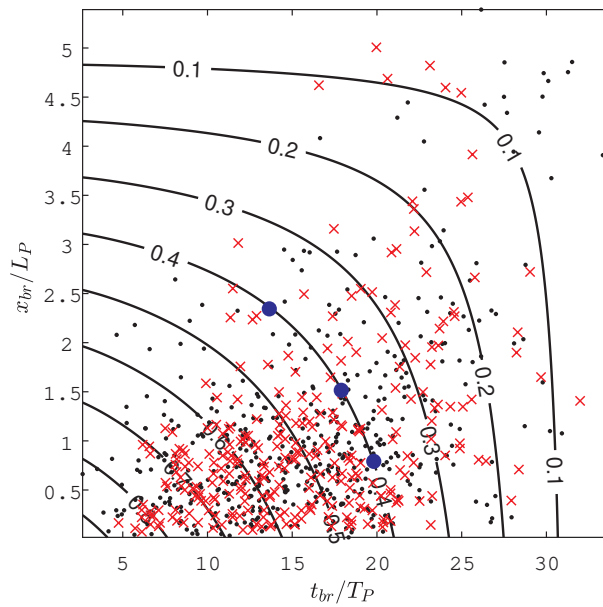


Figure 5.17.: Exceedance probability P_E calculated with the GUMBEL copula for the test runs with spectral steepness $s_{Z,i} = 0.033$, with original NWF simulated data (red cross markers) and copula generated data (black round markers).

5.2.2. Uncertainty assessment

Firstly, uncertainties emerged from estimating the structure of dependence or the copula parameter, Θ , respectively, from a random sample of the considered parameters. Further uncertainties resulted from fitting univariate distribution functions to the marginal parameters and from choosing certain bivariate models. However, the application of four GoF tests to choose proper copula functions minimised the uncertainties.

5.3. Optimal Sample Size

Since the phenomenon of wave breaking is random and intermittent, its output parameters such as time, location and shape of the breaking wave are strongly scattered. In order to determine the necessary number of test runs for a robust determination of the phenomenon, a convergence analysis was carried out on the basis of the output parameter time of breaking onset t_{br} . In the first step, only the NWF simulated data was used for this, and then the existing data base was expanded by the data generated from the GUMBEL copula which represented the relationship of $(t_{br}/T_P, x_{br}/L_P)$ well. The result was the optimal sample size N_{opt} , which was determined for each initial spectral steepness $s_{Z,i}$ and the permissible deviations 1%, 2%, 5% and 10%. N_{opt} was determined dependent upon $s_{Z,i}$, since the scattering of the parameter t_{br} depended on $s_{Z,i}$ and thus the optimal sample size N_{opt} did, too. The original data basis was extended with the data generated from the GUMBEL copula since the optimal sample size N_{opt} depended on the initial sample size.

5.3.1. Optimal Sample Size Based on NWF Data

For the determination of the optimal sample size N_{opt} , a convergence analysis was performed with the normalised time of breaking onset t_{br}/T_P . The data sample with breaking wave trains was selected in which only the input parameter $s_{Z,i}$ was variable and all other input parameters were fixed². Since the scatter of t_{br}/T_P depends significantly on the initial spectral steepness $s_{Z,i}$, a convergence analysis was performed for each $s_{Z,i}$. In the convergence analysis, the median was formed from the normalised time of breaking onset t_{br}/T_P by increasing the number n of the considered test runs. That is, in the first step, the median from $(t_{br}/T_P)_n$ was determined with $n = 1$, in the second step from $(t_{br}/T_P)_n$ with $n = 2$, etc. until n equates to the maximum available test run number n_{max} . The resulting vectors were projected to zero by subtracting the median

² $N_W = 192, h = 0.7\text{m}, \gamma = 3.3.$

5. Variability of Breaking Onset

$(\widetilde{t_{br}/T_P})_{n_{max}}$, and then normalised by dividing them by the median, see Eqs. (5.7) and (5.8).

$$(\widetilde{t_{br}/T_P}) = \begin{cases} x_{\frac{n+1}{2}} & n \text{ odd} \\ \frac{1}{2} (x_{\frac{n}{2}} + x_{\frac{n}{2}+1}) & n \text{ even} \end{cases} \quad (5.7)$$

$$\Delta(\widetilde{t_{br}/T_P})^*(n) = \frac{(\widetilde{t_{br}/T_P})(n) - (\widetilde{t_{br}/T_P})}{(\widetilde{t_{br}/T_P})} \quad (5.8)$$

Because the course of $\Delta(\widetilde{t_{br}/T_P})^*$ depended strongly on the order of values in t_{br}/T_P , the original vectors of t_{br}/T_P were uniformly random distributed before each analysis. This process was repeated 10,000 times. In Fig. 5.18 the convergence analysis for the normalised time of breaking onset t_{br}/T_P is shown exemplarily for $s_{Z,i} = 0.033, 0.044, 0.055, 0.071$ and, for a better representation, with only 3,000 repetitions. It can be observed that the bandwidth of resulting differences between $(\widetilde{t_{br}/T_P})$ and $(\widetilde{t_{br}/T_P})(n)$ decreased with increasing number of considered test runs. Furthermore, it can be observed that as the spectral steepness $s_{Z,i}$ increased, the difference of the normalised median $\Delta(\widetilde{t_{br}/T_P})^*$ converged more rapidly; this was because with increasing spectral steepness, the scatter of the normalised time of breaking onset t_{br}/T_P decreased.

Then the sample size n for $\Delta(\widetilde{t_{br}/T_P})^* = 0.01, 0.02, 0.05, 0.10$ was determined from the mean value of all convergence curves; these values were the optimal sample size N_{opt} with permissible deviations 1%, 2%, 5% and 10%.

Tab. 5.13 summarises the results of N_{opt} , median value \tilde{x} , standard deviation σ and the coefficient of variation $cv = \sigma/\tilde{x}$ (mean value \tilde{x}).

The results in Tab. 5.13 and Fig. 5.19 show that the larger the permissible deviation the smaller the optimal sample size N_{opt} . For example, for $s_{Z,i} = 0.033$ $N_{opt} = 245$ was required to be able to determine t_{br}/T_P with an deviation of 1%, but only $N_{opt} = 59$ with an deviation of 5%.

The dependence of the optimal sample size on the spectral steepness, or rather, on the scattering of the parameter, on the permissible deviation, and on the initial sample size n_{max} was clearly visible. Generally speaking, the optimum sample size N_{opt} decreased with increasing spectral steepness $s_{Z,i}$, i.e. the greater the spectral steepness the fewer tests were required to determine the time of breaking onset with a certain error. This was due to the fact that the scatter of t_{br}/T_P decreased with increasing spectral steepness $s_{Z,i}$. Please note, that the ratio of standard deviation and mean value, which is the

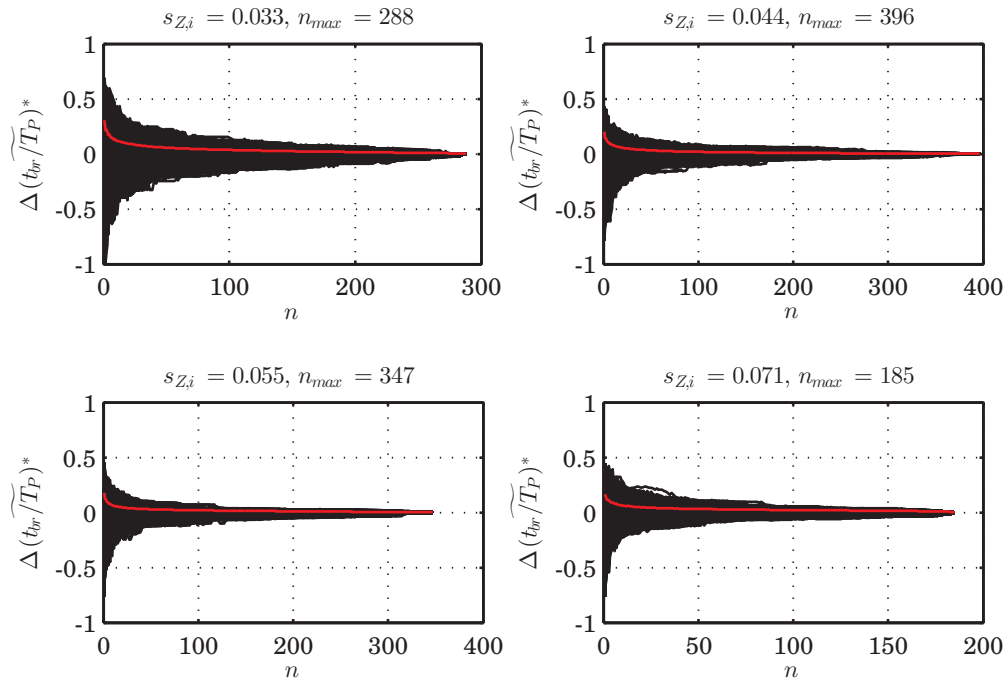


Figure 5.18.: Convergence analysis for the normalised time of breaking onset t_{br}/T_P against the number of considered test runs for $s_{Z,i} = 0.033, 0.044, 0.055, 0.071$ with mean value of all convergence curves (red). Repeats: 3,000.

5. Variability of Breaking Onset

Table 5.13.: Optimal sample size N_{opt} for the median value of the normalised time of breaking onset t_{br}/T_P with a permissible deviation of 1%, 2%, 5% and 10% based on the NWF data. Repeats: 10,000.

$s_{Z,i}$	n_{max}	\tilde{x}	σ	cv	1%	2%	5%	10%
0.010	85	133	10	0.08	4	2	1	1
0.020	69	102	22	0.21	16	10	4	2
0.027	99	22	12	0.49	96	84	50	21
0.033	288	15	6	0.35	245	174	59	17
0.035	171	10	3	0.28	134	96	33	7
0.044	396	8	2	0.24	182	94	24	5
0.050	142	7	1	0.20	95	61	15	3
0.055	347	6	1	0.21	202	93	17	3
0.067	146	5	1	0.21	104	56	11	3
0.071	185	5	1	0.21	172	109	17	3

coefficient of variation cv , had a significant influence on the optimum sample size, which can be seen for the results for the spectral steepnesses $s_{Z,i} = 0.02$ and $s_{Z,i} = 0.027$. The optimal sample size was largest for the spectral steepness $s_{Z,i} = 0.027$, although the scatter of the parameter was larger for $s_{Z,i} = 0.02$. This observations can be explained by the coefficient of variation cv : although the mean value of t_{br}/T_P for $s_{Z,i} = 0.027$ is only 1.5 times the mean value for $s_{Z,i} = 0.044$, the coefficient of variation is six times larger. In order to investigate the influence of the sample size n_{max} on the optimal sample size N_{opt} , the sample size was increased by means of the GUMBEL copula function and the convergence analysis was repeated, see next subsection 5.3.2. Before that, however, the influence of the number of repetitions of the convergence analysis on the optimal sample size was investigated. As mentioned above, the order of the values in t_{br}/T_P had an influence on the convergence analysis, so the vectors of t_{br}/T_P were uniformly random distributed for each repetition. It can be observed that for $repeats \geq 1,000$ the number of repetitions had no significant influence on the resulting optimal sample size N_{opt} .

5.3.2. Optimal Sample Size Based on Copula Generated Data

In section 5.2 it was shown that the output parameters $(t_{br}/T_P, x_{br}/L_P)$ followed the GUMBEL copula. By means of this copula function, any number of random value pairs following the GUMBEL function can be generated. Thus, the existing sample size was

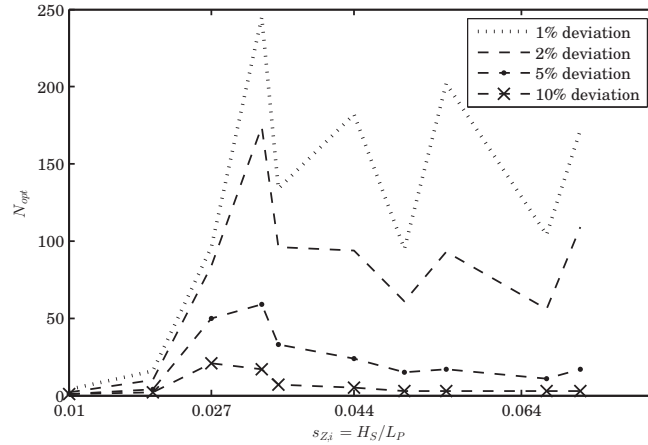


Figure 5.19.: Optimal sample size N_{opt} for the median value of the normalised time of breaking onset t_{br}/T_P with a permissible deviation of 1%, 2%, 5% and 10% based on the NWF data for all $s_{Z,i}$. Repeats: 10,000.

increased and the convergence analysis repeated with this increased sample to investigate the influence of the initial sample size n_{max} on the optimal sample size N_{opt} . In a first step, the same sample sizes per $s_{Z,i}$ as in the NWF simulations were generated by means of the GUMBEL copula function to show that the copula generated data led to the same results for the optimal sample size N_{opt} as the NWF data. Subsequently, the sample size n_{max} with which the convergence analysis was carried out was increased step by step to show its influence on the resulting optimal sample size N_{opt} .

The optimal sample sizes N_{opt} for the NWF data and the copula generated data are shown in Fig. 5.21. The initial sample size for the convergence analysis with the copula generated data corresponded to the sample size of the NWF data. It can be seen that the differences between the copula generated data and the NWF data were largest with a permissible deviation of 1%. However, the differences of N_{opt} decreased rapidly with increasing permissible deviation. Therefore, the GUMBEL copula was used to increase the sample size and to repeat the convergence analysis with an enlarged sample. The optimal sampling sizes N_{opt} are shown in Fig. 5.22 depending on the permissible deviation and the initial sample size. The larger the permissible deviation the lower the influence of the initial sample size on the optimal sample size. For a permissible deviation of 1% and 2%, the initial sample size had a significant influence on the resulting optimal sample size N_{opt} ; the influence was negligible only from an initial sample size of $n \geq 5,000$ test runs. With a permissible deviation of 5% or 10%, the influence of the initial sample size on the

5. Variability of Breaking Onset

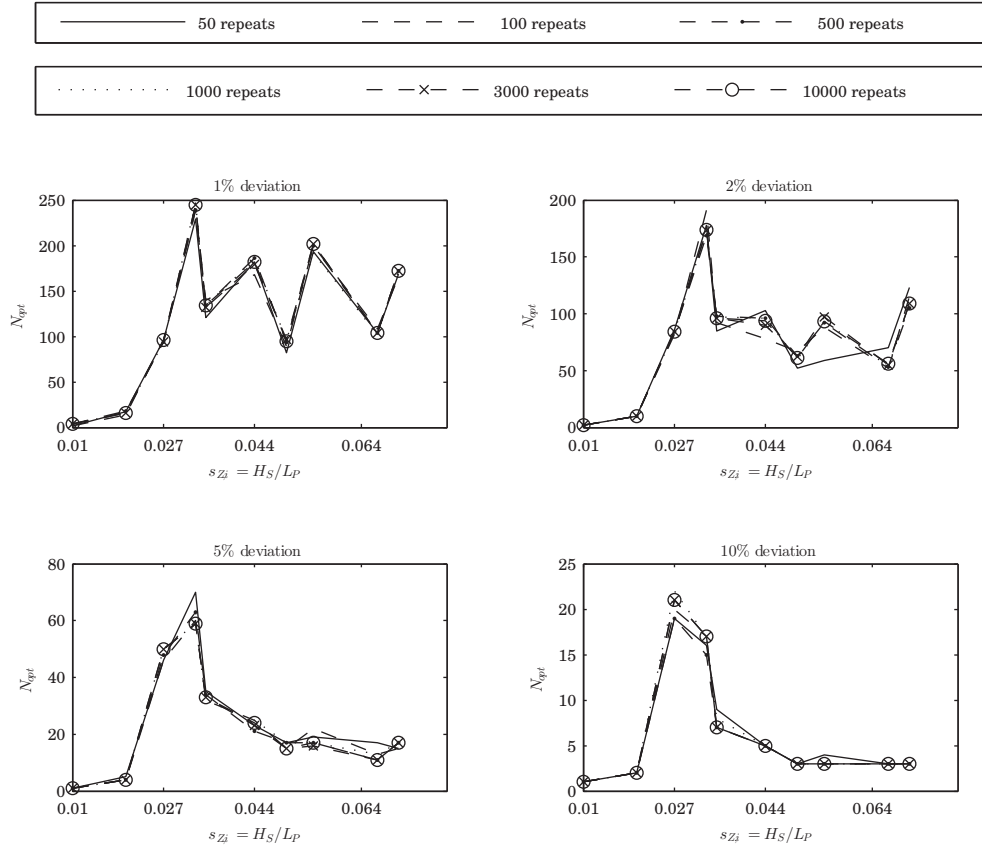


Figure 5.20.: Optimal sample size N_{opt} for the median value of the normalised time of breaking onset t_{br}/T_P with a permissible deviation of 1%, 2%, 5% and 10% based on the NWF data for different repetitions of the convergence analysis.

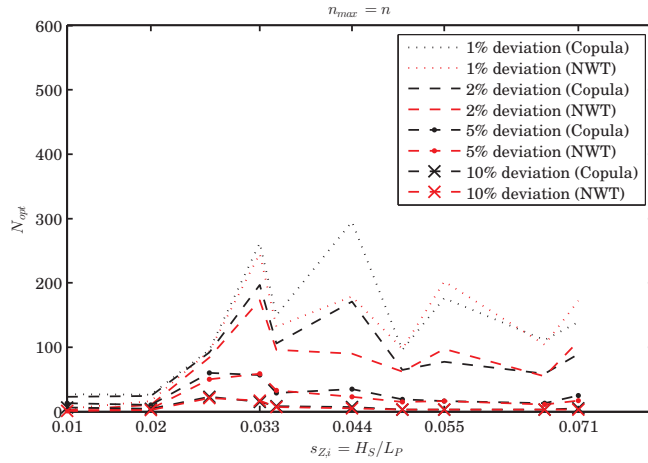


Figure 5.21.: Optimal sample size N_{opt} for the median value of the normalised time of breaking onset t_{br}/T_P with a permissible deviation of 1%, 2%, 5% and 10% based on the NWT data and copula generated data with the same initial sample size per spectral steepness. Repeats: 3,000.

optimal sample size was negligible from an initial sample size of $n \geq 1,000$. It is unclear why the initial sample size had a significant influence on the optimal sample size; for example, with a permissible deviation of 1% an initial sample size of at least 5,000 test runs had to be considered to conclude that the optimal sample size was approximately 1,800 test runs. In Tab. 5.14 the results for the optimal sample sizes N_{opt} based on the simulated NWT data and the GUMBEL copula generated data are listed. The median value, the standard deviation, and the coefficient of variation for the normalised time of the wave breaking t_{br}/T_P were quasi identical for both data sets; this suggests that the data generated from the GUMBEL copula represented well the behaviour of the time and location of breaking onset. The resulting optimal sample sizes N_{opt} from the two data sets differed significantly for a permissible deviation of 1% and 2%; except for a deviation of 2% and a spectral steepness of $s_{Z,i} = 0.055$ and $s_{Z,i} = 0.071$. With a permissible deviation of 5% and 10%, the differences between the two data sets were not significant. Considering all initial spectral steepnesses and a permissible deviation of 1%, approximately 1,800 test runs were sufficient to determine the median of the normalised time of breaking onset t_{br}/T_P , see Fig. 5.22. With a deviation of 2% it was $N_{opt} = 580$, with a deviation of 5% it was $N_{opt} = 100$, and with a deviation of 10% it was $N_{opt} = 25$.

5. Variability of Breaking Onset

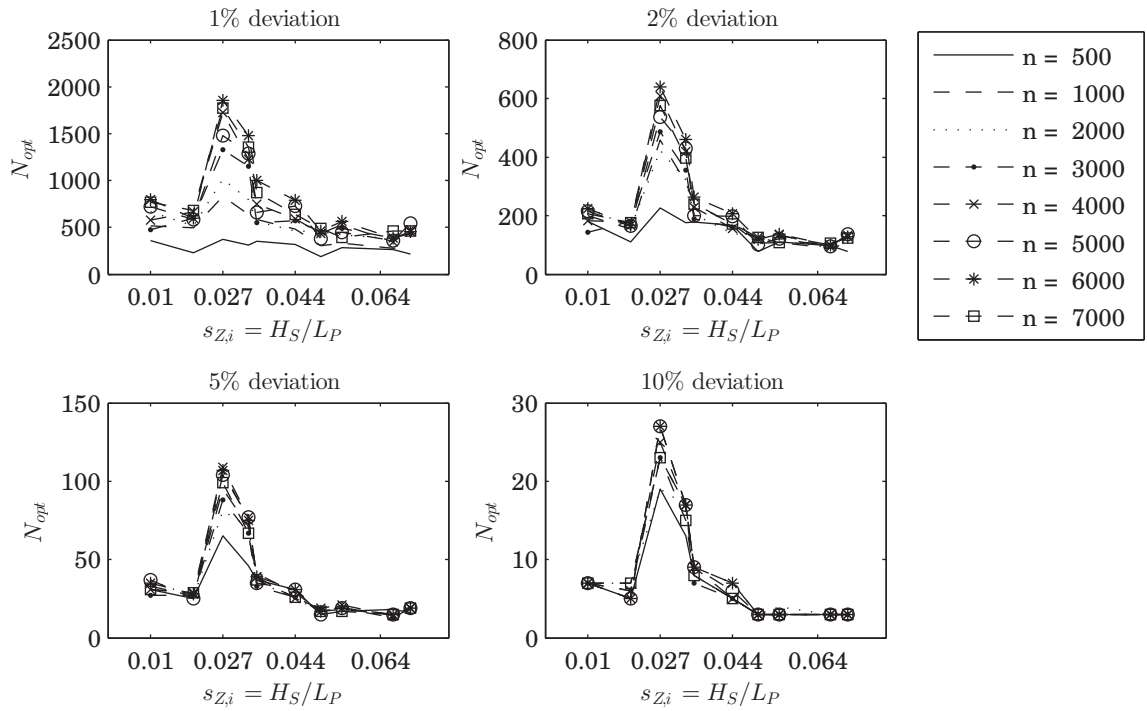


Figure 5.22.: Optimal sample size N_{opt} for the median value of the normalised time of breaking onset t_{br}/T_P with a permissible deviation of 1%, 2%, 5% and 10% based on copula generated data with different initial sample sizes n_{max} . Repeats: 3,000.

Table 5.14.: Optimal sample size N_{opt} for the median value of the normalised time of breaking onset t_{br}/T_P with a permissible deviation of 1%, 2%, 5% and 10% based on the NWF simulated data and copula generated data (in italic) for the test runs with initial spectral steepness $s_{Z,i} = 0.033, 0.044, 0.055, 0.071$. Repeats: 10,000 (NWF) and 3,000 (GUMBEL copula).

$s_{Z,i}$	n_{max}	\tilde{x}	σ	cv
0.033	288/7,000	15/15	6/6	0.35/0.37
0.044	396/7,000	8/8	2/2	0.24/0.25
0.055	347/7,000	6/6	1/1	0.21/0.22
0.071	185/7,000	5/5	1/1	0.21/0.22

$s_{Z,i}$	1%	2%	5%	10%
0.033	245/1,495	174/427	59/73	17/17
0.044	182/752	94/196	24/31	5/7
0.055	202/464	93/125	17/19	3/3
0.071	172/453	109/117	17/19	3/3

Conclusions

To determine the median of the normalised time of breaking onset t_{br}/T_P :

- with a permissible deviation of 1%, approximately 1,800 test runs are sufficient.
- with a permissible deviation of 2%, approximately 580 test runs are sufficient.
- with a permissible deviation of 5%, approximately 100 test runs are sufficient.
- with a permissible deviation of 10%, approximately 25 test runs are sufficient.

6. Detection and Prediction of Breaking Onset in Wave Trains

In the following chapter, the deformation and development of breaking and non-breaking wave crests and wave trains are compared with each other in order to identify indicators for wave breaking, which were used for the detection and prediction of wave breaking onset.

The first section presents the physical model tests and their results, which were used to detect and predict wave breaking in time series of water surface elevation. Then the NWF model tests were used to investigate the deformation of the wave crest shortly before breaking onset to indicate precursors of breaking onset. In the third section the wave trains at the location of breaking onset are analysed and by means of the MARKOV chain precursors of breaking onset are identified.

6.1. Detection of Breaking Onset in Wave Trains

To develop a detection method of wave breaking in time series, laboratory experiments in the wave flume with random and regular wave trains were carried out. The model tests were carried out in the WKS wave flume of the Ludwig-Franzius-Institute with its overall dimensions of 110 m length, 2.2 m width and 2.0 m height. The piston type wave maker was hydraulically driven and capable of generating regular and irregular waves with wave heights up to 0.40 m while using a stroke of up to ± 0.30 m by a water depth of up to 1.2 m. In the rear part of the flume, a beach was installed as a passive wave absorber in order to minimize reflections.

It should be noted that parts of the physical and hydronumerical tests were conducted on the basis of scientific investigations in the framework of the research project “Probabilistic Safety Assessment of Offshore Wind Turbines (PSA) - work package 2”, founded by the Ministry for Science and Culture in Lower Saxony (support code GZZM2547), see Wilms and Schlurmann (2012), Wilms and Schlurmann (2014), Hansen (2014) and Hansen (2015).

6. Detection and Prediction of Breaking Onset in Wave Trains

6.1.1. Test Setup

The water surface elevation were measured using eight capacitive type wave gauges installed along the flume and covering a testing area of 45 m. As additional measurement equipment, three video cameras were installed to record the tests and to determine the wave breaking in post-processing. A sketch of the test setup is given in Fig. 6.1. The cameras were installed with such a viewing direction, so that they faced wave gauges WG1 (video camera 3), WG2 to WG7 (video camera 2), and WG8 to WG4 (video camera 1). Wave gauge WG1 was used to determine the incident wave spectrum. The position of testing area in the flume was a compromise between minimal distance to the wave maker (at least 5 times maximum wavelength) and maximum distance to the beach (to avoid wave reflections in the testing area).

6.1.2. Test Program and Procedure

The model tests were carried out in a length scale of 1:40, which was a compromise between possible wave generation and possible water depths. After the wave gauges and the video cameras were installed, the flume was filled to still water level of the required water depth. A test program with 20 test runs with random waves, and seven tests with regular waves were compiled, see Tabs. 6.1 and 6.2. As a spectrum, a narrow-band JONSWAP spectrum with enhancement factor $\gamma = 3.3$ and enhancement width $\sigma_L = 0.07$ and $\sigma_H = 0.09$ were used. The peak period varied between $T_P = 1.3 - 2.2$ s, the significant wave height H_S varied between $H_S = 0.2 - 0.25$ m, number of generated waves was $N_W = 50$ and $N_W = 100$, and the wave maker theory (wmt) was first and second order. The initial spectral steepness $s_{Z,i} = H_S/L_P$ varied between $s_{Z,i} = 0.026 - 0.082$, with the peak wavelength L_P calculated with $L_P = g/(2\pi)T_P^2$ and $g = 9.80655$ m/s² as acceleration of gravity. The water depth to wavelength ratio varied between $h/L = 0.13 - 0.31$. In Tab. 6.1 the random phase angle φ is indicated as “a”, “b”, “c”, “d” and “e”, and refers to five fix sets of random phase angle distributions (uniformly distributed between 0 and 2π), which were generated before the tests were carried out and stored. That way, the wave spectrum, characterized with significant wave height H_S and peak period T_P , could be transformed repeatedly to time domain and resulting in the same wave train every time. This means, test number 1, 2 and 3 were the same wave train, and test number 4 and 5 were the same wave train; they had the same phase angle distributions. Those retests were done, to analyse the reproducibility of the wave trains and number of breaking waves accordingly.

During each test run, all wave gauges and video cameras were continuously collecting

6.1. Detection of Breaking Onset in Wave Trains

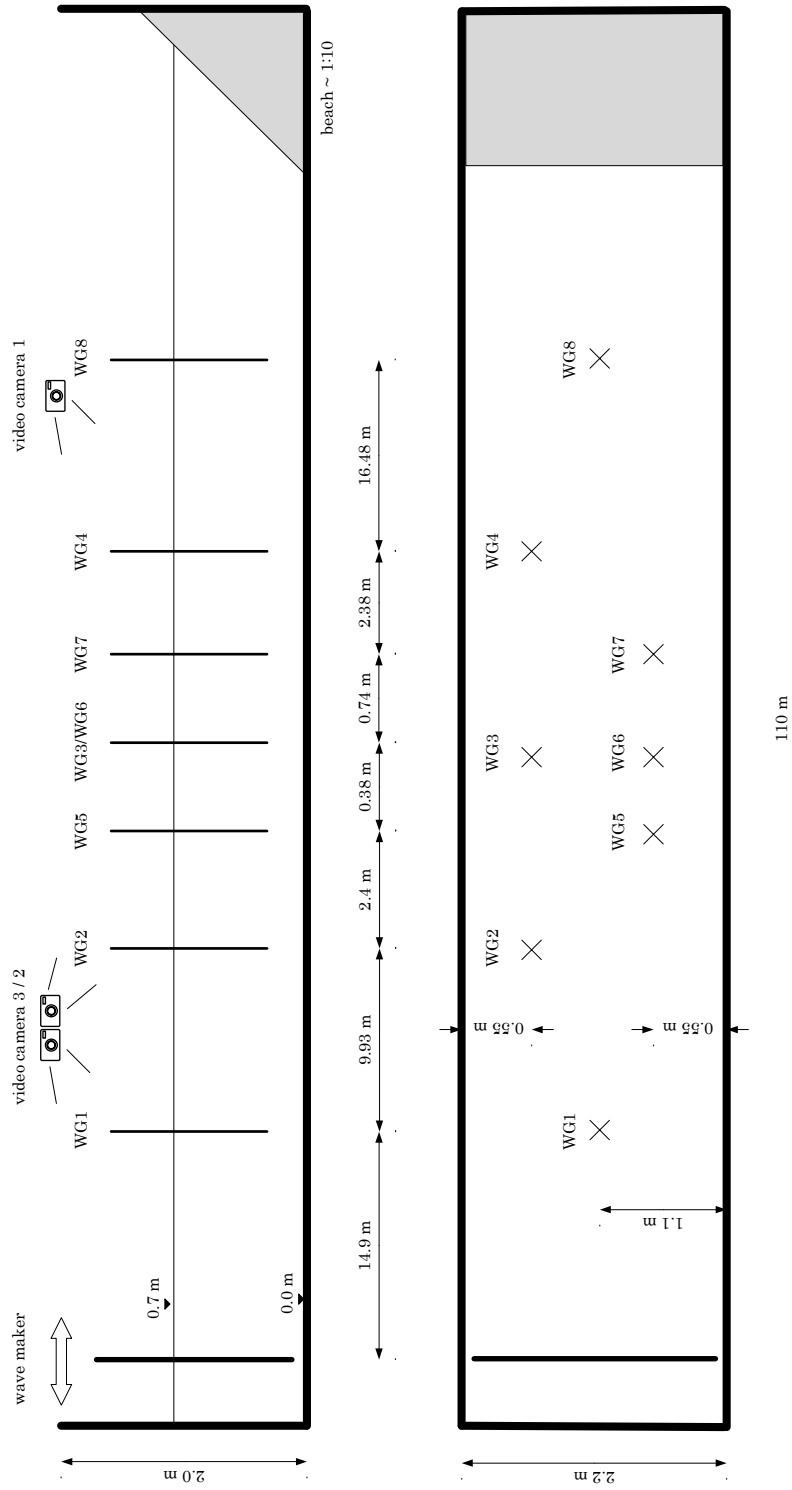


Figure 6.1.: Test setup in the wave flume. Top: side view of setup. Bottom: top view of setup. wg: wave gauge.

6. Detection and Prediction of Breaking Onset in Wave Trains

data. The wave gauges had an analogue output system (voltage outputs) and the data were sampled by a HBM analogue-digital converter in digital form. For data storage, the HBM sampling and control software catmanEasy was used and Mathworks Matlab was used for post-processing. Based on experience, a waiting time of at least 10 min between each test ensured no remaining oscillations, thus no interference, from the previous test run.

6.1.3. Results and Extended Detection Method

In the first step, the test runs were analysed in regard to plausibility (comparison of target value and actual value) and reproducibility (comparison of retests). The analysis of plausibility showed a mean deviation of 3.5% for the significant wave height H_S and a mean deviation of 1.8% for the peak period T_P , both determined in frequency domain with the Fast FOURIER Transform (FFT). The mean deviations were small and the targeted wave parameters were generated. The analysis of reproducibility showed a mean coefficient of determination of $R^2 = 0.998$ for test runs 1, 2 and 3, and $R^2 = 0.997$ for test runs 4 and 5. Fig. 6.2 shows exemplarily the first 20 s of the time series with $H_S = 0.2$ m and phase angle distribution “a”. The analysis showed that the time series were reproduced very well and therefore the resulting numbers of breaking waves were reliable. In the second step, the number of breaking waves were determined by re-watching the video camera data. The observed breakers were classified in “spilling breaker” and “whitecapping”.

In Tab. 6.3 the results for the number of breaking waves are compiled with their respective time stamp in relation to the start of the wave maker. The results of the retests 2 and 3 were the same as for test 1, as well as the results for the retest 5 is the same as for test 4; the reproducibility was again verified, which is why the results for retests 2, 3 and 5 are not shown in Tab. 6.3. For direct comparison, the results in Tab. 6.3 are sorted by phase angle distribution and then significant wave height H_S .

The resulting wave breaking probability $P_{br} = n_{br}/n_{tot}$ is summarised in Fig. 6.3 for all tests with water depth $h = 0.7$ m. The breaking probability ranged from $P_{br} = 0\%$ to $P_{br} = 6\%$; the result depended heavily on the phase angle distribution (wave sequence in the time series). An efficient investigation of the wave breaking probability in physical model tests was not possible with this large scatter in the results.

The following results were observed:

1. The initial steepness of the spectrum $s_{Z,i}$ had a great influence on the number of breaking waves, whereby the change of T_P had a greater influence than the change

6.1. Detection of Breaking Onset in Wave Trains

Table 6.1.: Compilation of conducted model test runs in the WKS wave flume with random wave trains.

Nr.	wmt	h	T_P	$\frac{h}{L}$	H_S	$s_{Z,i}$	N_W	φ
[-]	[-]	[m]	[s]	[-]	[m]	[-]	[-]	[-]
1	1st	0.7	1.7	0.18	0.200	0.044	50	a
2	1st	0.7	1.7	0.18	0.200	0.044	50	a
3	1st	0.7	1.7	0.18	0.200	0.044	50	a
4	1st	0.7	1.7	0.18	0.200	0.044	50	b
5	1st	0.7	1.7	0.18	0.200	0.044	50	b
6	1st	0.7	1.7	0.18	0.200	0.044	50	c
7	1st	0.7	1.7	0.18	0.225	0.050	50	a
8	1st	0.7	1.7	0.18	0.250	0.055	50	a
9	1st	0.7	1.7	0.18	0.200	0.044	50	d
10	1st	0.7	1.7	0.18	0.200	0.044	50	e
11	1st	0.7	1.9	0.15	0.200	0.035	50	a
12	1st	0.7	2.2	0.13	0.200	0.026	50	a
13	1st	0.7	1.7	0.18	0.200	0.044	100	a
14	1st	0.7	1.7	0.18	0.200	0.044	100	a
15	2nd	0.7	1.7	0.18	0.200	0.044	50	a
16	2nd	0.7	1.7	0.18	0.200	0.044	50	a
17	1st	0.8	1.7	0.20	0.200	0.044	50	a
18	2nd	0.8	1.7	0.20	0.200	0.044	50	a
19	1st	0.8	1.4	0.27	0.250	0.082	50	a
20	2nd	0.8	1.4	0.27	0.250	0.082	50	a

6. Detection and Prediction of Breaking Onset in Wave Trains

Table 6.2.: Compilation of conducted model test runs in the WKS wave flume with regular wave trains.

Nr.	wmt	h	T	$\frac{h}{L}$	H	$\frac{H}{L}$	N_W	φ
[-]	[-]	[m]	[s]	[-]	[m]	[-]	[-]	[-]
21	1	0.7	1.7	0.18	0.20	0.051	50	$-\pi$
22	1	0.7	1.7	0.18	0.20	0.051	50	$-\pi$
23	1	0.7	1.3	0.27	0.25	0.098	25	$-\pi$
24	1	0.7	1.3	0.27	0.25	0.098	12	$-\pi$
25	2	0.7	1.3	0.27	0.25	0.098	25	$-\pi$
26	1	0.8	1.7	0.20	0.20	0.049	25	$-\pi$
27	2	0.8	1.3	0.31	0.25	0.097	25	$-\pi$

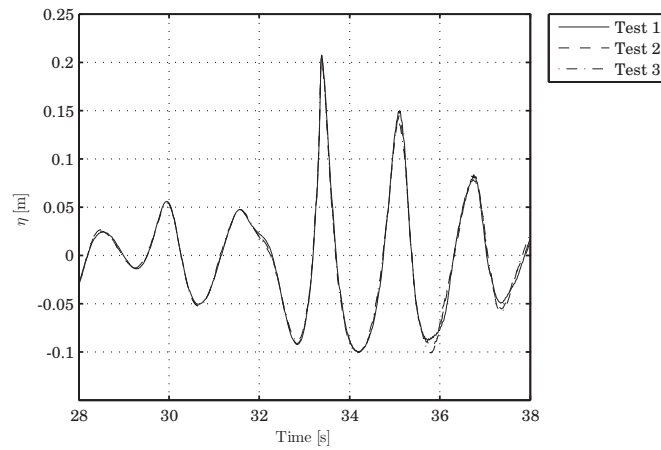


Figure 6.2.: Reproducibility of test run with $H_S = 0.2$ m and phase angle distribution "a".

6.1. Detection of Breaking Onset in Wave Trains

Table 6.3.: Compilation of results of number of breaking waves with their respective time stamp relative to the start of the wave maker.

Nr.	H_S	phase angle	Time	breaker type
	[m]		[s]	
1	0.200	a	00:47	spilling
			00:52	whitecap.
			00:55	whitecap.
			01:15	spilling
			01:20	whitecap.
			01:23	whitecap.
7	0.225	a	00:47	spilling
			00:52	whitecap.
			01:15	spilling
			01:19	whitecap.
			01:23	whitecap.
8	0.250	a	00:48	spilling
			01:10	whitecap.
			01:15	spilling
4	0.200	b	00:55	whitecap.
			00:59	whitecap.
6	0.200	c	01:03	whitecap.

6. Detection and Prediction of Breaking Onset in Wave Trains

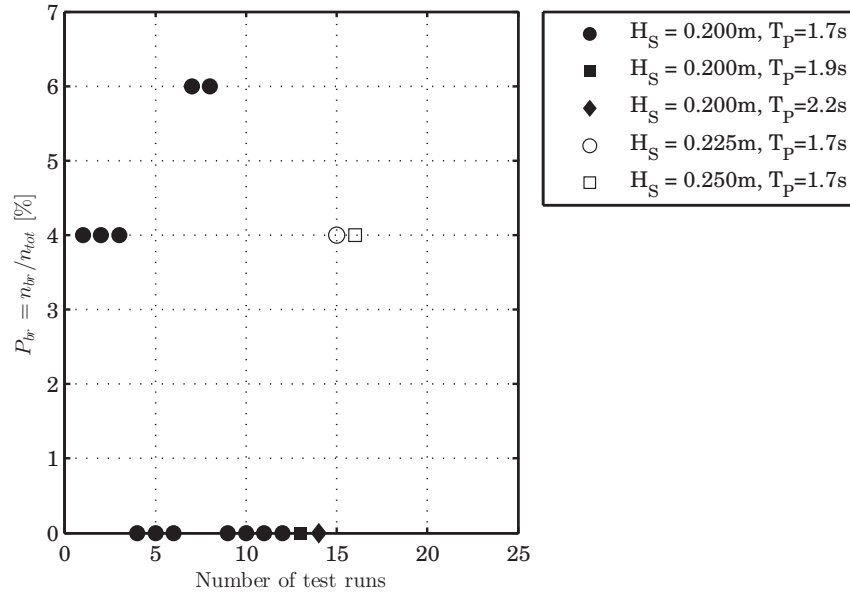


Figure 6.3.: Wave breaking probability P_{br} for the test runs with $h = 0.7$ m.

of H_S .

2. For the same phase angle distribution φ , the number of breaking waves was constant, and the wave breaking occurred temporally and spatially at the same positions.
3. An increasing significant wave height resulted in a decreasing number of whitecaps.
4. Even the second spilling breaker in a wave train was reproducible, which concluded that the first spilling breaker broke always in the same way, though the breaking process is a highly non-linear and turbulent process. The reproducibility of the physical model test is validated.
5. The randomness of the phase angle distribution, and thereby the randomness of the wave sequence in the time series, had a significant influence on the number of breaking waves; different realizations of the same energy density spectra in time domain did not produce same numbers of breaking waves; in contrast to phase angle distribution “a” with two spilling breakers, phase angle distributions “b” and “c” caused no breaking waves, only whitecapping, although all three spectra had the same theoretical energy density. There might be two reasons for that: either

the record length were too short (50-100 waves) or an exemplary time series could not represent all possible time series from one sea spectrum.

6.1.3.1. Extended Detection Method

Indicators to detect wave breaking should have the following features: They are measurable directly in the field or can be determined from the standard parameters like H_S and T_P . Based on the investigation from Babanin et al. (2007, 2010), the measured time series were analysed and plotted against the geometrical parameters for every single wave (zero-downcrossing), namely: wave steepness $s_Z = H/L$, frequency $f_0 = 1/T$, skewness $S_K = a_C/a_T - 1$ and asymmetry $A_S = L''/L' - 1$. It should be noted that in contrast to the experiments from Babanin et al., who used near-monochromatic deep water two-dimensional wave trains, the wave trains in this thesis were generated from JONSWAP spectra with large characteristic steepness $s_{Z,i} = H_S/L_P$. As an exemplary analysis of the wave train modulation as a function of time, the time series of wave gauge WG2 for test run 1 and the corresponding geometrical parameters are given in Fig. 6.4.

The two spilling breakers occurred at approximately 33 s and 61 s; their positions are marked with dashed lines. The only parameter here with a clear behaviour was the wave steepness s_Z which reached its maximum at the moment of wave breaking (for the first breaker), a behaviour also observed by Babanin et al. (2007). The other geometrical parameters did not behave in a unique way at breaking onset, in contrast to Babanin's observations for near-monochromatic wave trains. The second breaker at $t = 66$ s did not reach a clear maximum for s_Z . The reason is that the second breaking wave was already in the developed breaking process when reaching wave gauge WG2; the actual incipient breaker was not measured.

The critical steepness for the conducted model tests was $s_Z \approx 0.11$, which was smaller than the thresholds given in literature. Again, the reason is, that not the exact incipient breaker, but the breaker in progress, was measured. However, these resembling results with Babanin et al. (2007) were not found for every measured test.

In Fig. 6.5, the results for the alternative steepnesses and asymmetries, as proposed by the IAHR, see Tab. 2.1 on page 9, are shown. It can be observed that the steepnesses showed a more definite behaviour, especially the crest front steepness s'_C and crest rear steepness s''_C which reached their maximum with $s'_C = 0.0115$ and $s''_C = 0.0069$. The critical limits of Kjeldsen and Myrhaug (1979b) were $s'_C = 0.78$ and $s''_C = 0.39$ and thus significantly larger than the values of this thesis. Reasons for this could be that 1) the wave gauges were not exactly at the position of breaking onset and thus the maximum values were not measured, 2) Kjeldsen and Myrhaug generated wave breaking with wave

6. Detection and Prediction of Breaking Onset in Wave Trains

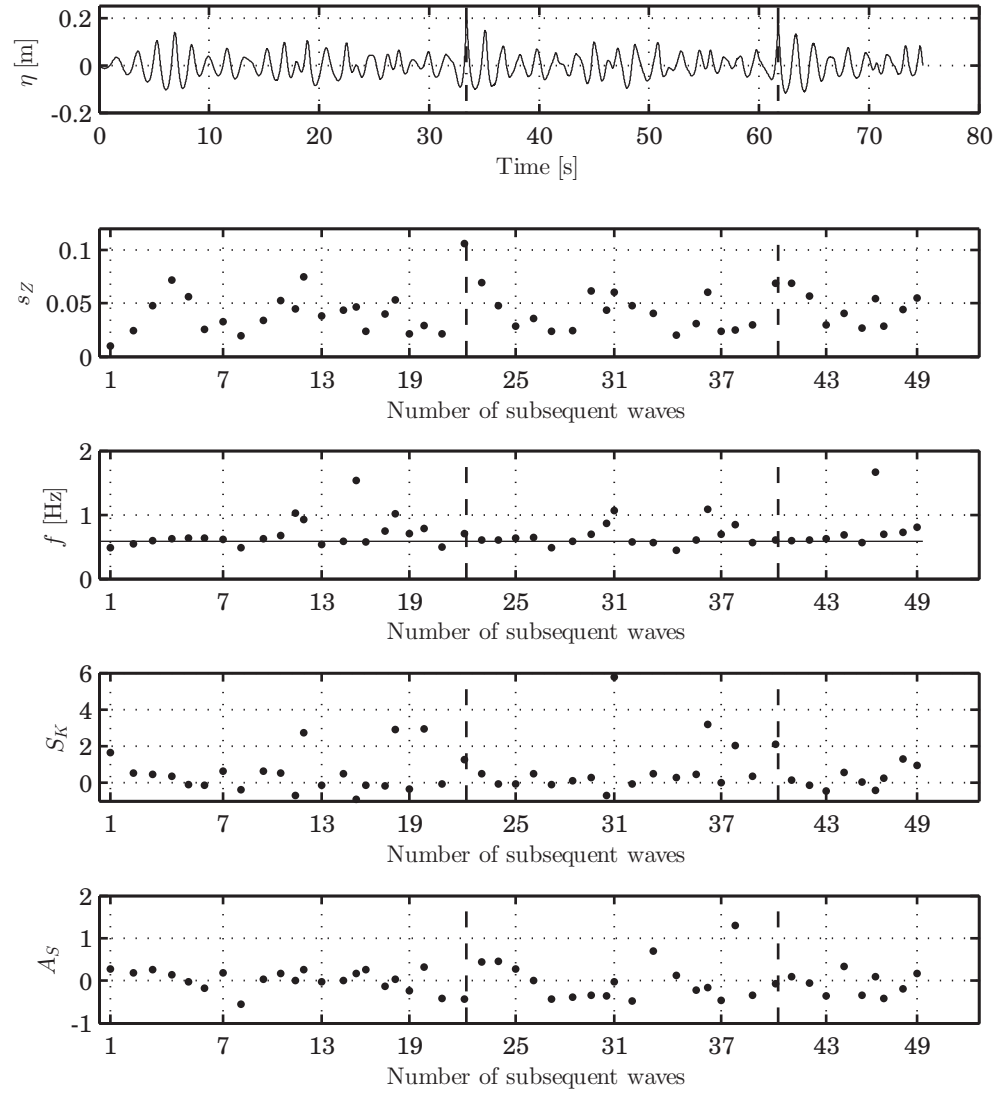


Figure 6.4.: Time series of test run 1 for wave gauge WG2 with $H_S = 0.2$ m and phase angle distribution “a” with the geometrical parameters wave steepness s_Z , frequency f , skewness $S_K = \frac{a_C}{a_T} - 1$ and asymmetry $A_S = \frac{L''}{L'} - 1$. Position of wave breaking is marked with dashed lines.

groups.

Babanin et al. (2007) stated, that incipient breaking waves were the steepest waves in a wave train, their skewness was positive (i.e. peaked up) and asymmetry was small (i.e. not tilted forward). At the point of breaking, the skewness increased very rapidly and immediately after the limit was reached the asymmetry became negative (i.e. the wave starts tilting forward at the point of breaking). Furthermore, at the point of breaking the frequency f_0 increased rapidly (modulation in the frequency). These observations, especially for the skewness, asymmetry and frequency, were hard to make in the measured irregular wave trains of this thesis.

Although Babanin postulated, that the wave steepness was the single robust criteria for wave breaking, it is, in the author's point of view, not a robust indicator in a wave train, because the time span of an incipient breaker (the exact point of breaking onset) is so short, and it is very unlikely to measure an incipient breaker (= the maximum/critical steepness) with a wave gauge. Therefore, further characteristics of a wave train with a breaking wave had to be established to develop a robust detection method.

Instantaneous parameters, derived from the analytical signal, seemed promising when describing a sudden and short-term change in the surface elevation, even when the wave gauge did not measure the exact point of breaking onset. An analytic signal in the signal theory is a complex-valued time signal whose imaginary part is the HILBERT transform of the real part. The term analytical expresses that the function is differentiable in the complex. This results in the fact that in the spectrum of an analytical signal no negative frequencies occur, in contrast to a real signal. In the field of signal processing, the HILBERT transform can be computed in a few steps: Firstly, the FOURIER transform of the given signal $X_r(t)$ is calculated. Secondly, the negative frequencies are rejected. Finally, the inverse FOURIER transform is calculated, and the result will be a complex-valued signal where the real and the imaginary parts form a HILBERT transform pair. To describe a signal simultaneously in time and space the instantaneous frequency $f(t)$ can be used. For that, the analytical signal $X(t)$ is derived, see Eq. (6.1), with $X_r(t)$ as the real function (original signal) and $X_i(t)$ the HILBERT transform of $X_r(t)$ (Schlurmann, 2005).

$$X(t) = X_r(t) + iX_i(t) \tag{6.1}$$

The time-variant variables are the instantaneous amplitude $a(t)$, instantaneous phase $\Theta(t)$ and the instantaneous angular frequency $\omega(t)$ or instantaneous frequency $f(t)$, see

6. Detection and Prediction of Breaking Onset in Wave Trains

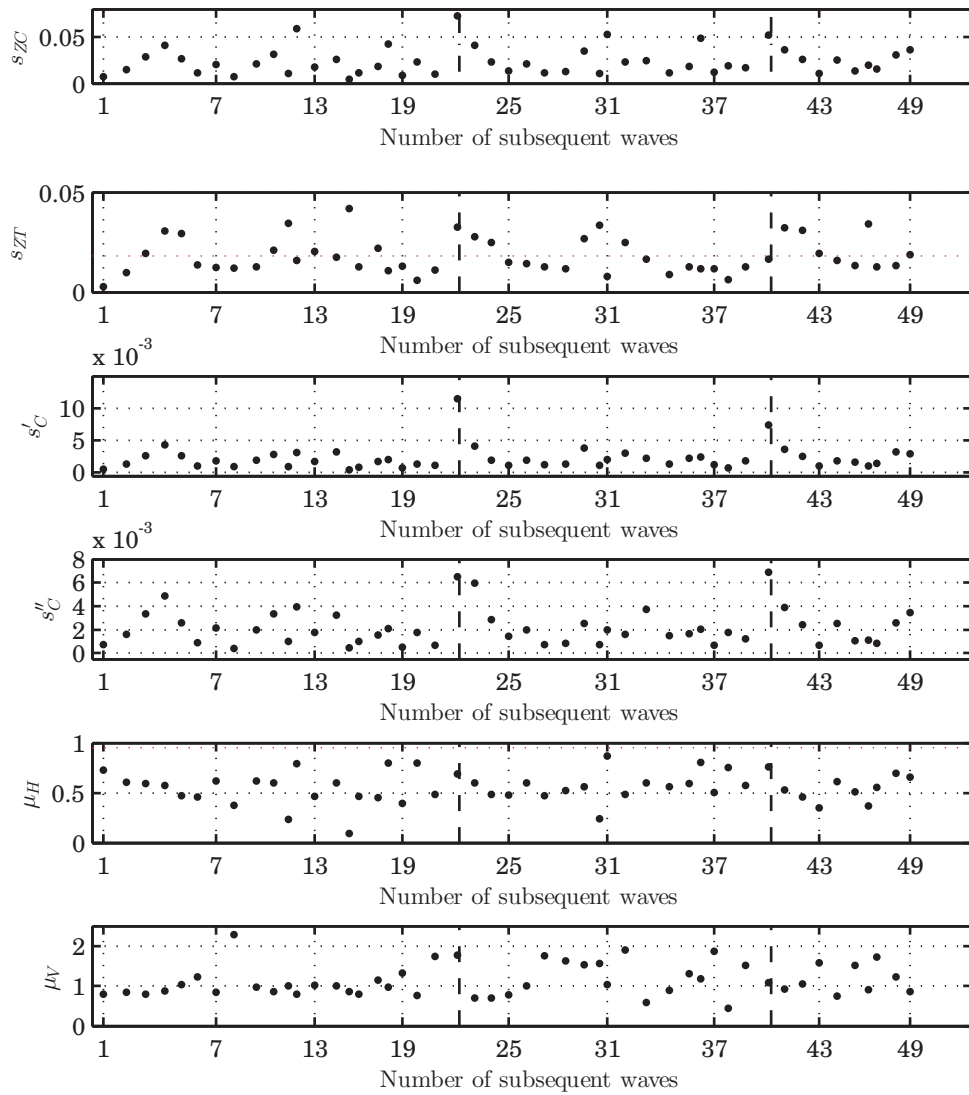


Figure 6.5.: Geometrical parameters for test run 1 for wave gauge WG2 with $H_S = 0.2$ m and phase angle distribution “a”. Position of wave breaking is marked with dashed lines.

6.1. Detection of Breaking Onset in Wave Trains

Eqs. (6.2) to (6.4).

$$a(t) = |X(t)| \quad (6.2)$$

$$\Theta(t) = \arg(X(t)) \quad (6.3)$$

$$\omega(t) = \frac{\partial \Theta(t)}{\partial t} \Rightarrow f(t) = \frac{1}{2\pi} \omega(t) \quad (6.4)$$

In order to establish a relationship between instantaneous amplitude $a(t)$ and instantaneous frequency $f(t)$ and thus extend the previous detection methods, the inverse of the instantaneous frequency was considered as an instantaneous period $T(t) = 1/f(t)$ and based on this the instantaneous “wavelength” $L(t)$ was determined. For the calculation of $L(t)$ the dispersion relation for intermediate water was used and iteratively calculated. This resulted in the instantaneous steepness $s_Z(t)$, see Eq. (6.5). Please note, that the HILBERT transform was computed from a water surface elevation over time here, therefore the instantaneous wavelength $L(t)$ had to be calculated with the approach of a instantaneous period $T(t) = 1/f(t)$ and the dispersion relation. When the HILBERT transform was computed from a water surface elevation over the flume length, the instantaneous wavelength was the reciprocal value of the instantaneous frequency $L(t) = 1/f(t)$.

$$s_Z(t) = \frac{2a(t)}{L(t)} \quad (6.5)$$

Comparing the author’s own approach to literature, one can see that the instantaneous wavelength $L(t)$ was calculated in the same way as the local wave number k from Song and Banner (2002), but without the application of a low-pass filter. As an envelope of the surface elevation, the author used the instantaneous amplitude $a(t)$, which was computed easily from the HILBERT transform as well, instead of the mean of the upper and lower envelopes $\mu(t)$ which was based on the wave energy and not directly on the wave amplitude.

In Fig. 6.6 the time series of test run 1 for wave gauge WG2 with $H_S = 0.2\text{m}$ and its corresponding instantaneous parameters $a(t)$, $f(t)$ and $s_Z(t)$ are shown. The suggested thresholds to detect the breaking waves were marked with dashed lines, see also Eqs. (6.6) to (6.8).

$$\eta(t) \geq 0.8H_S \quad (6.6)$$

6. Detection and Prediction of Breaking Onset in Wave Trains

$$f(t) \geq 2.2f_P \quad (6.7)$$

$$s_Z(t) \geq 0.4 \quad (6.8)$$

Fig. 6.4 shows that the detection of wave breaking with the wave steepness s_Z as an indicator was only unambiguously possible if the wave gauge was at the location of breaking onset. On the other hand, the instantaneous wave steepness $s_Z(t)$ was even distinctly developed in the second wave breaking ($t \approx 61$ s), which did not take place directly at the position of the wave gauge.

It can be observed that the instantaneous frequency $f(t)$ and steepness $s_Z(t)$ had high oscillations after a wave breaking. This oscillation was caused by ripples on the surface elevation, which occurred after wave breaking. Presumably, these ripples were caused by the breaking process (air entry and impulse of the breaker). A comparison with measurements carried out in the Large Wave Flume of Forschungszentrum Küste (FZK) (Hildebrandt (2013)) showed that this phenomenon was not measured by the wave gauges of the Large Wave Flume. The reasons for this were probably the different kind of used wave gauges and the position of wave gauges (close to the flume wall). Therefore, those oscillations are not an universal indicator for wave breaking.

6.1.3.2. Conditions of the Breaking Detection Method

Taking into account all laboratory tests carried out in this thesis (with an initial spectral slope of $s_{Z,i} = 0.044$), the following thresholds were found to detect wave breaking in a time series:

1. The amplitude of the wave crest has to be at least 80% of H_S .

$$\eta(t) \geq 0.8H_S$$

2. The instantaneous wave steepness has to be greater than 0.4

$$s_Z(t) \geq 0.4$$

3. The wave steepness has to be greater than 0.08.

$$s_Z \geq 0.08$$

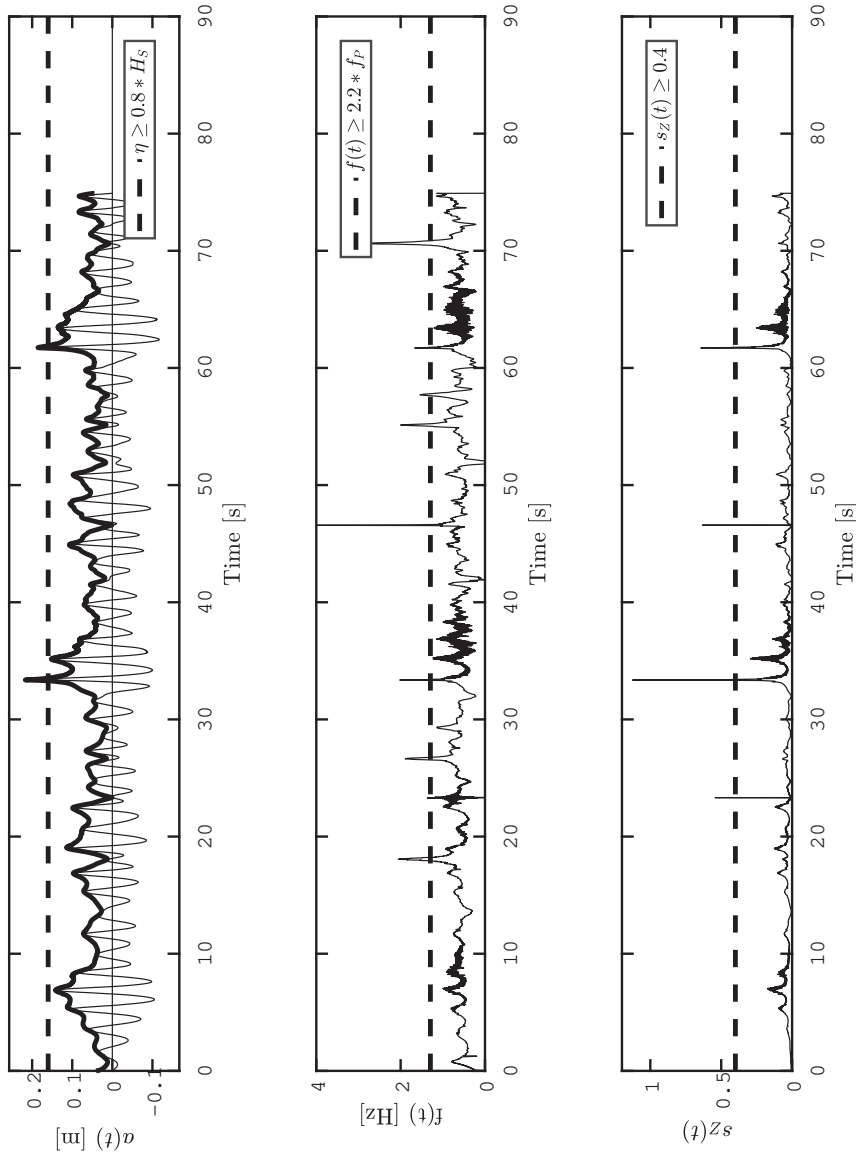


Figure 6.6.: Time series of test run 1 for wave gauge WG2 with $H_s = 0.2$ m and phase angle distribution “a” with the instantaneous parameters $a(t)$ (instantaneous amplitude), $f(t)$ (instantaneous frequency) and $s_z(t)$ (instantaneous steepness). The two spilling breakers occur at approximately 33 s and 61 s. The suggested thresholds are marked with dashed lines.

6. Detection and Prediction of Breaking Onset in Wave Trains

4. The instantaneous frequency has to be greater than $2.2f_P$

$$f(t) \geq 2.2f_P$$

5. The crest front steepness has to be greater than 0.009.

$$s'_C \geq 0.009$$

6. The crest rear steepness has to be greater than 0.005.

$$s''_C \geq 0.005$$

It must be noted that wave breaking is characterised inevitably not only by fixed values, but also by the history of the time series. The investigation showed that a breaking wave crest had a minimum wave amplitude (condition #1) and the maximum steepness (instantaneous and geometrical) from the entire time series (condition #2 and #3). The consideration of all these boundary conditions, i.e. a combination of parameters and thresholds, formed a reliable detection method. A single parameter or threshold is not sufficient.

Zimmermann and Seymour (2002) carried out model tests with irregular two-dimensional wave trains in deep water, similar to this thesis. The sea spectrum was a JONSWAP spectrum with $1.6 \text{ s} \leq T_P \leq 2.0 \text{ s}$ and $0.23 \text{ m} \leq H_S \leq 0.38 \text{ m}$. The phase-time method was used as the detection method and two conditions were derived: $\eta \geq 0.38H_S$ and $f(t) \geq 0.85f_P$. Further steepnesses and asymmetries had also been investigated, but according to Zimmermann and Seymour did not improve the detection method since it was not possible to distinguish between steep but non-breaking waves and breaking waves. This result is confirmed by the author's own comparison of non-breaking and breaking wave crests, see subsection 6.2.2; the main result was that only the ratios a_C/H_S and $a(t)/H_S$ differ significantly between a non-breaking and breaking wave crest.

Conclusions

- The detection of breaking onset in physical model tests is non-trivial because breaking onset is an extreme short-term state of wave dynamics and difficult to measure exactly with wave gauges.
- Therefore, the novel parameter of instantaneous steepness is introduced and defined as $s_Z(t) = 2a(t)/L(t)$. The instantaneous steepness $s_Z(t)$ describes the relation between the envelope of surface elevation and the rate of change of the surface elevation, which are both maximal at breaking onset. Even when the wave gauge did not measure the exact point of breaking onset in the physical model tests, the instantaneous steepness $s_Z(t)$ was able to detect wave breaking in an unambiguous way.
- Based on the physical model tests with irregular wave trains and an initial spectral steepness of $s_{Z,i} = 0.044$, the following threshold parameters were found for a detection method: $\eta(t) \geq 0.8H_S$, $s_Z(t) \geq 0.4$, and $s_Z \geq 0.08$. But most importantly those indicative parameters reached their maximum at breaking onset. That means, in order to detect dominant wave breaking in irregular wave trains, the largest, steepest, and fastest deforming wave has to be found.

6.2. Deformation of Wave Crests before Breaking Onset

In this section, the deformation of the breaking wave crest within the last 2 s before breaking onset is investigated more precisely in order to obtain further valuable information for the detection of breaking onset. The development of the geometrical and instantaneous parameters of the wave crest over time towards breaking onset was considered and the reached thresholds were determined. Subsequently, the results of the breaking wave crests were compared with the results of non-breaking wave crests in order to determine indicators that only occur during wave breaking. Finally, the results were compared with the physical model tests of Bonmarin and Ramamonjiarisoa (1985) and Bonmarin et al. (1989). Bonmarin et al. conducted model tests with monochromatic wave trains with an initial wave steepness in the order of magnitude of $H/L_0 = 0.08$, which broke because of modulational instability. The deformation of the breaking wave crest was recorded spatially by means of high-speed cameras. These differences in the generation and type of wave breaking had to be taken into account when compared with the results of this

6. Detection and Prediction of Breaking Onset in Wave Trains

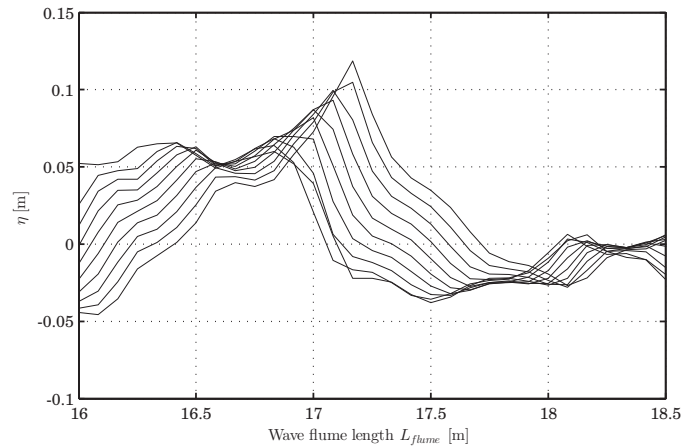


Figure 6.7.: Computed wave crest evolution (chronological) until breaking onset with time step $\Delta t = 0.04$ s.

thesis.

6.2.1. Deformation of Wave Crests before Breaking Onset

In Fig. 6.7 the temporal development of a wave crest before breaking onset is plotted against the flume length; the last ten time steps ($10 \cdot 0.04$ s = 0.4 s) before breaking onset are shown. The flat wave trough and the rapidly rising wave crest can be seen. The geometrical and instantaneous parameters of these waves which are about to break are examined in more detail below. For a better representation, the results of the test runs with the initial spectral steepness between $0.027 \leq s_{Z,i} \leq 0.071$ are shown separately, see Fig. 6.8 to Fig. 6.10, and for $s_{Z,i} = 0.01, 0.02$, see Figs. C.1 to C.3 in the annex. The figures show the development of the geometrical and instantaneous parameters within 2 s before breaking onset with a time step of $\Delta t = 0.04$ s, and the breaking onset as the last time step.

It can be observed that between time step 30-40, i.e. 0.4s-0.8s, before breaking onset, the wave crest began to deform significantly geometrically. The larger the initial spectral steepness $s_{Z,i}$ the later the deformation began and the smaller the change. The crest amplitude a_C and the instantaneous amplitude $a(t)$ increased rapidly and reached their maximum with breaking onset. The crest amplitude a_C doubled and the instantaneous amplitude $a(t)$ tripled within the last 2s before breaking onset. The wave frequency f_0 did not change significantly, rather decreased slightly, i.e. the wavelength increased slightly. Thus the increase of the wave amplitude a_C was responsible for the increase

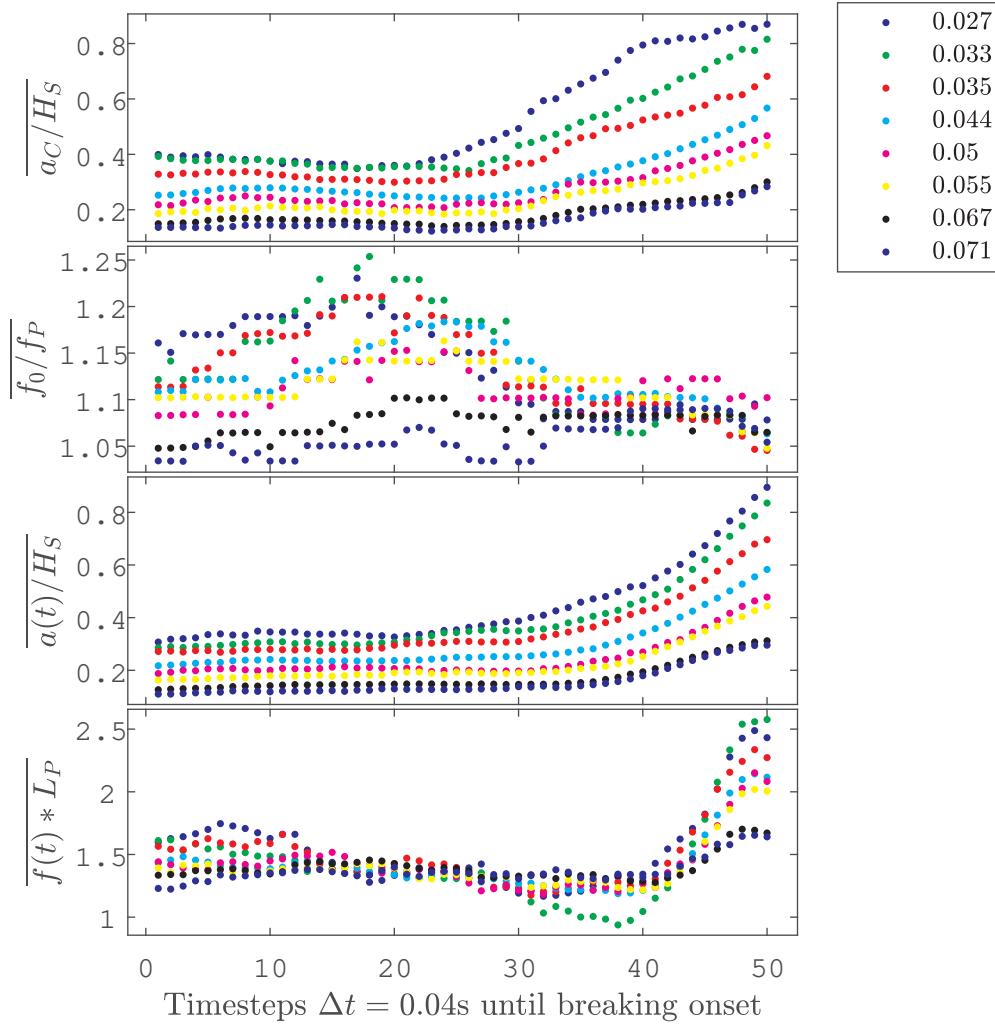


Figure 6.8.: Development of the median of the geometrical parameters against the time step ($\Delta t = 0.04\text{s}$) until breaking onset with the simulated NWF data for the test runs with different spectral steepnesses $s_{Z,i}$ (part 1, amplitudes and frequencies).

6. Detection and Prediction of Breaking Onset in Wave Trains

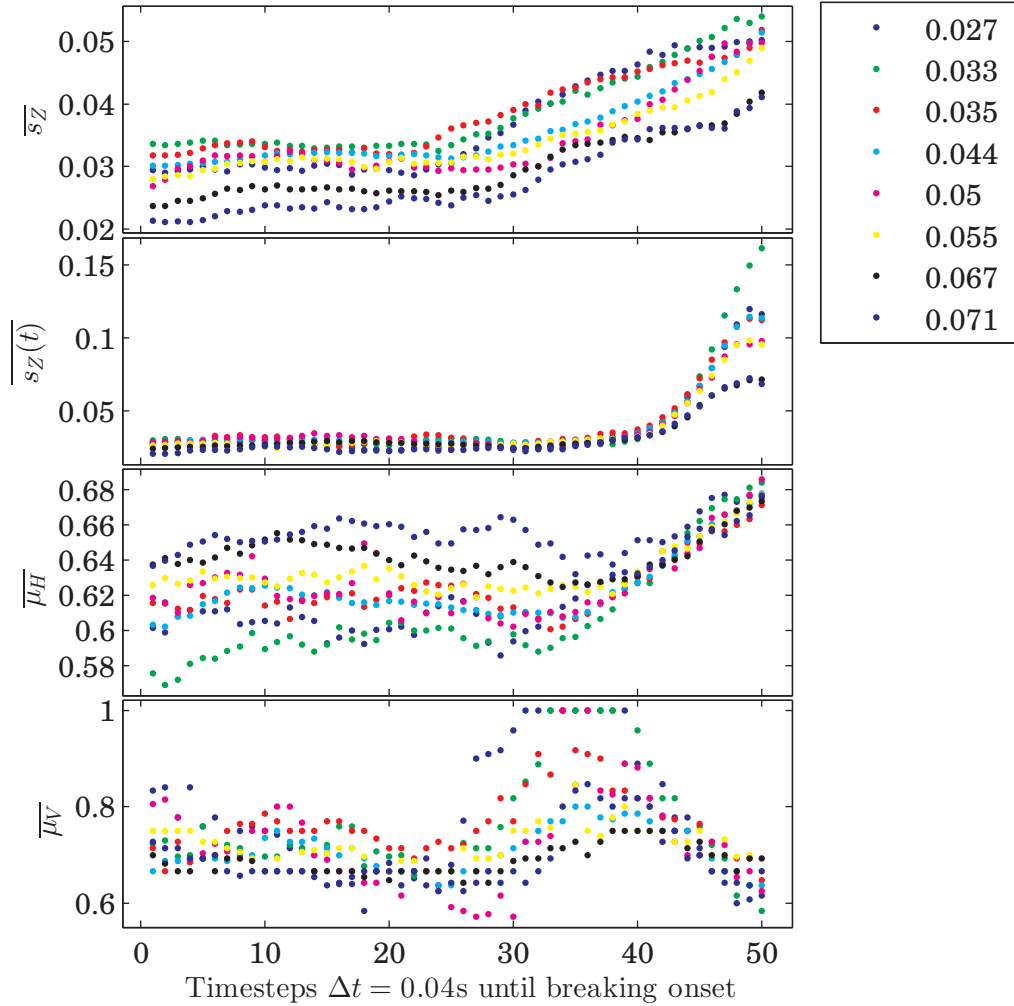


Figure 6.9.: Development of the median of the geometrical parameters against the time step ($\Delta t = 0.04$ s) until breaking onset with the simulated NWF data for the test runs with different spectral steepnesses $s_{Z,i}$ (part 2, steepnesses and asymmetries).

6.2. Deformation of Wave Crests before Breaking Onset

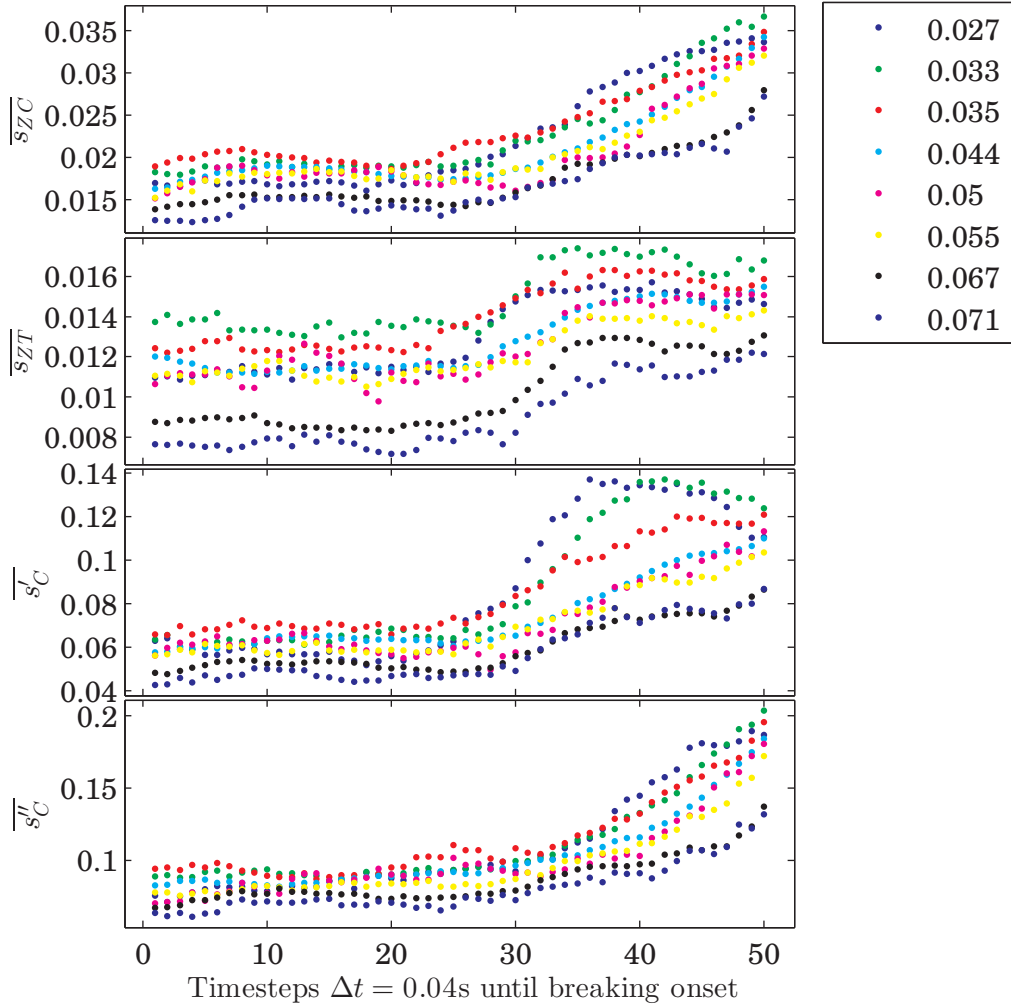


Figure 6.10.: Development of the median of the geometrical parameters against the time step ($\Delta t = 0.04\text{s}$) until breaking onset with the simulated NWF data for the test runs with different spectral steepnesses $s_{Z,i}$ (part 3, steepnesses).

6. Detection and Prediction of Breaking Onset in Wave Trains

of the wave steepness s_Z . It can be observed that approximately 0.7s before breaking onset, the wave frequency f_0 reached similar values for all initial spectral steepnesses. The instantaneous frequency $f(t)$ decreased slightly about 0.5s before breaking onset and then increased significantly (up to triple) and reached its maximum with breaking onset. The instantaneous wave steepness $s_Z(t)$ was constant up to about 0.4s before breaking onset and then increased promptly (up to five-fold); in comparison, the geometrical wave steepness s_Z increased slightly already from 2s before breaking onset, and then increased twofold 0.8s before breaking onset. The larger the initial spectral steepness $s_{Z,i}$ the smaller the wave steepness s_Z of the breaking wave crest.

The alternative wave steepnesses besides s_Z , which were $s_{ZC} = a_C/L$, $s_{ZT} = a_T/L$, $s'_C = a_C/L'$ and $s''_C = a_C/L''$, behaved similarly to s_Z and doubled in the last 2s before breaking onset. Approximately 0.8s before breaking onset the crest steepness s_{ZC} and the crest rear steepness s''_C reached their maximum at breaking onset. The trough steepness s_{CT} was 0.4s before breaking onset almost constant; this indicates that the through amplitude a_T became smaller as the wavelength L increased. The crest front steepness s'_C behaved similar to the wave steepness s_Z for large initial spectral steepnesses $s_{Z,i} \geq 0.044$; it increased 0.8s before breaking onset and reached its maximum at breaking onset. For small initial spectral steepnesses $s_{Z,i} \leq 0.035$, however, the crest front steepness decreased 0.4s before breaking onset. This suggests that for small initial spectral steepnesses, where the wave train had time to develop, the wave crest not only rose, but also tended forward as the crest front wavelength L' shortened. This could be a reference to different types of breakers. With values between $0.04 \leq s'_C \leq 0.14$ and $0.05 \leq s''_C \leq 0.2$ the wave crest was off from a symmetric shape with $s'_C = s''_C = 0.40$ (for a second-order STOKES wave in deep water).

In the case of the geometrical parameters for the asymmetry, the horizontal asymmetry $\mu_H = a_C/H$ started to increase approximately from 0.4s to 0.8s before breaking onset and reached its maximum with breaking onset; the larger the initial spectral steepness $s_{Z,i}$ the earlier the increase started. For the vertical asymmetry $\mu_V = L''/L'$, however, the parameter decreased slightly in the first 1.2s, and then increased until 0.4s before breaking onset, reached its maximum and then decreased toward breaking onset. This also indicates the shortening of the crest front wavelength L' and thus the inclination of the wave crest forward. With values between $0.6 \leq \mu_H \leq 0.7$ and $0.6 \leq \mu_V \leq 0.8$ the wave crest was off from a symmetric shape with $\mu_H = 0.61$ and $\mu_V = 1$ (for a second-order STOKES wave in deep water).

In Tab. 6.4 the median values are summarised for all geometrical and instantaneous parameters for every fifth time step (every 0.2s). To quantitatively describe the change

6.2. Deformation of Wave Crests before Breaking Onset

Table 6.4.: Median values for every geometrical and instantaneous parameter for every 5th time step (every 0.2s) until time of breaking onset (tbo) for the test runs with initial spectral steepness $s_{Z,i} = 0.044$.

	1st	5th	10th	15th	20th	25th	30th	40th	45th	tbo
a_C/H_S	0.27	0.28	0.27	0.25	0.24	0.26	0.32	0.38	0.45	0.57
f_0/f_P	1.12	1.11	1.14	1.16	1.18	1.14	1.10	1.10	1.09	1.06
$a(t)/H_S$	0.23	0.24	0.23	0.24	0.25	0.25	0.28	0.34	0.45	0.58
$f(t) * L_P$	1.44	1.38	1.44	1.34	1.32	1.27	1.22	1.21	1.66	2.12
s_Z	0.03	0.03	0.03	0.03	0.03	0.03	0.04	0.04	0.04	0.05
$s_Z(t)$	0.03	0.03	0.03	0.03	0.03	0.03	0.03	0.03	0.07	0.11
μ_V	0.69	0.75	0.71	0.67	0.64	0.71	0.80	0.79	0.70	0.64
μ_H	0.61	0.63	0.62	0.62	0.61	0.61	0.61	0.63	0.65	0.68
s_{ZC}	0.02	0.02	0.02	0.02	0.02	0.02	0.02	0.02	0.03	0.03
s_{ZT}	0.01	0.01	0.01	0.01	0.01	0.01	0.01	0.02	0.01	0.02
s'_C	0.06	0.06	0.07	0.06	0.06	0.07	0.08	0.09	0.10	0.11
s''_C	0.09	0.08	0.09	0.09	0.09	0.10	0.10	0.12	0.14	0.18

of the median values over the time steps, the absolute values of the gradients of the median values are summarised in Tab. 6.5. It can be observed how most of the changes happened in the last 0.4s - 0.8s before breaking onset and the parameters reached their maximum or minimum values with breaking onset.

Tabs. 6.6 and 6.7 summarises the minimum and maximum values of the geometrical and instantaneous parameters at breaking onset for every initial spectral steepness $s_{Z,i}$. The parameters were within those ranges when the breaking onset happened. The maximum values can be taken as thresholds for detection. Those results confirm that there is no universal value to detect wave breaking. All these wave crest broke and covered a large range of values. The geometrical and instantaneous parameters showed that wave breaking onset is an absolute immediate phenomenon. The later the wave train broke, i.e. the more time the wave train had to develop, the less it changed in the last 2s before breaking onset. Since the wave frequency did not change significantly, this could be an indication that the majority of wave crests broke due to wave-wave interaction, i.e. the wave energy accumulated by the superposition of waves and thereby the waves broke. This assumption is supported by the fact that just approximately 3% of the test runs fulfilled the conditions that the kurtosis of the wave trains is $k > 3$ and the relative water

6. Detection and Prediction of Breaking Onset in Wave Trains

Table 6.5.: Absolute value of the gradient of the median values for every geometrical and instantaneous parameter for every 5th time step (every 0.2 s) until time of breaking onset (tbo) for the test runs with initial spectral steepness $s_{Z,i} = 0.044$.

	1st	5th	10th	15th	20th	25th	30th	40th	45th	tbo
a_C/H_S	0.0099	0.0014	0.0145	0.0123	0.0066	0.0384	0.0560	0.0669	0.0953	0.1132
f_0/f_P	0.0132	0.0102	0.0271	0.0206	0.0101	0.0405	0.0196	0.0054	0.0210	0.0303
$a(t)/H_S$	0.0110	0.0021	0.0020	0.0076	0.0073	0.0138	0.0454	0.0870	0.1199	0.1312
$f(t) * L_P$	0.0570	0.0011	0.0210	0.0560	0.0351	0.0540	0.0284	0.2197	0.4519	0.4602
s_Z	0.0012	0.0008	0.0001	0.0005	0.0009	0.0028	0.0034	0.0040	0.0056	0.0067
$s_Z(t)$	0.0001	0.0003	0.0007	0.0007	0.0001	0.0003	0.0032	0.0188	0.0399	0.0473
μ_V	0.0577	0.0110	0.0417	0.0390	0.0238	0.0818	0.0357	0.0500	0.0747	0.0636
μ_H	0.0112	0.0037	0.0045	0.0042	0.0039	0.0027	0.0092	0.0228	0.0253	0.0244
s_{ZC}	0.0013	0.0005	0.0006	0.0007	0.0004	0.0018	0.0028	0.0036	0.0050	0.0060
s_{ZT}	0.0002	0.0000	0.0001	0.0000	0.0007	0.0015	0.0011	0.0002	0.0002	0.0007
s'_C	0.0039	0.0026	0.0002	0.0025	0.0008	0.0099	0.0132	0.0111	0.0089	0.0070
s''_C	0.0038	0.0004	0.0032	0.0033	0.0035	0.0058	0.0098	0.0198	0.0344	0.0409

6.2. Deformation of Wave Crests before Breaking Onset

Table 6.6.: Minimum and maximum values of the geometrical and instantaneous parameters at breaking onset for initial spectral steepness $s_{Z,i} = 0.01 - 0.035$.

$s_{Z,i}$	0.01		0.02		0.027		0.033		0.035	
a_C/H_S	0.73	2.11	0.79	1.92	0.16	1.41	0.22	1.21	0.21	1.21
f_0/f_P	1.02	4.12	1.02	2.26	0.83	1.93	0.76	1.97	0.78	2.28
$a(t)/H_S$	0.74	2.17	0.80	1.92	0.17	1.42	0.22	1.23	0.21	1.21
$f(t) * L_P$	3.00	13.61	2.25	8.14	1.17	7.15	1.02	8.03	1.21	6.54
s_Z	0.02	0.26	0.03	0.11	0.01	0.10	0.02	0.12	0.01	0.12
$s_Z(t)$	0.05	0.47	0.07	0.61	0.01	0.42	0.03	0.36	0.02	0.38
μ_V	0.00	7.00	0.11	4.75	0.14	3.29	0.06	5.67	0.10	2.50
μ_H	0.49	0.99	0.62	1.00	0.46	1.00	0.48	1.00	0.43	0.97
s_{ZC}	0.01	0.25	0.02	0.11	0.01	0.09	0.01	0.11	0.01	0.12
s_{ZT}	0.00	0.06	0.00	0.02	0.00	0.03	0.00	0.03	0.00	0.03
s'_C	0.03	0.58	0.09	0.34	0.02	0.27	0.02	0.37	0.01	0.30
s''_C	0.03	0.98	0.05	0.95	0.03	0.88	0.04	1.47	0.03	0.56

Table 6.7.: Minimum and maximum values of the geometrical and instantaneous parameters at breaking onset for initial spectral steepness $s_{Z,i} = 0.044 - 0.071$.

$s_{Z,i}$	0.044		0.05		0.055		0.067		0.071	
a_C/H_S	0.08	1.61	0.13	0.83	0.11	1.58	0.06	0.74	0.08	0.61
f_0/f_P	0.73	2.33	0.80	2.45	0.74	2.22	0.69	2.22	0.76	1.98
$a(t)/H_S$	0.08	1.62	0.14	0.87	0.12	1.60	0.06	0.75	0.09	0.62
$f(t) * L_P$	0.36	8.44	0.89	7.11	0.88	11.56	0.78	7.89	0.84	5.35
s_Z	0.01	0.13	0.01	0.15	0.01	0.16	0.00	0.10	0.01	0.10
$s_Z(t)$	0.01	1.22	0.02	0.29	0.02	2.05	0.01	0.35	0.01	0.26
μ_V	0.04	3.67	0.06	3.50	0.08	3.33	0.04	4.40	0.08	5.25
μ_H	0.44	1.00	0.47	0.99	0.43	1.00	0.42	1.00	0.41	0.99
s_{ZC}	0.00	0.12	0.01	0.14	0.01	0.14	0.00	0.10	0.01	0.10
s_{ZT}	0.00	0.04	0.00	0.04	0.00	0.04	0.00	0.03	0.00	0.03
s'_C	0.01	0.44	0.03	0.32	0.01	0.47	0.01	0.35	0.01	0.27
s''_C	0.02	1.15	0.02	0.55	0.02	0.69	0.01	1.03	0.02	0.51

6. Detection and Prediction of Breaking Onset in Wave Trains

depth is $h/L > 0.5$, which are the conditions for modulational instability to be present which may lead to wave breaking; thus wave breaking due to modulational instability was unlikely in these test runs. Furthermore, the almost constant wave frequency and therefore wavelength indicated that the waves did not shorten which rather happens for depth-induced wave breaking.

Conclusions

- Based on the hydronumerical model tests, the deformation of breaking wave crest was analysed with a time step of $\Delta t = 0.04\text{s}$ and for the time period of 2s. The deformation of breaking wave crest began approximately 0.4s - 0.8s before breaking onset.
- The larger the initial spectral steepness $s_{Z,i}$, the later the deformation began, the smaller the change of the parameters, and the smaller the wave steepness s_Z of the breaking wave crest. In other words, the earlier the wave train broke, i.e. the less time the wave train had to develop, the faster the deformation happened.
- The results confirm that there is no universal value to detect wave breaking. All breaking wave crests covered a large range of values of geometrical and instantaneous parameters.

6.2.2. Comparison of Breaking and Non-Breaking Wave Crests

In Figs. 6.11, 6.12 and 6.13, the normalised instantaneous amplitude $a(t)/H_S$, the normalised instantaneous frequency $f(t) * L_P$ and the instantaneous steepness $s_Z(t) = 2 * a(t)/L(t)$ are shown for both the breaking and non-breaking wave crests. For the breaking wave crests, the median value of the corresponding parameter was taken with all test runs considered. In the case of non-breaking wave crests, there were only four wave trains (three wave trains with $s_{Z,i} = 0.01$ and one with $s_{Z,i} = 0.02$) which had no instability during their simulation and the simulation ran until the simulation end was reached. Therefore, one wave crest per initial spectral steepness is plotted exemplarily; the chosen wave crest was the maximum crest in the wave train at the end of simulation. In the two test runs chosen here, the highest wave was also the steepest wave. It can thus be judged whether a distinction between a breaking wave and a very steep but non-breaking wave is possible.

It can be observed that the breaking wave was strongly deformed about 0.4s before

6.2. Deformation of Wave Crests before Breaking Onset

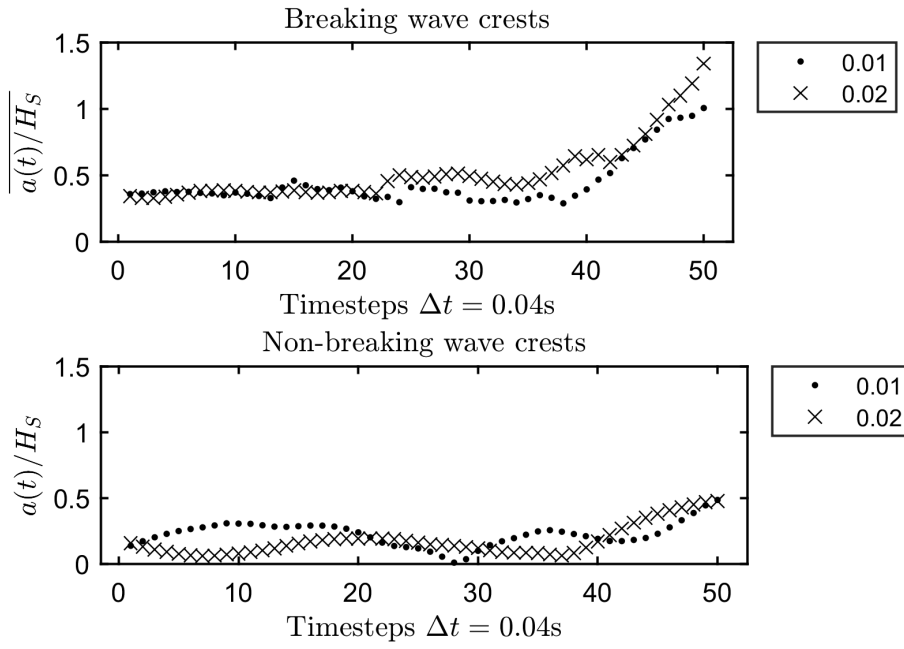


Figure 6.11.: Normalised instantaneous amplitude of the breaking and non-breaking wave crest for the test runs with initial spectral steepness $s_{Z,i} = 0.01$ and $s_{Z,i} = 0.02$. In case of the breaking wave crest, the parameter is a median of all test runs.

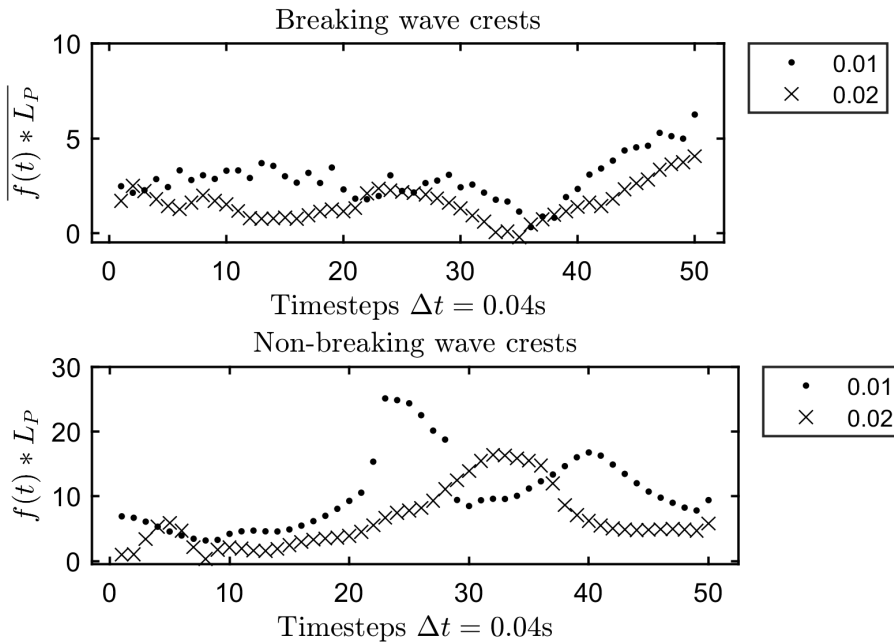


Figure 6.12.: Normalised instantaneous frequency of the breaking and non-breaking wave crest for the test runs with initial spectral steepness $s_{Z,i} = 0.01$ and $s_{Z,i} = 0.02$. In case of the breaking wave crest, the parameter is a median of all test runs.

6. Detection and Prediction of Breaking Onset in Wave Trains

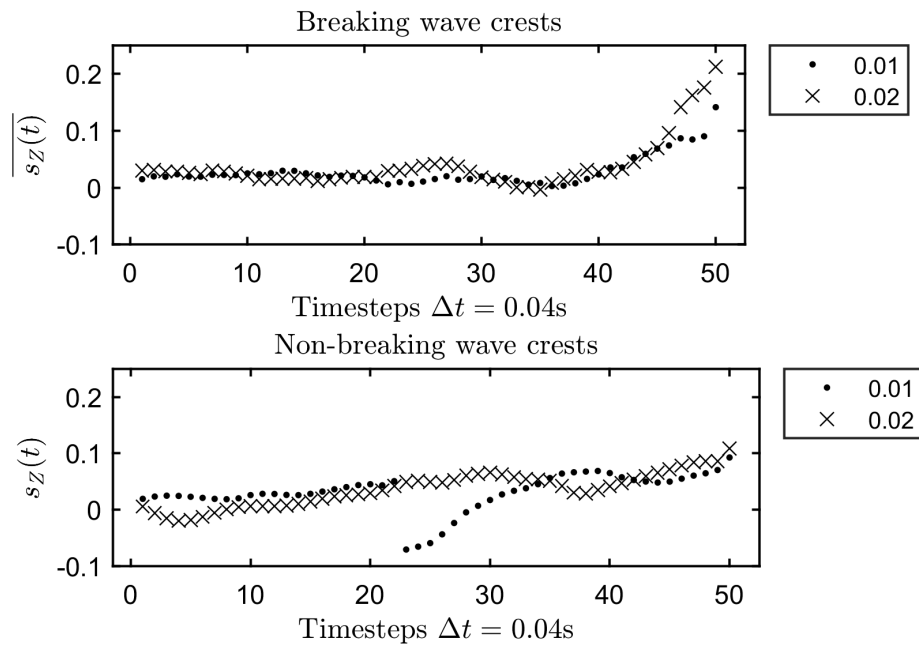


Figure 6.13.: Instantaneous steepness of the breaking and non-breaking wave crest for the test runs with initial spectral steepness $s_{Z,i} = 0.01$ and $s_{Z,i} = 0.02$. In case of the breaking wave crest, the parameter is a median of all test runs.

6.2. Deformation of Wave Crests before Breaking Onset

breaking onset, and the instantaneous amplitude, frequency and correspondingly steepness increased. The non-breaking wave, on the other hand, increased in amplitude, but its frequency dropped. Overall, the non-breaking wave crest did not reach the maximum values of the breaking wave crest. The breaking wave crest reached a three times larger instantaneous amplitude and a two times greater instantaneous steepness. A clear distinction between a breaking and a very steep wave was therefore possible in this example. The breaking wave crest reached the following thresholds for the test runs with an initial spectral steepness $s_{Z,i} = 0.01$:

$$\overline{a(t)/H_{S_{max}}} = 1.0$$

$$\overline{f(t) * L_{P_{max}}} = 6.3$$

$$\overline{s_Z(t)_{max}} = 0.14$$

The following thresholds were reached for the test runs with an initial spectral steepness $s_{Z,i} = 0.02$:

$$\overline{a(t)/H_{S_{max}}} = 1.3$$

$$\overline{f(t) * L_{P_{max}}} = 4.1$$

$$\overline{s_Z(t)_{max}} = 0.21$$

These thresholds differ from the findings in subsection 6.1.3.2, because the initial spectral steepness $s_{Z,i}$ of the investigated test runs differ. Comparing Tab. 6.7, one will find that $s_Z(t)$ is between 0.01 and 1.22 for $s_{Z,i} = 0.044$ and thus the findings in subsection 6.1.3.2 lay in this value range.

In Tab.6.8, the geometrical and instantaneous parameters for the non-breaking and breaking wave crests at the time of simulation end t_{simul} are shown. It can be observed that only the parameters a_C/H_S and $a(t)/H_S$ differed significantly between a non-breaking and breaking wave crest. Otherwise, the values of the non-breaking wave crests were in the value ranges of the breaking wave crests. The crest amplitude a_C for a breaking wave was at least 1.5 times larger than for a non-breaking wave. This res-

6. Detection and Prediction of Breaking Onset in Wave Trains

Table 6.8.: Geometrical and instantaneous parameters for the highest (and steepest) wave crest at the time of simulation end for non-breaking test runs, and minimum and maximum values for the breaking test runs.

	Non-Breaking Wave Crest		Breaking Wave Crest			
	$s_{Z,i} = 0.01$	$s_{Z,i} = 0.02$	$s_{Z,i} = 0.01$	$s_{Z,i} = 0.02$	$s_{Z,i} = 0.01$	$s_{Z,i} = 0.02$
a_C/H_S	0.48	0.47	0.73	2.11	0.79	1.92
f_0/f_P	3.57	2.92	1.02	4.12	1.02	2.26
$a(t)/H_S$	0.49	0.48	0.74	2.17	0.80	1.92
$f(t) * L_P$	9.41	5.79	3.00	13.61	2.25	8.14
s_Z	0.07	0.09	0.02	0.26	0.03	0.11
$s_Z(t)$	0.09	0.11	0.05	0.47	0.07	0.61
μ_V	1.00	0.67	0.00	7.00	0.11	4.75
μ_H	0.88	0.92	0.49	0.99	0.62	1.00
s_{ZC}	0.06	0.08	0.01	0.25	0.02	0.11
s_{ZT}	0.01	0.01	0.00	0.06	0.00	0.02
s'_C	0.25	0.16	0.03	0.58	0.09	0.34
s''_C	0.25	0.24	0.03	0.98	0.05	0.95

ult agrees with the observation from the field measurements of Holthuijsen and Herbers (1986), who observed that the average crest amplitude of breaking waves was about 1.6 times greater than the average crest amplitude of all the measured waves.

Conclusions

It can be observed that only the parameters a_C/H_S and $a(t)/H_S$ differed significantly between a non-breaking and breaking wave crest of a steep wave. The crest amplitude a_C for a breaking wave was at least 1.5 times larger than for a non-breaking wave. Otherwise, the values of the non-breaking wave crests were in the value ranges of the breaking wave crests.

6.2.3. Comparison with Physical Model Tests

Bonmarin and Ramamonjiarisoa (1985) and Bonmarin et al. (1989) conducted physical model tests with monochromatic wave trains with an initial wave steepness in the order of magnitude of $H/L_0 = 0.08$, which broke because of modulational instability. The

deformation of the breaking wave crest was recorded spatially by means of high-speed cameras. Those differences in the generation and type of wave breaking had to be taken into account when compared with the results of this thesis.

In Fig. 6.14, the measured values of the geometrical parameters of Bonmarin and Ramamonjiarisoa (1985) are shown with the simulated NWF data for the tests with an initial spectral steepness of $s_{Z,i} = 0.071$. It can be observed that the crest amplitudes a_C were similar for the simulated and measured data and were of the same order of magnitude. For the remaining geometrical parameters, the measured values of Bonmarin et al. exceeded the simulated values. In addition, the behaviour of the trough steepness $s_{ZT} = a_T/L$ and the crest front steepness $s'_C = a_C/L'$ differed from the measured values. The differences in the behaviour and in the magnitudes of the values can be explained by several causes: Bonmarin and Ramamonjiarisoa (1985) investigated monochromatic wave trains, no sea state spectra, and generated wave breaking through modulational instabilities rather than wave-wave interaction.

The differences between the results of Bonmarin and the NWF data also showed that a transfer of the model experiments to the nature is not easily possible, since natural waves are directional seas with a spectrum of frequencies. Bonmarin and Ramamonjiarisoa (1985), as well as the author of this thesis, concluded that there are no universal values for the geometrical parameters which define breaking onset.

6.3. Prediction of Breaking Onset

In this section the results of the analysis of the development of the wave train towards breaking onset are presented, focusing on the geometrical and instantaneous parameters and their distribution. The wave train, which was analysed, was read out at the location of the highest wave crest at the time of breaking onset. It contained the ten waves before the breaking wave; the wave which was about to break itself was not taken into account. Characteristic phenomena of the wave train before breaking onset were determined in order to not only detect but also to predict the breaking onset. The threshold method was applied again to detect breaking onset and the MARKOV chain method was carried out to predict breaking onset.

In Figs. 6.15 to 6.17, the median values of the geometrical and instantaneous parameters of the single waves in the wave train are plotted for the test runs with an initial spectral steepness of $s_{Z,i} = 0.027, 0.044, 0.067$. It can be observed that approximately five to six waves before breaking onset the wave train started clearly to deform. The crest amplitude a_C and the instantaneous amplitude $a(t)$ increased towards breaking on-

6. Detection and Prediction of Breaking Onset in Wave Trains

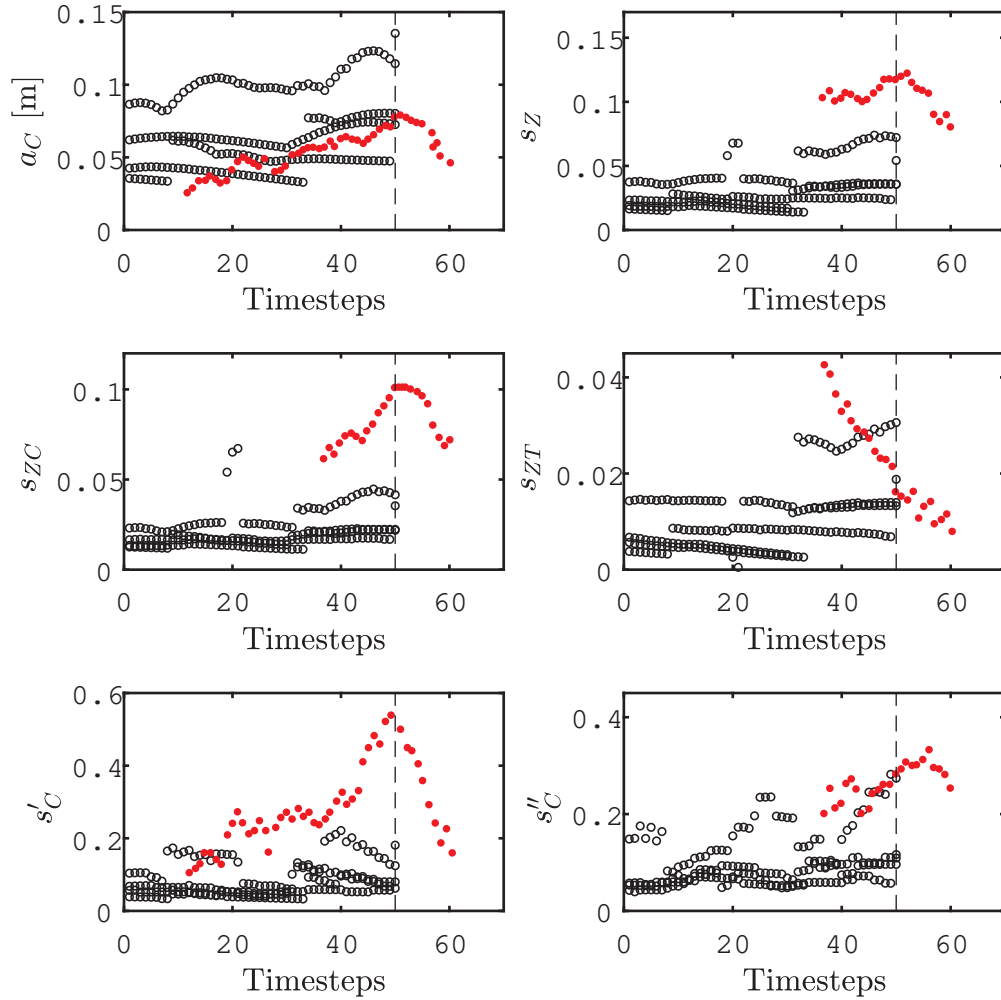


Figure 6.14.: Development of geometrical parameters against time steps ($\Delta t = 0.04\text{s}$) with the simulated NWF data (black circle markers) for the test with $s_{Z,i} = 0.071$ and the measured data (filled red circle markers) by Bonmarin and Ramamonjarisoa (1985). The breaking onset is marked by a dashed line.

set and reached their maximum with the last wave before the breaking wave. The larger the initial spectral steepness $s_{Z,i}$ the smaller the median values of a_C/H_S and $a_C(t)/H_S$, but the larger the gradient from the 1st to the 10th wave. For small spectral steepnesses $s_{Z,i}$ the wave train had time to develop and to reach a critical amplitude or steepness. For large spectral steepnesses this increase of amplitude and steepness happened quickly. The wave frequency f_0 and the instantaneous frequency $f(t)$ did not change significantly in the wave train and they did not show uniform behaviour for all initial spectral steepnesses $s_{Z,i}$. This behaviour was consistent with the results of the physical model tests, see section 6.1. Since the frequency did not change significantly indicates that the wave, which was about to break, was part of a wave group and broke likely due to wave-wave interaction and not due to modulational instability.

The wave steepness s_Z increased towards breaking onset; the larger the initial spectral steepness $s_{Z,i}$ the larger the gradient. For small spectral steepnesses $s_{Z,i}$ the wave steepness s_Z hardly increased. This different behaviour depending on the spectral steepness $s_{Z,i}$, suggests that different physical phenomena caused the wave breaking or different types of wave breaking occurred.

The instantaneous steepness $s_Z(t)$ increased quickly in the last five waves before breaking onset, whereby the increase was greater for the large initial spectral steepnesses.

The horizontal asymmetry $\mu_H = a_C/H$ increased only for the small initial spectral steepness $s_{Z,i} = 0.027$ in the last three waves before breaking onset. The vertical steepness $\mu_V = L''/L'$ changed significantly for small spectral steepnesses $s_{Z,i}$. For spectral steepnesses $s_{Z,i} \geq 0.044$ the vertical asymmetry increased in the last four waves before breaking onset.

The alternative wave steepnesses besides s_Z , which were $s_{ZC} = a_C/L$, $s_{ZT} = a_T/L$, $s'_C = a_C/L'$ and $s''_C = a_C/L''$, behaved similarly to s_Z and increased their values 1.5 times for small initial spectral steepnesses $s_{Z,i}$ and doubled them for large initial spectral steepnesses. For the initial spectral steepnesses $s_{Z,i} = 0.044$ and $s_{Z,i} = 0.067$, the steepnesses increased clearly in the last four to five waves before breaking onset. For the small initial spectral steepness $s_{Z,i} = 0.027$, the steepnesses acted slightly different, namely they did not change significantly in the last three waves before breaking onset. This indicates a wave group which broke due to modulational instability. That assumption was also supported by the observation that μ_H was not pronounced asymmetric as it is typical for a deep water bore breaking wave with $\mu_H = 0.9$, which is a highly non-linear wave-wave interaction, see Kjeldsen and Myrhaug (1981).

Tabs. 6.9 and 6.10 summarises the minimum and maximum values of the geometrical and instantaneous parameters for the last wave before the breaking wave for every initial

6. Detection and Prediction of Breaking Onset in Wave Trains

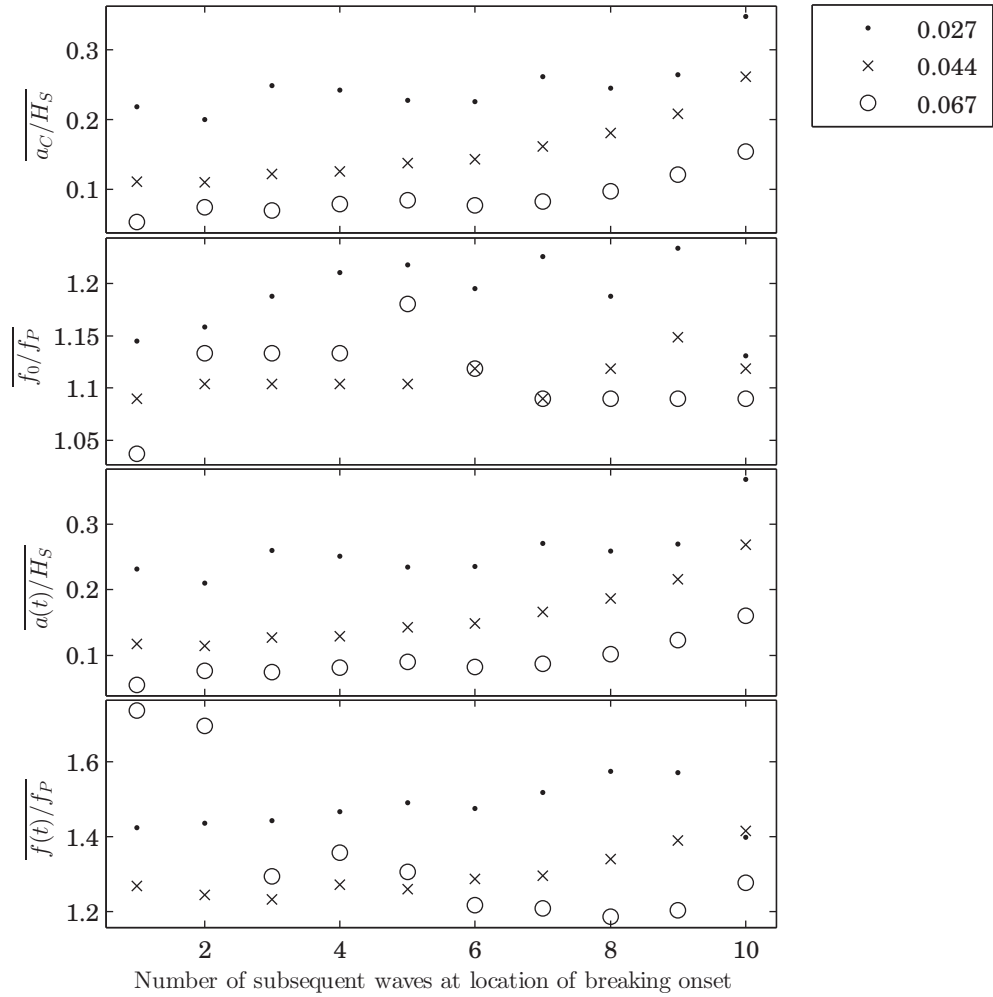


Figure 6.15.: Development of geometrical and instantaneous parameters (part 1, amplitudes and frequencies) of the wave train at location of breaking onset for the test runs with initial spectral steepness $s_{Z,i} = 0.027, 0.044, 0.067$ over the last ten waves before the breaking wave.

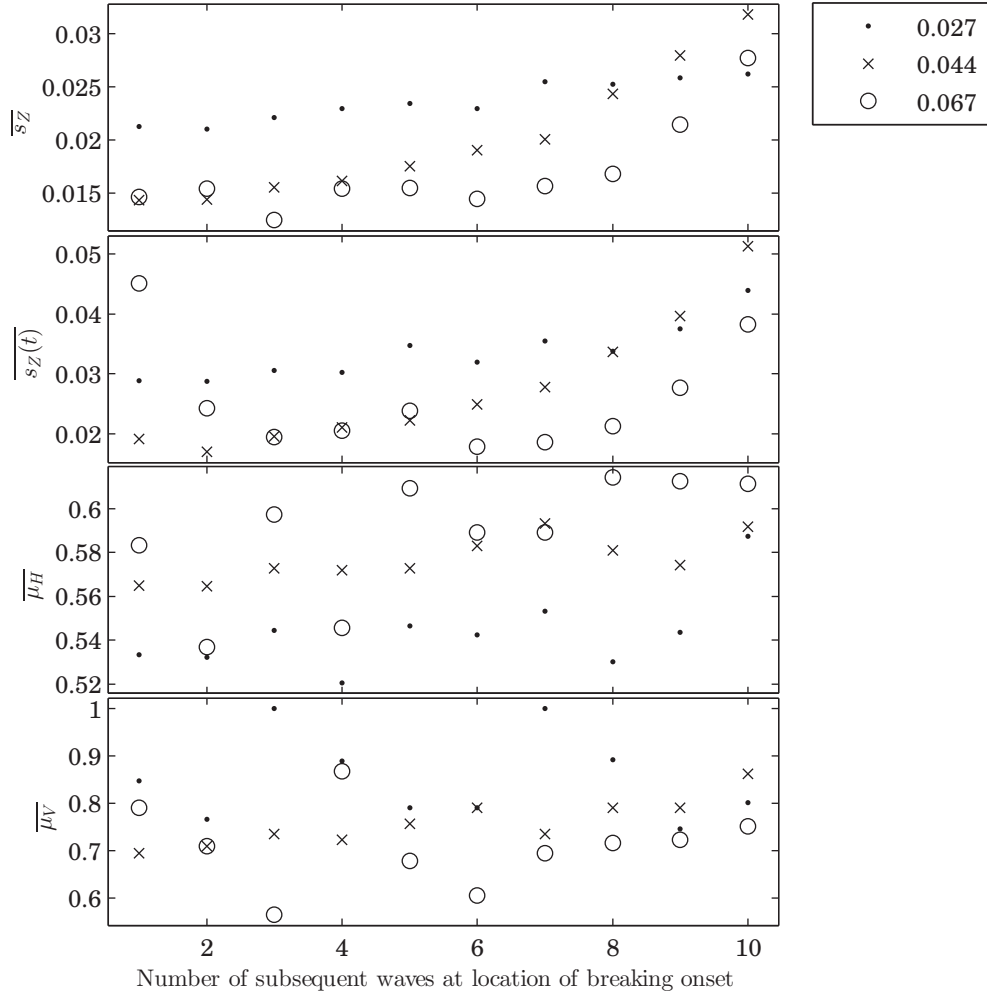


Figure 6.16.: Development of geometrical and instantaneous parameters (part 2, steepnesses and asymmetries) of the wave train at location of breaking onset for the test runs with initial spectral steepness $s_{Z,i} = 0.027, 0.044, 0.067$ over the last ten waves before the breaking wave.

6. Detection and Prediction of Breaking Onset in Wave Trains

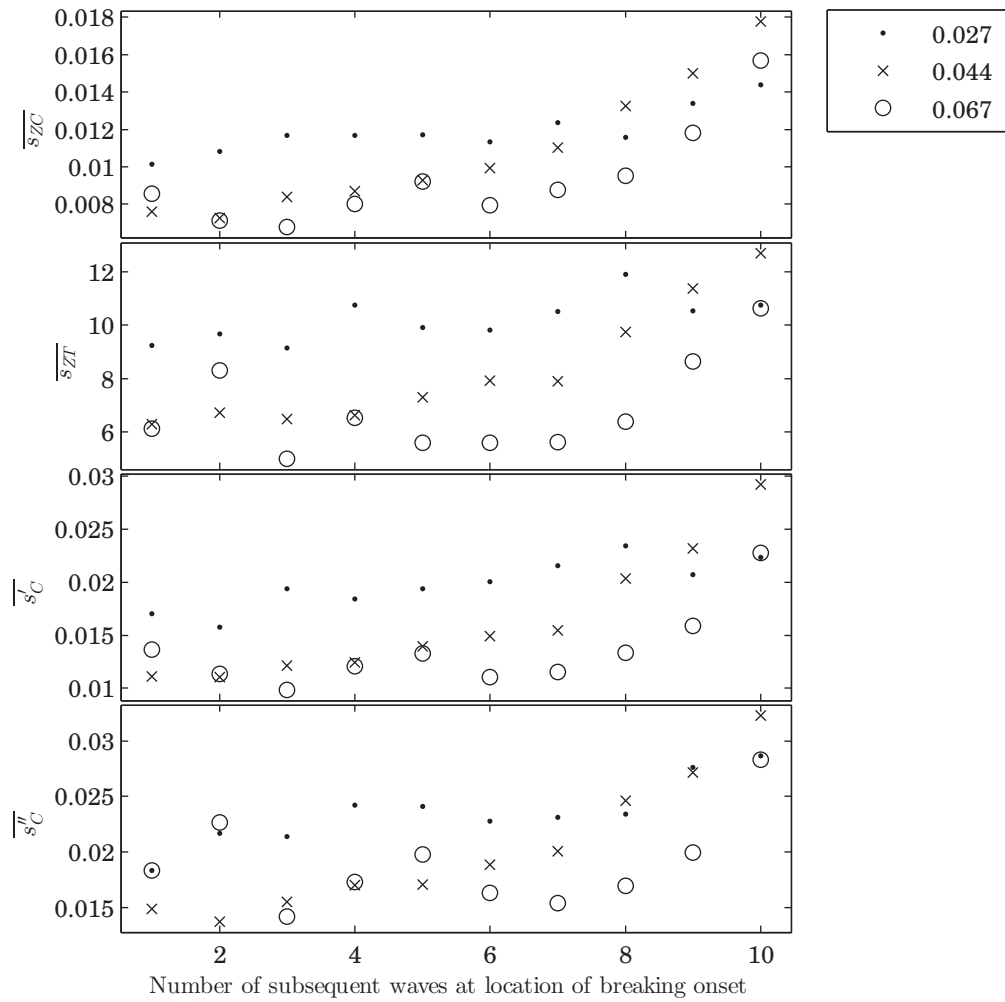


Figure 6.17.: Development of geometrical and instantaneous parameters (part 3, steepnesses) of the wave train at location of breaking onset for the test runs with initial spectral steepness $s_{Z,i} = 0.027, 0.044, 0.067$ over the last ten waves before the breaking wave.

spectral steepness $s_{Z,i}$. The parameters were within these ranges before the wave broke. The maximum values can be taken as thresholds for detection. Those results confirm that there is no universal value to detect wave breaking. All these wave trains broke and covered a large range of values.

6.3.1. Markov Chain

In order to allow a prediction of breaking onset, the development of the wave train is stochastically described by means of the MARKOV chain in this section. The MARKOV chain is a mathematical model that describes the probabilities of observing a certain sequence of discrete states. At each step of the process, the model may generate an output, or emission, depending on which state it is in, and then make a transition to another state. Here, the sets of states $i = i_1, i_2, \dots, i_r$ were the ten waves ($r = 10$) before the breaking wave and the emissions for every step were the geometrical and instantaneous parameters. It is possible to determine, for example, the probability that the 10th wave had a crest amplitude with the median value $a_C/H_S = 0.2$, if the 5th wave had the median value $a_C/H_S = 0.1$. The MARKOV chain starts in the initial state i_0 at step 0. The chain then transition to state i_1 with probability T_{1i_1} (transition probability) and emits an output s_{k1} with probability $E_{i_1k_1}$ ($k = 12$, since there are 12 geometrical and instantaneous parameters). Consequently, the probability of observing the sequence of state $i_1i_2\dots i_r$ and the sequence of emissions $s_{k1}s_{k2}\dots s_{kr}$ in the first r steps is $p = T_{1i_1}E_{i_1k_1} * T_{i_1i_2}E_{i_2k_2} \dots * T_{i_{r-1}i_r}E_{i_rk_r}$. Since the transition from one wave to the next can only happen in one direction, namely towards the 10th wave, the transition probability from, for example, state i_2 (2nd wave) to state i_1 (1st wave) is $T_{i_2i_1} = 0$. Thus, the transition probability is $T_{i_1i_2} = T_{i_2i_3} = \dots = T_{i_9i_{10}} = 1$. The emission probabilities $E_{i_rk_r}$ were the relative frequencies of the geometrical and instantaneous parameters. In Figs. 6.18 to 6.20 the boxplots of the geometrical and instantaneous parameters of the single waves in the wave train at the location of breaking onset are plotted for the test runs with an initial spectral steepness of $s_{Z,i} = 0.044$. As noted in section 6.3, the wave train began to alter significantly approximately five to six waves before the breaking wave. The median values of the last six waves before breaking onset are summarised in Tab. 6.11 for all geometrical and instantaneous parameters. In order to quantify the change in the wave train, the absolute value of the gradients of the median values are summarised in Tab. 6.12. It is observed that the median values and their gradients increased towards breaking onset.

As mentioned above, the probability of a particular sequence of events occurring is the product of their single probabilities. Since the relative frequencies were known here,

6. Detection and Prediction of Breaking Onset in Wave Trains

Table 6.9.: Minimum and maximum values of geometrical and instantaneous parameters for the 10th wave (last wave before the breaking wave) for the test runs with initial spectral steepness $s_{Z,i} = 0.01 - 0.035$.

$s_{Z,i}$	0.01		0.02		0.027		0.033		0.035	
a_C/H_S	0.006	1.00	0.009	0.68	0.004	1.04	0.006	0.85	0.001	0.81
f_0/f_P	0.897	4.58	0.878	3.17	0.709	5.94	0.659	8.50	0.543	7.92
$a(t)/H_S$	0.048	1.45	0.039	0.69	0.033	1.05	0.032	0.86	0.040	0.81
$f(t)/f_P$	-2.999	24.67	-0.506	3.40	-2.337	8.71	-0.104	6.23	-1.586	5.94
s_Z	0.008	0.31	0.009	0.05	0.005	0.07	0.008	0.12	0.006	0.16
$s_Z(t)$	0.007	2.33	0.001	0.13	0.000	0.30	0.001	0.43	0.001	0.69
μ_V	0.000	25.00	0.103	15.21	0.000	27.80	0.023	87.11	0.000	26.01
μ_H	0.017	0.97	0.034	0.62	0.018	0.96	0.021	0.99	0.005	0.99
s_{ZC}	0.000	0.21	0.002	0.02	0.001	0.05	0.001	0.11	0.000	0.12
s_{ZT}	0.002	0.10	0.004	0.05	0.001	0.05	0.000	0.09	0.000	0.07
s'_C	0.004	6.95	0.004	0.04	0.001	0.13	0.001	0.16	0.001	0.39
s''_C	0.003	0.34	0.002	0.12	0.001	0.56	0.001	0.73	0.001	0.27

Table 6.10.: Minimum and maximum values of geometrical and instantaneous parameters for the 10th wave (last wave before the breaking wave) for the test runs with initial spectral steepness $s_{Z,i} = 0.044 - 0.071$.

$s_{Z,i}$	0.044		0.05		0.055		0.067		0.071	
a_C/H_S	0.001	0.79	0.001	0.54	0.002	0.53	0.001	0.53	0.001	0.43
f_0/f_P	0.518	9.44	0.341	9.44	0.500	7.08	0.423	4.47	0.497	3.93
$a(t)/H_S$	0.005	0.79	0.010	0.54	0.011	0.54	0.008	0.54	0.008	0.43
$f(t)/f_P$	-3.989	31.23	-1.741	5.06	-26.271	5.21	-1.538	17.63	-5.032	6.37
s_Z	0.003	0.32	0.002	0.11	0.004	0.12	0.003	0.21	0.002	0.12
$s_Z(t)$	0.000	1.49	0.000	0.33	0.000	1.39	0.000	1.38	0.000	0.50
μ_V	0.000	49.00	0.000	21.16	0.000	49.00	0.000	60.06	0.000	38.21
μ_H	0.003	1.00	0.012	0.99	0.027	0.99	0.015	1.00	0.011	0.98
s_{ZC}	0.000	0.27	0.000	0.10	0.001	0.11	0.000	0.18	0.001	0.09
s_{ZT}	0.000	0.15	0.001	0.08	0.000	0.05	0.000	0.09	0.000	0.08
s'_C	0.000	1.06	0.000	0.60	0.001	1.14	0.000	0.69	0.000	1.56
s''_C	0.000	1.57	0.002	0.23	0.001	0.23	0.001	1.03	0.001	0.25

Table 6.11.: Median values for every geometrical and instantaneous parameter for the last six waves before the breaking wave for the test runs with initial spectral steepness $s_{Z,i} = 0.044$.

	5th wave	6th wave	7th wave	8th wave	9th wave	10th wave
a_C/H_S	0.14	0.14	0.16	0.18	0.21	0.26
f_0/f_P	1.10	1.12	1.09	1.12	1.15	1.12
$a(t)/H_S$	0.14	0.15	0.17	0.19	0.22	0.27
$f(t)/f_P$	1.26	1.29	1.29	1.34	1.39	1.41
s_Z	0.02	0.02	0.02	0.02	0.03	0.03
$s_Z(t)$	0.02	0.02	0.03	0.03	0.04	0.05
μ_V	0.76	0.79	0.73	0.79	0.79	0.86
μ_H	0.57	0.58	0.59	0.58	0.57	0.59
s_{ZC}	0.01	0.01	0.01	0.01	0.02	0.02
s_{ZT}	0.01	0.01	0.01	0.01	0.01	0.01
s'_C	0.01	0.01	0.02	0.02	0.02	0.03
s''_C	0.02	0.02	0.02	0.02	0.03	0.03

those were taken. The number of classes were calculated with Eq. (5.1) and $m = 14$ was selected. In Tab. 6.13 the relative frequencies of the medians and their products are summarised for all parameters and for the six last waves in the wave train. The product describes the probability that the parameters in the last six waves will take the values of the medians. In Tab. 6.14, on the other hand, the maximum relative frequencies and their product are summarised, i.e. the most probable sequence of the parameters is described here. The corresponding value ranges are summarised in Tab. 6.15. For example, the 5th wave in the wave train had for its relative crest amplitude a_C/H_S a maximum relative frequency of 0.22 and it ranged from 0.05 to 0.1. The median value of the same wave was $a_C/H_S = 0.14$ with a relative frequency of 0.19.

6. Detection and Prediction of Breaking Onset in Wave Trains

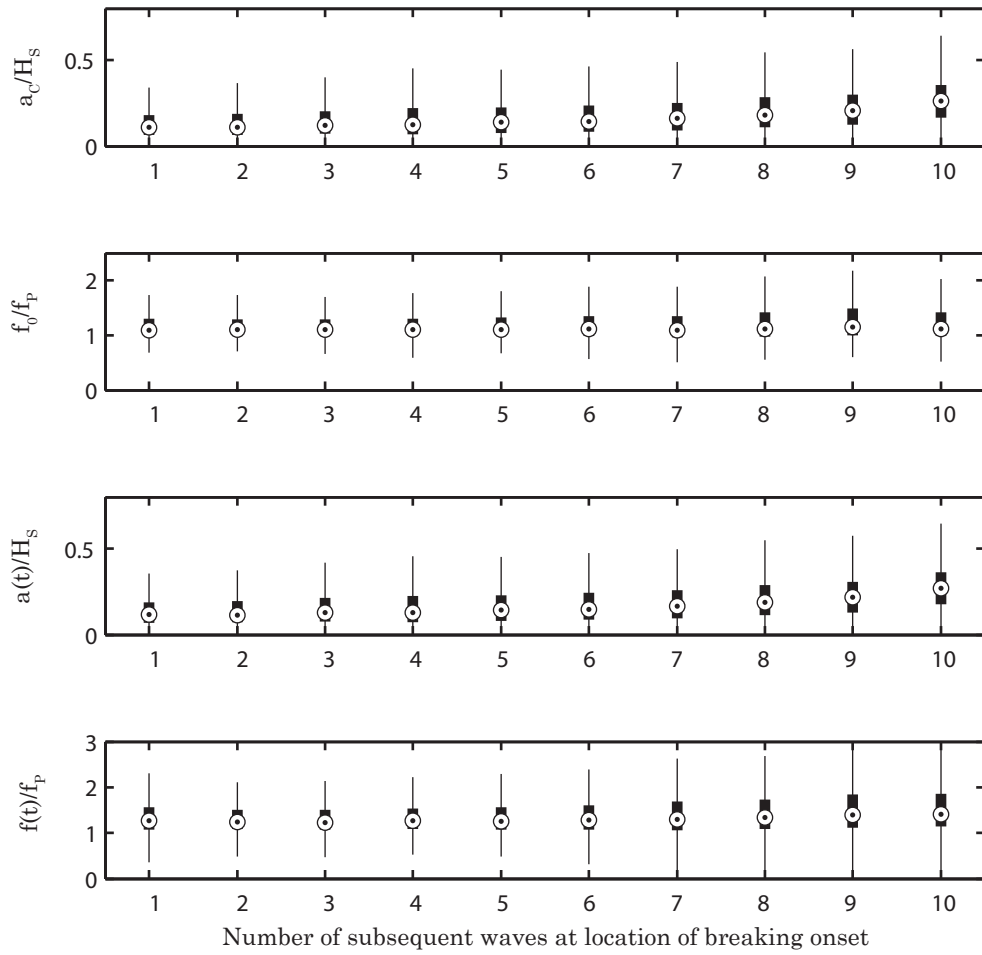


Figure 6.18.: Boxplots of geometrical and instantaneous parameters (part 1, amplitudes and frequencies) of the wave train at location of breaking onset for $s_{Z,i} = 0.044$ over the last ten waves before the breaking wave.

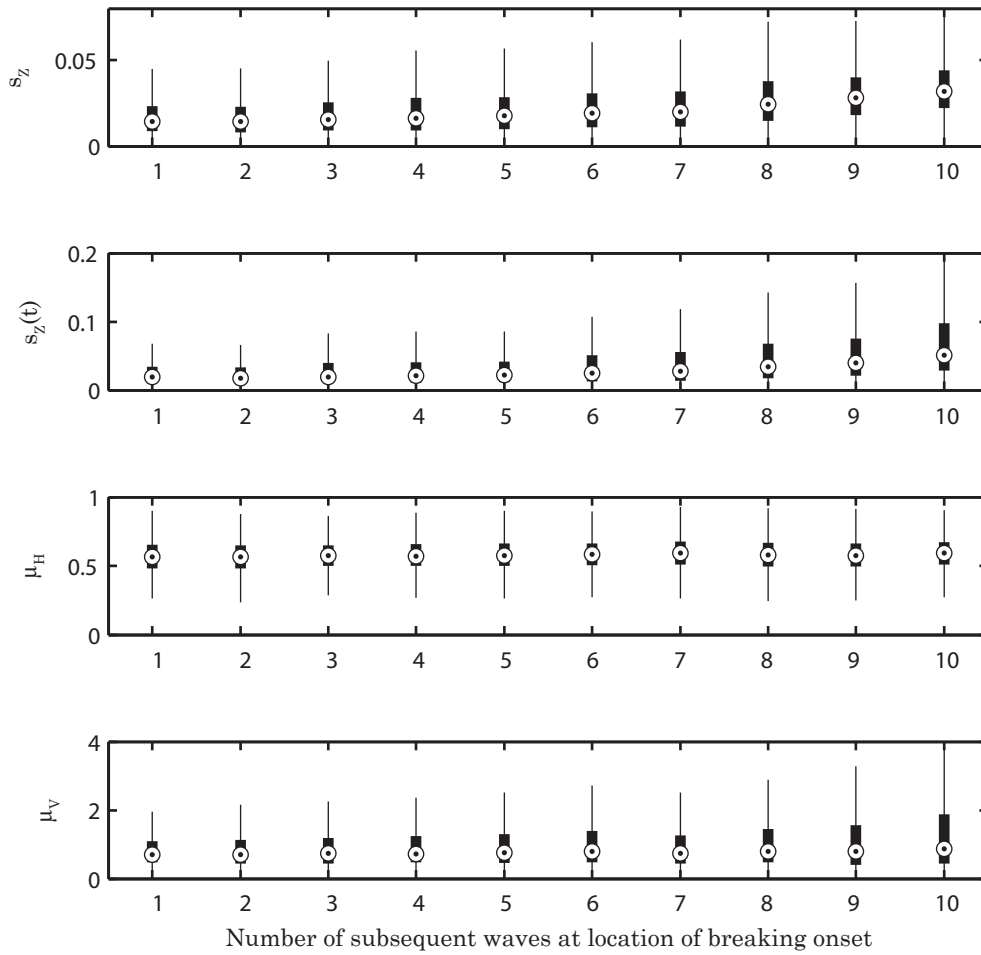


Figure 6.19.: Boxplots of geometrical and instantaneous parameters (part 2, steepnesses and asymmetries) of the wave train at location of breaking onset for $s_{Z,i} = 0.044$ over the last ten waves before the breaking wave.

6. Detection and Prediction of Breaking Onset in Wave Trains

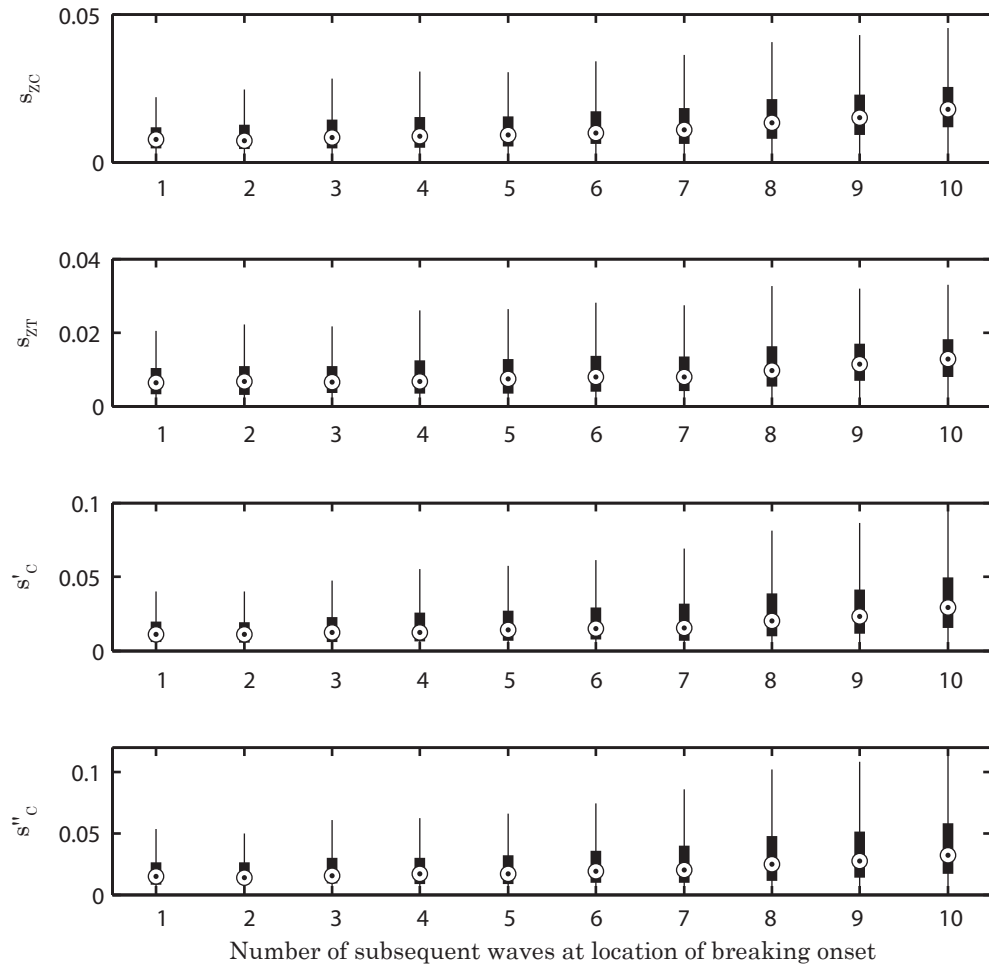


Figure 6.20.: Boxplots of geometrical and instantaneous parameters (part 3, steepnesses) of the wave train at location of breaking onset for $s_{Z,i} = 0.044$ over the last ten waves before the breaking wave.

Table 6.12.: Absolute value of the gradient of the median values for every geometrical and instantaneous parameter for the last six waves before the breaking wave for the test runs with initial spectral steepness $s_{Z,i} = 0.044$.

	5th wave	6th wave	7th wave	8th wave	9th wave	10th wave
a_C/H_S	0.0088	0.0114	0.0186	0.0232	0.0407	0.0543
f_0/f_P	0.0073	0.0071	0.0000	0.0295	0.0000	0.0302
$a(t)/H_S$	0.0096	0.0116	0.0188	0.0251	0.0415	0.0531
$f(t)/f_P$	0.0072	0.0157	0.0273	0.0492	0.0366	0.0242
s_Z	0.0014	0.0013	0.0027	0.0039	0.0037	0.0040
$s_Z(t)$	0.0019	0.0026	0.0044	0.0060	0.0089	0.0119
μ_V	0.0311	0.0107	0.0019	0.0277	0.0361	0.0721
μ_H	0.0057	0.0099	0.0012	0.0093	0.0058	0.0175
s_{ZC}	0.0007	0.0009	0.0016	0.0020	0.0023	0.0028
s_{ZT}	0.0006	0.0003	0.0009	0.0017	0.0015	0.0013
s'_C	0.0012	0.0008	0.0027	0.0038	0.0044	0.0060
s''_C	0.0009	0.0015	0.0029	0.0036	0.0039	0.0051

6. Detection and Prediction of Breaking Onset in Wave Trains

Table 6.13.: Relative frequency of the median values for every geometrical and instantaneous parameter for the last six waves before the breaking wave for the test runs with initial spectral steepness $s_{Z,i} = 0.044$.

	5th wave	6th wave	7th wave	8th wave	9th wave	10th wave	Product
a_C/H_S	0.19	0.20	0.22	0.18	0.18	0.18	0.00005
f_0/f_P	0.99	0.96	0.81	0.87	0.96	0.54	0.34685
$a(t)/H_S$	0.20	0.17	0.21	0.18	0.17	0.17	0.00004
$f(t)/f_P$	0.61	0.87	0.70	0.96	0.93	0.81	0.26778
s_Z	0.65	0.97	0.32	0.94	0.68	0.48	0.06282
$s_Z(t)$	0.84	0.87	0.82	0.72	0.82	0.78	0.27650
μ_V	0.83	0.91	0.95	0.94	0.97	0.87	0.56840
μ_H	0.25	0.24	0.24	0.23	0.21	0.25	0.00017
s_{ZC}	0.67	1.00	0.32	0.97	0.89	0.57	0.10487
s_{ZT}	0.59	0.28	0.64	0.56	0.41	0.43	0.01036
s'_C	0.76	0.94	0.90	0.94	0.75	0.88	0.40287
s''_C	0.80	0.87	0.95	0.66	0.70	0.93	0.28851

Table 6.14.: Maximum relative frequency for every geometrical and instantaneous parameter for the last six waves before the breaking wave for the test runs with initial spectral steepness $s_{Z,i} = 0.044$.

	5th wave	6th wave	7th wave	8th wave	9th wave	10th wave	Product
a_C/H_S	0.22	0.20	0.22	0.18	0.18	0.18	0.00005
f_0/f_P	0.99	0.96	0.81	0.87	0.96	0.54	0.34685
$a(t)/H_S$	0.22	0.20	0.21	0.18	0.17	0.17	0.00005
$f(t)/f_P$	0.61	0.87	0.70	0.96	0.93	0.81	0.26778
s_Z	0.65	0.97	0.32	0.94	0.68	0.48	0.06282
$s_Z(t)$	0.84	0.87	0.82	0.72	0.82	0.78	0.27650
μ_V	0.83	0.91	0.95	0.94	0.97	0.87	0.56840
μ_H	0.25	0.24	0.24	0.23	0.23	0.25	0.00018
s_{ZC}	0.67	1.00	0.32	0.97	0.89	0.57	0.10487
s_{ZT}	0.59	0.38	0.64	0.56	0.41	0.43	0.01408
s'_C	0.76	0.94	0.90	0.94	0.75	0.88	0.40287
s''_C	0.80	0.87	0.95	0.66	0.70	0.93	0.28851

6. Detection and Prediction of Breaking Onset in Wave Trains

Table 6.15.: Minimum and maximum values of the geometrical and instantaneous parameters for their respective maximum relative frequencies (see Tab. 6.14) for the last six waves before the breaking wave for the test runs with initial spectral steepness $s_{Z,i} = 0.044$.

	5th wave		6th wave		7th wave		8th wave		9th wave		10th wave	
a_C/H_S	0.05	0.10	0.10	0.14	0.12	0.18	0.15	0.20	0.16	0.22	0.23	0.28
f_0/f_P	0.51	3.51	0.57	2.55	0.50	1.48	0.39	1.88	0.61	2.59	0.52	1.16
$a(t)/H_S$	0.05	0.10	0.10	0.14	0.06	0.12	0.15	0.20	0.17	0.22	0.23	0.28
$f(t)/f_P$	0.37	1.37	-0.30	1.98	1.06	2.92	0.30	3.64	0.74	3.30	1.04	3.56
s_Z	0.00	0.02	0.00	0.06	0.01	0.03	0.00	0.06	0.00	0.04	0.03	0.05
$s_Z(t)$	0.00	0.06	0.00	0.08	0.00	0.07	0.00	0.06	0.00	0.10	0.00	0.11
μ_V	0.00	1.86	0.00	2.95	0.00	5.07	0.00	5.28	0.00	7.50	0.00	3.50
μ_H	0.51	0.57	0.57	0.64	0.57	0.64	0.57	0.64	0.50	0.57	0.57	0.64
s_{ZC}	0.00	0.01	0.00	0.06	0.01	0.01	0.00	0.05	0.00	0.03	0.00	0.02
s_{ZT}	0.00	0.01	0.00	0.01	0.00	0.01	0.00	0.01	0.01	0.02	0.01	0.02
s'_C	0.00	0.03	0.00	0.07	0.00	0.06	0.00	0.08	0.00	0.04	0.00	0.08
s''_C	0.00	0.04	0.00	0.05	0.00	0.09	0.00	0.04	0.00	0.05	0.00	0.11

Conclusions

- The wave train started to deform five to six waves before breaking onset. Wave trains with small initial spectral steepnesses $s_{Z,i}$ had time to develop and reached large median values for a_C/H_S and $a_C(t)/H_S$. Wave trains with large initial spectral steepnesses $s_{Z,i}$ broke fast, thus, had less time to develop, and reached smaller median values for a_C/H_S and $a_C(t)/H_S$; their deformation happened quickly.
- MARKOV chains were determined for the last six waves before breaking onset and their median values of geometrical and instantaneous parameters for each initial spectral steepnesses $s_{Z,i}$ were presented.

7. Summary & Outlook

7.1. Summary

The main objective of this study was to analyse the variability of wave breaking onset, in order to gain deeper knowledge of the frequency and likelihood of occurrence of wave breaking, allowing many applications to a more economic design and safety of offshore structures. Breaking onset is defined as an instantaneous state of wave dynamics where a wave has not started to break but cannot return to a stable state either. In this context, investigations on breaking onset in irregular wave trains (JONSWAP sea spectrum) in intermediate water depth were carried out using laboratory and hydronumerical model tests. A numerical wave tank was applied to generate a large data set of parameters of breaking onset for a reliable probabilistic analysis, in contrast to many previous studies in literature which analysed single wave breaking events in mono-/quasi-monochromatic wave trains and focused on energy dissipation or slamming forces on structures. Present investigations focused on the evolution of wave trains towards and at breaking onset to describe the stochastic process of breaking onset, to find precursors and indicators of breaking onset, and to determine the optimal sample size of test runs to get a reliable result of the parameters of breaking onset. By this means, insights on the variability of breaking onset and its distribution function could be achieved, which have not been available beforehand.

The physical model tests were carried out in the wave flume of the Ludwig-Franzius-Institute in a length scale of 1:40. In parallel, hydronumerical model tests using a numerical wave flume developed by Sriram (2008) and Sriram et al. (2006; 2007; 2010), based on the fully non-linear potential flow theory (semi-arbitrary Lagrangian-Eulerian Finite Element Method (SALE-FEM, structured version)), were conducted in the same length scale to complement the laboratory investigations and to increase the possible test run length and number. The hydronumerical simulations terminated before simulation end when the water surface became discontinuous. That point of termination of simulation was defined as physical breaking onset when the wave with the maximum wave crest and the wave with the maximum wave steepness were the same wave or less than one single

7. Summary & Outlook

wave apart. Breaking onset was characterised by the time to breaking onset t_{br} (temporal distance from simulation start to end) and location of breaking onset x_{br} (spatial distance from inlet to peak of breaking wave crest). As design database the wave measurements of research platform FINO1 in the North Sea for the time period 2004-2011 were used and JONSWAP spectra were selected in such a way that the initial spectral steepness $s_{Z,i} = H_S/L_P$ covered daily and storm events. Further input parameters were water depth, enhancement factor of JONSWAP spectrum, phase angle distribution, and number of waves in a wave train. By means of the random phase angle distribution, every considered spectrum was transformed multiple times (up to 500 times) to artificial, but physically-sound time series of water surface elevations.

The cause-effect relationship between input wave train and breaking onset was investigated with a dimensional analysis (BUCKINGHAM π theorem) and an analysis of the uni- and bivariate (copula) distribution functions. The optimal sample size of test runs was derived by means of a convergence analysis. Indicators of breaking onset were detected by analysing the surface elevation (over time and over flume length) and applying the threshold method which assumed that breaking onset happens when a parameter exceeds a certain threshold value. Precursors of breaking onset were presented with MARKOV chains of the geometrical and instantaneous parameters, which described the conditions that had to be met stochastically for wave instability to occur.

Influencing Factors on Wave Breaking Onset

The sensitivity of the input wave train ($H_S, T_P, \gamma, N_W, h, \varphi$) to breaking onset (t_{br}, x_{br}) was firstly analysed individually and subsequently with a dimensional analysis based on the hydronumerical model tests.

1. The experiments showed that breaking onset was highly sensitive to the sequence of waves in the input wave train (phase angle distribution φ), to the initial spectral steepness $s_{Z,i} = H_S/L_P$, and to the number of waves in the input wave train N_W . Different realizations of the same energy density spectra in time domain resulted in a large scatter of values for the breaking onset (t_{br}, x_{br}). The scattering of the results showed the influence of the sequence of waves in the input wave train.
2. The greater the initial spectral steepness $s_{Z,i}$, the earlier the wave train broke and the smaller the scatter of t_{br} and x_{br} . For small spectral steepnesses $s_{Z,i} \leq 0.044$, the sequence of waves in the input wave train was the main influence on breaking onset. For larger spectral steepnesses, the initial spectral steepness $s_{Z,i}$, especially H_S and, thus, the spectral energy, was the main influence on breaking onset. Even

wave trains with low spectral steepness broke when duration of simulation was chosen long enough. The inverse time of breaking onset $1/t_{br}$ is almost quadratically dependent on $s_{Z,i}$.

3. The larger the number of waves in the input wave train N_W , the later the wave train broke. For test runs with the same initial spectral steepness $s_{Z,i}$, the number of waves in the input wave train N_W had a linear influence on breaking onset. A change in water depth h or a change in enhancement factor γ did not influence breaking onset.
4. For the dimensional analysis all breaking test runs with $a_C/H_S \geq 0.9$ were considered to focus on the interesting data range. The power function $y = ax^b$ was used as a basic relation. Because the shape of the input spectrum and wave groups play an important role in wave breaking phenomenon, they were described with the spectral width ν_W , the dimensionless time of the first wave group in the input wave train $WaGoTime/T_P$, and the dimensionless number of waves in that first wave group $WaGoNum/N_W$.
5. To investigate which input variables were relevant for the dimensional analysis, three groups of input variables were formed and their results were compared with one another. Group 1 considered all parameters. Group 2 considered $s_{Z,i}$, N_W , H_S/h , and γ . Group 3 considered $s_{Z,i}$ and H_S/h .
6. The resulting equations for the predicted time and location of breaking onset based on Group 1 were

$$\frac{t_{br,pred}}{T_P} = 0.0294 s_{Z,i}^{-1.43} N_W^{0.49} \left(\frac{H_S}{h}\right)^{-0.3} \gamma^{-0.71} \left(\frac{WaGoNum}{N_W}\right)^{-0.02} \left(\frac{WaGoTime}{T_P}\right)^{0.002} \nu_W^{0.76}$$

$$\frac{x_{br,pred}}{L_P} = 0.0053 s_{Z,i}^{-2.09} N_W^{0.05} \left(\frac{H_S}{h}\right)^{-0.11} \gamma^{-1.36} \left(\frac{WaGoNum}{N_W}\right)^{-0.01} \left(\frac{WaGoTime}{T_P}\right)^{-0.05} \nu_W^{0.44}$$

Coefficients of determination were for $t_{br,pred}$ $R^2 = 0.958$ and for $x_{br,pred}$ $R^2 = 0.906$. The resulting equations for the predicted time and location of breaking onset based on

7. Summary & Outlook

Group 3 were

$$\frac{t_{br,pred}}{T_P} = 0.158s_{Z,i}^{-1.43} \left(\frac{HS}{h} \right)^{-0.04}$$

$$\frac{x_{br,pred}}{L_P} = 0.0008s_{Z,i}^{-2.09} \left(\frac{HS}{h} \right)^{-0.09}$$

Coefficients of determination were for $t_{br,pred}$ $R^2 = 0.885$ and for $x_{br,pred}$ $R^2 = 0.906$. N_W and γ were influential variables for the time of breaking onset t_{br} , but not for the location of breaking onset x_{br} . The spectral width ν_W and the wave group parameters $WaGo_{Time}$ and $WaGo_{Num}$ showed no influence on the coefficient of determination.

Variability of Wave Breaking Onset and Optimal Sample Size

The scattering of the normalised time and location of breaking onset t_{br}/T_P and x_{br}/L_P , respectively, is analysed with univariate and bivariate (copula) distribution functions. Because the scatter depended on the initial spectral steepness $s_{Z,i}$, the analyses were carried out for each $s_{Z,i}$ separately.

1. For the analysis with univariate distribution functions the probability density functions and cumulative distribution functions for GUMBEL, Gamma, WEIBULL, GAUSSIAN Normal, and RAYLEIGH were considered. The analysis showed that the larger the initial spectral steepness $s_{Z,i}$, the better all theoretical distribution functions followed the empirical distribution functions of t_{br}/T_P and x_{br}/L_P due to the decreasing scatter. The normalised time of breaking onset t_{br}/T_P was best described by the GUMBEL distribution functions. The normalised location of breaking onset x_{br}/L_P was best described by the WEIBULL distribution function.
2. Because t_{br}/T_P and x_{br}/L_P did not follow the same distribution functions, the classical multivariate approach could not be used. Instead, the ARCHIMEDEAN copulas GUMBEL, CLAYTON, and FRANK were chosen for the analysis. The analysis showed that the larger the initial spectral steepness $s_{Z,i}$ the smaller the copula parameter Θ , that is, for larger spectral steepnesses the theoretical copula did not need to be adjusted to the empirical copula as much as for smaller spectral steepnesses. The empirical copula for $(t_{br}/T_P, x_{br}/L_P)$ follows the GUMBEL copula best and data generated from the GUMBEL copula represented the behaviour of the time and location of breaking onset well. Based on the GUMBEL copula, the

cumulative distribution functions and exceedance probabilities for breaking onset were determined and can be used to estimate where and when breaking onset may occur.

3. The optimal sample size N_{opt} is the required number of test runs for a robust determination of breaking onset and was determined based on the normalised time of breaking onset t_{br}/T_P and for each initial spectral steepness $s_{Z,i}$ and the permissible deviations 1%, 2%, 5% and 10%. In the first step, only the data from the hydronumerical model tests was used and then expanded by data generated from the GUMBEL copula. The convergence analysis showed that the larger the initial spectral steepness $s_{Z,i}$ and the larger the permissible deviation, the smaller the required number of test runs N_{opt} . Considering all initial spectral steepnesses, the optimal sample size with permissible deviation of 1% was $N_{opt} = 1,800$, with a deviation of 2% it was $N_{opt} = 580$, with a deviation of 5% it was $N_{opt} = 100$, and with a deviation of 10% it was $N_{opt} = 25$.

Detection of Wave Breaking Onset in a Wave Train

The geometrical deformation and development of breaking and non-breaking wave crests and wave trains were compared with each other in order to identify indicators for breaking onset.

1. The detection of breaking onset in physical model tests was non-trivial because breaking onset is an extreme short-term state of wave dynamics and difficult to measure exactly with wave gauges. Therefore, a novel parameter based on the HILBERT transform was introduced that established a relationship between instantaneous amplitude $a(t)$ and instantaneous frequency $f(t)$. The instantaneous steepness was defined as $s_Z(t) = 2a(t)/L(t)$, where $L(t)$ was the instantaneous wavelength, which was $L(t) = 1/f(t)$ when the HILBERT transform was computed from a water surface elevation over the flume length. When the HILBERT transform was computed from a water surface elevation over time, $L(t)$ needed to be calculated using the dispersion relation and the approach of an instantaneous period $T(t) = 1/f(t)$. The instantaneous steepness $s_Z(t)$ described the relation between the envelope of surface elevation and the rate of change of the surface elevation, which are both maximal at breaking onset.
2. Based on the physical model tests with irregular wave trains and an initial spectral steepness of $s_{Z,i} = 0.044$, the following threshold parameters were found for

7. Summary & Outlook

a detection method: $\eta(t) \geq 0.8H_S$, $s_Z(t) \geq 0.4$, and $s_Z \geq 0.08$. But most importantly those indicative parameters reached their maximum at breaking onset. That means, in order to detect dominant wave breaking in irregular wave trains, the largest, steepest, and fastest deforming wave had to be found. Even when the wave gauge did not measure the exact point of breaking onset, the instantaneous steepness $s_Z(t)$ was able to detect wave breaking in an unambiguous way. The other geometrical parameters did not behave in a unique way at breaking onset, in contrast to observations for monochromatic wave trains from literature.

3. Based on the hydronumerical model tests, the deformation of breaking wave crest was analysed with a time step of $\Delta t = 0.04$ s and for the time period of 2 s. The deformation of breaking wave crest began approximately 0.4 s - 0.8 s before breaking onset.
4. The larger the initial spectral steepness $s_{Z,i}$, the later the deformation began, the smaller the change of the parameters, and the smaller the wave steepness s_Z of the breaking wave crest. In other words, the earlier the wave train broke, i.e. the less time the wave train had to develop, the faster the deformation happened.
5. For wave trains with small initial spectral steepnesses, where the wave train had time to develop, the wave crest not only rose, but also tended forward. The more time the wave train had to develop, the less it changed in the last 2 s before breaking onset. This could be an indication to different types of breakers. Since the wave frequency did not change significantly, this could be an indication that the majority of wave crests broke due to wave-wave interaction, i.e. the wave energy accumulated by the superposition of waves and thereby the waves broke. This assumption was supported by the fact that just approximately 3% of the test runs fulfilled the conditions for the presence of modulational instability, thus, wave breaking due to modulational instability was unlikely. Furthermore, the almost constant wave frequency and therefore wavelength indicated that the waves did not shorten which rather happens for depth-induced wave breaking.
6. When comparing breaking wave crests with steep, but non-breaking wave crests, it was observed that only the parameters a_C/H_S and $a(t)/H_S$ differed significantly between a non-breaking and breaking wave crest. The crest amplitude a_C was at least 1.5 times larger for a breaking wave than for a non-breaking wave. Those results confirm that there is no universal value to detect wave breaking. All these wave crest broke and covered a large range of values.

Prediction of Wave Breaking Onset

Based on the hydronumerical model test, the time series of surface elevation were read out at the location of breaking onset $\eta(x_{br}, t)$ and the last ten waves before the breaking wave were analysed to predict breaking onset. The wave which was about to break was not taken into account.

1. The wave train started to deform five to six waves before breaking onset. Wave trains with small initial spectral steepnesses $s_{Z,i}$ had time to develop and reached large median values for a_C/H_S and $a_C(t)/H_S$. Wave trains with large initial spectral steepnesses $s_{Z,i}$ broke fast, thus, had less time to develop, and reached smaller median values for a_C/H_S and $a_C(t)/H_S$; their deformation happened quickly. Since the frequency did not change significantly indicated that the wave, which was about to break, was part of a wave group and broke likely due to wave-wave interaction and not due to modulational instability.
2. MARKOV chains were determined for the last six waves before breaking onset and their median values of geometrical and instantaneous parameters for each initial spectral steepnesses $s_{Z,i}$ were presented. Furthermore, MARKOV chains were determined for the parameter values with the highest relative frequencies. This novel prediction tool provided insights how irregular wave trains deformed before breaking onset, and which median values and value ranges they most probably took on.

7.2. Outlook

Focus of this thesis was time and location of wave breaking onset and their relation to the input signal. The data of geometry of the breaking wave was used for detection and prediction of breaking onset in time series of water surface elevation. In future works, the relation between input signal and geometry of the breaking wave could be investigated by means of dimensional analysis and copula functions. Furthermore, the relation between time of breaking onset and geometry of the breaking wave could be analysed. The bivariate copula analysis carried out here could be extended to a trivariate analysis in order to investigate the relationship between time and location of breaking onset and, for example, the steepness of the breaking wave. Such an analysis would provide deeper knowledge about the frequency and likelihood of occurrence of different wave breaking geometries, which is of interest because the geometry of a breaking wave has a significant influence on slamming forces on offshore structures. Furthermore, determination of the

7. Summary & Outlook

distribution functions of the geometrical and instantaneous parameters would provide their probability density functions and improve the MARKOV chains.

Besides an extended analysis of the geometrical output data, future works could consider a complete probabilistic approach where the probability of occurrence of the sea spectra is taken into account to improve the prediction of breaking onset. In addition, future works could contain tests with different sea spectra than the JONSWAP spectrum to vary the shape of the spectrum which has an influence on wave groups and therefore on wave breaking.

Finally, the data set of very steep, but non-breaking wave trains could be extended to improve the comparison of their geometrical differences to breaking wave trains and based on that determine the maximum possible ratio of wave amplitude to significant wave height and wave steepness. More information on the transitional area of very steep, but non-breaking wave trains to breaking wave trains would improve the detection and prediction method.

Bibliography

- Babanin, A. V. (2011). *Breaking and dissipation of ocean surface waves*. Cambridge University Press, Cambridge and UK and , New York.
- Babanin, A. V., Chalikov, D., Young, I. R., and Savelyev, I. (2007). Predicting the breaking onset of surface water waves. *Geophysical Research Letters*, 34(7).
- Babanin, A. V., Chalikov, D., Young, I. R., and Savelyev, I. (2010). Numerical and laboratory investigation of breaking of steep two-dimensional waves in deep water. *Journal of Fluid Mechanics*, 644:433–463.
- Babanin, A. V. and Polnikov, V. G. (1995). On the non-gaussian nature of wind waves. *Journal of Physical Oceanography*, 6(3):241–245.
- Babanin, A. V., Waseda, T., Kinoshita, T., and Toffoli, A. (2011a). Wave breaking in directional fields. *Journal of Physical Oceanography*, 41(1):145–156.
- Babanin, A. V., Waseda, T., Shugan, I., and Hwung, H.-H. (2011b). Modulational instability in directional wave fields, and extreme wave events. pages 409–415.
- Babanin, A. V., Young, I. R., and Banner, M. L. (2001). Breaking probabilities for dominant surface waves on water of finite constant depth. *Journal of Geophysical Research*, 106(C6):11659–11676.
- Banner, M. L., Babanin, A. V., and Young, I. R. (2000). Breaking probability for dominant waves on the sea surface. *Journal of Physical Oceanography*, 30(12):3145–3160.
- Banner, M. L. and Tian, X. (1998). On the determination of the onset of breaking for modulating surface gravity water waves. *Journal of Fluid Mechanics*, 367:107–137.
- Barthélémy, X., Banner, M. L., Dias, F., Peirson, W. L., and Allis, M. J. (2011). Numerical study of a breaking wave threshold parameter. In *20th Australasian Coastal and Ocean Engineering Conference 2011 and the 13th Australasian Port and Harbour Conference 2011, COASTS and PORTS 2011*, pages 281–286.

BIBLIOGRAPHY

- Bonmarin, P. and Ramamonjarihoa, A. (1985). Deformation to breaking of deep water gravity waves. *Experiments in Fluids*, 3(1):11–16.
- Bonmarin, P., Rochefort, R., and Bourguel, M. (1989). Surface wave profile measurement by image analysis. *Experiments in Fluids*, 7(1):17–24.
- Bowman, A. W. and Azzalini, A. (2004). *Applied smoothing techniques for data analysis: The kernel approach with S-Plus illustrations*, volume 18 of *Oxford statistical science series*. Clarendon Press, Oxford, reprinted. edition.
- Buckingham, E. (1914). On physically similar systems; illustrations of the use of dimensional equations. *Physical Review Letters*, 4(4):345–376.
- Chalikov, D. (2005). Statistical properties of nonlinear one-dimensional wave fields. *Nonlinear Processes in Geophysics*, 12(5):671–689.
- Chalikov, D. (2007). Numerical simulation of the benjamin-feir instability and its consequences. *Physics of Fluids*, 19(1).
- Chalikov, D. and Babanin, A. V. (2012). Simulation of wave breaking in one-dimensional spectral environment. *Journal of Physical Oceanography*, 42(11):1745–1761.
- Chang, K. A. and Liu, P. L.-F. (1998). Velocity, acceleration and vorticity under a breaking wave. *Physics of Fluids*, 10(1):327–329.
- Clayton, D. G. (1978). A model for association in bivariate life tables and its application in epidemiological studies of familial tendency in chronic disease incidence. *Biometrika*, 65(1):141–151.
- Dawson, T. H., Kriebel, D. L., and Wallendorf, L. A. (1991). Experimental study of wave groups in deep-water random waves. *Applied Ocean Research*, 13(3):116–131.
- Dawson, T. H., Kriebel, D. L., and Wallendorf, L. A. (1993). Breaking waves in laboratory-generated jonswap seas. *Applied Ocean Research*, 15(2):85–93.
- Deheuvels, P. (1979). La fonction de dependance empirique et ses propriétés. un test non paramétrique d’independance. *Bull. Cl. Sci., V. Sér., Acad. R. Belg.*, 65:274–292.
- Ding, L. and Farmer, D. M. (1994). Observations of breaking surface wave statistics. *Journal of Physical Oceanography*, 24(6):1368–1387.
- Diorio, J. D., Liu, X., and Duncan, J. H. (2009). An experimental investigation of incipient spilling breakers. *Journal of Fluid Mechanics*, 633:271–283.

BIBLIOGRAPHY

- Dold, J. W. and Peregrine, D. H. (1986). Water-wave modulation. *Proceedings of the 20th International Conference on Coastal Engineering*, I, New York, U.S.A., Am. Soc. Civ. Engrs., 1987, Part I, Chapter 13.
- Donelan, M., Longuet-Higgins, M. S., and Turner, J. S. (1972). Periodicity in whitecaps. *Nature*, 239(5373):449–451.
- Drazen, D. A., Melville, W. K., and Lenain, L. (2008). Inertial scaling of dissipation in unsteady breaking waves. *Journal of Fluid Mechanics*, 611:307–332.
- Duncan, J. H. (1981). An experimental investigation of breaking waves produced by a towed hydrofoil. *Proceedings of the Royal Society A: Mathematical, Physical and Engineering Sciences*, 377(1770):331–348.
- Frank, M. J. (1979). On the simultaneous associativity of $f(x, y)$ and $x+y-f(x, y)$. *Aequationes Mathematicae*, 19(1):194–226.
- Fu, S. (1987). On the joint distribution of the periods and heights of sea waves. *Acta Oceanologica Sinica*, 6(4):503–509.
- Genest, C. and Favre, A.-C. (2007). Everything you always wanted to know about copula modeling but were afraid to ask. *Journal of Hydrologic Engineering*, 12(4):347–368.
- Goda, Y. (2010). *Random seas and design of maritime structures*, volume 33 of *Advanced series on ocean engineering*. World Scientific, New Jersey, 3 edition.
- Griffin, O. M., Peltzer, R. D., Wang, H. T., and Schultz, W. W. (1996). Kinematic and dynamic evolution of deep water breaking waves. *Journal of Geophysical Research*, 101(C7):16515–16531.
- Gudmestad, O. T. (1993). Measured and predicted deep water wave kinematics in regular and irregular seas. *Marine Structures*, 6(1):1–73.
- Gumbel, E. J. (1960). Distributions des valeurs extrêmes en plusieurs dimensions. *Publications de l'Institut de statistique de l'Université de Paris*, 9:171–173.
- Hansen, M. (2014). *Probabilistic Safety Assessment of Offshore Wind Turbines: Annual Report 2013*. Leibniz Universität Hannover, Hannover, Germany.
- Hansen, M. (2015). *Probabilistic Safety Assessment of Offshore Wind Turbines: Final Report*. Leibniz Universität Hannover, Hannover, Germany.

BIBLIOGRAPHY

- Hildebrandt, A. (2013). *Hydrodynamics of Breaking Waves on Offshore Wind Turbine Structures: Dissertation*. Franzius-Institut für Wasserbau, Ästuar- und Küsteningenieurwesen, Leibniz Universität Hannover.
- Holthuijsen, L. H. and Herbers, T. H. (1986). Statistics of breaking waves observed as whitecaps in the open sea. *Journal of Physical Oceanography*, 16(2):290–297.
- Hua, F. and Yuan, Y. (1992). Theoretical study of breaking wave spectrum and its application. In Banner, M. L. and Grimshaw, R. H. J., editors, *Breaking waves*, pages 277–282. Springer Berlin Heidelberg, Berlin, Heidelberg.
- Huang, N. E., Long, S. R., Bliven, L. F., and Tung, C.-C. (1984). Non-gaussian joint probability density function of slope and elevation for a nonlinear gravity wave field. *Journal of Geophysical Research*, 89(C2):1961–1972.
- Huang, N. E., Shen, Z., and Long, S. R. (1999). A new view of nonlinear water waves: The hilbert spectrum. *Annual Review of Fluid Mechanics*, 31(1):417–457.
- Huang, N. E., Shen, Z., Long, S. R., Wu, M. C., Shih, H. H., Zheng, Q., Yen, N.-C., Tung, C.-C., and Liu, H. H. (1998). The empirical mode decomposition and the hilbert spectrum for nonlinear and non-stationary time series analysis. *Proceedings of the Royal Society A: Mathematical, Physical and Engineering Sciences*, 454(1971):903–995.
- Hwang, P. A., Xu, D.-l., and Wu, J. (1989). Breaking of wind-generated waves: measurements and characteristics. *Journal of Fluid Mechanics*, 202:177–200.
- IAHR (1989). List of sea-state parameters. *Journal of Waterway, Port, Coastal and Ocean Engineering*, 115(6):793–808.
- Kennedy, R. M. and Snyder, R. L. (1983). On the formation of whitecaps by a threshold mechanism: Part ii: Monte carlo experiments. *Journal of Physical Oceanography*, (13):1493–1504.
- Kjeldsen, S. P. (1989). The experimental verification of numerical models of plunging breakers. In *Proceedings of 19th Conference on Coastal Engineering*, volume 1, pages 15–30. American Society of Civil Engineers, Houston, TX.
- Kjeldsen, S. P. and Myrhaug, D. (1979a). Breaking waves in deep water and resulting wave forces. *Proceedings of the 11th Annual Offshore Technology Conference*, 4, Dallas, U.S.A., Offshore Technol. Conf., 1979, OTC 3646:2515–2522.

- Kjeldsen, S. P. and Myrhaug, D. (1979b). *Formation of wave groups and distributions of parameters for wave asymmetry: Dannelse av bølgegrupper og statistiske fordelinger for beskrivelse av asymmetriske bølger*. Ships in rough seas = Skip i sjøgang. Part 4. Vassdrags- og havnelaboratoriet ved Norges tekniske høgskole, Trondheim.
- Kjeldsen, S. P. and Myrhaug, D. (1981). Wave-wave interactions, current-wave interactions and resulting extreme waves and breaking waves. *Proceedings of the 17th International Conference on Coastal Engineering*, 3, New York, U.S.A., Am. Soc. Civ. Engrs., 1981, Part 3, Chapter 137.
- Kraaiennest (2015). Breaking wave types: Redrawn after u.s. department of transportation - federal highway agency (fhwa) by s.l. douglas and j. krolak, fhwa: Licensed under cc by-sa 3.0 via wikimedia commons.
- Kriebel, D. L. (2000). Breaking waves in intermediate-depths with and without current. *Coastal Engineering 2000 - Proceedings of the 27th International Conference on Coastal Engineering, ICCE 2000*, 276.
- Kriebel, D. L. and Dawson, T. H. (1991). Nonlinear effects on wave groups in random seas. *Journal of Offshore Mechanics and Arctic Engineering*, 113(2):142–147.
- Kwoh, D. S. and Lake, B. M. (1984). A deterministic, coherent, and dual-polarized laboratory study of microwave backscattering from water waves, part i: Short gravity waves without wind. *IEEE Journal of Oceanic Engineering*, 9(5):291–308.
- Liu, P. C. and Babanin, A. V. (2004). Using wavelet spectrum analysis to resolve breaking events in the wind wave time series. *Annales Geophysicae*, 22(10):3335–3345.
- Longuet-Higgins, M. S. (1969). On wave breaking and equilibrium spectrum of wind-generated waves. 310(1501):151–159.
- Longuet-Higgins, M. S. (1983). On the joint distribution of wave periods and amplitudes in a random wave field. *Proceedings of the Royal Society London*, (A389):241–258.
- Longuet-Higgins, M. S. (1985). Accelerations in steep gravity waves. In *Journal of Physical Oceanography*, volume 15, pages 1570–1579.
- Longuet-Higgins, M. S. and Fox, M. J. H. (1977). Theory of the almost-highest wave: The inner solution. *Journal of Fluid Mechanics*, 80(04):721.

BIBLIOGRAPHY

- Manasseh, R., Babanin, A. V., Forbes, C., Rickards, K., Bobevski, I., and Ooi, A. (2006). Passive acoustic determination of wave-breaking events and their severity across the spectrum. *Journal of Atmospheric and Oceanic Technology*, 23(4):599–618.
- McCowan, J. (1891). On the solitary wave. *London, Edinburgh & Dublin philosophical magazine and journal of science*, 32(5).
- Melville, W. K. (1996). The role of surface-wave breaking in air-sea interaction. *Annual Review of Fluid Mechanics*, 28:279–321.
- Melville, W. K., Loewen, M. R., and Lamarre, E. (1992). Sound production and air entrainment by breaking waves: A review of recent laboratory experiments: Breaking waves: Iutam symposium sydney, australia 1991. In Banner, M. L. and Grimshaw, R. H. J., editors, *Breaking Waves. IUTAM Symposium, Sydney, Australia, 1991*, pages 139–146. Springer Berlin Heidelberg, Berlin, Heidelberg.
- Melville, W. K. and Rapp, R. J. (1988). The surface velocity field in steep and breaking waves. *Journal of Fluid Mechanics*, 189 , Apr. 1988:1–22.
- Miche, R. (1944). Mouvements ondulatoires de la mer en profondeur croissante ou décroissante. In *Annales des Ponts et Chaussées*.
- Michell, J. H. (1893). The highest waves in water. *Philosophical Magazine*, 5(36):430–437.
- Nath, J. H. and Ramsey, F. L. (1976). Probability distributions of breaking wave heights emphasizing the utilization of the jonswap spectrum. *Journal of Physical Oceanography*, (6):316–323.
- Nelsen, R. B. (2006). *An introduction to copulas*. Springer Series in Statistics. Springer, New York, 2nd ed. edition.
- Nepf, H. M., Wu, C. H., and Chan, E. S. (1998). A comparison of two- and three-dimensional wave breaking. *Journal of Physical Oceanography*, 28(7):1496–1510.
- Neumann, T., Nolopp, K., Strack, M., Mellinshoff, H., Söker, H., Mittelstädt, E., Gerasch, W. J., and Fischer, G. (2003). Erection of german offshore measuring platform in the north sea. *DEWI Magazin*, (23):32–46.
- Ochi, M. K. (2005). *Ocean waves: The stochastic approach*. Cambridge University Press, Cambridge and U.K. and , New York.

- Ochi, M. K. and Tsai, C.-H. (1983). Prediction of occurrence of breaking waves in deep water. *Journal of Physical Oceanography*, (13):2008–2019.
- Papula, L. (2002). *Mathematik für Ingenieure und Naturwissenschaftler: Band 3*. Viewegs Fachbücher der Technik. Vieweg, Braunschweig, 4. edition.
- Perlin, M., Choi, W., and Tian, Z. (2013). Breaking waves in deep and intermediate waters. *Annual Review of Fluid Mechanics*, 45:115–145.
- Perlin, M., He, J., and Bernal, L. P. (1996). An experimental study of deep water plunging breakers. *Physics of Fluids*, 8(9):2365–2374.
- Phillips, O. M. (1985). Spectral and statistical properties of the equilibrium range in wind-generated gravity waves. *Journal of Fluid Mechanics*, 156:505–531.
- Ramberg, S. E. and Griffin, O. M. (1987). Laboratory study of steep and breaking deep water waves. *Journal of Waterway, Port, Coastal and Ocean Engineering*, 113(5 , Sep. 1987, p.493-506).
- Rapp, R. J. and Melville, W. K. (1990). *Laboratory measurements of deep-water breaking waves*. Royal Society, London.
- Schlurmann, T. (2005). *Time-frequency analysis methods in hydrology and hydraulic engineering: Zugl.: Wuppertal, Univ., Habil.-Schr., 2004*, volume 14 of *Bericht / Lehr- und Forschungsgebiet Wasserbau und Wasserwirtschaft*. Univ, Wuppertal.
- Sharkov, E. A. (2007). *Breaking ocean waves: Geometry, structure and remote sensing*. Springer-Praxis books in geophysical sciences. Springer, Berlin and New York.
- She, K., Greated, C. A., and Easson, W. J. (1994). Experimental study of three-dimensional wave breaking. *Journal of Waterway, Port, Coastal and Ocean Engineering*, 120(1):20–36.
- Skjelbreia, J. E., Berek, G., Bolen, Z. K., Gudmestad, O. T., Heideman, J. C., Ohmart, R. D., and Spidsoe, N. (1991). Wave kinematics in irregular waves. In *Proceedings of the International Conference on Offshore Mechanics and Arctic Engineering*, volume 1A, pages 223–228. The American Society of Mechanical Engineers.
- Sklar, M. (1959). Fonctions de répartition à n dimensions et leurs marges. In *Publications de l'Institut de statistique de l'Université de Paris*, volume 8, pages 229–231.

BIBLIOGRAPHY

- Snyder, R. L. and Kennedy, R. M. (1983). On the formation of whitecaps by a threshold mechanism. part i: Basic formalism. *Journal of Physical Oceanography*, (13):1482–1492.
- Snyder, R. L., Smith, L., and Kennedy, R. M. (1983). On the formation of whitecaps by a threshold mechanism. part iii: Field experiment and comparison with theory. *Journal of Physical Oceanography*, (13):1505–1518.
- Song, J.-B. and Banner, M. L. (2002). On determining the onset and strength of breaking for deep water waves: Part i: Unforced irrotational wave groups. *Journal of Physical Oceanography*, 32(9):2541–2558.
- Song, J.-B., Lou, S.-l., and Tian, J.-w. (1997). Calculations of wave breaking probability and distribution of breaking wave heights in deep water. *Chinese Journal of Oceanology and Limnology*, 15(3):252–257.
- Sriram, V. (2008). *Finite element simulation of nonlinear free surface waves*. Dissertation, Indian Institute of Technology, Chennai.
- Sriram, V., Sannasiraj, S. A., and Sundar, V. (2006). Simulation of 2-d nonlinear waves using finite element method with cubic spline approximation. *Journal of Fluids and Structures*, 22(5):663–681.
- Sriram, V., Sannasiraj, S. A., and Sundar, V. (2007). 2d nonlinear wave body interaction using semi-ale. In *Journal of Coastal Research: Proceedings of the 9th International Coastal Symposium*, pages 394–399.
- Sriram, V., Sannasiraj, S. A., Sundar, V., Schlenkhoff, A., and Schlurmann, T. (2010). Quantification of phase shift in the simulation of shallow water waves. *International Journal for Numerical Methods in Fluids*, 62(12):1381–1410.
- Stansell, P. and MacFarlane, C. (2002). Experimental investigation of wave breaking criteria based on wave phase speeds. *Journal of Physical Oceanography*, 32(5):1269–1283.
- Stokes, G. G. (1847). *On the theory of oscillatory waves*, volume vol. 8 pt. 4 of *Transactions of the Cambridge Philosophical Society*. Printed at the Pitt Press, Cambridge.
- Tian, Z., Perlin, M., and Choi, W. (2008). Evaluation of a deep-water wave breaking criterion. *Physics of Fluids*, 20(6).

- Tian, Z., Perlin, M., and Choi, W. (2010). Energy dissipation in two-dimensional unsteady plunging breakers and an eddy viscosity model. *Journal of Fluid Mechanics*, 655:217–257.
- Tian, Z., Perlin, M., and Choi, W. (2012). An eddy viscosity model for two-dimensional breaking waves and its validation with laboratory experiments. *Physics of Fluids*, 24(3):036601.
- Toffoli, A., Babanin, A. V., Onorato, M., and Waseda, T. (2010). Maximum steepness of oceanic waves: Field and laboratory. *Geophysical Research Letters*, 37(5).
- Tulin, M. P. and Waseda, T. (1999). Laboratory observations of wave group evolution, including breaking effects. *Journal of Fluid Mechanics*, 378:197–232.
- Wahl, T., Mudersbach, C., and Jensen, J. (2012). Assessing the hydrodynamic boundary conditions for risk analyses in coastal areas: A multivariate statistical approach based on copula functions. *Natural Hazards and Earth System Science*, 12(2):495–510.
- Wilms, M. and Schlurmann, T. (2012). Investigation on wave-breaking probability in deep water. In *The 6th Chinese-German Joint Symposium on Hydraulic and Ocean Engineering (JOINT 2012)*.
- Wilms, M. and Schlurmann, T. (2014). A laboratory study on wave-breaking probability of two-dimensional wave trains depending on their input parameters. In *The 7th Chinese-German Joint Symposium on Hydraulic and Ocean Engineering (JOINT 2014)*.
- Wu, C. H. (2004). Laboratory measurements of limiting freak waves on currents. *Journal of Geophysical Research*, 109(C12).
- Wu, C. H. and Nepf, H. M. (2002). Breaking criteria and energy losses for three-dimensional wave breaking. *Journal of Geophysical Research*, 107(10):41–1.
- Xu, D.-l., Hwang, P. A., and Wu, J. (1986). Breaking of wind-generated waves. *Journal of Physical Oceanography*, 16(12):2172–2178.
- Yao, A. and Wu, C. H. (2005). Incipient breaking of unsteady waves on sheared currents. *Physics of Fluids*, 17(8):082104–1–082104–10.
- Yuan, Y., Han, L., Hua, F., Zhang, S., Qiao, F., Yang, Y., and Xia, C. (2009). The statistical theory of breaking entrainment depth and surface whitecap coverage of real sea waves. *Journal of Physical Oceanography*, 39(1):143–161.

BIBLIOGRAPHY

- Yuan, Y., Hua, F., Zhang, S., and Han, L. (2008). Statistical model on the surface elevation of waves with breaking. *Science in China, Series D: Earth Sciences*, 51(5):759–768.
- Yuan, Y., Tung, C.-C., and Huang, N. E. (1986). Statistical characteristics of breaking waves. In Phillips, O. M. and Hasselmann, K. L., editors, *Wave dynamics and radio probing of the ocean surface*, pages 265–272. Springer US, Boston, MA.
- Zakharov, V. E. and Shamin, R. V. (2012). Statistics of rogue waves in computer experiments. *JETP Letters*, 96(1):66–69.
- Zheng, G.-Z. and Xu, D.-l. (2004). Probabilistic models for the probability of wave breaking and whitecap coverage based on kinematic breaking criterion. *China Ocean Engineering*, 18(3):357–370.
- Zimmermann, C.-A. and Seymour, R. (2002). Detection of breaking in a deep water wave record. *Journal of Waterway, Port, Coastal and Ocean Engineering*, 128(2):72–78.

A. Test Program of Hydronumerical Model Tests

Table A.1.: Test program of the hydronumerical model tests.

Nr.	$s_{Z,i}$	H_S	T_P	γ	h	N_W	L_{flume}	σ_H	σ_L	n_{max}
	[-]	[m]	[s]	[-]	[m]	[-]	[m]	[-]	[-]	[-]
1	0.010	0.043	1.65	3.3	0.7	192	50	0.090	0.070	1
2	0.010	0.043	1.65	3.3	0.7	192	100	0.090	0.070	88
3	0.020	0.083	1.65	3.3	0.7	192	50	0.090	0.070	2
4	0.020	0.083	1.65	3.3	0.7	192	100	0.090	0.070	75
5	0.027	0.150	1.90	3.3	0.7	192	50	0.090	0.070	104
6	0.027	0.150	1.90	3.3	0.7	768	50	0.090	0.070	43
7	0.027	0.150	1.90	3.3	0.7	1536	50	0.090	0.070	36
8	0.027	0.150	1.90	3.3	0.7	3072	50	0.090	0.070	30
9	0.033	0.150	1.70	3.3	0.7	192	50	0.090	0.070	81
10	0.033	0.150	1.70	3.3	0.7	192	100	0.090	0.070	212
11	0.035	0.200	1.90	3.3	0.7	192	50	0.090	0.070	174
12	0.035	0.200	1.90	3.3	0.7	768	50	0.090	0.070	40
13	0.035	0.200	1.90	3.3	0.7	1536	50	0.090	0.070	40
14	0.035	0.200	1.90	3.3	0.7	3072	50	0.090	0.070	32
15	0.044	0.200	1.70	2.0	0.7	192	50	0.090	0.070	25
16	0.044	0.200	1.70	2.0	0.7	192	50	0.095	0.065	47
17	0.044	0.200	1.70	2.0	0.7	192	50	0.100	0.060	49
18	0.044	0.200	1.70	2.0	0.7	192	50	0.105	0.055	51

A. Test Program of Hydronumerical Model Tests

Table A.1.: Test program of the hydronumerical model tests.

Nr.	$s_{Z,i}$	H_S	T_P	γ	h	N_W	L_{flume}	σ_H	σ_L	n_{max}
	[-]	[m]	[s]	[-]	[m]	[-]	[m]	[-]	[-]	[-]
19	0.044	0.200	1.70	3.3	0.5	192	50	0.090	0.070	240
20	0.044	0.200	1.70	3.3	0.6	192	50	0.090	0.070	144
21	0.044	0.200	1.70	3.3	0.7	192	50	0.090	0.070	167
22	0.044	0.200	1.70	3.3	0.7	192	100	0.090	0.070	238
23	0.044	0.200	1.70	3.3	0.7	768	50	0.090	0.070	24
24	0.044	0.200	1.70	3.3	0.7	1536	50	0.090	0.070	3
25	0.044	0.200	1.70	3.3	0.8	192	50	0.090	0.070	267
26	0.044	0.200	1.70	3.3	0.9	192	50	0.090	0.070	368
27	0.044	0.200	1.70	5.0	0.7	192	50	0.090	0.070	68
28	0.044	0.200	1.70	5.0	0.7	192	50	0.095	0.065	47
29	0.044	0.200	1.70	5.0	0.7	192	50	0.100	0.060	39
30	0.044	0.200	1.70	7.0	0.7	192	50	0.095	0.065	35
31	0.044	0.200	1.70	7.0	0.7	192	50	0.100	0.060	49
32	0.050	0.225	1.70	3.3	0.7	192	50	0.090	0.070	143
33	0.055	0.250	1.70	3.3	0.7	192	50	0.090	0.070	110
34	0.055	0.250	1.70	3.3	0.7	192	100	0.090	0.070	239
35	0.055	0.250	1.70	3.3	0.7	768	50	0.090	0.070	48
36	0.055	0.250	1.70	3.3	0.7	1536	50	0.090	0.070	47
37	0.055	0.250	1.70	3.3	0.7	3072	50	0.090	0.070	13
38	0.067	0.300	1.70	2.0	0.7	192	50	0.090	0.070	86
39	0.067	0.300	1.70	2.0	0.7	192	50	0.095	0.065	49
40	0.067	0.300	1.70	2.0	0.7	192	50	0.100	0.060	48
41	0.067	0.300	1.70	2.0	0.7	192	50	0.105	0.055	39
42	0.067	0.300	1.70	3.3	0.7	192	50	0.090	0.070	149

Table A.1.: Test program of the hydronumerical model tests.

Nr.	$s_{Z,i}$	H_S	T_P	γ	h	N_W	L_{flume}	σ_H	σ_L	n_{max}
	[-]	[m]	[s]	[-]	[m]	[-]	[m]	[-]	[-]	[-]
43	0.067	0.300	1.70	5.0	0.7	192	50	0.090	0.070	25
44	0.067	0.300	1.70	5.0	0.7	192	50	0.095	0.065	48
45	0.067	0.300	1.70	5.0	0.7	192	50	0.100	0.060	49
46	0.067	0.300	1.70	7.0	0.7	192	50	0.090	0.070	45
47	0.067	0.300	1.70	7.0	0.7	192	50	0.095	0.065	42
48	0.067	0.300	1.70	7.0	0.7	192	50	0.100	0.060	49
49	0.071	0.300	1.65	3.3	0.7	192	50	0.090	0.070	186

B. Additional Figures (copula)

This chapter contains additional figures of the cumulative distribution function $H(x, y)$ and of the exceedance probability P_E of the normalised time and location of breaking onset t_{br}/T_P and x_{br}/L_P , respectively, which were determined with the GUMBEL copula. All breaking test runs with initial spectral steepnesses $s_{Z,i} = 0.01, 0.02, 0.027, 0.035, 0.044, 0.05, 0.055, 0.067, 0.071$ are considered; the results for $s_{Z,i} = 0.033$ are in the main text of the thesis.

B. Additional Figures (copula)

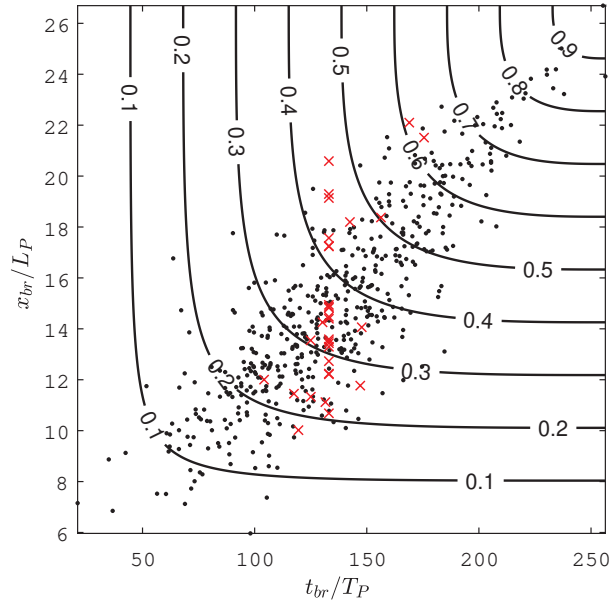


Figure B.1.: Cumulative distribution function $H(x, y)$ with the Gumbel copula for the test runs with spectral steepness $s_{Z,i} = 0.01$, with original NWF simulated data (red cross markers) and copula generated data (black round markers).

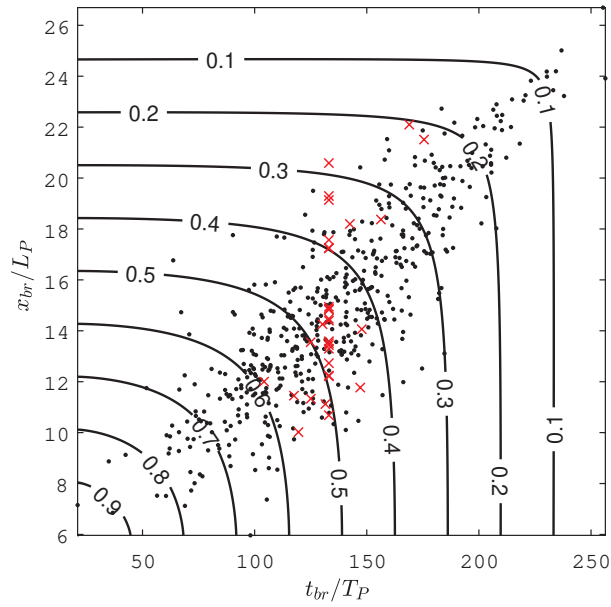


Figure B.2.: Exceedance probability P_E for the test runs with spectral steepness $s_{Z,i} = 0.01$, with original NWF simulated data (red cross markers) and copula generated data (black round markers).

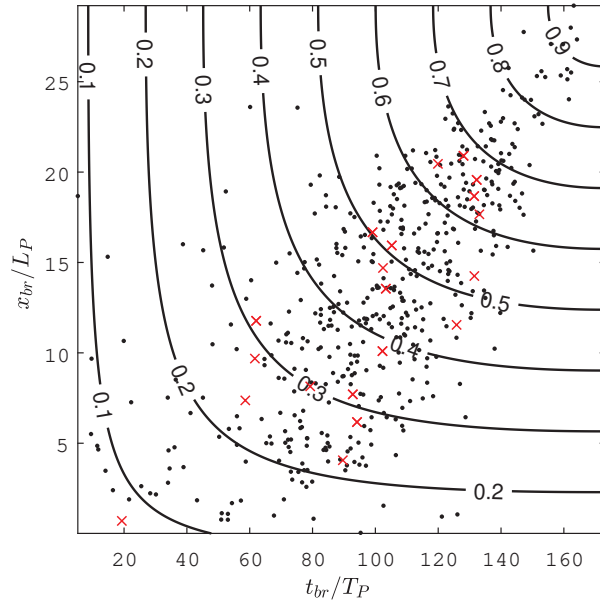


Figure B.3.: Cumulative distribution function $H(x, y)$ with the Gumbel copula for the test runs with spectral steepness $s_{Z,i} = 0.02$, with original NWF simulated data (red cross markers) and copula generated data (black round markers).

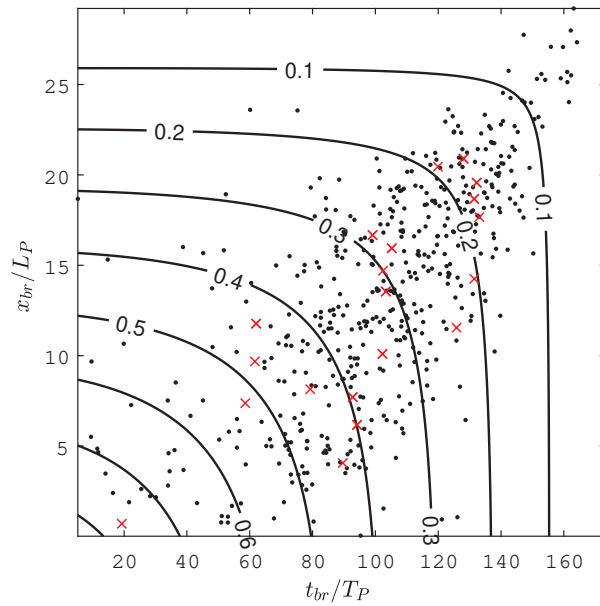


Figure B.4.: Exceedance probability P_E for the test runs with spectral steepness $s_{Z,i} = 0.02$, with original NWF simulated data (red cross markers) and copula generated data (black round markers).

B. Additional Figures (copula)

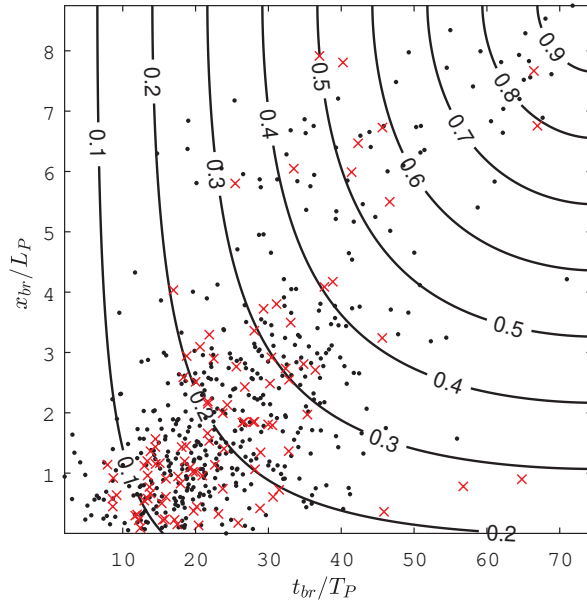


Figure B.5.: Cumulative distribution function $H(x, y)$ with the Gumbel copula for the test runs with spectral steepness $s_{Z,i} = 0.027$, with original NWF simulated data (red cross markers) and copula generated data (black round markers).

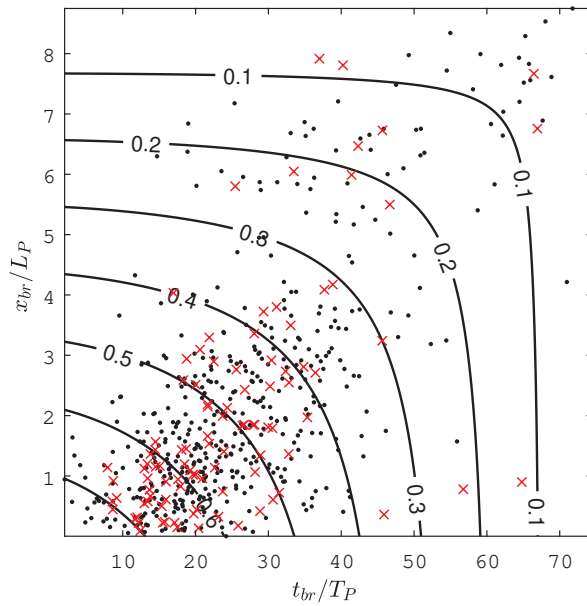


Figure B.6.: Exceedance probability P_E for the test runs with spectral steepness $s_{Z,i} = 0.027$, with original NWF simulated data (red cross markers) and copula generated data (black round markers).

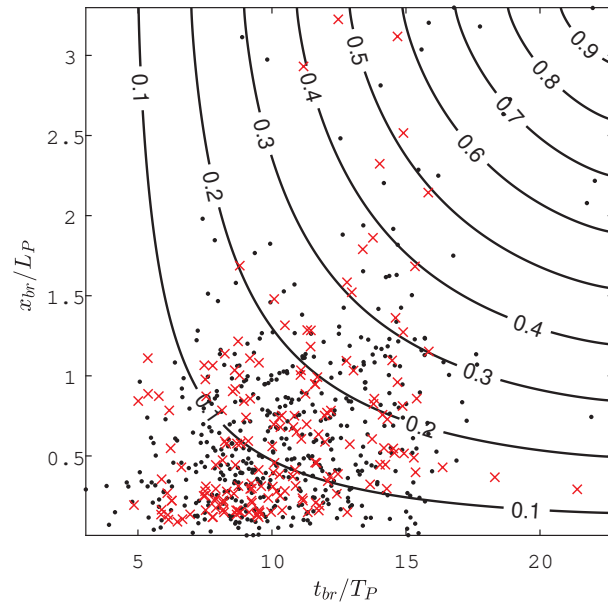


Figure B.7.: Cumulative distribution function $H(x, y)$ with the Gumbel copula for the test runs with spectral steepness $s_{Z,i} = 0.035$, with original NWF simulated data (red cross markers) and copula generated data (black round markers).

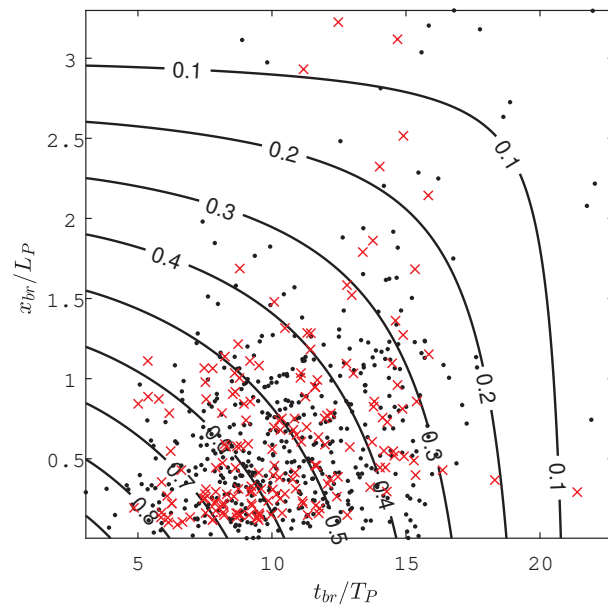


Figure B.8.: Exceedance probability P_E for the test runs with spectral steepness $s_{Z,i} = 0.035$, with original NWF simulated data (red cross markers) and copula generated data (black round markers).

B. Additional Figures (copula)

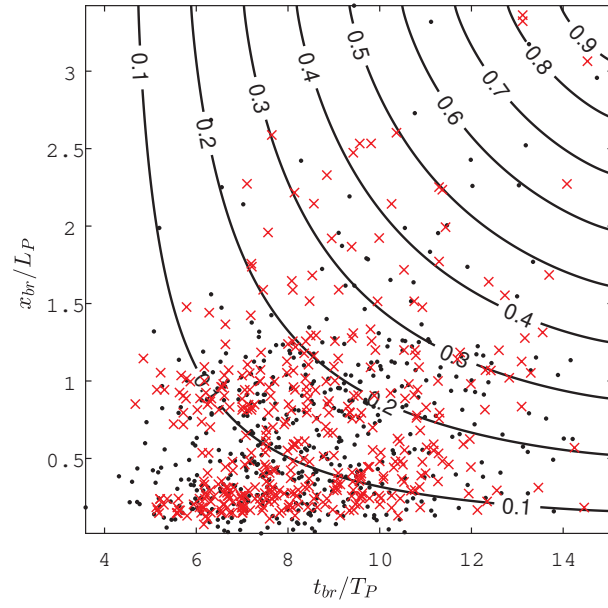


Figure B.9.: Cumulative distribution function $H(x, y)$ with the Gumbel copula for the test runs with spectral steepness $s_{Z,i} = 0.044$, with original NWF simulated data (red cross markers) and copula generated data (black round markers).

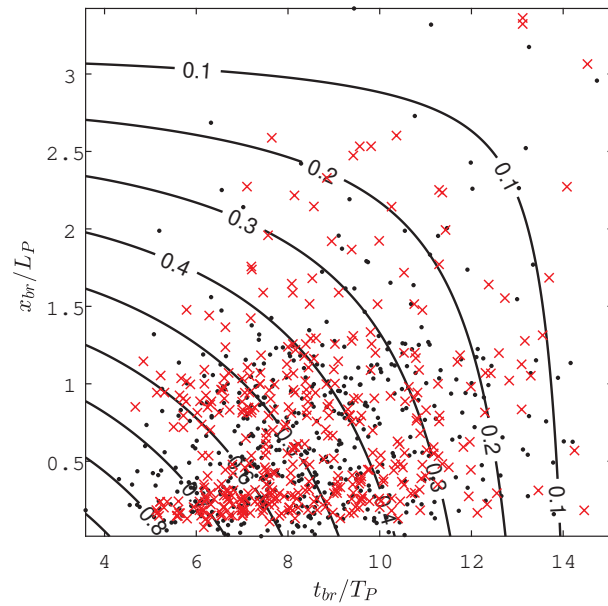


Figure B.10.: Exceedance probability P_E for the test runs with spectral steepness $s_{Z,i} = 0.044$, with original NWF simulated data (red cross markers) and copula generated data (black round markers).

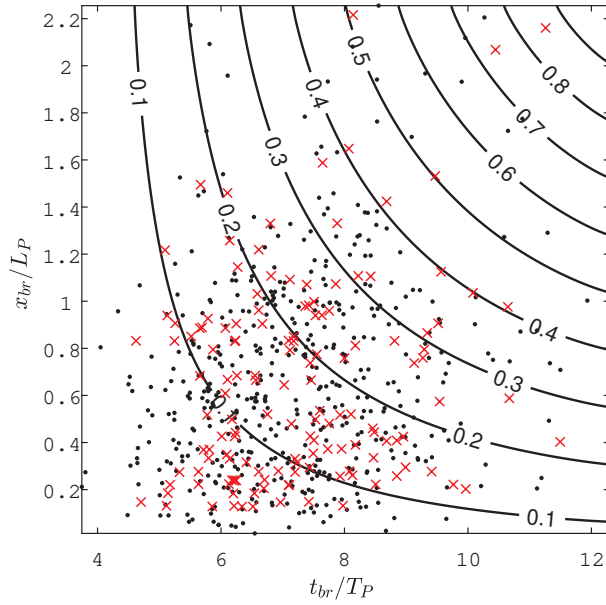


Figure B.11.: Cumulative distribution function $H(x, y)$ with the Gumbel copula for the test runs with spectral steepness $s_{Z,i} = 0.05$, with original NWF simulated data (red cross markers) and copula generated data (black round markers).

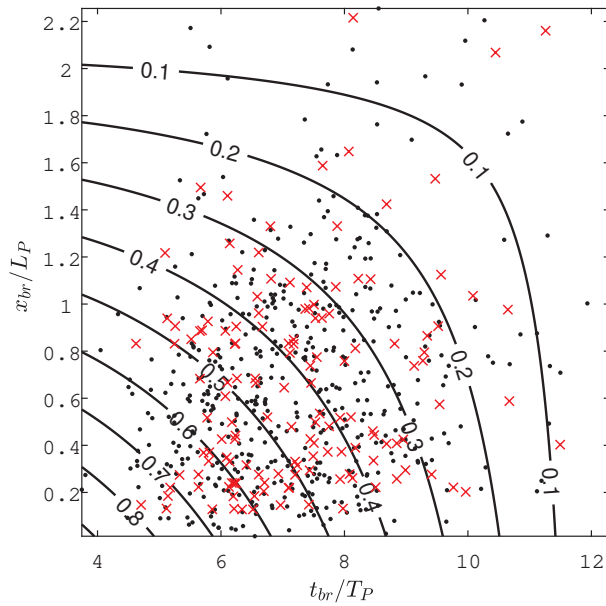


Figure B.12.: Exceedance probability P_E for the test runs with spectral steepness $s_{Z,i} = 0.05$, with original NWF simulated data (red cross markers) and copula generated data (black round markers).

B. Additional Figures (copula)

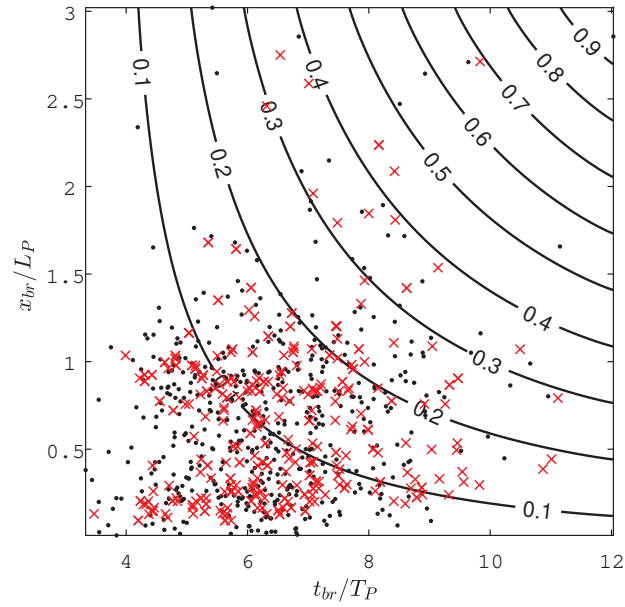


Figure B.13.: Cumulative distribution function $H(x, y)$ with the Gumbel copula for the test runs with spectral steepness $s_{Z,i} = 0.055$, with original NWF simulated data (red cross markers) and copula generated data (black round markers).

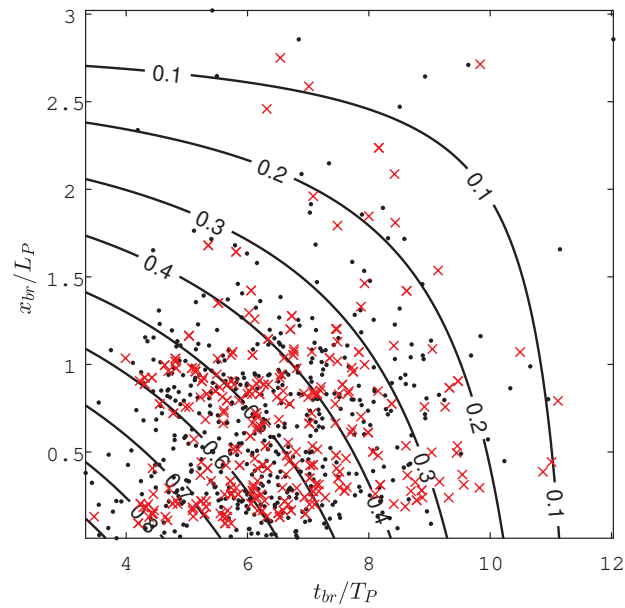


Figure B.14.: Exceedance probability P_E for the test runs with spectral steepness $s_{Z,i} = 0.055$, with original NWF simulated data (red cross markers) and copula generated data (black round markers).

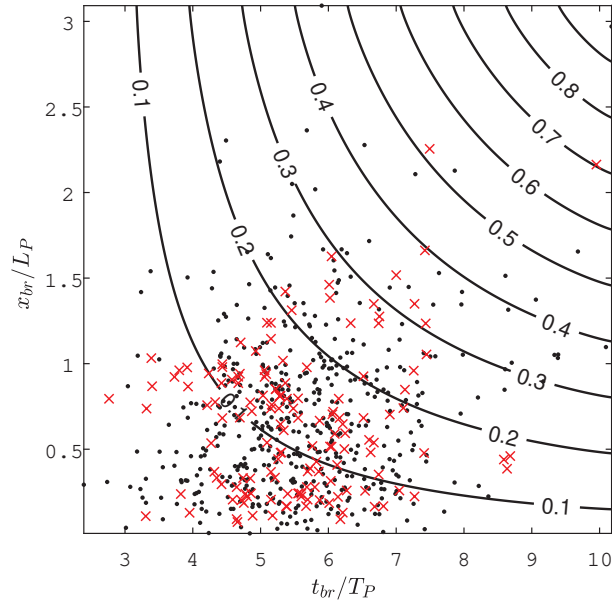


Figure B.15.: Cumulative distribution function $H(x, y)$ with the Gumbel copula for the test runs with spectral steepness $s_{Z,i} = 0.067$, with original NWF simulated data (red cross markers) and copula generated data (black round markers).

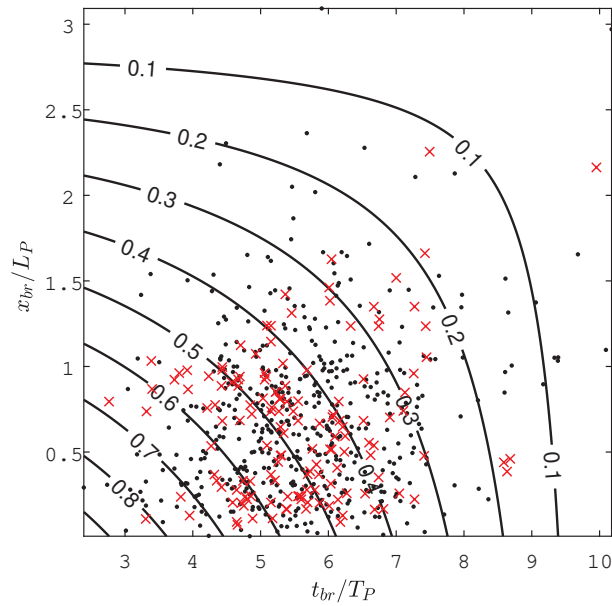


Figure B.16.: Exceedance probability P_E for the test runs with spectral steepness $s_{Z,i} = 0.067$, with original NWF simulated data (red cross markers) and copula generated data (black round markers).

B. Additional Figures (copula)

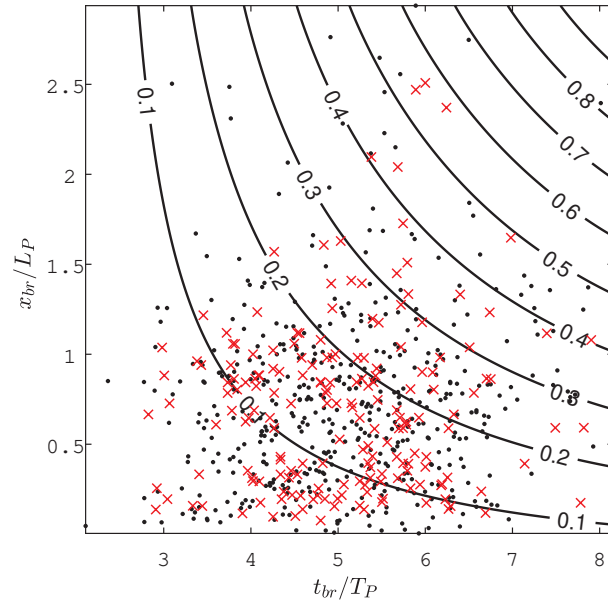


Figure B.17.: Cumulative distribution function $H(x, y)$ with the Gumbel copula for the test runs with spectral steepness $s_{Z,i} = 0.071$, with original NWF simulated data (red cross markers) and copula generated data (black round markers).

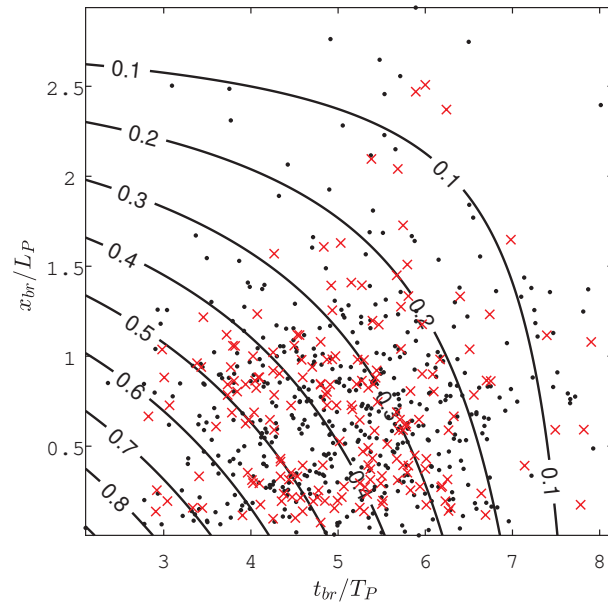


Figure B.18.: Exceedance probability P_E for the test runs with spectral steepness $s_{Z,i} = 0.071$, with original NWF simulated data (red cross markers) and copula generated data (black round markers).

C. Additional Figures (deformation of wave crest)

C. Additional Figures (deformation of wave crest)

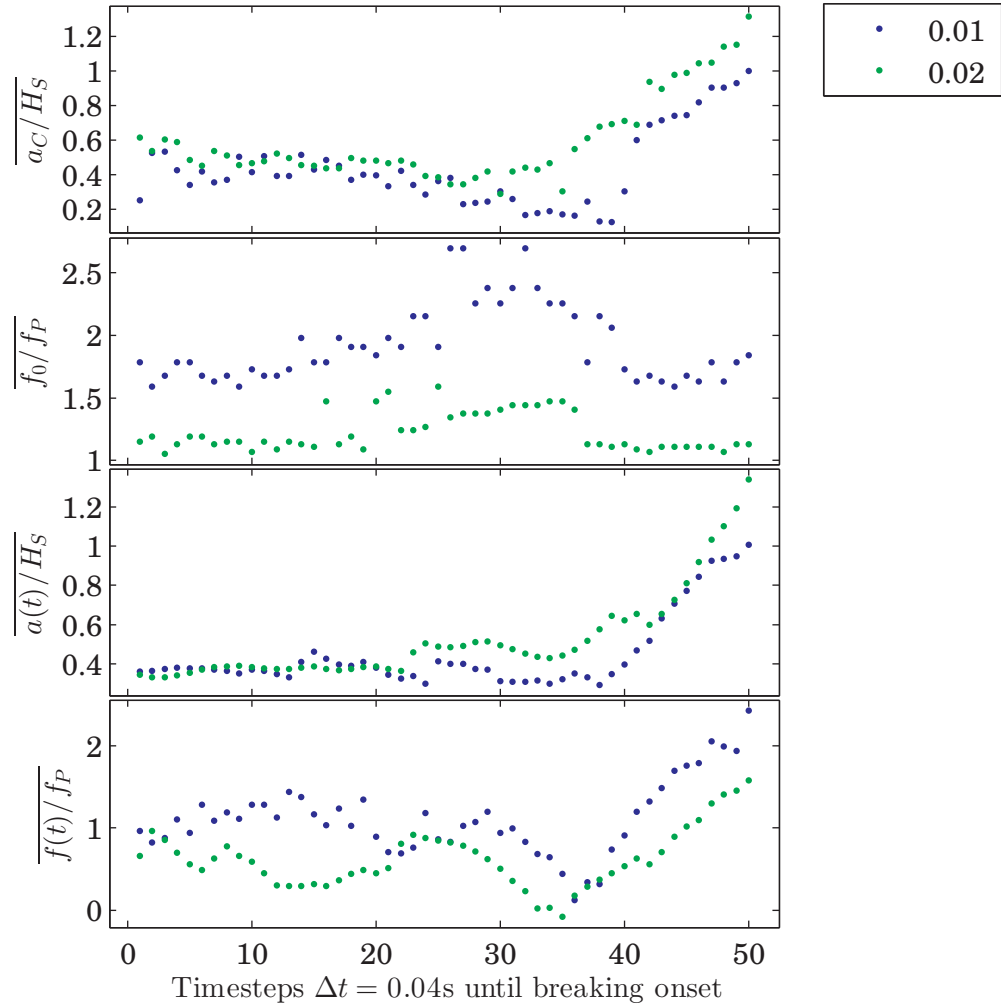


Figure C.1.: Development of the median of the geometrical parameters against time steps ($\Delta t = 0.04s$) until breaking onset with the simulated NWF data for different spectral steepnesses $s_{Z,i}$ (part 1, amplitudes and frequencies).

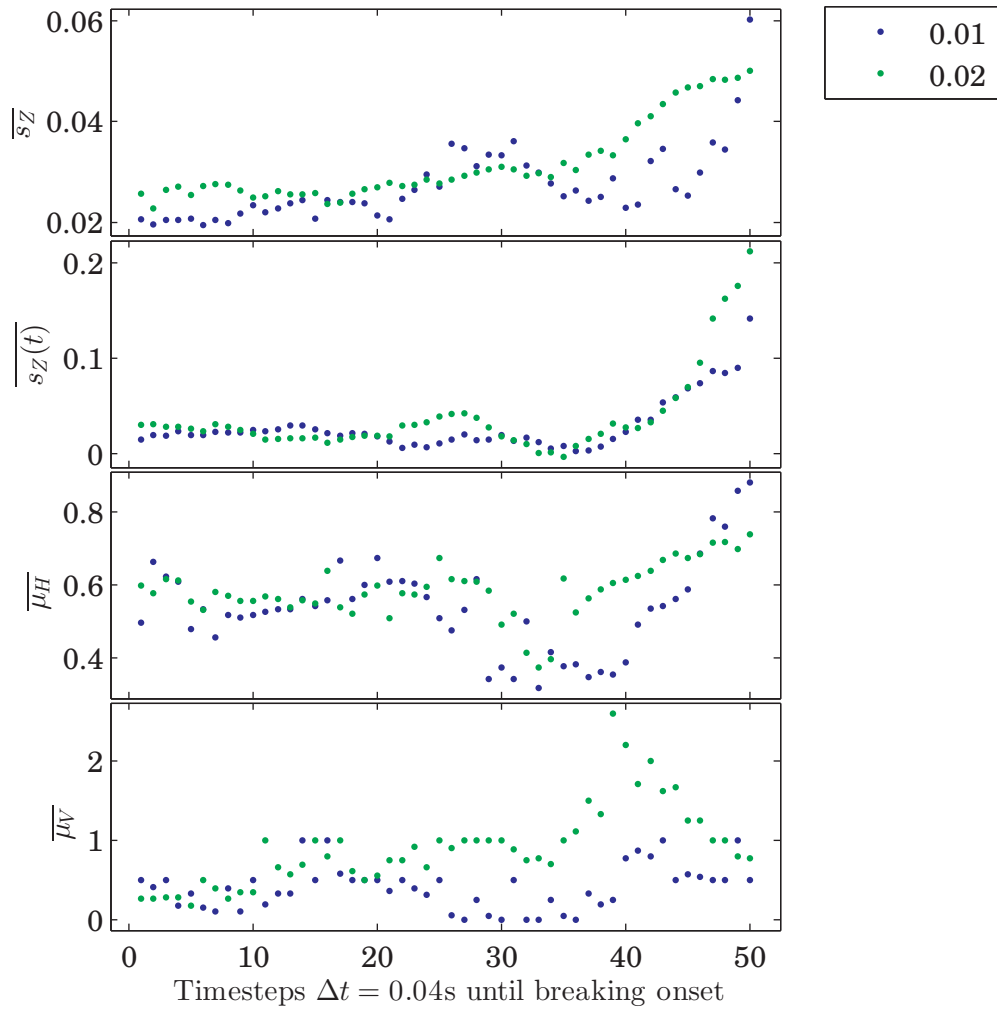


Figure C.2.: Development of the median of the geometrical parameters against time steps ($\Delta t = 0.04s$) until breaking onset with the simulated NWF data for different spectral steepnesses $s_{Z,i}$ (part 2, steepnesses and asymmetries).

C. Additional Figures (deformation of wave crest)

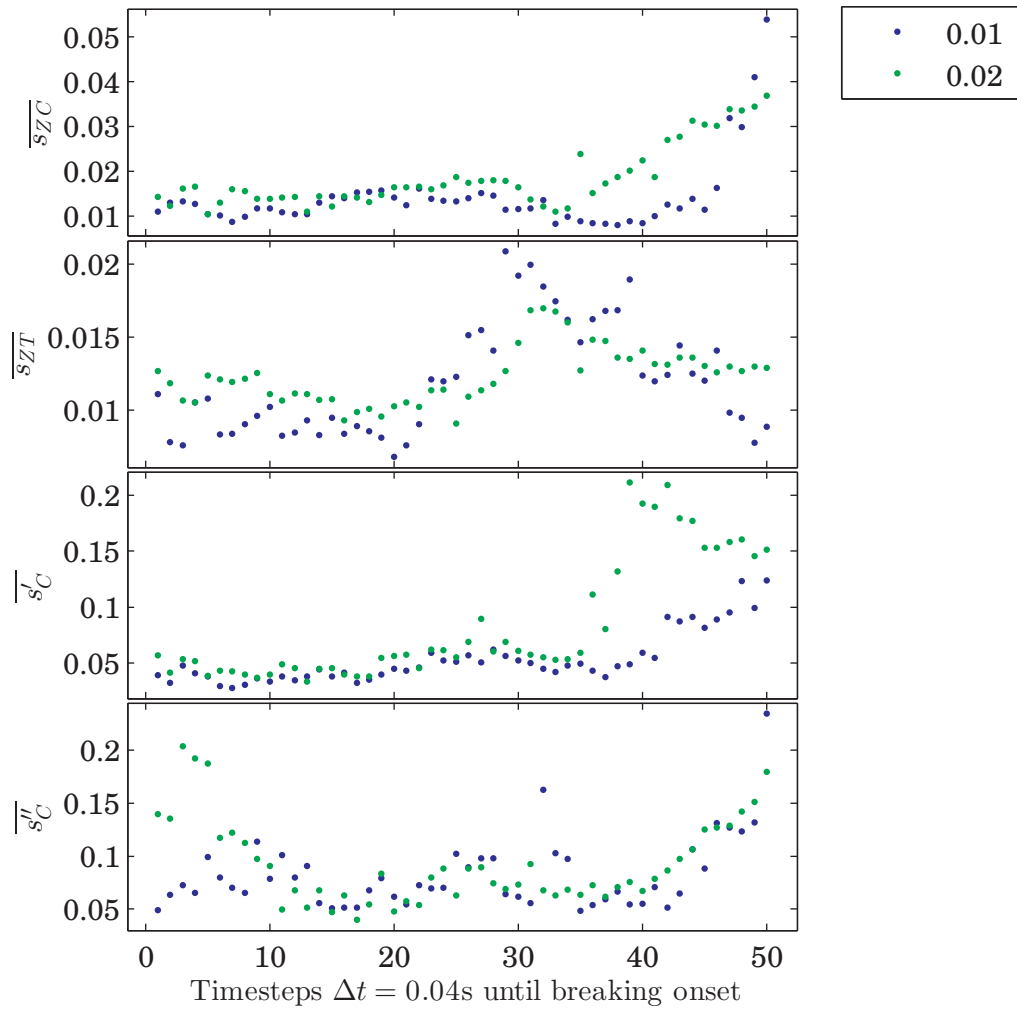


Figure C.3.: Development of the median of the geometrical parameters against time steps ($\Delta t = 0.04s$) until breaking onset with the simulated NWF data for different spectral steepnesses $s_{Z,i}$ (part 3, steepnesses).

D. Curriculum Vitae

Personal Data

Name	Mayumi Louise Wilms
Date of Birth	September 21, 1982
Place of Birth	Wuppertal, Germany

Work Experience

04/2009 – 09/2015	Research Associate, Ludwig-Franzius-Institute for Hydraulic, Estuarine and Coastal Engineering, Leibniz Universität Hannover
-------------------	--

Education

09/2008 – 02/2009	Diploma thesis at Leibniz Universität Hannover
04/2007 – 09/2007	Student research project at MARIN (Maritime Research Institute Netherlands)
10/2002 – 03/2009	University education in Verkehrswesen (Mechanical Engineering) at Technische Universität Berlin Degree: Diplomingenieurin (equivalent to Master Degree) Specialization: Naval Architecture and Ocean Engineering
09/1993 – 05/2002	School education at the Carl-Duisberg-Gymnasium Wuppertal, Germany Graduated with German Abitur (equivalent to A-levels)